

Pressure Mapping Of Medical Compression Bandages Used For Venous Leg Ulcer Treatment

by

Jawad Ameen Jawad Al Khaburi

Submitted in accordance with the requirements
for the degree of Doctor of Philosophy

The University of Leeds
School of Mechanical Engineering

July, 2010

The candidate confirms that the work submitted is his own and that the appropriate credit has been given where references have been made to the work of others.

This copy has been supplied on the understanding that it is copyright material and that no quotation from the report may be published without proper acknowledgement.

© 2010 The University of Leeds and Jawad Ameen Jawad Al Khaburi.

Abstract

Chronic leg ulcers affect 1% of the adult population in the developed countries. The majority of leg ulcers are due to venous disease. The impact of venous ulcers on the quality of life is significant, and it costs the NHS £300 – 600m annually. Medical compression bandages (MCBs) are the cornerstone in the treatment of chronic venous ulcers. MCBs should be applied with a pressure gradient reducing from the ankle to the knee. Visual inspection of bandages in situ for the amount of extension and overlap in the MCBs is normally what nurses use in day by day clinical practice to control the pressure they apply to patients' legs. Interface pressure produced by a bandage is proportional to the tension which, in turn, is proportional to the extension of the bandage, and pressure is inversely proportional to the limb radius. Experts in the field believe that applying MCBs with a constant extension will enable users to achieve the required gradient pressure profile, as the circumference of the leg increases from the ankle towards the mid-calf. Despite the many studies published investigating the effectiveness of different MCBs, very little work has been done to understand the underpinning physics of how MCBs apply pressure to the leg. In addition, although many types of pressure measurement systems have been developed and used by various researchers, most of these devices have not been systematically tested for their performance and measurement reliability.

In this thesis, the physics behind compression therapy is investigated and modeled using mathematical equations, some of which are validated experimentally. Analytical results suggest that ignoring MCBs thickness when computing the interface pressure will have a negligible effect on the accuracy of the pressure calculation produced by single-layer MCBs. However, MCBs thickness should be considered in computing the interface pressure produced by multi-layer MCBs. Moreover, a model developed by other researchers to explain the impact of the pressure sensor's physical dimensions on the interface pressure is tested experimentally. Results suggest that the model is not sufficient to estimate the amount of perturbation in the pressure, and a better model is needed.

Furthermore, the thesis outlines experiments conducted to study MCBs and obtain polynomial expressions to describe the MCBs tension-elongation curves. The polynomial expressions are used in conjunction with mathematical models to compute the interface pressure induced by MCBs. In addition, the thesis demonstrates how the information obtained from these experiments is used in line with a mathematical model to classify compression bandages and simulate the impact of limb shape change secondary to calf muscle activity on the interface pressure.

Moreover, the thesis reports on the evaluation of various types of resistive-based flexible pressure sensors. It illustrates that FlexiForce outperforms other resistive-based flexible sensors in static evaluation for sensitivity to low pressures, nonlinearity, repeatability, hysteresis and drift. However, the typical accuracy of FlexiForce sensor is found to be $\pm 12\%$ full scale, where full scale in this case is $120mmHg$. The accuracy error is further reduced to approximately $\pm 6\%$ full scale by arranging the sensors in arrays and using

averaging techniques.

Arrays of FlexiForce sensors are used then to map the interface pressure under MCBs applied to different mediums. The pressure maps obtained by FlexiForce sensors are compared with the maps obtained using microelectromechanical systems (MEMS) force sensors and PicoPress transducer, a commercial medical pressure transducer used currently to study the pressure induced under MCBs. Furthermore, the measured pressures in all these cases are compared with the pressures computed theoretically from the bandage extension. Results show low levels of agreement or, in some cases, no agreement between the measured and computed pressures, which lead to question the reliability of using extension as a feedback method to control the interface pressure applied by MCBs. Additionally, in spite of some deficiencies in the performance of FlexiForce sensors, the thesis demonstrates that they could be used to obtain pressure maps for qualitative purposes. This, in some cases, is found to provide more reliable pressure readings than commercial sensors like PicoPress. Generally, current medical pressure transducers are thick; thus, they tend to overestimate the pressure applied by compression bandages significantly.

The thesis details the assessment of pressure-mapping bandage prototypes and the associated tests carried out to evaluate their performance. Preliminary results suggest that the pressure-mapping bandage prototypes cannot be used to have accurate measurements. Nevertheless, they can provide the user with qualitative information about the pressure profile in terms of pressure levels and gradient.

Finally, the thesis presents the usage of a pressure-mapping leg for training purposes for student nurses. This involved studying student nurses' bandaging techniques and pinpointing their main bandaging technique pitfalls. Compared with experienced nurses, fewer of the student nurses applied MCBs with reverse pressure gradient.

To my parents
As a token of gratitude and appreciation

To the person I love most
Isra
As a pledge of love and affection

Acknowledgements

Although a PhD is a journey that someone has to travel on his/her own, in my case, there have been a number of people who have played a significant role in helping me reach my destination. I would like ,therefore, to express my deep thanks for them.

Firstly, I would like to express my gratitude to my supervisors, Dr. Abbas Dehghani and Prof. Andrea Nelson. They have proved to be a constant source of assistance, encouragement and advice throughout the project, and I would have been truly lost in this project without their guidance.

Secondly, I would like to thank ConvaTec to sponsor this project. I would like also to express my great thanks for Dr. Jerry Hutchinson and the rest of ConvaTec team who have offered continuous invaluable support throughout the project phases.

Thirdly, I would like to thank the Ministry of Higher Education in the Sultanate of Oman for providing me with a PhD scholarship to cover my maintenance expenses.

Fourthly, I would like to thank the various members of technical and workshop staff who have helped to source materials and/or assist with machining parts. Special mentions go to Mick Martin, Dave Readman, Tony Weise, Abbas Ismail, Steve Caddick, Graham Blyth, Margaret Gibson and Ted Allwood who have been very helpful whenever I needed any kind of assistance or support.

Fifthly, I would like to thank the researchers in the iESD and especially my colleagues in the mechatronics and robotics group who have inspired me with wonderful suggestions and ideas.

Sixthly, I would like to express my deep appreciation and thanks for my parents for their continuous support and love.

Finally, many thanks to my precious wife, Isra. This thesis was not going to see the light without her unlimited support and infinite love. I would like also to express my gratitude for her for spending her valuable time in reading the thesis and fixing the spelling and grammatical errors.

Contents

1	Introduction	1
1.1	Aims and Objectives	2
1.1.1	Aims of the PhD	2
1.1.2	Objectives of the PhD	2
1.2	Organization of the Thesis	3
2	Literature Review	5
2.1	Chronic Venous Disorder	5
2.1.1	Definition	5
2.1.2	Epidemiology	5
2.1.3	The Venous System in the Lower Limb	7
2.1.4	Pathophysiology	13
2.1.5	Venous Ulcer Management	16
2.2	Compression Therapy	17
2.2.1	Pathophysiological Effects of Compression Therapy	17
2.2.2	Interface Pressure and Optimum Pressure Profile	19
2.2.3	Risks of Compression	20
2.2.4	Medical Compression Bandages (MCBs)	21
2.3	Measurement of the Interface Pressure	30
2.3.1	Interface Pressure Measurement Systems: Need and Use	30
2.3.2	Ideal Interface Pressure Measurement System	31
2.3.3	Impact of Sensor Dimensions on the Measured Interface Pressure	32
2.3.4	Sites of Pressure Measurement Under a Compression Device	34

2.3.5	Review of Interface Pressure Measurement Systems	34
2.3.6	Other Forms of Interface Pressure Measurement System	41
2.4	Flexible Pressure Sensors	43
2.4.1	Capacitive Flexible Pressure Sensors	43
2.4.2	Piezo-resistive Flexible Pressure Sensors	47
2.4.3	Other Potential Flexible Sensors	51
2.5	Synopsis of the Literature Review	51
2.6	The Project Overall Methodology	52
2.7	Contribution of this Project to the Body of Knowledge	55
3	Sub-Bandage Interface Pressure: Mathematical Examination	57
3.1	Introduction	57
3.2	Forces Interaction Between the Compression Bandages and the Lower Limb	58
3.3	Effect of Bandage Thickness on the Interface Pressure	59
3.3.1	Interface Pressure Model Using Thin Wall Cylinder Theory	60
3.3.2	Interface Pressure Model Using Thick Wall Cylinder Theory	61
3.3.3	Comparison Between Thin and Thick Cylinder Wall Theories	62
3.3.4	Experimental Validation for the Models	64
3.4	Interface Pressure Induced by Multi-Layered MCBs	68
3.4.1	Multi-Layer Bandage Interface Pressure Modeled Using Thin Wall Cylinder Theory	69
3.4.2	Multi-Layer Bandage Interface Pressure Modeled Using Thick Wall Cylinder Theory	69
3.4.3	Computational Comparison Between the Multi-Layer Bandage Pres- sure Models	69
3.4.4	Experimental Validation	72
3.5	Effect of Biaxial Tension Forces on the Interface Pressure	75
3.5.1	Mathematical Modeling	75
3.5.2	Theoretical Simulation for the Effect	76
3.6	Effect of Angle of Application on the Interface Pressure	76
3.6.1	Mathematical Modeling	77

3.6.2	Theoretical Simulation for the Angle Effect	78
3.7	Impact of Change in Limb Shape on the Interface Pressure	80
3.7.1	Thin Cylinder Wall Theory Model	80
3.7.2	Thick Cylinder Wall Theory Model	81
3.7.3	Comparison between the Two Models and Theoretical Simulation	82
3.8	The Effect of Sensor's Physical Dimensions on the Interface pressure	84
3.8.1	Experimental Work to Investigate the Effect of Sensor Physical Dimensions on the Interface Pressure	84
3.9	Summary	91
4	Medical Compression Bandages: Selection and Experimental Evaluation	93
4.1	Introduction	93
4.2	MCB Selection	94
4.3	MCB Width and Thickness Measurement	95
4.4	Evaluation of MCB Tension-Elongation Interconnection	99
4.5	MCB Biaxial Force Evaluation	104
4.6	New Method to Classify MCB	105
4.6.1	Results, Analysis and Discussion	108
4.7	Computing Pressure from Extension in MCBs	109
4.8	Summary	110
5	Sensors Characteristics	112
5.1	Introduction	112
5.2	Instrumentation Specification Terms: Background Information	113
5.2.1	Calibration	113
5.2.2	Span or Full Scale (FS)	113
5.2.3	Nonlinearity Error	114
5.2.4	Hysteresis Error	114
5.2.5	Repeatability Error	115
5.2.6	Drift	115
5.2.7	Calibration Fitting Line Error	116
5.2.8	Accuracy	116

5.2.9	Uncertainty	116
5.2.10	Response Time	117
5.3	Sensor Selection	117
5.3.1	Commercial Medical Pressure Sensor	117
5.3.2	MEMS Force Sensor	117
5.3.3	Flexible Sensors	118
5.4	Evaluation of PicoPress Sensor	118
5.4.1	Static Characteristics of PicoPress Sensor	118
5.4.2	Evaluation of the effect of PicoPress Physical Dimensions on the Measured Interface Pressure	119
5.5	Evaluation of MEMS FS01 Force Sensor	121
5.5.1	Evaluation of FS01 Force Sensor over Flat Surface	122
5.5.2	Evaluation of FS01 Force Sensor Over Curved Surface	124
5.6	Evaluation and Comparison of Flexible Resistive-Based Sensors	126
5.6.1	Evaluation of Flexible Resistive-Based Sensors Using Deadweights	126
5.6.2	Evaluation of Flexible Resistive-Based Sensors Using Aneroid Sphyg- momanometer	129
5.7	FlexiForce Sensors: Other Issues	131
5.7.1	FlexiForce Dynamic Response to Step Input	131
5.7.2	FlexiForce Temperature Sensitivity	136
5.7.3	FlexiForce Averaging Technique	137
5.8	Summary	138
6	Pressure-Mapping Reference Systems	140
6.1	Introduction	140
6.2	Pressure-Mapping Systems Over Rigid Cylinders	141
6.2.1	Pressure-Mapping Cylinder Using PicoPress Sensors	141
6.2.2	Pressure-Mapping Cylinder Using FS01 Force Sensors	146
6.2.3	Pressure-Mapping Cylinder Using FlexiForce Sensors	152
6.2.4	Comparison Between the Different Pressure-Mapping Cylinders	160

6.2.5	Comparison Between the Different Pressure Sensing Technologies on the Same Cylinder	161
6.3	Pressure-Mapping Systems Over Rigid Mannequin Leg	167
6.3.1	3D Scan and Curvature Measurements for Rigid mannequin Leg . . .	168
6.3.2	Pressure-Mapping Mannequin Leg Using PicoPress Sensors	170
6.3.3	Pressure-Mapping Mannequin Leg Using FS01 Force Sensors	176
6.3.4	Pressure-Mapping Mannequin Leg Using FlexiForce Sensors	181
6.3.5	Comparison Between the Different Pressure-Mapping Mannequin Legs	189
6.4	Pressure-Mapping Systems Over Soft Leg Model	192
6.4.1	3D scan and Curvature Measurements for Leg Model	193
6.4.2	Pressure-Mapping Leg Using PicoPress Sensors	194
6.4.3	Pressure-Mapping Leg Using FlexiForce Sensors	198
6.4.4	Comparison Between the Different Pressure-Mapping Legs	208
6.5	Summary	211
7	Pressure-Mapping Measurement System	214
7.1	Introduction	214
7.2	Design and Development	214
7.2.1	Hardware	214
7.2.2	Sensors Calibration	215
7.2.3	Interface and Pressure Measurement Program	216
7.3	3D scan and Curvature Measurements for Human Participant Leg	217
7.4	Validation Using Computational Pressure From Extension	217
7.4.1	Methods and Materials	219
7.4.2	Results, Analysis and Discussion	221
7.5	Validation Using PicoPress Measured Pressures	224
7.5.1	Methods and Materials	225
7.5.2	Results, Analysis and Discussion	227
7.6	Summary	232
8	Pressure-Mapping Bandage	234
8.1	Introduction	234

8.2	Pressure-Mapping Bandage: First Prototype	235
8.2.1	Bandage Selection	235
8.2.2	Sensors, Sensors Attachments, Processing Unit and Data Acquisition	235
8.2.3	Sensors Calibration	236
8.2.4	Pressure-Mapping Bandage Interface and Program	236
8.2.5	Experimental Validation for the Pressure-Mapping Bandage	237
8.3	Pressure-Mapping Bandage: Second Prototype	242
8.3.1	Bandage Selection	242
8.3.2	Sensors, Sensor Attachments, Processing Unit and Data Acquisition	242
8.3.3	Sensors Calibration	243
8.3.4	Pressure-Mapping Bandage Interface and Program	243
8.3.5	Experimental Validation for the Pressure-Mapping Bandage	243
8.4	Summary	248
9	Compression Bandages Training System	250
9.1	Introduction	250
9.2	Methods and Materials	250
9.3	Results, Analysis and Discussion	255
9.4	Summary	257
10	Summary and Conclusions	259
10.1	Summary of the Findings and Contribution to the Field	259
10.1.1	Mathematical Examination of the Interface Pressure	260
10.1.2	Experimental Evaluation of Medical Compression Bandages	261
10.1.3	Pressure Sensors Characteristics	261
10.1.4	Pressure-Mapping Reference Systems	262
10.1.5	Pressure-Mapping Measurement System	262
10.1.6	Pressure-Mapping Bandage	263
10.1.7	Compression Bandages Training System	263
10.2	Assessment of the Research Objectives	263
10.3	Conclusions	265
10.4	Future Work	266

References	269
Appendices	
A Documentation for the Clinical Study: Lower Limb Shape, Temperature and Pressure Measurement Under Compression Bandages	286
B Documentation for the Clinical Study: Using a Model Leg With Embedded Pressure Sensors for Training Student Nurses to Apply Compression Bandages: Feasibility, Acceptability and Initial Results	293
C List of Publications	300

List of Figures

2.1	CVD abnormalities	6
2.2	Body planes	7
2.3	Great and small saphenous veins	8
2.4	Deep veins of the lower limb	8
2.5	Perforator veins	9
2.6	Blood pressure in various blood vessels of the systemic circulation	10
2.7	Musculovenous pump	11
2.8	Sequences of venous pump action during ambulation	12
2.9	Fluid flow at capillaries	12
2.10	Healthy and incompetent vein valves	14
2.11	The weight of blood column	14
2.12	The effects of walking on reducing pressure in normal individuals, and those with degrees of CVD	15
2.13	Resting vs. working pressures	23
2.14	Typical tension-elongation curves for commercial inelastic and elastic bandages.	26
2.15	Schematic representation of the interface perturbation effect of a sensor placed beneath an extensible bandage	33
2.16	Schematic representation of the interface perturbation effect of a sensor placed beneath an extensible bandage over a curved surface	33
2.17	PicoPress®	35
2.18	Air-Pack Type Analyzer	36
2.19	Kikuhime®	37

2.20	MST MK <i>IV</i>	38
2.21	ConTacts discrete sensors with ConTacts C500	44
2.22	Novel S2011 single sensor with 10 <i>mm</i> diameter	45
2.23	XSENSOR X3 LX100	46
2.24	FSR layers	47
2.25	FlexiForce® sensor	49
2.26	FlexiForce sensor construction layers	49
2.27	The project flow chart	54
3.1	Force Body Diagram for the bandage limb interaction	59
3.2	Dynamic bandage-limb interaction	59
3.3	Half of a thin cylinder subjected to internal pressure	60
3.4	Stresses within the cylinder wall	60
3.5	Thick cylinder subjected to internal pressure	61
3.6	Percentage difference in tension/pressure ratio between the thin and thick wall cylinder theories vs. limb diameter/bandage thickness ratio	63
3.7	Pressure calculated using the models based on thin and thick wall cylinder theory vs. limb radius	63
3.8	The simulated pressure map over a real leg when single-layer bandage is applied to the leg. The pressure calculated using the pressure model derived using thin wall cylinder theory	64
3.9	The simulated pressure map over a real leg when single-layer bandage is applied to the leg. The pressure calculated using the pressure model derived using thick wall cylinder theory	64
3.10	Rig used in the experiment	65
3.11	The experimental results in validating the model developed to study the effect of bandage thickness on the interface pressure	67
3.12	Pressure calculated using three models; Thomas model, thin wall cylinder model and thick wall cylinder model vs. radius	70

3.13	The simulated pressure map over a real leg when four layers of bandage are applied to the leg. The pressure calculated using the pressure model reported by Thomas	71
3.14	The simulated pressure map over a real leg when four layers of bandage are applied to the leg. The pressure calculated using the pressure model based on thin cylinder wall theory	71
3.15	The simulated pressure map over a real leg when four layers of bandage are applied to the leg. The pressure calculated using the pressure model based on thick cylinder wall theory	71
3.16	The pressure of individual layers as a percentage of the first layer pressure for variable limb circumference	72
3.17	The experimental results in validating the models developed to calculate the pressure applied by multi-layer MCBs	74
3.18	The effect of biaxial forces on the interface pressure	77
3.19	Tension forces in bandage when applied in angle	78
3.20	The effect of changing the application angle on the interface pressure	79
3.21	The effect of changing the application angle on the interface pressure when the tension in the width direction of the bandage is set to $0.1N$	79
3.22	Poisson's ratio for a bandage [thin cylinder wall]	80
3.23	The percentage difference in pressure pulsation calculated using thin and thick wall cylinder theories	83
3.24	Change in interface pressure caused by $10mm$ change in the limb circumference.	83
3.25	FlexiForce sensors' arrangement	86
3.26	Class 3C MCB is used to apply pressure to FlexiForce sensors	86
3.27	The effect of sensor aspect ratio on measured pressure (deadweights calibration)	87
3.28	The effect of sensor aspect ratio on measured pressure (Aneroid Sphygmomanometer calibration)	87
4.1	Comprilan Bandage	94

4.2	SurePress Bandage	95
4.3	Shirly thickness gauge and the mechanical arrangement used in the experiment	96
4.4	Instron 4301	100
4.5	Tension-elongation curves for Comprilan and SurePress bandages for the 0 – 60% elongation range.	100
4.6	1 st and 5 th cycles tension-elongation curves for Comprilan bandage of dif- ferent elongation ranges.	101
4.7	1 st and 5 th cycles tension-elongation curves for SurePress bandage of differ- ent elongation ranges.	101
4.8	(a) Change in peak tension over 5 cycles for Comprilan and SurePress ban- dages for the elongation range 0 – 60%. (b) Change in elongation value where tension starts over 5 cycles for Comprilan and SurePress bandages for the elongation range 0 – 60%. (c) Change in elongation value where tension ends over 5 cycles for Comprilan and SurePress bandages for the elongation range 0 – 60%	102
4.9	Tension-elongation curves for Comprilan bandage in the transverse direction for 0 – 10% elongation range	105
4.10	Tension-elongation curves for Comprilan bandage in the transverse direction for 0 – 4% elongation range	106
4.11	Young’s modulus and Chord modulus	107
4.12	Chord modulus for both bandages for the elongation range 45 – 55%	108
4.13	Change in tension at 45% elongation when cyclic load is applied to the two bandages	109
4.14	Change in tension at 55% elongation when cyclic load is applied to the two bandages	109
4.15	Change in peak-peak tension when cyclic load is applied to the two bandages	110
4.16	4 th order polynomial fitting-lines for the 1 st loading cycle for the tension- elongation curves for the range 0 – 60% elongation for Comprilan [top] and SurePress [bottom] bandages	111
5.1	FS01 force sensor from Honeywell	117

5.2	PicoPress sensor, the aneroid sphygmomanometer and the cylinder used to evaluate the sensor	119
5.3	PicoPress sensor output for five repeats when tested with aneroid sphygmomanometer	119
5.4	Rig used to evaluate the impact of PicoPress probe's physical dimensions on the interface pressure	120
5.5	The pressures measured, estimated and corrected during the experimental setup to study the impact of PicoPress probe's physical dimension on the interface pressure	121
5.6	The test rig and the arrangement used to test the FS01 force sensor	122
5.7	FS01 force sensor output for five repeats when tested with deadweights . .	123
5.8	The test rig and arrangement used to test FS01 over a curved surface . . .	124
5.9	FS01 force sensor output for five repeats when tested with aneroid sphygmomanometer	125
5.10	FlexiForce, Tactilus, big FSR and small FSR sensors	126
5.11	The test rig and the arrangement used to test Tactilus force sensor	127
5.12	FlexiForce sensor output for five repeats when tested with deadweights . . .	128
5.13	Tactilus sensor output for five repeats when tested with deadweights	129
5.14	The arrangement to test nonlinearity and repeatability of FlexiForce, Tactilus, big FSR and small FSR sensors using aneroid sphygmomanometer . .	130
5.15	FlexiForce sensor output for twenty repeats when tested with aneroid sphygmomanometer	131
5.16	Tactilus sensor output for twenty repeats when tested with aneroid sphygmomanometer	132
5.17	Big FSR sensor output for twenty repeats when tested with aneroid sphygmomanometer	132
5.18	LCAE-600G load cell used to study the FlexiForce step response to a step input	133
5.19	The output of the load cell and the FlexiForce sensor 1, when connected in a potential divider arrangement	134

5.20	The output of the load cell and the FlexiForce sensor 1, when connected in a gain-filter circuit arrangement	134
5.21	The time difference in response time of the output of the load cell and the FlexiForce sensor 1, when connected in a potential divider arrangement. . .	135
5.22	The time difference in response time of the output of the load cell and the FlexiForce sensor 1, when connected in a gain-filter circuit arrangement [one cycle]	135
5.23	Oven used in the experiment	136
5.24	The output voltage of the FlexiForce sensor vs. change in temperature . . .	137
5.25	The size of pressure map before and after using window averaging, when 16 FlexiForce sensors are arranged in 4×4 matrix over a cylinder	138
6.1	PVC cylinder with PicoPress sensors in a 5×3 array	142
6.2	Comprilan: computed, measured and corrected measured pressures	145
6.3	SurePress: computed, measured and corrected measured pressures	145
6.4	Bland-Altman plot for computed pressures and corrected measured pressures for Comprilan	146
6.5	Bland-Altman plot for computed pressures and corrected measured pressures for SurePress	146
6.6	PVC cylinder with FS01 force sensors embedded in its wall	147
6.7	The arrangement of FS01 force sensors	148
6.8	Calibration of FS01 force sensors using aneroid sphygmomanometer	149
6.9	The front panel of the display program	149
6.10	The flow chart of the display program	150
6.11	Comprilan: computed and measured pressures	151
6.12	SurePress: computed and measured pressures	152
6.13	Bland-Altman plot for computed pressures and measured pressures for Comprilan	152
6.14	Bland-Altman plot for computed pressures and measured pressures for SurePress	153
6.15	PVC cylinder with FlexiForce sensors mounted in the form of 8×7 matrix	154

6.16	The conditioning circuit used to power up and process the output signals of 16 FlexiForce sensors	154
6.17	The front panel of the display program for FlexiForce cylindrical pressure-mapping system	155
6.18	The flow chart of the display program for FlexiForce cylindrical pressure-mapping system	156
6.19	Comprilan and SurePress pressure maps	157
6.20	Comprilan: computed and measured pressures	159
6.21	SurePress: computed and measured pressures	159
6.22	Bland-Altman plot for computed pressures and measured pressures for Comprilan	160
6.23	Bland-Altman plot for computed pressures and measured pressures for SurePress	160
6.24	PVC cylinder with FlexiForce sensors mounted in the form of 8×7 matrix	162
6.25	Summary of computed pressures, measured pressures using PicoPress sensors, FS01 sensors and FlexiForce sensors using fitting-lines obtained from two calibration methods and the PicoPress corrected pressures at two levels for four Comprilan bandages	164
6.26	Summary of computed pressures, measured pressures using PicoPress sensors, FS01 sensors and FlexiForce sensors using fitting-lines obtained from two calibration methods and the PicoPress corrected pressures at two levels for four SurePress bandages	164
6.27	Bland-Altman plot for PicoPress sensors vs. FlexiForce deadweights calibration	167
6.28	Bland-Altman plot for PicoPress sensors with correction vs. FlexiForce aneroid sphygmomanometer calibration	167
6.29	Bland-Altman plot for PicoPress sensors with correction vs. FS01 force sensors	168
6.30	Bland-Altman plot for FS01 force sensors vs. FlexiForce aneroid calibration	168
6.31	NextEngine's 3D scanner and the mannequin leg. The mannequin leg is painted in white for scanning purposes	169

6.32	The mannequin leg's mesh data as displayed in 3D Scan Studio	169
6.33	The 3D mannequin leg solid model with the cross sectional digital profiles at seven levels	170
6.34	Plastic mannequin leg with PicoPress sensors mounted	171
6.35	The arrangement of the PicoPress sensors on the mannequin leg	171
6.36	Comprilan: computed, measured and corrected measured pressures	174
6.37	SurePress: computed, measured and corrected measured pressures	174
6.38	Bland-Altman plot for computed pressures and corrected measured pres- sures for Comprilan	175
6.39	Bland-Altman plot for computed pressures and corrected measured pres- sures for SurePress	175
6.40	Plastic mannequin leg with FS01 force sensors embedded in its wall	176
6.41	The arrangement of FS01 force sensors	177
6.42	The front panel of the display program	178
6.43	The flow chart of the display program	178
6.44	Comprilan: computed and measured pressures	180
6.45	SurePress: computed and measured pressures	180
6.46	Bland-Altman plot for computed pressures and corrected measured pres- sures for Comprilan	181
6.47	Bland-Altman plot for computed pressures and corrected measured pres- sures for SurePress	181
6.48	Plastic mannequin leg with FlexiForce sensors mounted in the form of 8×5 matrix	182
6.49	The front panel of the display program for FlexiForce mannequin leg pressure- mapping system	183
6.50	The flow chart of the display program for FlexiForce mannequin leg pressure- mapping system	184
6.51	Comprilan and SurePress pressure maps	185
6.52	Comprilan: computed and measured pressures	187
6.53	SurePress: computed and measured pressures	187

6.54	Bland-Altman plot for computed pressures and measured pressures for Comprilan	188
6.55	Bland-Altman plot for computed pressures and measured pressures for SurePress	188
6.56	Comprilan measured over computed pressure ratio maps	190
6.57	SurePress measured over computed pressure ratio maps	191
6.58	NextEngine's 3D scanner and the soft leg model. The white stickers with red marks were used for scanning purposes	193
6.59	The 3D ankle-to-knee solid model of the soft leg showing the planes where the cross sectional digital profiles were obtained	193
6.60	The leg model with PicoPress sensors mounted	194
6.61	The arrangement of the PicoPress sensors on the leg model	195
6.62	Comprilan: computed, measured and corrected measured pressures	197
6.63	SurePress: computed, measured and corrected measured pressures	197
6.64	Bland-Altman plot for computed pressures and corrected measured pressures for Comprilan	199
6.65	Bland-Altman plot for computed pressures and corrected measured pressures for SurePress	199
6.66	Soft leg model with FlexiForce sensors mounted in the form of 8×6 matrix	200
6.67	The front panel of the display program for FlexiForce soft leg pressure-mapping system	201
6.68	The flow chart of the display program for FlexiForce soft leg pressure-mapping system	202
6.69	Silicon rubber adhesive padding disc attached to the sensitive area of the FlexiForce sensor.	203
6.70	Comprilan and SurePress pressure maps	205
6.71	SurePress: computed and measured pressures	206
6.72	SurePress: computed and measured pressures	207
6.73	Bland-Altman plot for computed pressures and measured pressures for Comprilan	207

6.74	Bland-Altman plot for computed pressures and measured pressures for Sure- Press	208
6.75	SurePress pressure maps reporting the effect of padding on the pressure measurement	209
6.76	Comprilan measured over computed pressure ratio maps	210
6.77	SurePress measured over computed pressure ratio maps	211
7.1	The pressure measurement system developed which can be used to map pressures under MCBs applied to human legs	215
7.2	The conditioning circuit used to power up 8 sensors and process their output signals	216
7.3	The front panel of the display program for the pressure-mapping system . .	217
7.4	The flow chart of the display program for the pressure-mapping system . .	218
7.5	NextEngine's 3D scanner and the left leg of the participant in the study. The red marks on the participant skin were used for scanning purposes . . .	219
7.6	The 3D ankle-to-knee solid model of the left leg of the participant showing the planes where the cross sectional digital profiles were obtained	219
7.7	FlexiForce sensors attached to the participant's leg	220
7.8	SurePress pressure maps	222
7.9	SurePress: computed and averaged measured pressures for both deadweights and aneroid sphygmomanometer calibration methods	224
7.10	Bland-Altman plot for computed pressures and averaged measured pres- sures using deadweights calibration for SurePress	224
7.11	Bland-Altman plot for computed pressures and averaged measured pres- sures using aneroid sphygmomanometer calibration for SurePress	225
7.12	FlexiForce sensors and PicoPress transducer attached to the participant leg	226
7.13	SurePress: computed pressures, PicoPress measured and corrected mea- sured pressures and FlexiForce averaged measured pressures for both cali- bration methods	228
7.14	Bland-Altman plot for computed pressures and PicoPress measured pressures	228

7.15	Bland-Altman plot for computed pressures and PicoPress corrected measured pressures	229
7.16	Bland-Altman plot for computed pressures and FlexiForce sensors averaged measured pressures using deadweights calibration	229
7.17	Bland-Altman plot for computed pressures and FlexiForce sensors averaged measured pressures using aneroid sphygmomanometer calibration	230
7.18	Bland-Altman plot for PicoPress measured pressures and FlexiForce load calibration measured pressures	231
7.19	Bland-Altman plot for PicoPress measured pressures and FlexiForce aneroid sphygmomanometer calibration measured pressures	231
7.20	Bland-Altman plot for PicoPress corrected measured pressures and FlexiForce load calibration measured pressures	232
7.21	Bland-Altman plot for PicoPress corrected measured pressures and FlexiForce aneroid sphygmomanometer calibration measured pressures	232
8.1	SurePress bandage with attached FlexiForce sensors	235
8.2	The front panel of the display program for the first prototype pressure-mapping bandage.	237
8.3	The flow chart of the display program for the first prototype pressure-mapping bandage.	238
8.4	The front panel of the display program for the program used in the experiment.	239
8.5	Pressure-mapping bandage applied to the pressure-mapping mannequin leg	240
8.6	The average output for the pressure-mapping bandage and the pressure-mapping mannequin leg	241
8.7	Bland-Altman plot for the measured pressures reported by the pressure mannequin leg and the averaged pressures reported by the pressure-mapping bandage	241
8.8	Bland-Altman plot for the anatomical level averaged pressures reported by the pressure mannequin leg and the averaged pressures reported by the pressure-mapping bandage	242
8.9	Tubular bandage with attached FlexiForce sensors	243

8.10	The front panel of the display program for the second prototype pressure-mapping bandage.	244
8.11	The flow chart of the display program for the second prototype pressure-mapping bandage.	245
8.12	The front panel of the display program for the program used in the testing experiment.	246
8.13	SurePress bandage applied to the second prototype pressure-mapping bandage and pressure-mapping mannequin leg	246
8.14	The average output for the second pressure-mapping bandage prototype and the pressure-mapping mannequin leg	247
8.15	Bland-Altman plot for the measured pressures reported by the pressure mannequin leg and the averaged pressures reported by the second pressure-mapping bandage prototype	248
8.16	Bland-Altman plot for the anatomical level averaged pressures reported by the pressure mannequin leg and the averaged pressures reported by the second pressure-mapping bandage prototype	248
9.1	The training pressure-mapping system.	251
9.2	The front panel of the display program for the training system.	252
9.3	The flow chart of the display program for the training system.	253
9.4	A nurse applying SurePress bandage to the training system.	254
9.5	Percentage of nurses applying higher, within and lower than the target pressure at ankle, gaiter, mid-calf and below knee.	258
9.6	Percentage of nurses applying mid-calf/ankle and below-knee/ankle pressure ratio higher than or equal to one and lower than 1.	258

List of Tables

2.1	The UK classification of bandages for the Drug Tariff	21
2.2	New recommended bandage classification according to the levels of pressure at B1 point	24
3.1	Summary of the experimental results in validating the model developed to study the effect of bandage thickness on the interface pressure	68
3.2	Summary of the experimental results in validating the models developed to calculate the pressure applied by multi-layer MCBs	73
3.3	Summary of the average pressure measured at each configuration	88
3.4	Summary of the average perturbation calculated from measured pressures at each configuration	89
3.5	Comparison between calculated pressure perturbation and the ones found experimentally. The ones found experimentally are reported as mean \pm overall error	90
4.1	Summary of the experimental results to measure the thickness and width of Comprilan bandage	97
4.2	Summary of the experimental results to measure the thickness and width of SurePress bandage	98
4.3	Summary of the peak tension and elongation where tension starts or ends for the 5 th cycle of all elongation ranges, the rate of drop in tension and the rate of increase in the elongation values where tension starts or ends for all elongation ranges for Comprilan and SurePress	103
5.1	Summary of PicoPress sensor's static characteristics	118

5.2	Summary of the experimental results for the impact of PicoPress probe's physical dimension on the interface pressure	121
5.3	Summary of FS01 sensor's static characteristics on flat surface	123
5.4	Summary of FS01 sensor's static characteristics on a curve surface	125
5.5	Summary of FlexiForce and Tactilus sensor's static characteristics using deadweights	128
5.6	Summary of FlexiForce, Tactilus, big FSR and small FSR sensor's drift error after applying $60mmHg$ on a flat surface	129
5.7	Summary of FlexiForce, Tactilus and big FSR sensors' static characteristics using aneroid sphygmomanometer	131
5.8	An example of the averaging technique for FlexiForce sensor. All values reported are for pressure in $mmHg$. The theoretical pressure is $19.51mmHg$	138
6.1	Summary of Comprilan and SurePress measured extensions, calculated tensions and pressures, measured pressures and corrected pressures	144
6.2	The percentage of cases where the difference between the computed and the measured and corrected measured pressures being within $\pm 5mmHg$ for Comprilan and SurePress	147
6.3	Summary of Comprilan and SurePress measured extensions, calculated tensions and pressures and measured pressures	151
6.4	Summary of Comprilan and SurePress measured extensions, calculated tensions and pressures and measured pressures	158
6.5	Summary of computed pressures, measured pressures using PicoPress sensors, FS01 sensors and FlexiForce sensors using fitting-lines obtained from two calibration methods and the PicoPress corrected pressures at two levels for four Comprilan bandages' applications	165
6.6	Summary of computed pressures, measured pressures using PicoPress sensors, FS01 sensors and FlexiForce sensors using fitting-lines obtained from two calibration methods and the PicoPress corrected pressures at two levels for four SurePress bandages' applications	166

6.7	Summary of Comprilan and SurePress measured extensions, calculated tensions and pressures, measured pressures and corrected pressures	173
6.8	Percentage of the cases where the difference between the computed and measured and corrected measured pressures being within $\pm 5mmHg$ for Comprilan and SurePress	176
6.9	Summary of Comprilan and SurePress measured extensions, calculated tensions and pressures and measured pressures	179
6.10	Summary of Comprilan and SurePress measured extensions, calculated tensions and pressures and measured pressures	186
6.11	Summary of Comprilan and SurePress measured extensions, calculated tensions and pressures, measured pressures and corrected pressures	196
6.12	The percentage of cases where the difference between the computed and the measured and corrected measured pressures being within $\pm 5mmHg$ for Comprilan and SurePress	198
6.13	Summary of Comprilan and SurePress measured extensions, calculated tensions and pressures and measured pressures	206
7.1	Summary of SurePress measured extensions, calculated tensions and pressures and averaged measured pressures for both calibration methods	223
7.2	Summary of SurePress measured extensions, calculated tensions and pressures, averaged measured pressures for both FlexiForce calibration methods and measured and corrected pressures for PicoPress sensor	227
7.3	The percentage of cases where the difference between the pressures being within $\pm 5mmHg$	230
9.1	Summary of average pressures applied by student nurses to the training pressure measurement system and the time they taken took to apply the padding bandage and SurePress bandage.	256
9.2	Summary of student nurses' response to the questionnaire.	257
9.3	Percentage of nurses applied the correct amount of pressures for at least one level, two levels, three levels and four levels.	257

List of Abbreviations & Symbols

List of Abbreviations:

ABPI	Ankle-Brachial Pressure Index
ARX	Autoregressive Model
ARMAX	Autoregressive Moving Average Model
CI	Confidence Interval
CVD	Chronic Venous Disorder
CVI	Chronic Venous Insufficiency
DAQ	Data Acquisition
DC	Direct Current
DSI	Dynamic Stiffness Index
FEA	Finite Element Analysis
FS	Full Span
FSR	Force Sensing Resistors
GSV	Great Saphenous Vein
IPC	Intermittent Pneumatic Compression
LCD	Liquid Crystal Display
LS	Long Stretch
MCB	Medical Compression Bandage
MCS	Medical Compression Stocking
MEMS	Microelectromechanical Systems
MRI	Medical Resonance Imaging
MST	Medical Stocking Tester
PCB	Printed Circuit Board
PPS	Pressure Profile Systems
QTC	Quantum Tunneling Composites
PVC	Polyvinyl Chloride
SD	Standard Deviation
SE	Standard Error
SS	Short Stretch

SSI	Static Stiffness Index
SSV	Small Saphenous Vein
USB	Universal Serial Bus

List of Symbols:

E	Youngs Modulus
Q	Blood Flow
P_B	Blood Pressure
R_P	Peripheral Resistance
HP_c	Capillary Hydrostatic Pressure
HP_{if}	Interstitial Fluid Pressure
OP_c	Capillary Osmotic Pressure
OP_{if}	Interstitial Fluid Osmotic Pressure
NFP	Net Filtration Pressure
P	Pressure
P_P	Pressure Perturbation
r	Limb or Cylinder Radius
R	Limb or Cylinder Radius
R_H	Limb or Cylinder Hoop Direction Radius
R_L	Limb or Cylinder Longitudinal Direction Radius
T	Tension
T_H	Limb or Cylinder Hoop Direction Tension
T_L	Limb or Cylinder Hoop Longitudinal Tension
T_E	Bandage Length Direction Tension
T_W	Bandage Width Direction Tension
σ_H	Hoop or Circumferential Stress
σ_L	Longitudinal Stress
σ_R	Radial Stress
t	Bandage Thickness
w	Bandage Width

w_W	Bandage Width
w_L	Bandage Length
n	Number of Bandage Layers
D	Cylinder or Limb Diameter
D_S	Sensor Diameter
d	Sensor Thickness
C_{PP}	Coefficient of Pressure Perturbation Due to Sensor Dimensions
C_{TP}	Coefficient of Pressure Perturbation Due to Bandage Local Stretch
L	Cylinder Length
θ	Angle Between the Length of the Bandage and the Limb
ν	Poisson's Ratio

Chapter 1

Introduction

Chronic leg ulcers affect 1% of the adult population in the developed countries, and the majority of leg ulcers are due to venous disease [1–5]. Venous ulcer’s impact on the quality of life is significant and it costs the NHS £300 – 600*m* annually [6]. Medical compression bandages (MCBs) are the cornerstone in the treatment of chronic venous ulcers. MCBs should be applied with a pressure gradient reducing from the ankle to the knee. Previous research has found that nurses sometimes apply compression bandages with a reverse pressure gradient [7]. Insufficient or non-sustained compression therapy will be less effective than sufficient and sustained compression due to an impaired hemodynamic effect. Excessive bandage pressure can lead to tissue damage, pressure sores and necrosis. Reverse gradient compression is likely to worsen the condition as it increases the pressure in the veins. Limb damage or treatment failure may result in limb amputation.

Despite the many studies published investigating the effectiveness of different compression bandages, very little work has been done to understand the underpinning physics of how compression bandages apply pressure to the leg. In addition, the current compression therapy techniques do not provide users with sufficient and accurate feedback concerning the interface pressures applied by them. This lack of control of therapeutic dose is unacceptable neither from the clinical perspective nor the scientific one [8]. Overcoming this problem will result in a considerable improvement with regards providing better care for the patients. One solution for the lack of feedback is the use of pressure measurement devices which can also be used for research, quality control and training purposes. Researchers all around the globe have developed various pressure measurement devices. Nevertheless, the performance and measurement reliability of most of these devices have not been systematically tested. Moreover, most of such devices fail to meet the specifications recommended by the experts in the field for the ideal pressure measurement device [9].

An advanced solution for the lack of control of pressures applied by MCBs may lie in integrating pressure transducers with MCBs to form pressure-mapping bandages. However, in order to achieve this ambitious goal, a solid understanding of the underpinning physics that govern the pressures applied by MCBs is needed. Flexible pressure sensors

have been available for around a couple of decades, and they might seem an attractive sensing solution that can be integrated or printed on MCBs. Nevertheless, current flexible pressure sensors suffer from various systematic errors [10]. These errors need to be addressed before using such sensors as sensing mediums in pressure-mapping bandages. Furthermore, even if pressure-mapping bandages are developed, they need to be validated with accurate pressure measurement systems. Unfortunately, with the absence of accurate pressure measurement systems, it is necessary to attempt to design a reference pressure measurement system before attempting to design a pressure-mapping bandage.

1.1 Aims and Objectives

1.1.1 Aims of the PhD

1. To design a pressure measurement system or systems that can measure and map accurately the interface pressure (a reference system).
2. To design and develop a prototype pressure-mapping bandage.

1.1.2 Objectives of the PhD

1. To theoretically investigate the factors that influence the sub-bandage interface pressures and model them mathematically. The models, then, need to be verified experimentally.
2. To explore flexible pressure sensors which can be utilized to design pressure-mapping bandages and evaluate their static performance in terms of accuracy, repeatability, hysteresis and drift.
3. To design pressure-mapping leg systems with distributed embedded or mounted pressure sensors in order to study MCBs and validate pressure-mapping bandages.
4. To design a pressure measurement system using custom arrays of flexible sensors in order to map the pressure applied by MCBs to a real leg.
5. To design a user interface that can acquire the signals from distributed sensors, convert the acquired signals to the equivalent pressure values, display the calculated pressure values using a graphical map, and store the measured values for post-processing.
6. To design a prototype pressure-mapping bandage by attaching flexible sensors to MCBs and test their performance with the pressure-mapping leg systems.
7. To test the feasibility and acceptability of using pressure-mapping systems for training purposes.

1.2 Organization of the Thesis

The thesis is divided into ten chapters. Chapter 2 reviews the literature on chronic venous ulcers: their epidemiology, aetiology and management, compression therapy: their pathophysiological effect, different types and the underpinning physics, current pressure measurement systems: their ideal specification, technology and performance, and flexible pressure sensors: their technology and static and dynamic performances.

Chapter 3 revises the current understanding of how MCBs deliver pressure. This includes work carried out to understand the effect of thickness, number of layers, biaxial forces, angle of application, change in limb size and sensor's physical dimensions on the interface pressure.

Chapter 4 details the experiments conducted to obtain tension-elongation curves for commercial MCBs for both longitudinal and transverse directions of the MCB, and it explains how the information can be used to compute the interface pressures and classify compression bandages.

Chapter 5 presents the experimental assessment of various resistive based flexible sensors such as FSR, FlexiForce and Tactilus pressure sensors. In addition, the chapter addresses the problem of calibration for flexible sensors, in particular on curved surfaces. It also explains the method used to reduce the uncertainty associated with FlexiForce sensors. Moreover, the chapter reports on the evaluation of PicoPress transducer and microelectromechanical systems (MEMS) FS01 force sensor.

Chapter 6 provides in depth information about the few reference pressure measurement systems developed in the course of the project. It compares among pressure maps obtained using arrays of FlexiForce sensors, arrays of PicoPress balloons and arrays of embedded FS01 force sensors when MCBs were applied to rigid cylinders. In all cases, the measured pressures were also compared to the pressure computed from extension. In addition, it describes the usage of arrays of the three mentioned sensing transducers over a mannequin leg to form pressure-mapping leg systems. MCBs were also applied to these three systems, and the measured pressures were again compared to the computed pressures in all experiments. Furthermore, the chapter makes a comparison between the pressure maps obtained using arrays of FlexiForce sensors and PicoPress sensors when MCBs were applied to a leg model with soft skin.

Chapter 7 describes the design and development of a pressure-mapping measurement system using FlexiForce sensors, which can be used to map the pressure applied by MCBs to a real leg. The developed system was tested on a human subject and the pressure maps obtained were compared to the ones obtained by arrays of PicoPress probes. Besides, the maps obtained using the pressure measurement system and PicoPress probes were compared with the pressure maps computed from the extension in the MCBs.

Chapter 8 reports on the design and development of two pressure-mapping bandages prototypes and the experimental work conducted to test these prototypes using the pressure-mapping mannequin leg with embedded FS01 force sensors. The chapter details the eval-

uations' outcomes and discusses them thoroughly.

Chapter 9 gives an account of a study carried out to assess the acceptability and usability of a pressure-mapping mannequin leg for training purposes. The study also assesses student nurses' bandaging techniques, pinpoints the common pitfalls and compares these mistakes with the skilled nurses' common mistakes.

Chapter 10 summarizes the work reported in this thesis, highlights the main findings and outlines future work.

Chapter 2

Literature Review

This chapter sets out the background to the research topic and presents the current literature concerning chronic venous ulcers, compression therapy, interface pressure measurement systems used to measure pressure under medical compression bandages and flexible pressure sensors. The chapter uses the outcome of the literature review to justify the aims and objectives of the study. In addition, the outcomes are used to justify the methodology proposed to address the aims of the study. The chapter ends with describing the aspects of novelty of the current work and their main contribution to the body of knowledge.

2.1 Chronic Venous Disorder

2.1.1 Definition

The term chronic venous disorder (CVD) includes the full spectrum of morphological and functional abnormalities of the venous system like telangiectasia, blue veins, varicose veins, ankle flare, oedema, pigmentation, eczema, lipodermatosclerosis, atrophie blanche and venous ulcers [11; 12]. Figure 2.1 represents some of these abnormalities. CVD might be associated with other symptoms like aching, pain, skin irritations, heaviness, muscle cramps, leg-tiredness, itching, sensation of burning and swelling [11; 12]. The term chronic venous insufficiency (CVI) implies a functional abnormality of the venous system with more advanced disease including those with edema, skin changes or venous ulcers [11; 12]. Thus, varicose veins in the absence of skin changes are not indicative of CVI and it is referred to as uncomplicated varicose veins [13; 14]. Venous ulcer is a chronic open wound in the epidermis, which is venous in aetiology and have a long healing tendency (more than four weeks) [2].

2.1.2 Epidemiology

CVI and chronic leg ulcers affect approximately 5% and 1% of the adult population in the developed countries respectively [1–5]. The high prevalence of venous disease is associated with the increased health care costs and substantial economic effects in terms of work lost



Figure 2.1: CVD abnormalities [11]

days and diminishing quality of life [13; 14]. CVI's impact on the lifestyle and quality of life is similar to that of other chronic diseases like cancer, diabetes and chronic pulmonary disease, reaching levels similar to the impact of heart failure on quality of life, at its worst i.e. healed and active venous ulcers [15]. In the UK, the Healthcare Commission has estimated that chronic venous ulcers cost the NHS £300 – 600m per year as cited by O'Meara et al. [6]. Overall, CVD has been estimated to consume 1 – 2% of the total health care budget of the European countries [4].

Venous ulceration is a chronic disease requiring long-term care and can result in a lifelong need for medical intervention. The overall recurrence rate of venous ulcers ranges from 60% to 70% [16; 17]. A recent study has showed that 56% of ulcers reoccur within one year after healing [17]. The majority of venous ulcers appear on the gaiter area of the lower limb [16].

There are some certain risk factors for CVD such as heredity, age, female gender, pregnancy, obesity, standing occupation, previous history of major leg trauma and conditions affecting the cardiovascular system including hypertension, diabetes and cholesterol [11; 14; 18; 19]. Family history, male gender, aging, obesity, standing occupation and previous history of trauma and conditions affecting the cardiovascular system are established risk factors for CVI [1; 5; 19]. Ulcer recurrence is positively associated with restricted ankle movement, number of previous episodes of leg ulcers [20], ulcer duration, cardiac disease, obesity, malnutrition and depression [17].

2.1.3 The Venous System in the Lower Limb

In order to understand the aetiology and pathophysiology of CVI and venous ulcers, it is important to give a brief background about the venous system in the lower limb. It should be mentioned at this point that the report uses the common terms of anatomical orientation and direction which are summarized in Figure 2.2.

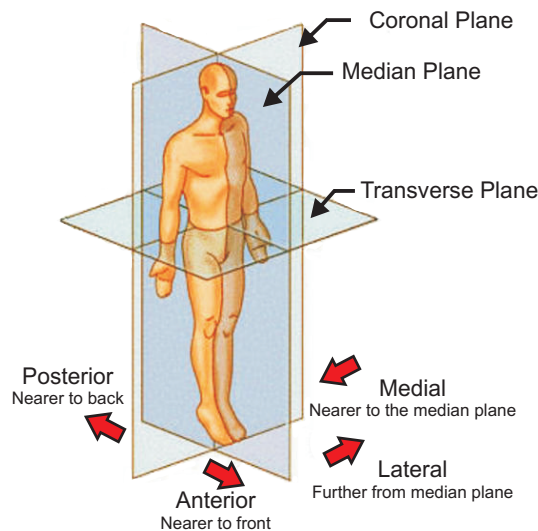


Figure 2.2: Body planes

Veins and Venous Valves

Veins carry the deoxygenated blood back to the heart from the extremities [21]. Due to of the lower blood pressure in the venous system compared to the arterial system, the walls of the veins are thinner than the companion arteries and they have larger diameters. Thin walls enable veins to have a large capacity for expansion. This and the large diameter explain why veins store about 60% to 75% of the blood [21; 22].

Most veins have valves to prevent reflux of blood distally [23]. The valves are cusps and attached by their convex edges to the venous wall. Their concave margins are directed with the flow and lie against the wall as long as the flow is towards the heart. When blood flow reverses, the valves close [23].

The venous network in the lower limb is divided into three systems that work together to return blood to the heart. These systems are: the superficial veins, the deep veins and the perforator veins [24].

Superficial Veins

Superficial veins are subcutaneous and lie in the superficial fascia [23]. The two major veins in this system are the great saphenous vein (GSV) and the small saphenous vein (SSV) (Figure 2.3). GSV is formed by the union of the dorsal vein of the great toe and

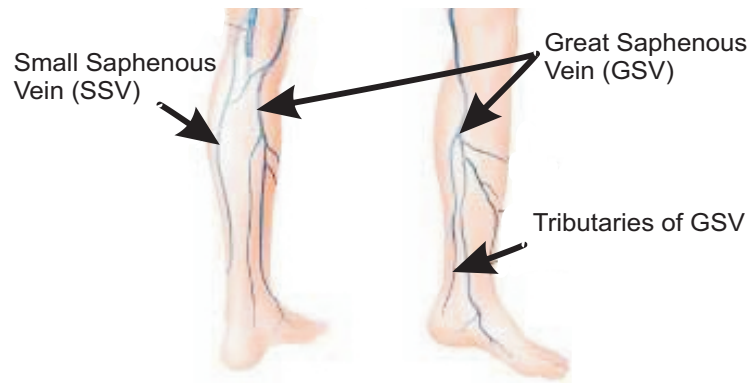


Figure 2.3: Great and small saphenous veins

the dorsal venous arch of the foot, and it empties in the femoral vein [21]. GSV receives numerous tributaries and communicates at several locations with SSV [21; 23]. SSV arises on the lateral side of the foot from the union of the dorsal vein of the little toe with the dorsal venous arch, and it empties into the popliteal vein in the popliteal fossa [23]. The communicating branches between the GSV and the SSV are oriented to direct the blood from the SSV to the GSV [24].

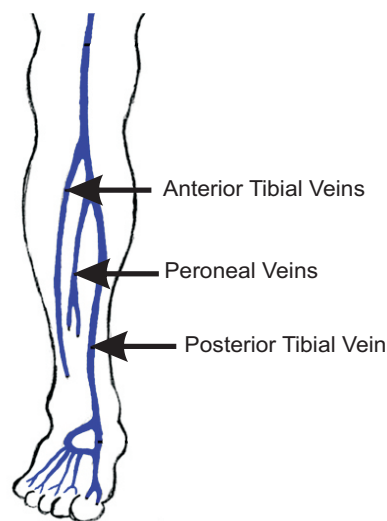


Figure 2.4: Deep veins of the lower limb

Deep Veins

These are found deep within muscle compartments, lie near the associated arteries and carry most of the blood out of the leg (Figure 2.4). There are three major deep veins below the knee: the anterior tibial vein, posterior tibial vein and peroneal vein. Above the knee, there are two major branches: the popliteal vein, which is formed by the tibial and peroneal veins, and the femoral vein which is the continuation of the popliteal vein

[23]. Venous sinuses are closely related to deep veins as they are embedded in the belly of the calf muscles and are able to dilate and hold a large amount of blood [24]. These veins play a significant role in the calf muscle pump function [25].

Perforator Veins

Perforator veins originate from the superficial veins and join with the deep veins or venous sinuses of the calf muscle [11]. They contain valves that allow only flow from the superficial veins to the deep veins (Figure 2.5). They pass through the deep fascia at an oblique angle so that they compress when the muscles contract [21].

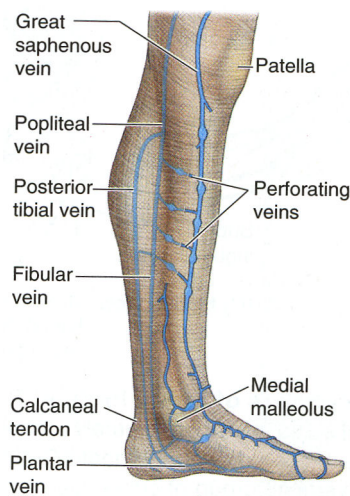


Figure 2.5: Perforator veins: direct flow from the superficial veins to the deep veins [21]

Hemodynamics

Hemodynamics is a term used to describe the flow of blood within the body organs and tissues [26]. As the name suggests, it deals with the dynamic state of blood; thus, it is important to define some relevant physiological terms and use them to describe the blood flow within the organs and tissues.

Blood flow is the volume of blood flowing through a vessel, an organ, or the entire circulation in a given time. In normal conditions, the blood flow through the body is equal to the cardiac output. However, the flow through the individual body organs varies widely [22].

Blood pressure is the force per unit area exerted on a vessel wall by the contained blood. It is expressed in millimeters of mercury (*mmHg*) [22].

Blood flow resistance is the opposition to flow and is a measure of the amount of friction blood encounters as it passes through the vessels [22]. Blood viscosity, blood vessel length and diameter are factors influencing blood flow resistance. Increasing the former two factors results in increasing the flow resistance, whereas increasing the vessel diameter results in reducing the flow resistance. The flow resistance is inversely proportional to fourth power of the vessel radius [22]. Both viscosity and vessel length are almost constant in a particular body. The factor that changes the most is the vessel diameter [22].

The relation between the flow (Q), the difference in blood pressure (ΔP_B) and the peripheral resistance (R_P) is summarized in Equation 2.1 [22]

$$Q = \frac{\Delta P_B}{R_P} \quad (2.1)$$

The equation illustrates the importance of the difference in the blood pressure to the flow. It can be concluded from the formula that the single factor which really matters in maintaining continuous flow and returning the blood back to the heart is to have a pressure gradient throughout the circuit [22]. Figure 2.6 shows the pressure in various vessels.

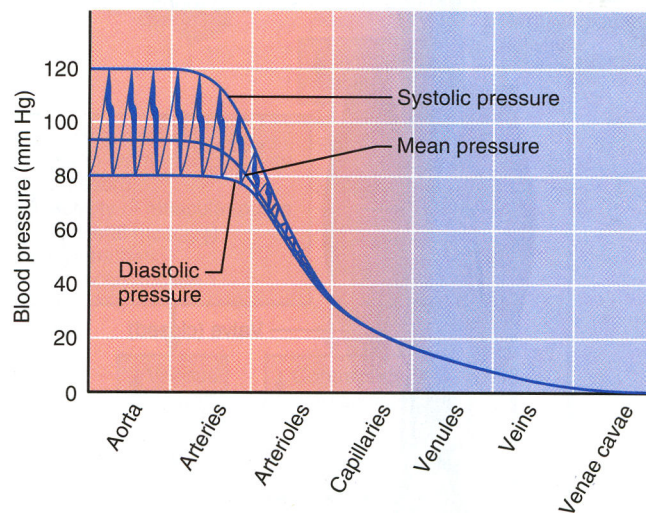


Figure 2.6: Blood pressure in various blood vessels of the systemic circulation [22]

Venous Blood Pressure and Venous Return

The primary function of the venous circulation is to return blood to the heart. Figure 2.6 shows that pressure within the venous system is low and not enough to promote adequate venous return, especially when a person is standing, for it needs to overcome the hydrostatic component of the pressure in the veins of the leg and pump blood against gravity. The hydrostatic component of pressure is related to the weight of the column of blood from

the right atrium to the foot [14]. This hydrostatic component of pressure works against the blood pressure, resulting in pooling of the blood within the lower limb veins when a person is standing. However, there are four different mechanisms which work together and assisted by venous valves to help venous return:

Respiratory pump: as people inhale, abdominal pressure increases, squeezing the veins in the ventral body cavity and forcing blood towards the heart. At the same time, pressure in the chest decreases, allowing thoracic veins to expand and speeding blood entry into the right atrium [22].

Accompanying veins: as a result of arteries expansion due to heart contraction, veins that accompany deep arteries get stretched and flattened, which aid in driving venous blood towards the heart [21].

Musculovenous pump: skeletal muscles function with the venous valves to move blood toward the heart. The outward expansion of the contracting muscles, limited by the deep fascia, compresses the veins, “milking” blood superiorly towards the heart (Figure 2.7) [21]. In the lower limb, there are three musculovenous pumps: the foot, the calf and the thigh. The most important of these is the calf as it has the largest blood capacitance and generates the highest pressures, which is found to be approximately 200mmHg during muscular contraction [25].

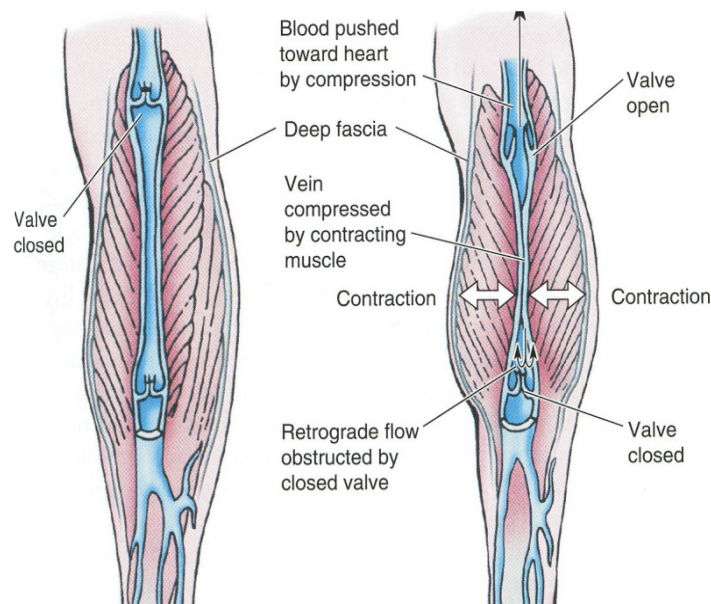


Figure 2.7: Musculovenous pump [21]

Foot pump due to weight bearing: weight bearing is thought to empty blood from the foot when the foot gets flat during a gait cycle [27].

During normal locomotion, the three venous pumps; the foot pump, the distal and proximal calf pumps work together to pump blood back to the heart. Before weight bear-

ing, the ankle is dorsiflexed, emptying the distal calf pump. Weight bearing empties the foot using foot pump. Immediately after the weight bearing, the ankle is plantarflexed and the proximal calf pump empties blood into the popliteal vein and femoral vein (Figure 2.8) [27].

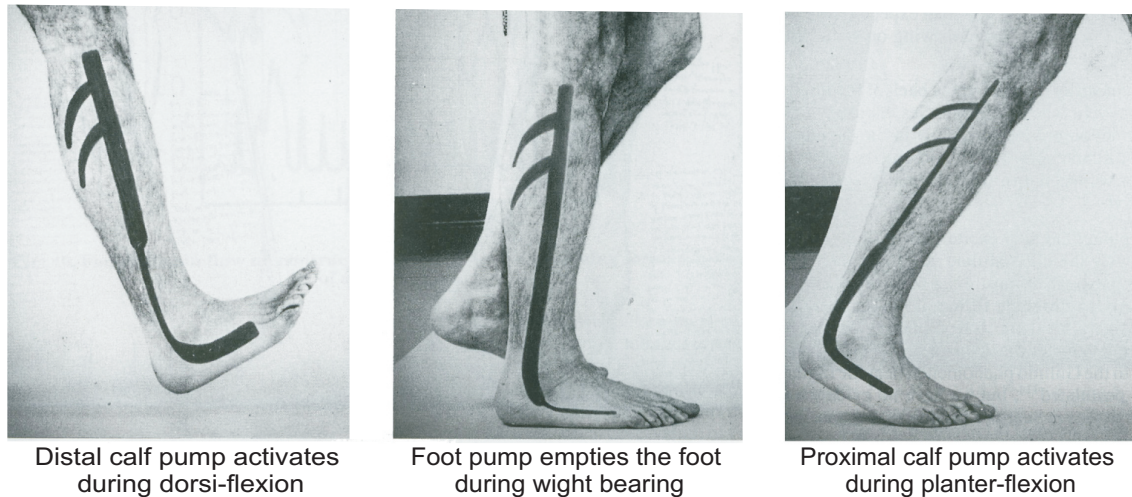


Figure 2.8: Sequences of venous pump action during ambulation [27]

Capillary Dynamics

Nutrient and gas exchanges occur across the capillary wall. Fluid is forced out of the capillaries at the arterial end of the capillaries bed and returns to the bloodstream at the venous end or via the lymphatic system. The direction and amount of fluid that flows across the capillary walls reflect the balance between the hydrostatic and osmotic pressures (Figure 2.9) [22].

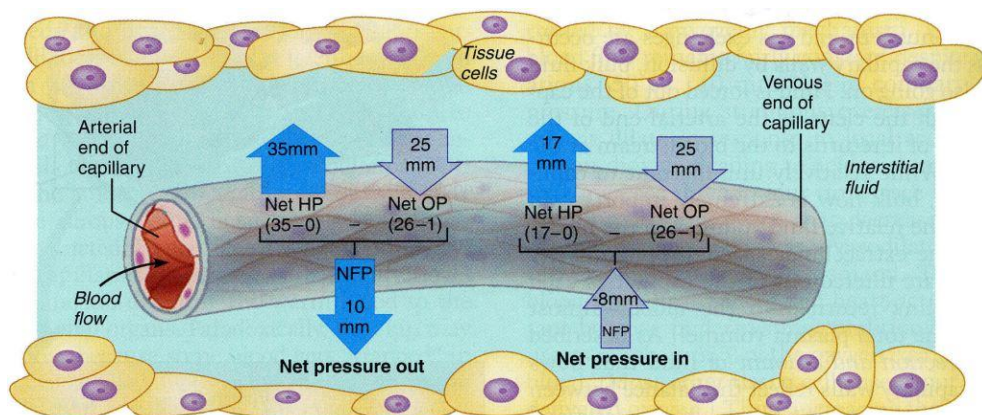


Figure 2.9: Fluid flow at capillaries [22]

Hydrostatic pressure is the force exerted by a fluid pressing against a wall. In capillaries, the hydrostatic pressure is as same as the capillary blood pressure, and it is called the

capillary hydrostatic pressure (HP_c). This pressure tends to force liquid through the walls in a process called filtration. At the arterial end, the HP_c is about $35mmHg$, whereas at the venous end it is about $17mmHg$. This pressure is opposed by the interstitial fluid hydrostatic pressure (HP_{if}) acting outside and pushing fluid back to the capillary. This has been assumed to be very small and negligible; thus, the net pressure is equivalent to the HP_c [22].

Colloid osmotic pressure is created by the difference in water concentration between the two sides of the capillary membrane. Capillary colloid osmotic pressure (OP_c) or the oncotic pressure, is approximately $26mmHg$, whereas interstitial fluid colloid osmotic pressure (OP_{if}) is about 0.1 to $5mmHg$. Osmotic pressure does not vary a lot between the two ends of the capillary [22].

The net filtration pressure (NFP) is the net gain or net loss of fluid from blood, and it depends on the interaction between the hydrostatic and osmotic pressures. This is summarized in the so called Starling's equation which is a summary of the Starling hypothesis (Equation 2.2)

$$NFP = k(HP_c - HP_{if}) - (OP_c - OP_{if}) \quad (2.2)$$

Where k is a filtration constant [28].

2.1.4 Pathophysiology

CVI is caused by primary abnormalities in the venous valves that may cause over-stretching of the vein valves, and distraction of the valves [11; 25]. Recent research suggests that valvular incompetence in the superficial veins is a secondary phenomenon resulted from dilatation of the vein wall with enlargement of the vein ring [25]. The other cause of CVI is the secondary changes resulting from deep venous thrombosis, which causes obstruction of the veins and valvular dysfunction [11; 25]. Competent valves prevent blood refluxing, and backward retrograde flow of blood. Incompetent valves allow reflux and retrograde flow of blood back into the veins (Figure 2.10). If this condition persists over time, it will result in vein dilation, ambulatory venous hypertension and increase of filtration within capillary beds; hence, tissue oedema [7; 11].

Dilated Veins

The superficial veins are considered to be low pressure systems, while the deep veins are considered to be high pressure systems. Perforating vein valvular dysfunction leads to the transmission of high pressure from the deep veins to the superficial system. This causes dilation of the superficial veins and their tributaries [29].

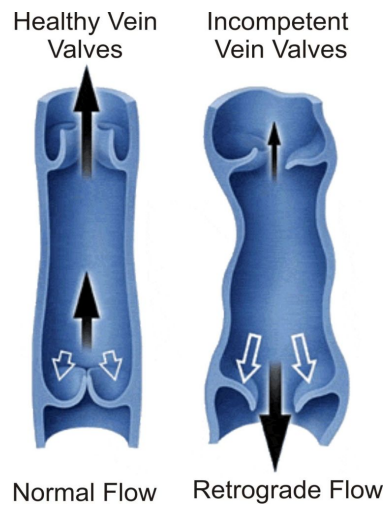


Figure 2.10: Healthy and incompetent vein valves

Ambulatory Venous Hypertension

CVI is always associated with ambulatory venous hypertension, a condition in which the venous pressure is higher than normal when the person exercises [11]. Pressure in the veins of the leg is determined by a hydrostatic component related to the weight of the column of blood from the right atrium to the foot and the hydrodynamic component related to pressure generated by contraction of the skeletal muscle of the leg and the pressure in the capillary network [14]. Both components are profoundly influenced by the action of venous valves [14].

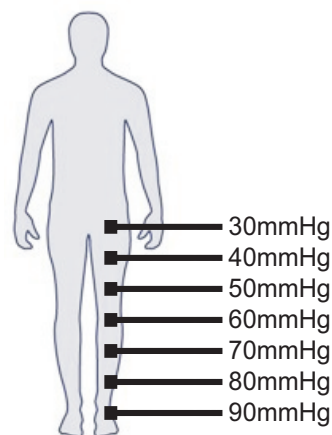


Figure 2.11: The weight of blood column [30]

In people with competent venous valves, venous pressure in the foot during standing may reach 80–90 $mmHg$ which represents the hydrostatic component of the pressure minus the capillary flow pressure (Figure 2.11). However, during ambulation, the venous pressure is reduced to less than 30 $mmHg$ as a consequence of skeletal muscle contraction [14; 25].

In people with incompetent valves, the decrease in venous pressure with leg movement is attenuated (Figure 2.12) [14]. In addition, in a healthy subject with a normal venous system, the hydrostatic pressure is restored in 30 – 40s, once the subject resumes static standing. Nevertheless, venous refill time gets shorter in people with CVI [25]. Sustained venous hypertension results in pathological effects on the skin subcutaneous tissues like edema, pigmentation and ulceration [25].

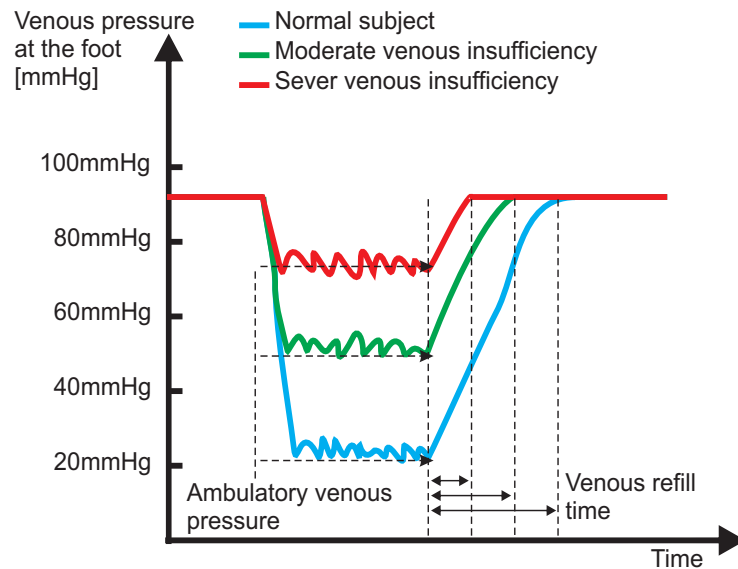


Figure 2.12: The effects of walking on reducing pressure in normal individuals, and those with degrees of CVD [30]

Starling Hypothesis and Edema Formation

As described in Section 2.1.3, the net filtration pressure in capillaries (NFP) is the net gain or net loss of fluid from blood. NFP depends on the interaction between the hydrostatic and osmotic pressure in the capillaries and the interstitial space. The Starling hypothesis is summarized in Equation 2.2.

At the arterial end of the capillaries, the normal hydrostatic pressure ($HP_c - HP_{if}$) is $35mmHg$ and the osmotic pressure ($OP_c - OP_{if}$) is $25mmHg$. This means that the NFP is positive. The normal hydrostatic pressure at the venous side of the capillaries is $17mmHg$; thus, the NFP is negative; hence, re-absorbing occurs (Figure 2.9) [22]. However, due to ambulatory venous hypertension, the pressure at the venous end of the capillaries is much higher than the normal values. This results in positive NFP; thus, more filtration of the fluid occurs from the intra-vascular space towards the interstitial space. This, in turn, results in edema and swelling of the leg [7].

Ulcer Formation

There are many theories put forward to explain venous ulcer formation:

The fibrin cuff theory suggests that fibrin cuffs form in the interstitial space due to fibrinogen from blood leaking out via permeable capillaries and act as a barrier to oxygen diffusion, which leads to ischemia and necrosis of the surrounding area [2; 25].

White cell rheology suggests that white blood cells can become trapped in the endothelial wall of the capillaries secondary to venous hypertension. The trapped white cells become activated and release free radicals, proteolytic enzymes and cytokines. These factors provoke tissue damage and ulceration [2; 25].

Macromolecules which leak to the dermis as a consequences of venous hypertension and endothelial injury. These macromolecules trap growth factors and matrix proteins, which result in failing the tissue repair process [2].

Microvascular ischemia is caused by the reduction in the number of skin capillaries. Microvascular ischemia leads to ulcer formation [2].

It is worth mentioning that only 70% of leg ulcers are purely venous in etiology, 20% of them are associated with arterial or arterial and venous disease. The rest are attributed to other causes [2; 31].

2.1.5 Venous Ulcer Management

In the case of uncomplicated varicose veins, compression, sclerotherapy and surgery are widely used to increase the quality of life for patients. A recent study suggests that regardless of intervention, all three treatments captioned above are associated with significant improvements in the quality of life at a cost which is well below the £30,000 upper limit suggested for therapies in the NHS in the UK [13].

The core principles for the management of venous ulceration are to obtain clean wound base and external compression [32]. Approximately 80% of venous patients are managed conservatively with compression therapy and wound dressing. The remainder may have venoactive drugs and adjuvant therapies and are treated surgically with vein stripping or endovenous ablation [2; 11; 33]. Skin grafts have also used for venous ulcer management [2; 32]. The other method in treating venous ulcers is to reconstruct the valves, which involves a surgery to repair the valves using various methods including internal and external valvuloplasty and external banding [11].

Other new methods for treating CVI have been introduced in the last few years such as radio-frequency and LASER ablation of GSV. These new methods require expensive instrumentation. However, no proper treatment-cost effectiveness comparisons between these methods and the traditional methods have been carried out to evaluate whether the additional costs are worth the degree of improvement achieved [25].

In order to prevent the recurrence of venous ulcers, patients are advised to wear the highest level of medical compression hosiery that is comfortable for them [17; 20]. They are also advised to undertake activities such as leg exercises and leg elevation in addition to maintaining healthy diet and weight [17].

2.2 Compression Therapy

Compression therapy in the form of bandaging is an ancient treatment that has been used since 3500BC to treat venous leg ulcers [34]. The term compression could be defined as squeezing part of the body by mechanical influence [30]. The logic behind using compression therapy in the treatment of venous ulcers is to provide an external pressure that works against the hydrostatic pressure and aids venous return [35]. There are several types of compression products which are used to apply compression to the lower limb including MCBs, medical compression stockings (MCSs), band devices and intermittent pneumatic compression devices (IPCs) [11; 29; 35]. All these compression devices are used to treat venous leg ulcers and prevent their recurrence [11; 17; 20; 36]. In a recent systematic review of the literature about compression therapy and venous ulcers, O'Meara et al. [35] concluded that compression increases the healing rates for venous ulcers compared with no compression and that high compression is more effective than moderate compression. In another systematic review of the clinical evidence about the usage of compression to prevent the recurrence of venous ulcers, Nelson et al. [36] concluded that recurrence of ulcers may be less with the usage of high compression compared to low compression; however, there is no evidence that high compression is more effective than moderate pressure for prevention (but there is limited research available).

2.2.1 Pathophysiological Effects of Compression Therapy

Compression therapy is a very effective treatment whose mechanisms are not yet fully understood [37]. The current understanding of the pathophysiological effects of compression has been addressed in several works [7; 11; 28; 37; 38] and can be summarized in the following points:

- Narrows or occludes superficial and deep veins. This results in improving venous pumping, reducing venous reflux, increasing the flow towards the heart and redistributing blood towards central parts of the body [28; 37; 39]. These effects improve ambulatory venous hypertension and venous return which comprise the main objectives of the treatment.

Lord and Hamilton [40] and Partsch and Partsch [41] used Doppler ultrasound to measure the reduction in vein cross-sectional diameter [40] and area [41] when external compression is applied to the leg. Partsch and Partsch [41] showed that 10 – 15mmHg is sufficient to decrease the vein diameter and increase the flow in supine position. Lord and Hamilton [40] showed using duplex ultrasound that MCS which are designed to apply 20 – 30mmHg are able to reduce the diameter of GSV and the deep veins in supine position. Nevertheless, the same MCS exerted non-statistically significant compression effect on the superficial and the deep veins at the upright position [40]. Partsch and Partsch [41] showed that a median 20mmHg and 50 – 70mmHg interface pressure are sufficient to occlude the leg veins at mid

calf region in the supine and upright positions respectively.

In his work to rationalize the need for medical compression bandages, Partsch [39] cited a previous work reported by Mostbeck et al. [42], who showed that an external pressure of 40mmHg is able to reduce the local blood volume by 30% and, at the same time, increase the blood volume in the central compartment of the body. The physical principle behind these results is that compression results in reduced venous diameter, which means that the cross sectional area of the vein will be reduced; hence, the blood volume [41].

Downie et al. [43] have shown using magnetic resonance imaging (MRI) that uncompressed deep veins are sometimes elliptical and not circular in cross section, while the compressed deep veins are always elliptical. Also, they have displayed that superficial uncompressed veins are circular in cross section and the GSV is often elliptical when bound close to the muscular fascia by the saphenous fascia [43]. Moreover, they have found that GSV moves longitudinally as a consequence of the forces exerted by compression. This will result in a problem in alignment which can be detected by MRI and not ultrasound [43]. Furthermore, they have found that a stocking which is designed to provide $18 - 21\text{mmHg}$ at ankle can result in a mean reduction of 64% in the diameter of the deep veins and 39% in the diameter of the superficial veins [43] at supine position. However, Downie et al. [43] were not able to study the MCS effect on the superficial and the deep veins at the upright position as MRI can only be obtained for the supine position [43].

- Increases the vein wall shear stress, decreases the reduction in local flow velocities (i.e. increases the blood flow through the microcirculation) and decreases the flow pulsatility index, which is defined as the maximum flow velocity minus the minimum flow velocity over the mean flow velocity [44]. These effects were more prevalent in the deep veins [44]. Downie et al. [44] obtained these findings by using MRI, pulsed Doppler ultrasound, and computational fluid dynamics. Accelerating blood flow in the microcirculation favours white cell detachment from the endothelium and prevents further adhesion [28]. This is important as the trapping of white cells in the capillaries is thought to be behind the changes in the skin and the formation of ulcers [7; 14; 29; 32].
- Increases local tissue pressure [37]. According to Starling's equation, (Equation 2.2) this will result in the increase in re-absorption. This, in turn, helps improve lymph drainage and reduces oedema [28; 37]. Damstra et al. [45] have shown that high compression can result in 6.7% reduction in leg volume in patients with lymph oedema.
- Reduces the elevated levels of vascular endothelial growth factor and tumor necrosis factor alpha in patients with venous ulcers [46]. This helps in pain relief and ulcer healing [28]

2.2.2 Interface Pressure and Optimum Pressure Profile

Interface pressure is used to refer to the pressure exerted by a compression device like the MCB on a specific skin area [37]. In the medical literature related to venous ulcers, clinicians use millimeters of mercury (*mmHg*) as a descriptive unit for the interface pressure instead of SI units (N/m^2), where $1mmHg = 133.33N/m^2$ [37].

Some medical experts believe that in order to have an effective compression therapy, the compression device should be able to provide intermittent occlusion of the incompetent veins during ambulation. This intermittent occlusion will result in an artificial valve that leads to a segmentation of venous reflux [41]. This means that compression devices should be applied with high pressures to be able to occlude the superficial and the deep veins [41]. From a biomedical engineering point of view, the applied external pressure should be greater than the intravenous pressure in order to achieve full occlusion, as some of the external pressures will be dissipated in the skin, fat and veins surrounding tissues. Besides, the external pressure will need to overcome the mechanical strengths of the vein wall [41]. In patients with impaired calf muscles and incompetent veins, the intravenous pressure is governed by the hydrostatic component of the pressure due to the blood column. Therefore, an external pressure of $90mmHg$ and $70mmHg$ is needed in order to achieve full vein occlusion at the ankle and calf regions respectively when a person is standing [41] (Figure 2.11). As noted in Section 2.2.1, Partsch and Partsch [41] showed that the median pressure to occlude SSV at calf region is about $70mmHg$, which is in agreement with this theoretical understanding [41].

Few researchers have attempted to use finite element analysis (FEA) in order to study the tissue deformation in the leg when compression is applied [47–49]. These attempts should provide researchers with a computational tool to simulate the results of different pressure profiles on the venous flow, which will ultimately help in arriving at an agreement for the recommended pressure profile. Dai et al. [47] reported an FEA model for the leg which included only the femoral vein. The model used $12kN/m^2$ as a module of elasticity for the calf muscle, obtained experimentally by applying loads to the calf region of the leg while the subject is sitting on a chair [47]. However, the model has not been verified experimentally and has been criticized by Narracott et al. [49] and Downie et al. [43] for the many assumptions used to generate the FEA model. Moreover, the method they have reported to obtain the modulus of elasticity seems to include the skin, fat, fascia and the muscle and not only the muscles tissue as they have used it in their model [47].

Narracott et al. [49] have reported another FEA model which included six deep vessels. They applied pressure profiles obtained experimentally [48] to the 2D computational mode. The deformation in the computational model was compared with the MRI of a volunteer's leg scanned with and without a compression device that apply the same pressure profile. [48]. The researchers have shown good agreement between their FEA model and the MRI [49] and they found that the elasticity modulus for the muscles tissue should be about twice the value reported by Dai et al. [47]. It is worth pointing out that the MRI scans

were taken with the leg in a horizontal position, and the elasticity modulus for the calf muscle was measured with the leg relaxed and in an upright position, which raise questions about the robustness of their work. In conclusion, the available up-to date FEA models cannot be used to compute the required pressure profile to produce intermittent occlusion for venous network in a lower leg.

In the medical literature, the optimum pressure profile that is most commonly described is a pressure of $40 - 45\text{mmHg}$ at the ankle, reducing gradually to $15 - 20\text{mmHg}$ at the knee [7; 50; 51]. These values do not appear to have been determined through a systematic study [7]. Burnand and Layer [52] cited that Stemmer [53] calculated that an external pressure of $35 - 40\text{mmHg}$ at the ankle is required to prevent capillary transudation in legs with severe CVD. The calculation was based on Starling's equation and known range of venous pressures measured at the ankle in normal, varicose and post-thrombosis legs [52]. A recent clinical trial suggests that the 40mmHg target pressure at the ankle is only beneficial for patients with small ulcers and small calf circumference [54]. Milic et al. [54] have suggested that the required ankle pressure should be calculated using a simple equation (calf circumference + (calf circumference/2)) [54].

Burnand and Layer [52] have reported that Sigg [55], who developed the first graduated compression stockings, greeted Van Der Molen with the idea of graduation of the level of elastic compression [52]. The main argument for the need of graduated pressures comes from a physical understanding of fluid flow. In order to move blood from the ankle to the knee, there is a need to apply a pressure gradient with high pressure at the ankle and low pressure at the knee [11]. However, there is very little clinical evidence for graduated pressure profile. In fact, no clinical data is published to compare the time takes for ulcers to heal while controlling both ankle and calf or below knee pressure to assess the level of gradient needed, if any, for the treatment of CVI [7; 56].

2.2.3 Risks of Compression

There are few risks associated with compression therapy:

- Compression therapy results in shifting blood into the central compartment of the body, and it is estimated to preload the heart by 5%; thus, it should be avoided with patients with borderline cardiac function [37].
- Compression therapy might result in a reduction in the arterial flow. Therefore, it is generally accepted that compression should not be used as a treatment for people with arterial occlusive disease, i.e. with ankle-brachial pressure index (ABPI) < 0.5 [37; 57]. ABPI is derived from the ratio of arm systolic pressure, taken as the best non-invasive estimate of central systolic pressure, and the highest ankle systolic pressure [57]. When the ABPI is > 1 , then arterial disease is usually eliminated [57].
- High levels of compression might result in damaging the skin tissues and forming of pressure ulcers [7; 30; 58]. Kosiak [59] studied the pressure and time conditions

necessary to damage the skin of animals, and he found that high pressures for a short period of time or low pressures for a long period of time will result in damaging the skin. Currently, there is no clinical evidence to indicate the safe levels of compression that might be applied to a limb [28]. However, a number of surgeons reported damages from compression which led to sever skin necrosis and amputation [58].

- Reverse gradient pressure, i.e. higher external pressures at calf compared to the applied pressure at the ankle, might result in reduction in the venous return. This is not supported by reliable clinical evidence [7] as it is based on theoretical understanding of human physiology and physics.

2.2.4 Medical Compression Bandages (MCBs)

Classification of MCBs

There is an absence of consistent international classification for bandages [11; 60]. The UK classification of bandages for the Drug Tariff is summarized in Table 2.1. From Table 2.1, it can be seen that only type-3 bandages are classified as compression bandages. However, in many parts of the world, inelastic short stretch bandages, type-2, are used to provide high levels of compression which are equivalent to type-3d bandages [37; 39; 61]. The following few paragraphs will attempt to summarize the different classification methods used in the medical literature.

Table 2.1: The UK classification of bandages for the Drug Tariff [30; 60; 61]

Type 1	Refer to retention, light weight and elastic bandages. These apply little or no pressure and are generally used to hold dressings in place.	
Type 2	Refer to support, short and inelastic bandages. These apply low pressure. However, some are capable of applying moderate levels of pressure.	
Type 3	Type 3a	They are capable of providing 12-17mmHg and are used to apply compression to patients with mixed venous-arterial disease or for those unable to tolerate high compression.
	Type 3b	They are capable of providing 18-24mmHg.
	Type 3c	They are capable of providing 25-35mmHg and are used in treatment of venous ulcers.
	Type 3d	They are extra high compression bandages and are capable to provide up to 60mmHg at the ankle.

Extensibility is the ability of the bandage to stretch when a force is applied to it [30].

Bandages can be split into three main categories according to their extensibility:

- No stretch bandages provides no extension when subjected to a force [37].
- Short stretch (SS) bandages. They are generally made of cotton without elastomers. They provide 40 – 90% extension when subjected to a force [30].
- Long stretch (LS) bandages. These lock out at over 140% extension as they contain elastomers [30].

Nevertheless, the definitions of SS and LS bandages differ among professionals [60; 61]. In addition, the terms no stretch, short stretch and long stretch are meaningless without a reference to the amount of tension associated with these levels of extensions [60].

Elasticity is the ability of a bandage to return to its original unstretched length when tension is removed from the bandage [30]. Bandages can be divided into two main categories according to their elasticity:

- Inelastic bandages: They are generally made of cotton without elastomers [30].
- Elastic bandages: They contain elastomers such as rubber or lycra [30].

This classification does not help in providing information about how bandages work, rather it provides information about whether a bandage will return to its original position or not. Many researchers in the field tend to use the terms “elastic bandages” to describe LS bandages and “inelastic bandages” to describe SS bandages and no stretch bandages [60; 61].

Stiffness is the increase of compression pressure per centimeter increase in the circumference of the leg [28; 62]. Researchers have used this concept of stiffness to classify bandages. They have proposed two different methods to evaluate stiffness:

- Static Stiffness Index (SSI) proposed by Partsch [8]. The SSI is defined as the difference in the interface pressure measured under bandages in standing and supine position [8; 61; 63]. Partsch [8] and others like Mosti and Mattaliano [63] suggested an SSI of 10mmHg as a differentiation line between inelastic and elastic bandages, with inelastic bandages being defined to have SSI more than 10mmHg .
- Dynamic Stiffness Index (DSI) proposed by Wegen-Franken et al. [64] and Stolk et al. [65] and it is defined as the increase in the pressure where the variation of the leg circumference equals to 1cm at a frequency of 1Hz [64]. However, their work was more concentrated on MCSs rather than MCBs. [64].

The importance of stiffness lies in the fact that bandages with different stiffnesses will behave differently in dynamic situations when the limb shape changes secondary to

calf muscle activity. Stiffness and the hysteresis in the tension-elongation relationship in compression bandages are thought to have a major impact on the interface pressure produced by compression bandages [61; 63; 64]. For example, bandages with high stiffness or inelastic bandages will have low resting pressure, the one continuously exerted by the bandage towards the tissues [30] and high working pressure, the one exerted by the muscles against the resistance of the bandage [30; 61]. On the other hand, low stiffness or elastic bandages will have high resting and working pressures (Figure 2.13). This has led some researchers to suggest that elastic bandages are uncomfortable for the users [37]. Partsch [37] believes that bandages with a high stiffness will provide the intermittent vein closure or artificial external valve that is thought to be more beneficial to the healing of venous ulcers [39].

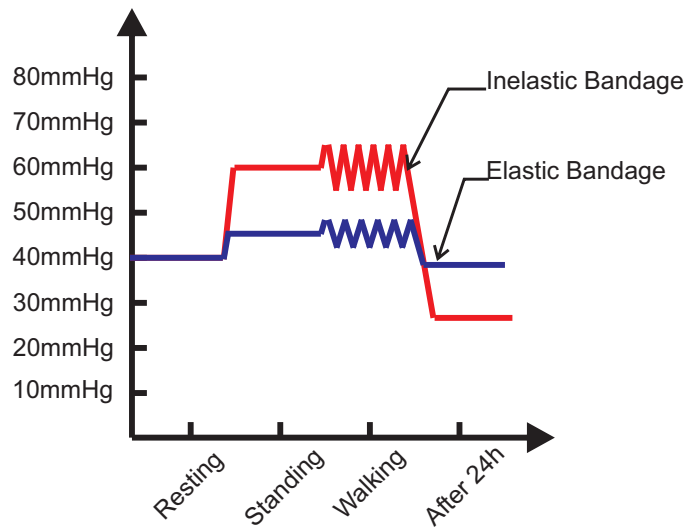


Figure 2.13: Resting vs. working pressures [28]

Interface Pressure . The pressure measured at the medial aspect of the lower leg, where the tendon changes into the muscular part of the gastrocnemius muscle when the bandage wearer is at supine position is used to classify MCBs [61]. The UK classification, for example, (Table 2.1) uses the pressure levels applied by compression bandages to divide them into four different categories. Partsch et al. [61] recommended another classification, which is summarized in Table 2.2. Classifying bandages according to the level of pressure might provide an easy interpreted classification for clinicians. However, from the engineering point of view, the pressure induced is a variable, which is dependent on many other factors. Using a dependent variable for classification might result in a rather weak classification system of MCBs. Moreover, limiting the definition of the interface pressure to one particular point is not based on clinical studies. In fact, the interface pressure in general can be defined as the pressure applied by the materials in contact. In this case, it is a bandage and the skin.

Table 2.2: New recommended bandage classification according to the levels of pressure at B1 point [61]

Bandage Classification	Pressure [mmHg]
Mild	<20mmHg
Medium	20-<40mmHg
Strong	40-<60mmHg
Very Strong	≥60mmHg

Number of components. Bandages can be classified according to whether they are applied alone or within a system that consists of a few different types of bandages:

- Single component compression bandage consists of one type of compression bandage that is commonly applied over a padding layer [61].
- Multi-layer single component compression bandage consists of a number of bandages applied usually on top of each other [61].
- Multi-component short stretch compression bandaging system consists of three to four different types of bandages and at least one of the components is a short stretch bandage [30; 35].
- Multi-component elastic compression bandaging system consists of three to four different types of bandages, and none of the components is classified as a short stretch bandage [30; 35].

Factors Influencing Sub-Bandage Pressure

Skill of the operator: In clinics, much of the variability in pressure is associated with the skill of the operator [66]. In many occasions, practitioners are unable to apply bandages to the optimum values of pressure, i.e. $40 - 45\text{mmHg}$ at ankle and a pressure gradient from ankle to knee. Keller et al. [67] have shown that only 9.5% of 63 nurses (0 to above 10 years of experience) were able to apply compression bandages with the target pressure of $35 - 45\text{mmHg}$ at the medial B1 point in a supine position. However, this figure has increased to 31.7% after providing nurses with an extended training with a pressure monitor (Kikuhime®), MediTrade, Denmark) for 10 – 14 weeks. Keller et al. [67] have reported that before the training intervention, 56.7% of nurses with above 10 years of work experience were applying bandages with insufficient levels of pressure (less than 20mmHg). After intervention, this reduced to only 3.3%.

Taylor et al. [68] have shown that only 31% of experienced nurses were able to apply $35 - 45\text{mmHg}$ of pressure at 4cm above the lateral malleolus, which increased to 50% immediately after a feedback session using a pressure monitor and reduced to 43% on a recall session after two weeks from the feedback session. They have also

demonstrated that only 31% of nurses were able to achieve good bandage proficiency, which they defined as having $30 - 50\text{mmHg}$ at 4cm above lateral malleolus and knee to ankle pressure ratio of less or equal to 0.70. This improved to 56% immediately after the feedback session and further improved to 57% at the recall session, which took place two weeks after the feedback session [68]. Furthermore, while the knee-ankle pressure ratio improved, the study have reported calf-ankle ratio of higher than 1 in 75% of cases before and after the feedback session. This figure was reduced to 50% at the follow up session [68]. Nevertheless, only 16 nurses were involved in their study.

Nelson [7] has reported that from 48 nurses only 22.9% were able to apply three different types of compression bandages with a pressure range of $18 - 50\text{mmHg}$ and a calf-ankle ratio less than 1. This was improved by training. She has reported that training nurses resulted in a significant improvement in the number of nurses who achieved calf-ankle ratio less than 1, when they used four component bandaging system. Before this intervention, only 29% of nurses were able to achieve acceptable pressure gradient. This increased to 60% after the intervention. However, she has not found any significant improvement in the pressure applied at the ankle with a mean pressure of 31.5mmHg before the training and 30.1mmHg after the training. Both values are lower than the target pressure of $40 - 45\text{mmHg}$ [7].

Hafner et al. [69] have reported that training of 156 participants in wound healing courses resulted in an improvement in the interface pressure from a mean of 33.8mmHg with 1.5 standard deviation (SD) ($15.8 - 79\text{mmHg}$) to a mean interface pressure of 35.6mmHg ($21 - 52\text{mmHg}$) in the fourth session. They have also shown that while experienced nurses improved their bandaging techniques after training and maintained their ability to achieve the target pressures of $35 - 45\text{mmHg}$ after two weeks of the training sessions, student nurses improved their bandaging skills after the training session but were not able to maintain these skills [69]. In addition, they have reported that some participants who attend the training courses were applying bandaging with dangerous levels of pressures (much higher than 60mmHg).

Tension in the fabric: According to Laplace's law, the sub-bandage compression pressure is proportional to the tension in the bandage [7; 66; 70; 71].

$$P \propto (T/R)$$

The tension in the bandage is proportional to the elongation of the bandage fabric. This is clearly illustrated in Figure 2.14 for two types of bandages. Figure 2.14 demonstrates that the tension-elongation relation cannot be described by a linear equation. In addition, there is significant hysteresis that governs the tension-elongation relation. In clinical situations, nurses are asked to apply MCBs by controlling the amount of elongation. In fact, the ability to control and apply MCBs

with the required elongation was used as a measure of nurses' consistency in applying MCBs in one trial [50]. This is usually maintained by marking the bandage at a constant interval and measuring the amount of elongation after application in order to check whether the bandage is applied with the manufacturer recommended elongation or not [50]. Currently, some bandages have geometrical shapes printed on them which change from rectangular to square or from oval to circle at the right elongation. This approach resulted in a significant reduction in the inter-operator variability and produced more consistent levels of compression in one study [71].

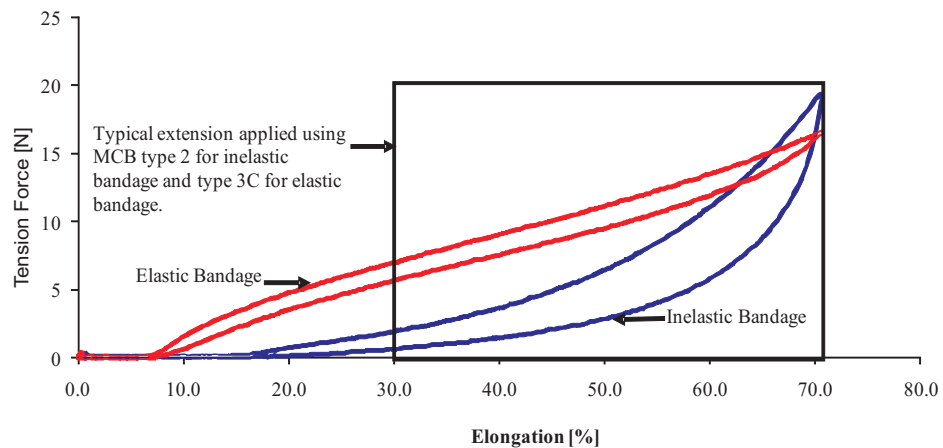


Figure 2.14: Typical tension-elongation curves for commercial inelastic and elastic bandages. This line graph is generated based on experimental data obtained in the course of this project. However, similar curves were reported in other published work [7; 30; 71].

Bandage Stiffness: As it has been mentioned earlier (2.2.4) stiffness is a major factor that influences the interface pressure when the limb shape changes secondary to calf muscle action or reduction in edema [61]. Lee et al. [56] have shown that there is not much difference in the pressure produced by inelastic, elastic non-cohesive and elastic-cohesive bandages when they are applied by the same operator to the same leg using the same technique at supine position. However, the physical properties of the bandages resulted in significant differences in pressure produced by these bandages when the participant changed her posture from supine to sitting and then to standing up. Lee et al. [56] have shown that inelastic bandages produce a higher pressure difference compared to non-cohesive elastic bandages when changing from supine to standing. This was more visible with spiral and Putter bandaging techniques compared to figure-of-eight bandaging technique. Besides, Lee et al. [56] have shown that the increase in pressure between supine and standing is higher at ankle and that it decreases towards the upper calf. These findings were echoed in many other studies [8; 61; 63; 72]

Creep in Bandage: Researchers have shown that the initial interface pressure that MCBs

apply will reduce with time. This reduction in the interface pressure was found to be up to 40% of the initial value for some inelastic bandages [61]. Many researchers believe that the reduction in edema and high stiffness nature of inelastic bandages make inelastic bandages unable to maintain the interface pressure [61]. However, a recent study by Damstra et al. [45] has found a poor correlation between the drop in the interface pressure and reduction in leg volume.

Ghosh et al. [73] have shown a reduction by $1mmHg$ in the interface pressure over $1000min$ when they applied a compression bandage to a mannequin leg. This reduction is the resultant effect of bandage creep and friction between bandage layers which work against the creep [73].

Shear Stiffness: Fabric stiffening under a constant shear extension is the main cause of friction forces between the fabric fibers [74]. Liu et al. [74] have found that the higher the shear stiffness for a stocking fabric, the higher the pressure it can apply to a leg.

Bending rigidity of the fabric: Fabric stiffness under bending deformation was found to influence the interface pressure that a compression garment can apply to a limb. Liu et al. [74] have found that as the bending rigidity of the fabric increases, its ability to apply high pressures increases. This may also be related to their findings which state that thick stocking garments with mean thickness of $1.32mm$ are able to apply higher amounts of pressure compared to thin stockings with mean thickness of $0.35mm$.

Leg dimensions and posture: According to Laplace's law, the sub-bandage compression pressure is inversely proportional to the radius of the leg if the tension is constant. As the leg circumference usually increases from the ankle to the calf, bandages should be able to apply a gradient pressure from the ankle to the calf if they were applied with constant tension [56]. Lee et al. [56] have shown that a skilled nurse who was asked to apply different bandages with constant tension was able to achieve pressure at ankle higher than the one at upper calf at the lateral side of the leg in all cases. However, in 29% of the cases, there was no progressive gradient over the four measuring points at the lateral side of the leg [56]. In addition, the assumption of constant tension was not verified by measuring the tension or even the extension of the bandage.

During exercise or change in posture, the leg dimensions like the circumference will change. The interaction between the change in limb size and the physical characteristics of the bandage will result in varying the interface pressure [56; 66]. This might provide a dynamic variation in pressure that could 'milk' the veins.

The leg itself is not uniformly circular. This means that the assumption of the constant tension will result in a pressure gradient is not an accurate assumption.

Furthemore, it implies that much higher interface pressure is expected over the bony structures of the leg such as the malleolus and the tibial crest [66].

Number of bandage layers and application technique: According to Moffatt [66], the more the number of bandage layers, the higher the pressure will be. In addition, application techniques such as figure-of-eight technique or the spiral technique will produce different levels of compression [66]. Lee et al. [56] have shown that while there was no much difference in pressure produced by spiral bandaging technique, figure-of-eight bandaging technique and Putter bandaging technique at supine position, there were significant differences at upright position.

Different application techniques result in bandages being applied at different angles of the leg [7]. Ghosh et al. [73] showed experimentally that as the angle between the bandage and the leg decreases, the interface pressure decreases as well.

Mathematical Model to Estimate the Sub-Bandage Interface Pressure

In order to design effective compression systems, improve practice and help nurses in achieving the optimum pressure gradient, many researchers have attempted to describe or predict the interface pressure theoretically [75; 76]. While De Bruyne and Dvořák [76] used trigonometry in order to relate the interface pressure to both the tension in the bandage component and limb radius'. Thomas [75] used the Law of Laplace, which is defined as the tension in the walls of a container being dependent on both the pressure of the container's content and its radius [77]. Macintyre et al. [78] have reported that the first work related between the Law of Laplace and the pressure applied by a garment is the work published by Cheng et al. [79]. The two methods; using Laplace's Law and the trigonometry, arrived at the same formula to describe the interface pressure (Equation 2.3).

$$P = \frac{T}{R} \quad (2.3)$$

Where, P is the interface pressure in Newton per metre square (N/m^2), T is the tension in bandage in (N) for ($1m$) width of fabric and R is the curvature radius in (m).

De Bruyne and Dvořák [76] extended their model to estimate the effect of both the tension in the hoop and longitudinal direction of the bandage i.e. across its length and width. By doing this, they arrived at the following expression:

$$P = \frac{T_H}{R_H} + \frac{T_L}{R_L} \quad (2.4)$$

Where, T_H is the tension in the bandage in the hoop or circumferential direction of the leg in (N) for $1m$ width of fabric, T_L is the tension in the bandage in the longitudinal direction of the leg in (N) for $1m$ width of fabric, R_H is the radius of the hoop curvature of the leg in (m) and R_L is the radius of the longitudinal curvature of the leg in (m).

Thomas [75] extended his model to estimate the interface pressure induced by multi-layer bandage application (Equation 2.5).

$$P = \frac{nT}{Rw} \quad (2.5)$$

Where, n is the number of bandage layers and w is the bandage width in (m).

He expressed his model with a version that contains more medical familiar terms (Equation 2.6). However, the use of simple multiplication of the numbers of layers with the pressure induced by one layer to express the overall interface pressure was questioned by Wertheim et al. [80].

$$Pressure(mmHg) = \frac{Tension(Kgf) \times Number\ of\ Layers}{Circumference(cm) \times Bandage\ Width(cm)} \times 4620 \quad (2.6)$$

Many researchers have used Equation 2.3 to estimate the interface pressure or describe the variation in the interface pressure [66; 70; 71; 73; 75; 77; 78; 80–84]. Some researchers like Macintyre et al. [78] and Melhuish et al. [84] expressed their doubts about using Laplace’s Law to estimate the pressure produced by pressure garments. Their main arguments are:

- The model is originally developed for solid cylindrical containers or elastic vessels like blood vessels filled with liquid and not for an elastic garment wrapped over a living limb.
- The model does not take into account the change in radius of the limb curvature.
- The model does not take into account the deformability of the living tissues.
- The model does not take into account the friction forces between bandage layers.

The first point can be counter-argued by the work reported by De Bruyne and Dvořák [76] who arrived at the same mathematical model using trigonometry and analyzing force body diagrams. The second point can be addressed by using local radius rather than using the overall radius of the leg cross section [81]. The third point can be dealt with by developing better FEA models for the leg [48]. The last point can be tackled by replacing the tension term in the mathematical model with a variable that represents the summation of the forces that influence the interface pressures.

Beside the mentioned doubts of the validity of using Laplace’s law to describe the interface pressure, Basford [77] have reported that Laplace’s law does not take into consideration the wall thickness. The error due to neglecting the wall thickness is as high as 5% when the ratio of vessel’s wall thickness to its radius is 1 : 10 [77; 85]. This might explain Macintyre et al. [78] findings, who have used an F-scan (Tekscan, Boston, USA) to compare the pressure measured under pressure garments, used for pressure delivery for hypertrophic scar treatment, and the predicted pressure by Equation 2.3 over number of uniform cylinders. They have found that the model they used predicted the pressure accurately for cylinders with large diameters and overestimated the pressure of cylinders

with low diameters. However, the results were poorly presented and no information was provided about the characteristics of the transducers they have used, except that the error inherent in the measurement system was $\pm 2.1\%$.

Melhuish et al. [84] have demonstrated in their work that as the tension in the applied bandage increases, the pressure increases. They have also shown that the pressure decreases as the radius of the solid cylinder increases. Nevertheless, they have reported that the amount of reduction in the applied pressure did not follow the predictions using Equation 2.3. In addition, they have illustrated that interface pressure would increase as the number of layers of bandage increases. However, they have not found a linear relationship between the applied pressure and the number of bandage layers as suggested by Thomas [75]. Moreover, they have shown that there is a significant effect of the softness of the medium, to which the bandage applied, on the interface pressure. Their last finding might be explained by the effect of the sensor's physical dimensions on the measured interface pressure [86]. The Fonatameter sensor used by Melhuish et al. [84] is *3mm* in thickness. This will result in bandage forming a curvature over the sensor when it is applied to a solid material. This, in turn, will cause perturbation in the level of the pressure measured. Nevertheless, as the softness of the material increases, the sensor will depress the material when pressure is applied to it, resulting in smaller local curvatures, i.e. less of the sensor presence is noticed. This will result in smaller a perturbation in the measured pressure (see Section 2.3.3 for more information) [86–88].

2.3 Measurement of the Interface Pressure

2.3.1 Interface Pressure Measurement Systems: Need and Use

The measurement of the interface pressure is one of the challenges addressed heavily in the field of medical engineering due to its wide-spread applications. For example, measuring the interface pressure is important to avoid the formation of pressure ulcers for patients who spend long times on bed and wheel chair [89]. Other applications for measuring the interface pressure are in the fields of orthopedics [90], sport science [90], diabetes [90], prosthetics [91; 92], human joint studies and replacements [93–95] and prevention of scars after burns [78; 79; 96–98]. Measuring the interface pressure applied by compression products, which are used in the treatment of chronic venous ulcers, is addressed in the work of many researchers. They have measured the interface pressure for various reasons:

- Study the impact of external compression pressures on the hemodynamics and different living tissues in the lower limb [48; 49; 72; 99; 100].
- Study the efficacy of compression products and their ability to heal venous ulcers and prevent their reoccurrence [45; 54; 99; 101–106].
- Evaluate nurses' ability to apply MCB with the correct pressure profile and, in some situations, provide nurses with a feedback about their bandaging techniques

[50; 67–69].

- Study the physics and working principles of compression therapy [80; 81; 84; 107–109].
- Study the influence of different bandage materials on the interface pressure [8; 56; 63; 81; 110–116].
- Study the effect of different postures on the interface pressure when a pressure garment is applied to the leg [56; 80; 111; 117; 118].
- Study the effect of ambulation on the interface pressure [111; 119; 120].

Measuring the interface pressure is important also for stockings and hosiery manufacturers, as it enables them to design better MCSs [64; 65; 116; 121].

2.3.2 Ideal Interface Pressure Measurement System

Researchers have built and used various types of pressure measurement transducers to measure the interface pressure under compression products. These transducers differ in their core technology, physical dimensions, accuracy and their ability to provide dynamic measurements. These wide differences have encouraged some leading researchers in the field of venous ulcers and compression therapy to define an ideal measurement system in an international consensus meeting in Vienna in 2005 [9]. The ideal measurement system is described to:

- be easy to calibrate before each measurement [9].
- have an external computer for continuous measurement with a high signal sampling rate during movement [9].
- be preferable to support several sensors for simultaneous measurements at different points [9].
- be low cost [9].
- be long lasting, reliable and accurate [9].
- have simple electronics [9].
- be insensitive to temperature and humidity changes [9].
- be linear response to applied pressure [9].
- have high resolution (time $< 0.1s$ and pressure $< 0.1mmHg$ ($< 13.1Pa$) [9].
- have low hysteresis [9].

- be thin ($< 0.5mm$), flexible and small in size (sensitive area) for mapping the circumferential pressure patterns [9].
- not cause irritation when in contact for a long period with the skin [9].
- be insensitive to bending and force concentration [9].
- have little drift to allow extended time pressure measurements [9].

The above definition for the ideal measurement system can be used as an evaluation tool for the interface pressure measurement transducers used and reported by researchers. In addition, the above definition can be used as the required specification for any device to be developed in future. However, the above definition used vague terms that need further clarification and agreement among researchers. For instance, accuracy, reliability, size in terms of its sensitive area, hysteresis and drift are not defined in exact numbers. In addition, the suggestion that the sensor thickness not to exceed $0.5mm$ is based on work done by Ferguson-Pell [87] on flat surfaces and not on curved surfaces.

2.3.3 Impact of Sensor Dimensions on the Measured Interface Pressure

As mentioned above, the recommendation to use sensors with thickness no more than $0.5mm$ is based on theoretical calculations for flat areas carried out by Ferguson-Pell [87]. Ferguson-Pell [87] derived a mathematical model to calculate the thickness of the sensor, if the pressure perturbation, MCB's thickness, MCB's Youngs modulus, and the sensor diameter are known (Equation 2.7). The model is based on the assumption that the MCB will form a constant radius curve over the transducer (Figure 2.15). The $0.5mm$ thickness figure was derived for a sensor with $14mm$ diameter, and the acceptable error tolerance was set to be $1mmHg$ ($133Pa$). However, Ferguson-Pell's findings [87] cannot be extended to transducers over curved surfaces.

$$d = \frac{D_S}{2\sqrt{\frac{D_S P_P}{2Et}}} \quad (2.7)$$

Where, d is the sensor thickness in (m), D_S is the sensor diameter in (m), P_P is the pressure perturbation in (N/m^2), E is the Youngs modulus for the MCB in (N/m^2) and t is the MCB thickness in (m).

Vinckx et al. [86] have worked analytically to analyze the perturbation in the measured pressure when a sensor is placed under a pressure garment applied to a curved surface like the lower limb. They proposed different models for cylindrical shapes sensors, rigid sensors and flexible thin plate sensors. They also studied the effect of depressing the soft tissue by the sensor, when compression garment is applied to it, on the sensor's reading. From all the reported models, the one which is in particular of interest to this project is the one they proposed for flexible thin plate sensors. The model they proposed (Equation 2.8) for thin plate flexible sensors was based on analyzing the geometry and the tension components

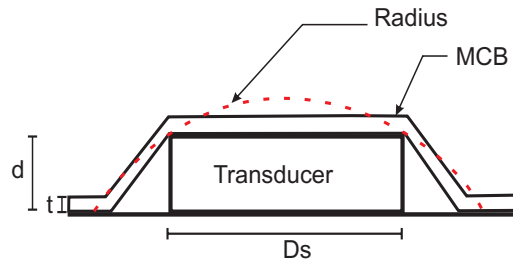


Figure 2.15: Schematic representation of the interface perturbation effect of a sensor placed beneath an extensible bandage [87]

(Figure 2.16). The main outcome of this model is that the pressure perturbation is not only dependent on the sensor aspect ratio (i.e. the sensors diameter and thickness) as in Ferguson-Pell's [87] model, but it is also dependent on the ratio of the sensor diameter to the limb radius. This means, for limb parts with small radii of curvature, the effect of perturbation will be larger [86]. However, no experimental results were reported to validate these findings.

$$\begin{aligned}
 C_{pp} &= 1 + 1.44f(\alpha)\sqrt{\frac{d}{D_S}} \\
 f(\alpha) &= \frac{\sqrt{\alpha}}{\tan(\alpha/2)} \\
 \alpha &= \frac{D_S}{R}
 \end{aligned} \tag{2.8}$$

Where, C_{PP} is the coefficient of pressure perturbation, R is the limb radius in (m).

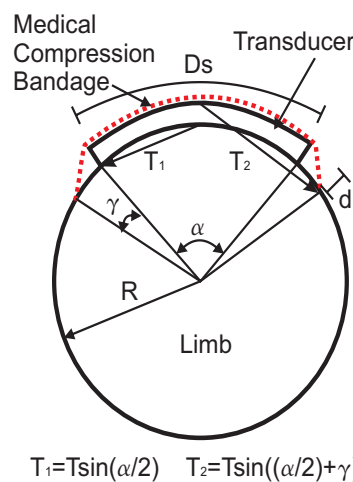


Figure 2.16: Schematic representation of the interface perturbation effect of a sensor placed beneath an extensible bandage over a curved surface [86]

2.3.4 Sites of Pressure Measurement Under a Compression Device

The definition for the ideal pressure measurement system reported in Section 2.3.2 suggests that the pressure measurement system should be able to support measuring the interface pressure at multiple points simultaneously. Nevertheless, the least number of sensors that the device should support was not specified. This might be due to the fact that there is no agreement about where the interface pressure should be measured under compression garments [9]. However, the International Consensus Meeting in Vienna in 2005 recommended several locations within the ankle-knee region for pressure measurements[9]:

- B: ankle at point of minimum girth. This area is made up primarily of tendon and bony structures; thus, pressure measurements at this area are expected to be significantly higher than the rest of the leg [9; 103]. However, this area has other complications; for instance, the radius tends to vary widely due to the bony prominence. This will probably result in local high pressure formation. In addition, the retro-malleolar fossae corresponds to concave radius and can only be compressed using pads [9].
- B1: area at which the Achilles tendon changes into the calf muscles (approximately 0.1 – 0.15m proximal to the medial malleolus) [9]. This point is found to be the location where the biggest change in leg circumference takes place due to muscle activity[65]. According to Partsch [8], the mean value of the difference in the circumference at the B1 level between lying down and standing for 20 healthy persons was $0.71 \pm 0.25cm$.
- C: calf at its maximum girth [9]. The ratio of the pressure measured at this level and the pressure at the ankle was used by some researchers to assess nurses ability to apply compression bandages correctly [7].
- D: just below the tibial tuberosity [9]. The ratio of the pressure at this level and the pressure at the ankle was used by some researchers to assess the bandaging skills of nurses [68].

Nevertheless, the above recommendations have not included whether the sensors should be placed medially, anteriorly, laterally or posteriorly. The only study found to recommend a side of the leg for measuring the interface pressure was the work reported by Coull et al. [50]. They have recommended measuring the interface pressure at the posterior side of the leg as they found it to be the most appropriate and accurate position. However, their recommendation was not justified by any kind of systematic approach [50].

2.3.5 Review of Interface Pressure Measurement Systems

As it has been mentioned earlier, researchers have built and used many pressure measurement systems, some of which are commercially available, to measure the interface pressure

under compression products used to treat CVD. This section will critically review some of these devices.

Pneumatic Based Interface Pressure Measurement Systems

Pneumatic pressure measurement systems are the most common type of pressure transducers used to measure the interface pressure under compression products. These pressure measurement systems use air as a medium to transfer the forces applied by compression products to an air pressure that can be converted into an electrical signal using electrical or piezoelectrical pressure transducers. In general, pneumatic devices have the advantages of being cheap and having thin and flexible probes [9]. However, they have some limitations, for example, the dynamic measurements are difficult. Moreover, they are sensitive to temperature and hysteresis [9]. A rundown on some of the pneumatic pressure measurement transducers reported in the compression and venous ulcers related literature are provided in the following few paragraphs.

- **PicoPress®** (Microlab Electronica, Ponte S. Nicolo PD, Italy) (Figure 2.17) is a portable pneumatic measuring system fitted with an ultra thin probe. The probe thickness is $0.2mm$ when it is not inflated and $3mm$ when it is inflated. The probe diameter is $50mm$. The device pressure measurement range is $0 - 200mmHg$ ($0 - 26.7kN/m^2$). Before the measurement, the probe is inflated with $2cc$ of air by means of electronically controlled syringe integrated in the system [122]. The transducer can be calibrated under the bandage and the pressure measured data can be stored on the device and/or transferred to a computer; enabling pressure measurements during dynamic tests [122].

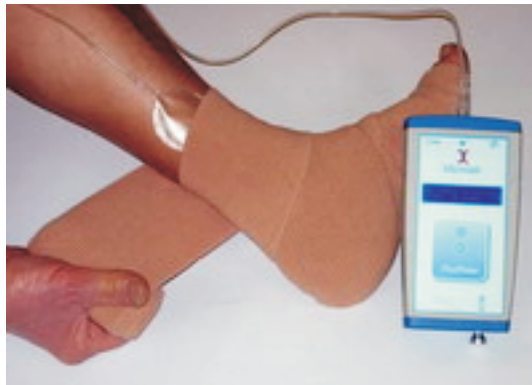


Figure 2.17: PicoPress® [124]

Mosti and Rossari [122] reported that the linearity and repeatability of the transducer are very good. Nevertheless, those performance evaluations were not reported using standard sensors evaluation method used in Engineering text books [123]. They have not tested the sensor performance for pressures lower than $20mmHg$ ($2.7kN/m^2$). Additionally, they have reported that PicoPress, outperformed Kikuhime® (TT

Medi Trade, Soro, Denmark) and the SIGaT® (Ganzoni-Sigvaris, St Gallen, Switzerland) [122]. The device was used by Partsch and Mosti [100] to study thigh compression.

- **Air-Pack Type Analyzer model 3037** (AMI Techno, Tokyo, Japan) (Figure 2.18) is a 2kg interface pressure measurement system, which is fitted with an ultra thin probe, 1mm thickness and 20mm diameter for its standard probe [125]. The 0 – 150mmHg (0 – 20kN/m²) is its lowest pressure sensitivity range. According to the manufacturer, the sensor accuracy at 23°C is ±1.5mmHg. The manufacturer recommends calibrating the sensor using a water column as the probe surface is extremely sensitive and when it is in contact with solid materials, the repeatability error of the sensor increases [125]. However, no information is available about the sensors static and dynamic performance. In addition, no information is available about transducers performance over curved surfaces. The transducer was used in a couple of recently published articles to evaluate the interface pressure and stiffness of various elastic stockings and bandages during posture change and exercises [111; 112]. The manufacturer used the transducer to measure the interface pressure produced by stockings for foot-abdomen length. The measurements were made at 25 different points with 12 sensors distributed over the ankle-knee region [125].

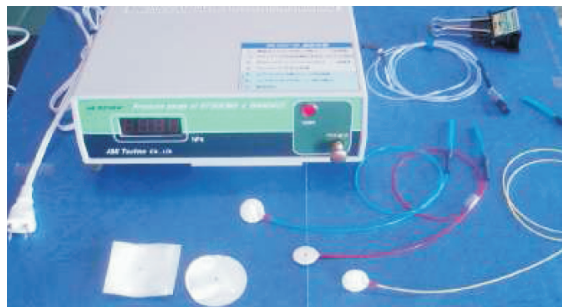


Figure 2.18: Air-Pack Type Analyzer [125]

- **Kikuhime®** (Figure 2.19) is a portable pressure transducer that is widely used in the last few years [8; 45; 54; 63; 67; 72; 106; 113–115; 126]. The sensor consists of an air-filled flexible probe which is connected to a pressure transducer. The probe is small, flexible and has a dimension of 30mm × 38mm × 3mm. Van den kerckhove et al. [98] reported that when the sensor was tested with a water column for the pressure range 0 – 30mmHg (0 – 4kN/m²), it showed an excellent linearity. However, they have not reported any nonlinearity error and the method of error reports was not done according to standard sensor static and dynamic characteristics tests [123].

Partsch [8] explored the accuracy and precision of the transducer by attaching the sensor to the legs of healthy subjects at the medial B1 point and then applying pressure using a cuff connected to a manometer with a mercury filled column. He reported that the sensor accuracy is good at high pressures. The sensor tended to

overestimate the pressure at low pressures 20 – 60 $mmHg$ and underestimate the pressure for pressure inputs larger than 80 $mmHg$. He also reported that the sensor coefficient of variation was a maximum of 7.1% at 20 $mmHg$ [8], which was called precision in his work. Moreover, the method did not test the variance in the sensor output for pressures lower than 20 $mmHg$. In addition, the so called precision in Partsch [8] work is close to what is known as sensors repeatability error but with small difference in the method of calculation.

Mosti and Rossari [122] also tested the accuracy and repeatability of the Kikuhime. They reported higher error levels at 20 $mmHg$ compared to the ones reported by Partsch [8]. Satpathy et al. [126] used method similar to the ones used by Van den kerckhove et al. [98] and Partsch [8] to calibrate the sensor and reported high linear correlation values between the input pressure and the measured pressure. However, no assessment for the error was reported in their work [106; 126].

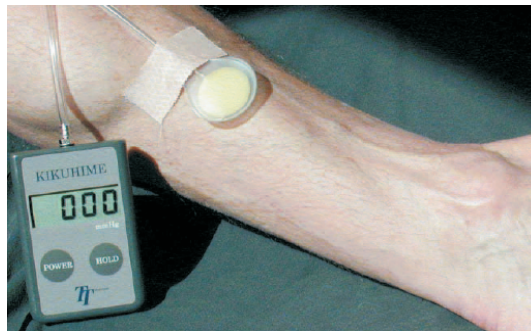


Figure 2.19: Kikuhime® [8]

- **Medical Stocking Tester (MST)** (Salzmann AG (SAG), ST. Gallen, Switzerland) (Figure 2.20) was widely used in measuring the interface pressure until recent times [49; 50; 56; 105; 121]. MST MK *IV* is the latest version of the MST devices and it consists of a measurement and a display unit that weighs 3 Kg and flat, air filled sleeves with large surface area, minimal volume and four to six paired electrical contact probes. The sleeves are inflated with air until the contacts are broken, which takes place when the pressure exerted by the air is greater than the pressure exerted externally by the compression garment [127; 128]. The system can be used to read the pressure at a maximum of 6 different points simultaneously [127]. The system can be used only to measure the interface pressure after applying MCB and cannot be used for continuous dynamic measurement [128].
- **The Oxford Pressure Monitor MK *II*** (Talley Medical Group Ltd, Hants, UK) measures the interface pressure by measuring the pressure of a small pulse of air that inflates 12 small plastic pockets (14 mm diameter and 1.5 mm thickness). The system can provide pressure measurement for 12 points with accuracy of $\pm 4mmHg$ [48; 128]. The system was reported to be used in a number of studies [48; 49; 129].



Figure 2.20: MST MK IV [127]

None of the mentioned studies reported a proper evaluation for the system. In addition, Allen et al. [88] reported that an earlier version of the system had a mean accuracy error ($\pm SD$) of $12 \pm 1\%$, where accuracy here is the percentage ratio of the difference between the measured pressures and the expected pressures, and the expected pressures. These findings cannot be extended to the current version of the system.

- **The Sigvaris Interface-Pressure Gauge advanced Tester (SIGaT®)** is a pneumatic sensor which works on similar principles to the MST and the Oxford Talley pressure monitor. The system consists of air pockets, which are placed between the leg and the MCB, air circuit with an injection pump that provides constant air flow, piezoelectric pressure sensors, which are used to measure the pressure of the air that flows to the individual plastic pockets, electronic circuits which are used to analyze the pressure readings, and a data logger or a PC with data acquisition card to store the pressure data. The system works on the following principle: as the pump starts to push the air through the air circuit towards the plastic pockets, the pressure increases gradually with a straight line due to the constant air flow. Once the pressure in air circuit is equal to the external pressure, the air pocket will start to inflate resulting in a change in the slope of the measured pressure (the gradient will decrease). The electronic circuit is designed to detect this dynamic change and report the pressure where this change occurs [81]. Gaied et al. [81] used the SIGaT working principles to measure the pressure under MCS. They reported calibrating the sensors using water column. Nevertheless, no proper evaluation for the errors was reported in their work. Mosti and Rossari [122] reported that the device can-

not be easily found in the market. Besides, they have stated that PicoPress and Kikuhime reported more accurate pressure readings compared to the SIGaT [122]. SIGaT was used in a recent study to compare the healing rates between the MCS and the MCB [130]. However, they did not mention anything about the accuracy and reliability of the system they have used in their study.

- Taylor and Taylor [131] developed a low cost interface pressure monitor which consists of three latex anorectal catheter balloons that are prolate ellipsoid in shape with nominal major/minor axes dimensions of $50mm/35mm$ and average thickness of $3mm$, tubing of $1.5m$ length and $5mm$ external diameter, which connects the latex balloons to the pressure monitor, three piezoelectric pressure sensors, and a differential amplifier processing circuit that amplifies the pressure sensor output and displays it on a liquid crystal display screen (LCD). Taylor and Taylor [131] evaluated the nonlinearity and hysteresis errors of the transducer and reported that the overall error of the transducer was $\pm 0.5mmHg$. This was obtained by calibrating the sensor over the pressure range $0 - 70mmHg$ ($0 - 9.3kN/m^2$) using a sphygmomanometer cuff over a nylon tube covered with a bubble-wrap to simulate the skin softness. They reported that the system overall cost was less than $\pounds 500$. However, they did not report their assessment for the repeatability error of the system and whether the system can be used for dynamic measurements. They used the system to evaluate the bandaging skills of nurses and aid in improving these skills [68].
- **Fontanometer sensor** (Gaelttec Ltd, Scotland, the UK) is a $12.6mm$ diameter and $3mm$ thick sensor. The sensor is a strain gauge mounted on a thin metal plate, which is sandwiched between two air-pockets with the same pressure. When pressure is applied to the upper air-pocket, it causes a change in the air pressure in that pocket, which results in a strain in the metal plate and a change in the resistance of the strain gauge [132; 133]. Gaelttec [132] claims that their sensor is linear over the pressure range $0 - 100mmHg$ with nonlinearity and hysteresis errors of less than $\pm 1\%FS$. The sensor is temperature compensated for the temperature range $15 - 40^\circ C$. The sensor was used by Wertheim et al. [134] to measure and study the interface pressure under MCBs and MCSs. They reported their work in a number of publications [80; 84; 118; 134–138]. However, they did not report their evaluation of the sensor characteristics in any of their publications.

Fluid-Based Interface Pressure Measurement Systems

In general, fluid-based pressure measurement systems use oil or water as a medium to transfer the forces applied by compression products to a pressure that can be converted to an electrical signal using electrical or piezoelectrical pressure transducers. Fluid-based pressure transducers have some limitations such as their bulkiness and problems associated with air bubbles and leakages in addition to the difficulties of using such systems to measure the interface pressure measurement during ambulation [9]. Over the last forty

years, researchers have developed few fluid-based pressure measurement systems, some of which are summarized in the following few paragraphs:

- Raj et al. [119] used water filled PVC envelopes connected to an electrical pressure transducer to measure the interface pressure at four positions. A sphygmomanometer was used to test the system. However, they did not report their transducers static and dynamic errors evaluation.
- Hafner et al. [69] used rubber bags ($50mm \times 30mm \times 5mm$) from baby-size sphygmomanometer cuffs, filled with silicon oil and connected to piezoelectric pressure transducer which, in turn, was connected to a processing and display unit. The system was tested against a sphygmomanometer cuff over fifty healthy volunteer legs for the pressure range of $0 - 120mmHg$. This was achieved by inflating the cuff by increments of $10mmHg$. Hafner et al. [69] reported that the maximum deviation of the interface pressure measured using their device under sphygmomanometer cuff was $\pm 3mmHg$ over the full scale. However, while this can be used as an assessment for the accuracy of the system, there is no information about the effect of hysteresis, temperature and sensor drift on the sensor's static measurements. Furthermore, they did not report a proper evaluation for the reproducibility and repeatability of their measurement system. Moreover, there is no information about the measurement system capabilities for dynamic measurements.
- Barbenel and Sockalingham [139] developed the Strathclyde Pressure Monitor which has been used in various studies [7; 110; 120]. The system consists of PVC probes ($14mm$ in diameter and $1.5mm$ in thickness) filled with vegetable oil connected to a nylon casing, which houses a piezo-resistive pressure transducer with its sensing element consisted of Wheatstone bridge implanted on integrated silicon wafer diaphragm. The transducer is then connected to a processing circuit and LCD screen to display the transducer output. The system was tested using a water column for the pressure range of $0 - 37.5mmHg$ and found to have a linearity error, hysteresis error and drift of less than $0.23mmHg$ for each of them [139]. When tested against a sphygmomanometer, the nonlinearity error was about $0.24mmHg$. Similar results were reported by Nelson [7].

Electrical Pressure Devices

These devices use the electrical properties of materials in which an applied force leads to a change in their resistance or capacitance. However, as pressure is the force over the area which the force is applied to, force sensors can be used to measure the interface pressure. These have the advantages of being thin, small and can be used for dynamic measurements. Some of these sensing devices are discussed below.

- Liu et al. [103] used 16 FlexiForce® sensors (Tekscan, Inc., Boston, USA) and a multichannel measuring system to measure the pressure underneath elastic compression

stocking. Liu et al. [103] calibrated the sensors using deadweights and reported that they have obtained a linear calibration relationships with correlation coefficient of > 0.98 for all sensors [103; 104; 117]. However, they did not report a proper assessment for the sensor's performance. More about this sensor's performance is provided in Section 2.4.2.

- Lurie et al. [99] used Tactilus Human Body Interface Sensor System (Sensor Products Inc, Madison, USA) to measure the interface pressure under IPCs. The system is matrix based tactile surface piezo-resistive sensors with pressure measurement range of $0 - 5171\text{mmHg}$. The 1024 sensing element sheet dimensions were $320 \times 320 \times 0.7\text{mm}$. They did not report any assessments for the device. In addition, the pressure range which the researchers were interested in was $0 - 100\text{mmHg}$, while the device pressure range was fifty times more than the required range. This raises many questions about the accuracy of the device and the results they have obtained with the device. This might explain why approximately $35 - 55\%$ of the sensing elements showed pressures more than 10mmHg (1.3kN/m^2) even when the IPC was deflated i.e. not applying any pressure [99]. More about Tactilus technology and its performance is provided in Section 2.4.2.

In addition to the above mentioned measurement systems, reviewing patents applications revealed other types of pressure measurement systems that are proposed to be used for measuring pressure under compression bandages. Taylor [140] proposed to use Quantum Tunneling Composites (QTC) as sleeves under compression products to measure the interface pressure (see Section 2.4.2 for more about QTC and its characteristics). However, the mentioned system has not been commercialized yet.

Ouchene and Counord [141] proposed to use a medical compression stocking that is made of two materials: non-stretchable material to cover the anterior side of the leg and a stretchable material to cover the rest of the leg, where the two materials are linked in the middle to form a sock. The front side of the sock contains inflatable balloons that provide external pressure just like IPCs. The rear extensible part of the sock contains attached MST sensors or other similar sensors to provide pressure readings which can be used to control the pressure generated by inflating the front balloons. Nevertheless, this system has not been commercialized yet.

2.3.6 Other Forms of Interface Pressure Measurement System

Section 2.3.5 summarized the interface pressure measurement transducers that were used over years to measure the interface pressure. However, all the above systems had a common factor that all of their sensing probes were to be attached to the measurement site. Studying the interface pressure was not only done by attaching external sensors to the human or dummy legs. In many occasions, researchers used dummy legs with embedded pressure sensors to study the interface pressure. Some of these systems are briefly discussed in the next few paragraphs:

- Horner et al. [102] used a latex balloon with controlled air flow and air pressure as a dummy leg. Stockings were positioned over the balloon and by controlling the air flow and pressure in the balloon Horner et al. [102] were able to measure the interface pressure profile. Horner et al. [102] did not report about the accuracy of their system.
- Stolk et al. [65] used an air filled drum to measure stockings DSI. This was done by controlling the air pressure and the increase in the circumference of the drum.
- Cornu-Thenard et al. [142] used a metal cylinder, which depressed when a stocking is applied to it. The metal cylinder contained an air circuit that pumped air into the cylinder to remove any depression caused by the tension forces in the stocking material. Cornu-Thenard et al. [142] measured the air pressure needed to remove these depressions and treated the measured pressure as the interface pressure.
- Strain gauges fitted over a thin sheet of bakelite were inserted at three positions into a dummy leg in a work reported by Ghosh et al. [73] to study the performance of compression bandages and compression garment. The strain gauges were calibrated using deadweights. However, no evaluation for the sensors static and dynamics characteristics was reported in the work [73].
- Rajendran and Anand [108] used strain gauges over cantilever beams, embedded within the structure of a leg mannequin to study their 3D padding. The sensing system worked on a very simple principle. A pin that protruded through the leg mannequin outer shell with 1mm clearance, bended a cantilever beam with mounted strain gauges when a bandage was applied to the mannequin leg. Rajendran and Anand [108] inserted eight of these transducers into their mannequin leg and calibrated the transducers using a sphygmomanometer cuff. However, no information is available about the accuracy of their mannequin leg system [108; 113; 116].

In addition to the above mentioned measurement systems, reviewing patents applications revealed a patented dummy leg to measure the interface pressure under compression stockings invented by Testud et al. [143]. The dummy leg is made of a two-layer wall: the outer layer is thin and the inner layer is thick. Strain gauges are mounted over the interior side of the outer layer. When pressure is exerted over the outer layer of the dummy leg by MCS, it results in a change in the strain gauge resistance, which is proportional to the pressure applied. Testud et al. [143] proposed to use 60 sensors to cover the ankle-thigh region, with 49 sensing points covering the ankle-knee region of the dummy leg. The patent also describes the usage of an air chamber to calibrate the 60 sensors while they are on the leg. However, the device has not commercialized yet.

Kuenzli et al. [144] proposed attaching MST sensors to the surface of their dummy leg, which then can be used to assess compression stockings. The difference between this system and the one proposed by Testud et al. [143], in addition to the different sensing

technology, is that they claim that their dummy leg can change its shape and mimics the change in the leg shape secondary to calf muscle activity. They have achieved that using mechanical levers which are used to change the shape of the leg. The system is commercially available under the name MST Professional [145].

Hansjoerg et al. [146] also proposed a pressure sensing dummy leg which can simulate the calf muscle motion. They used elastic materials that covered empty cavities. These cavities when inflated or filled with liquid would expand to mimic the calf muscle motion. They proposed the use piezo-force sensors to measure the pressure. However, they did not mention the nature or type of these force sensors. The system has not been commercialized yet.

2.4 Flexible Pressure Sensors

One of the objectives of this project is to combine the interface pressure measurement system with medical compression bandages. In order to realize such an advance bandaging system, the sensing material should be flexible, ultra thin and at the same time reliable and accurate. In addition, in order to test such a system, it is essential to design an accurate pressure measurement system first. The force and pressure transducers used in these pressure measurement systems should be as thin as possible as it was mentioned in Section 2.3.2. As nearly all pressure transducers reported in the last section are thick except flexible electrical sensors, it seems reasonable to consider these sensors for developing a new pressure measurement system that can be used to measure forces under compression products and, at the same time, be used to test any high tech bandage that would be developed throughout the course of the project. This section will review these commercial flexible pressure sensors.

2.4.1 Capacitive Flexible Pressure Sensors

Capacitive flexible pressure sensors have been around for some time. They are mainly constructed of three layers: two conductive layers and one non-conductive elastomer with high dielectric constant [10]. These sensors work on this principle: when a pressure or a force is applied to them, the distance between the conductive layers decreases and the capacitance increases. The capacitance change is normally in the order of pF or even lower. Therefore, highly sensitive, precise and stable read-out electronics are needed to process these sensors output signals[10]. In general, capacitive flexible sensors are more stable, more durable. and less sensitive to temperature and humidity than piezo-resistive flexible sensors [10]. However, they are much more expensive than piezo-resistive flexible sensors. In addition, like all other flexible sensors they suffer from high hysteresis errors and creep which is mainly due to limitations related to the polymeric material used [10].

Pressure Profile Systems

Pressure Profile Systems (PPS) sensors (PPS, Los Angeles, USA) are formed by separating electrodes using a compressible dielectric matrix, which acts like a spring. When pressure is applied to the sensor, the distance between the electrodes decreases and the capacitance increases [147]. PPS capacitive sensors come as a single-point sensing element or in grid matrix form sensing elements [147].

ConTacts discrete pressure measurement system (Figure 2.21) is a single-point tactile sensor designed by PPS. The sensor comes in three different types; conformable, industrial rigid and hybrid (combination of the last two). The smallest dimensions of the conformable sensors are $10 \times 10 \times 1 \text{ mm}$. The manufacturer claims that the sensor repeatability error is $< 2\%FS$. The lowest pressure range of the standard form of these sensors is $0 - 258.55 \text{ mmHg}$ ($0 - 34.5 \text{ kN/m}^2$). The manufacturer claims that they can provide sensors with pressure range as low as $0 - 103.42 \text{ mmHg}$ ($0 - 13.8 \text{ kN/m}^2$) ([148]. No information is available about the nonlinearity, hysteresis and drift of the sensor. Unfortunately, the manufacturer does not sell individual sensors, rather they supply the sensors with their high performance conditioning circuit ConTacts C500 [148]. The sale price for the individual conformable sensors in conjunction with ConTacts C500 is higher than £800. This makes the system very expensive and form a custom array from such a system will be highly impractical.



Figure 2.21: ConTacts discrete sensors with ConTacts C500 [147]

TactArray distributed pressure measurement system is the matrix form of pressure measurement system offered by PPS. The system comes in four different types: conformable TactArray, industrial rigid TactArray, stretchable TactArray and 3D molded TactArray (combines the features of conformable and industrial) [149]. The minimum pressure range for both conformable and stretchable TactArray is $0 - 51.7 \text{ mmHg}$ ($0 - 6.9 \text{ kN/m}^2$). The conformable TactArray is made of conductive cloth, while the stretchable TactArray is made of lycra. The thickness of the conformable and stretchable TactArray is 1 mm and 3 mm respectively [149]. The stretchable TactArray can be stretched linearly up to 10%. However, no information is available about these sensors static and dynamic performances.

Novel sensors

Novel sensors (Novel GmbH, Munich, Germany) are capacitive sensors constructed as closed condenser with an elastic dielectric layer [93]. The company manufactures single sensors (Figure 2.22) as well as array sensors with the smallest range of pressure being $15 - 1500\text{mmHg}$ ($2 - 200\text{kN/m}^2$) [150]. Lai and Li-Tsang [97] used Novel's single sensor to measure pressures as low as 5mmHg (666.7Pa). There is very little information on the Novel website about their sensor's performance. Lai and Li-Tsang [97] reported that the single sensor they have used had a linearity error of less than 1mmHg (133Pa) and very low repeatability error when the sensor was tested using deadweights for the pressure range $0 - 50\text{mmHg}$ ($0 - 6.67\text{kN/m}^2$). In addition, they reported that the maximum deviation between the pressure applied over soft tissues by sphygmomanometer cuff and the sensor was $\pm 1.451\text{mmHg}$ ($\pm 193\text{N/m}^2$). However, the data on their graphs show higher repeatability error than the one they have reported, approximately $\pm 3\text{mmHg}$ at 28mmHg . They did not report any information about the hysteresis error or other static or dynamic errors in their work. It should be mentioned that the sensor dimension used by Lai and Li-Tsang [97] was 10mm in diameter and less than 1mm in thickness and it was used in conjunction with Pliance X system electronic analyzer. The system overall cost including the sensor, the electronic analyzer and the software is approximately $US\$21,250$ according to Lai and Li-Tsang [97]. When contacted, the manufacturer was only interested in selling the single sensors with the Pliance X system.



Figure 2.22: Novel S2011 single sensor with 10mm diameter [150]

Rikli et al. [93] used much higher pressure range of Novel pressure transducer ($40 - 1600\text{kN/m}^2$). The transducer they used consisted of 32 sensing elements. They have reported that the sensor had an hysteresis error of less than $7\%FS$, temperature dependency of $-0.06\text{N}/^\circ\text{C}$, slight humidity dependency and no sterilization effect. However, these findings cannot be extended to the lower pressure range single and array sensors.

XSENSOR®

XSENSOR pressure imaging (XSENSOR® Technology Corporation, Calgary, Canada) comprised of two grid of parallel conductive stripes separated by a thin compressible elastomer layer [151]. These sensors come only in matrix form sensing arrangement pads with the smallest pad being (PX100:100.50.10) from their X3 PX series with physical dimensions of $250 \times 120 \times 1\text{mm}$. The pad comes with 2500 sensing element points with three pressure calibration ranges: $5\text{--}50\text{mmHg}$, $5\text{--}100\text{mmHg}$ and $10\text{--}200\text{mmHg}$ ($0.665\text{--}6.65\text{kN/m}^2$, $0.665\text{--}13.3\text{kN/m}^2$ and $1.33\text{--}26.6\text{kN/m}^2$). According to the manufacturer, the X3 series is accurate within $\pm 10\%FS$ [152].

Fergenbaum et al. [153] reported that an earlier version of XSENSOR's sensor, X2 series, outperformed the F-scan® (Tekscan, Boston, USA) and FSA (Vista Medical, Manitoba, Canada) on flat surfaces, with XSENSOR X2 being more sensitive to low pressures and showing better repeatability. In their following work over constant curved surfaces, they found that XSENSOR sensor had only 2% accuracy error compared to 72% for F-scan if the readings were taken after 5 minutes from loading the sensor. However, if readings were to be taken 2 minutes after applying the load to a curved surface, the XSENSOR and F-scan have an accuracy error of 33% and 27% respectively. When both systems were tested over a hip model, XSENSOR showed only 4% error compared to 53% for F-scan. However, it should be mentioned that the F-scan pressure range was $0\text{--}1810\text{mmHg}$ which is much higher than the pressure range tested in the reported apparatus. The researchers concluded that the XSENSOR pressure imaging sensor should only be used for static measurement with considerable resting time [154]



Figure 2.23: XSENSOR X3 LX100 [155]

XSENSOR have introduced recently their X3 LX100 series (Figure 2.23) which has repeatability error of $\pm 3\text{mmHg}$, hysteresis error of $\pm 2.6\text{mmHg}$, 5% drift after one hour of keeping the load at 100mmHg and 5% error at 100mmHg after 100,000 loading cycles i.e. the sensor has very high stability and can be used for a long time without the need for re-calibration. Nevertheless, the mentioned systems' smallest pad has an external physical dimension of $457 \times 457 \times 1\text{mm}$ [155].

2.4.2 Piezo-resistive Flexible Pressure Sensors

Piezo-resistive flexible pressure sensors are constructed of thin flexible polymer sheets sandwiching a conductive polymeric sheet. These sensors work on the principle of decreasing the resistance of the material when an external force is applied to its surface [10]. Several sensors from this category are available in the market while others are under development. These sensors differ in their wiring configuration, wiring material, the polymeric conductive material and the method which the conductive material is placed between the flexible polymer sheets [10; 156; 157]. In general, piezo-resistive sensors are cheap, their driving circuitry is very simple and have low sensitivity to electromagnetic fields. However, they have high non-linearity, high hysteresis, temperature and humidity dependency, creep problem, poor stability and limited durability [10].

Force Sensing Resistor (FSR®)

Force Sensing Resistor (FSR) (Interlink Electronics, Camarillo, USA) is a polymer thick film device which exhibits a decrease in resistance when a force is applied to its active surface (Figure 2.24) [158]. The sensor's minimum thickness, diameter and active diameter is about $0.3mm$, $7.6mm$ and $5mm$ respectively [158]. The company states that the sensor cannot be used for precision measurements as the force repeatability part-to-part is $\pm 15\%$ to $\pm 25\%$ of established nominal resistance and the single part force repeatability $\pm 2\%$ to $\pm 5\%$ of established nominal resistance [158]. In addition, the sensor's pressure sensitivity range according to the manufacturer is $77.6 - 776mmHg$ or in terms of forces it is $1 - 100N$ [158]. According to the manufacturer, dynamic measurement is possible with FSR for qualitative purposes only with rise time between $1 - 2ms$ [158]. The sensor is relatively cheap with price tag of $\pounds 2 - 3$ for the standard small size sensors.

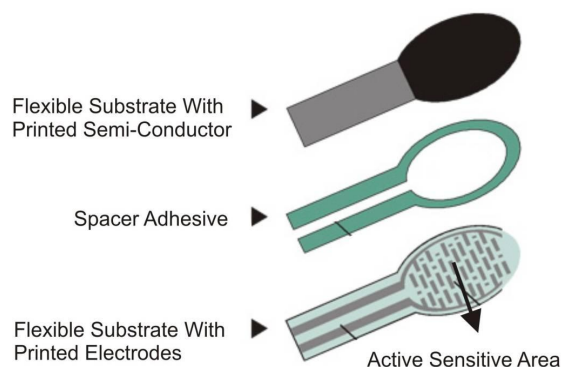


Figure 2.24: FSR layers[158]

Vecchi et al. [159] found that the $12mm$ diameter FSR had $\pm 2.2N$ linearity error, very high repeatability error and $8 - 15\%$ of initial value drift within 10 minutes of measurement. Average dynamic errors found to be 5% of initial value quasi-static $0.5Hz$ loading, with measurements taken after $10s$ from the start of loading the sensor. It should be mentioned

that they have directed the load to the sensitive area by using a dome which increased the sensor thickness to $4mm$.

Castro and Cliquet [160] used a 7th order calibration fitting line to fit the sensor's force range $0-15N$. They reported that hysteresis was within 6% of loading cycle measurement. They also directed the force to the sensor active area using two $1mm$ thick plates and adhesives under and above the sensor.

Hall et al. [161] used a polynomial equation with terms dependent on past loading history in the calibration equation to compensate for the hysteresis and drift errors of FSR. They also subjected the sensor to prolonged shear loading in two orthogonal directions in order to eliminate the shear force effect on the sensor and convert it to pure compression sensor. They used a $3mm$ thick dome to direct the forces directly towards the sensitive area of the sensor. [161].

Lebosse et al. [162] reported that FSR sensors with physical dimension of $43.7 \times 43.7mm$ have hysteresis errors below $8\%FS$, nonlinearity error of $7\%FS$ and repeatability error of $2.1\%FS$, with full scale defined as $7N$. They also reported that the sensor drifted by 4% in 20 minutes of loading the sensor. Additionally, they found that the time constant for the sensor is $35ms$ for a step response and it shows a linear reduction in its output for sinusoidal low frequencies (quasi-static) input. This reduction can reach up to 30% of the sensor initial value output just after 20 minutes from the start of applying the sinusoidal force. They used nonlinear modeling to compensate the dynamic nonlinearity effect [162].

Marechal et al. [163] used the smallest size of FSR sensors in their application. They reported problems with calibrating the sensors. However, they did not publish any evaluation for the sensor in their published work [163–165].

FlexiForce® Sensor

Tekscan's thin film pressure sensors are the most used and reported flexible sensors in the literature related to pressure-mapping and force measurements in the medical field [78; 90–92; 94; 98; 153; 154; 166–171]. Some of these studies did report extensive evaluation for the different Tekscan matrix form sensors like: F-scan and I-scan. However, in all these studies the sensors were used to measure much higher interface pressure than the ones required for this study, thus; the published evaluations are not reported here. Nevertheless, it is worth mentioning that Tekscan has manufactured a custom pressure measurement system that can measure interface pressure compression garment which Tekscan has called The Garment System [172]. No information is available about the static and dynamic characteristics of the system on the company's website.

The FlexiForce ultra-thin ($0.203mm$) flexible sensor is the Tekscan's single point free form solution for measuring the interface pressure (Figure 2.25). The sensor is constructed of two layers of substrate film with silver conductive material applied over the substrates, followed by a layer of pressure sensitive ink. Adhesives are used to laminate the two layers of substrate together to form the sensor. Silver is used as conductive leads for the sensor



Figure 2.25: FlexiForce® sensor [173]

(Figure 2.26) [173]. Applying force to the sensitive area of the sensor results in a decrease in the resistance of the sensor and increase in its conductance. The sensor comes in three force ranges with the lowest range of force is $0 - 4.4N$ which means that the smallest range of pressures the sensor can be utilized to measure is $0 - 462.6mmHg$ ($0 - 57.7kN/m^2$) [173].

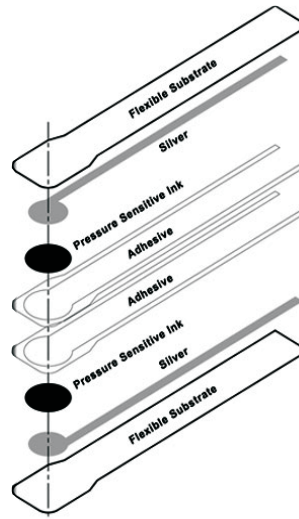


Figure 2.26: FlexiForce sensor construction layers [174]

Tekscan claims that the sensor's nonlinearity error in its three ranges is less than $\pm 3\%FS$, repeatability error is less than $\pm 2.5\%FS$, hysteresis is less than $4.5\%FS$, drift is less than 5% of initial value per logarithmic time scale, response time is less than $5\mu s$ and temperature sensitivity up to 0.36% per degree Celsius [173]. The sensor has been used in various studies [103; 104; 117; 159; 162; 169; 170; 175–182].

Komi et al. [169] found that the medium force range sensor $0 - 110N$ has an average accuracy error of $10\%FS$, hysteresis error of $6.3\%FS$, and repeatability error of 4.5%. They reported that the drift was -0.5% of the initial value a minute after loading of the sensor, and its performance was affected by bending it over curved surfaces, applying shear forces and applying dynamic forces with the sensor accuracy changing from 10% at static to -25% at $100Hz$ dynamic load.

For the same force range, Vecchi et al. [159] reported that the sensor nonlinearity was improved by directing the force to the sensitive area using a $4mm$ thick dome. They also

reported that the sensor repeatability was $3\%FS$ on average with their full scale set to $30N$. Nikonovas et al. [181] found that at the same force range FlexiForce sensor showed an agreement with $\pm 6\%$ between its output when it was applied to a flat surface compared to its output when wrapped over a cylinder with $5mm$ radius. They cited that Wasserman et al. [183] reported that the sensor output was uniform over the force range $0 - 2kHz$.

Ferguson-Pell et al. [176] have reported that the $0 - 4.4N$ FlexiForce sensor have an accuracy error of 5.1% , hysteresis error of 5.4% , repeatability error of 2.3% at $50g$ load and a drift of 1.7% per logarithmic scale for the $50g$ load. They also have reported an effect of bending on the sensor performance and recommended not to use the sensor over curvatures with radii smaller than $32mm$.

The same force range sensor was reported by Lebosse et al. [162] to have a nonlinearity error of 5% , hysteresis error of less than $10\%FS$, repeatability error of $3.6\%FS$, time drift of 6% over 20 minutes, time constant of $30ms$ for step input and 68% loss of output when a $0.44N$ load was applied to the sensor with $0.5Hz$ for 20 minutes. However, the authors did push the sensor beyond the manufacturer's recommendations and used the sensor for the force range $0 - 7N$. Finally, It is worth mentioning at this point that each FlexiForce sensor is about $\pounds 8$ when purchased in pack of 8.

In a recent published work, Paredes-Madrid et al. [182] showed that the capacitance of the highest FlexiForce force range changes linearly with the applied force. They also demonstrated that using capacitance instead of conductance results in a higher repeatability performance for FlexiForce sensor. In addition, they reported lower mean squared error for FlexiForce sensors when they used the combined average of both the resistance and the capacitance models of the sensor. Furthermore, they demonstrated that using a neural network to process the sensors variation in conductance and capacitance did result in a further reduction in the mean squared error of the sensor [182].

FSA

FSA (Vista Medical Ltd., Manitoba, Canada) consists of a piezo-resistive semi conductive polymer sandwiched between two layers of highly conductive rip stop nylon fabric. The conductive polymer is floating between the conductive layers which, according to the manufacturer, allow comfortability of the compound over curved surfaces [184]. Some of the array sensing systems developed by Vista Medical Ltd are for the pressure range of $0 - 100mmHg$. However, the mentioned systems are about $4mm$ thick. No other information about the sensor performance is available on the company's website [184].

Quantum Tunneling Composites (QTC) Force Sensors

Quantum tunneling is a term which describes the probability of electrons to be found on the other side of a non-conductive barrier due to the electrons wave properties. QTCs shows this electron behavior when the composite is subjected to external pressures which induce conductance within the composite [185].

QTC sheets (Peratech Ltd., Durham, UK) were customized by Komi et al. [169] to measure the forces applied by the hand during a golf shot. They found that their custom made QTC sensors had a second order or higher polynomial calibration fitting line for the forces range $0 - 105N$, accuracy error of $13\%FS$, hysteresis error of $20\%FS$, repeatability error of 7.1% , drift by 51% of the initial value within a minute of loading the sensor, a large decrease in the sensor's output when the sensor was tested over curved surfaces, sensitive to shear forces and high impact of dynamic forces on the sensor performance with indications for sensor degradation due to the high frequency forces [169]. QTC material is also used extensively by Eleksen, which is a Peratech company, as textile integrated wearable switches [186]

Tactilus

Tactilus pressure-mapping is available in both matrix and free form sensors. The company on its website claims that their piezoresistive/resistive matrix has an accuracy of $\pm 10\%$, repeatability error of $\pm 2\%$, hysteresis error of $\pm 5\%$, nonlinearity of $\pm 1.5\%$ and can measure pressure as low as $5.2mmHg$ [187]. The system was used by Lurie et al. [99] to measure the interface pressure under IPCs. The manufacturer also provides free form sensors which unlike their matrix form are only resistive-based [188]. After contacting the company it has been revealed that their smallest pressure range for the free form is $0 - 260mmHg$ with $8mm$ sensor diameter and a price tag of $\pounds 65$ for each sensor including postal services. No other information was available on the company's website about the free form sensor.

2.4.3 Other Potential Flexible Sensors

Ochoteco et al. [156] are developing a flexible force sensor composed of two thin layers of conductive polymers on plastic substrates. The conductive material is made of plastic polymer rather than metallic polymers which are used in other piezo-resistive flexible sensors described earlier. The sensor has not been commercialized yet.

2.5 Synopsis of the Literature Review

From the literature review reported in Section 2.1 and Section 2.2 it can be concluded that, to provide better care for venous ulcers patients, more work should be carried out in the following areas:

- The etiology and pathophysiology of the CVD and ulcers formation.
- The effect of external pressure on venous hypertension, hemodynamics, the vascular system and ulcers healing.
- The consequences of external pressures over the living tissues and the amount of pressure passing through these tissues into the deep veins.

- The underpinning physics of pressure delivery using MCBs.
- The pressure profile required to be applied to venous ulcer patients' legs to assist healing the ulcer and the different variables' which impact the levels of pressure needed. This includes a systematic study to verify the need for gradient pressure.
- Providing tools for training purposes for nurses to help them learn and practice applying MCBs in the correct way, which also needs to be defined.
- Designing better compression products with better control tools that enable clinicians to tailor their bandaging techniques according to the individual patient needs.

All the above areas except the first one require reliable and accurate pressure measurement systems. However, from Section 2.3 it is clear that current pressure measurement systems are not verified for their accuracy and reliability. Indeed, some of the new measurement products like PicoPress seem to be very promising. In addition, the sensor's physical dimensions will affect the reliability of the measurement readings provided by any pressure measurement system with sensor's thickness exceeding $0.5mm$. Therefore, even devices like PicoPress might not be as reliable as it is thought to be due to the fact that the sensor thickness increases to $3mm$ when it is inflated under the bandage. Hence, more work is needed in order to check the accuracy and reliability of the current pressure medical devices and to design pressure measurement devices that use ultra thin flexible sensors. Moreover, systematic research is needed to figure out the number of pressure measurement sites on the lower limb to provide enough information to judge the effectiveness of MCBs.

Section 2.4 shows that flexible sensors suffer from high static and dynamic errors. The capacitive sensors seem to be less effected by these systematic errors at least at static measurements. Nevertheless, they are very expensive and their thickness is more than the $0.5mm$ used to describe the ideal pressure measurement system (Section 2.3). The resistive sensors, on the other hand, are very cheap compared to the capacitive ones and are much thinner than $0.5mm$. However, the literature suggests that their static systematic errors are quite large, making them more useful for qualitative purposes rather than exact measurements. Thus, it is important to exert effort and spend time to either design new reliable and cheap flexible sensors or use the available ones with software algorithms to reduce the error.

2.6 The Project Overall Methodology

This thesis tries to fill some of the gap in the body of knowledge and answer some of the questions identified through the literature review. These questions are summarized in the following few points:

- What is the impact of MCB physical dimensions, number of layers and method of

application, leg local radius of curvature and the sensor physical dimensions on the interface pressure from theoretical point of view?

- Can the extension in the MCB be used to provide accurate and adequate information about the interface pressure applied by this MCB?
- Are the pressure readings provided by current commercial medical pressure transducers like PicoPress accurate?
- Which of the resistive-based flexible sensors will provide more accurate pressure readings?
- Can resistive-based flexible sensors be used to form a new pressure-mapping measurement system that can map the pressure under compression bandages with high resolution?
- Can resistive-based flexible pressure sensors attached to MCBs be used to form pressure-mapping bandage and provide clinicians with accurate pressure measurements and hence replace the current feedback method of using elongation to control the pressure applied by MCBs?
- Can dummy legs with embedded pressure sensors be used for training purposes?

In order to answer the above questions, the project has been divided into three main phases with tasks assigned for each phase (Figure 2.27).

The first phase of the project has been designed to address issues prerequisite to addressing the aims of the project:

- Exploring the physics behind how MCBs deliver pressure. This aimed at developing a mathematical model that enables calculating the interface pressure applied by multi-layer MCBs and testing the model proposed by other researchers to estimate the impact of sensor dimensions on the measured interface pressure.
- Obtaining a mathematical description for the tension-elongation curves for different MCBs. Nurses normally assess their bandaging technique by measuring extension and checking bandage overlap. However, no systematic review has been found in the literature to check the effectiveness of using extension to control the pressure applied by MCBs. Due to the absence of any gold standard that can be used to validate any new pressure measurement system, it has been proposed to use the computed pressure from the extension as a part of multi-way evaluation method for the systems to be developed in this project. At the same time this will help in studying the reliability of using extension to control the pressure.
- Evaluating the flexible resistive-based force sensors in static and selecting the best among them to be used in the next phase of the project. In addition, a current

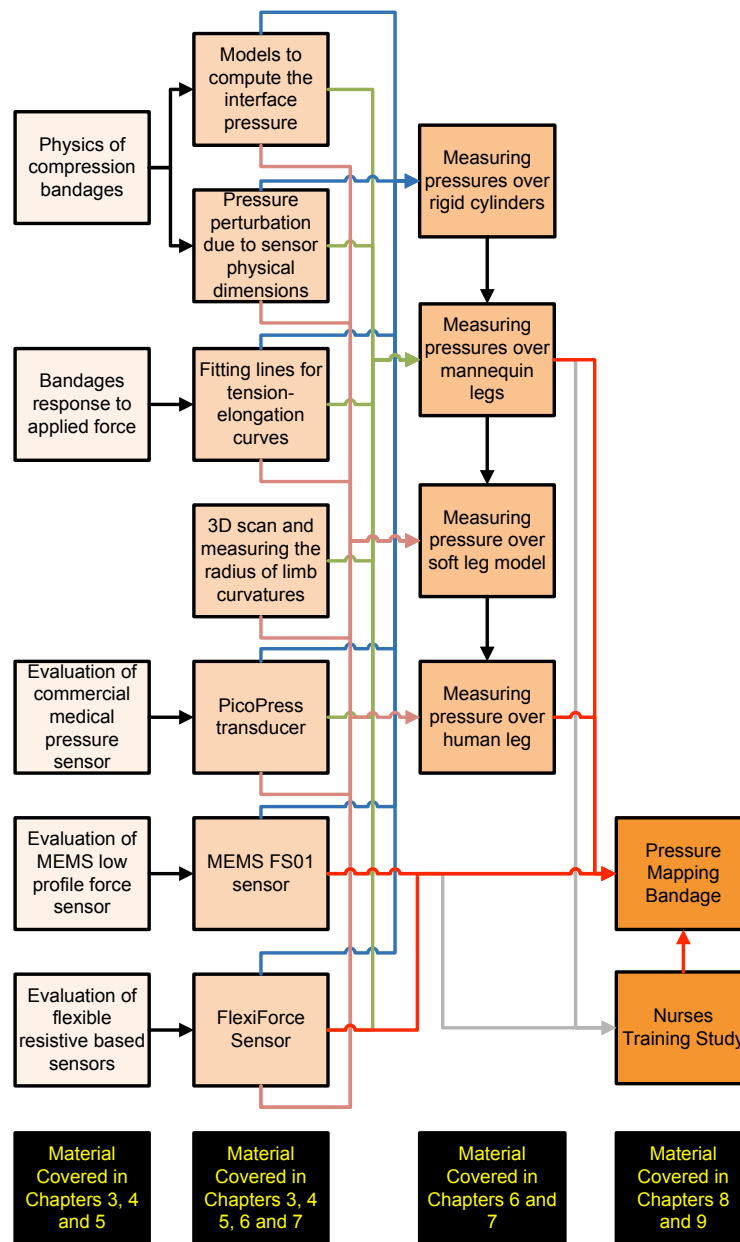


Figure 2.27: The project flow chart

commercial medical pressure transducer has been tested so that it can be used as a multi-way validation for any new pressure measurement system. Moreover, an MEMS low profile force sensor has also been tested in this phase for the same reason.

The second phase of the project aimed at designing pressure-mapping reference systems that can be used to validate and test pressure-mapping bandages and designing a pressure-mapping measurement system that can be used to study and map the pressure under MCBs when they are applied to a real leg. This phase was divided into four main sub-phases:

- The three sensors selected to be used in this phase of the project, flexible resistive

pressure sensor, the commercial medical pressure sensor and the MEMS force sensor, have been used in array form to map and measure the pressure applied by MCBS to a rigid cylinder. The pressures measured have been compared to the computed pressure from extension. The results obtained have been used to answer questions about the reliability and accuracy of using extension to control the pressure, the reliability of the medical pressure transducer, the reliability of the MEMS force sensor, the reliability of using flexible force sensors to measure the pressure and some other questions as well.

- Arrays of the three sensor types mentioned above have been used to map and measure the pressure applied by compression bandages to a rigid mannequin legs. As in the previous sub-phase, the pressure measured using these arrays of sensors have been compared to the computed pressure from extension. The outcomes have been used to answer similar questions to ones addresses in the previous sub-phase. Furthermore, as the mannequin leg does not have constant radius of curvature, a 3D model of the leg has been obtained using a 3D scanner. A computer software has been used to acquire the required dimensions from the 3D model.
- In the third sub-phase, the medical transducer and the flexible sensor have been used to map the pressure applied by MCBs to a soft leg. The main objective is to study the effect of softness on the two sensors performances.
- In the last sub-phase, the knowledge gained from the previous three sub-phases has been used to design a pressure-mapping measurement system using arrays of flexible sensors. The system has been tested against the medical transducer on a real leg. The pressure measured using the two sensing technologies have been compared to each other and to the computed pressure

The third phase of the project involved developing and testing a prototype pressure-mapping bandage. The prototype bandage has been evaluated by applying it to the MEMS pressure-mapping leg. The same leg has been used to train student nurses and study their bandaging techniques. Indeed, the work does not directly serve the aims of the project. However, student nurses feedback was important to decide about the nature of the pressure feedback: numerical numbers or colored maps.

2.7 Contribution of this Project to the Body of Knowledge

The project main novelty can be summarized in the following points:

- Mathematical modeling for the interface pressure applied by single-layer and multi-layer MCBs. The models were experimentally validated.
- Mathematical modeling for the effect of angles and bi-axial force on the interface pressure.

-
- Mathematical modeling for the change in the interface pressure due to change in limb size.
 - Studying experimentally the effect of sensors aspect ratio on the measured interface pressure.
 - Comparing between the computed pressures and the measured pressures in different situations and demonstrating that controlling the bandage application by extension results in pressure maps that are not in agreement with the measured pressure maps.
 - Illustration for the pressure overestimation problem caused by using thick sensors like PicoPress to measure the pressures applied by MCBs.
 - Designing and implementing of pressure-mapping reference systems which can be used for testing and studying compression products.
 - Designing and implementing a high resolution custom made pressure-mapping measurement system which can be used to study MCBs when applied to healthy participants.
 - Designing and implementing a pressure-mapping bandage prototype which can be used to provide qualitative feedback on the pressure profile.
 - Designing and implementing a training pressure-mapping system that can provide pressure maps for nurses and can be used to train nurses and improve their bandaging skills.

Chapter 3

Sub-Bandage Interface Pressure: Mathematical Examination

*This chapter presents the theoretical work carried out to re-examine the underpinning physics of compression therapy and how bandages deliver the required pressure. First, it provides a short summary of the current understanding of how MCBs apply pressure. This is followed by a general description for the forces that govern the pressure induced by MCBs. The chapter then reports the work carried out to examine the effect of bandage thickness on the interface pressure. Next, it describes models developed to estimate pressure applied by multi-layer MCBs. The effect of MCBs biaxial forces and angle of application on the interface pressure is then reported. After that, the impact of the change in the limb shape on the interface pressure is presented. Finally, experimental work to study the effect of sensors' physical dimensions on the interface pressure is detailed. Some of the work reported in this chapter have been presented in the 12th Mechatronics Forum Biennial International Conference (“Effect of Sensor Thickness and Length on Interface Pressure Measurement Induced by Medical Compression Bandages”), and two articles have been accepted for publication in *Phlebology* (“Impact of Multi-Layered Compression Bandages on Sub-Bandage Interface Pressure: a Model” and “Impact of Variation in Limb Shape on Sub-Bandage Interface Pressure”).*

3.1 Introduction

As reviewed in Section 2.2.4, the current understanding of how MCBs apply pressure to a limb is based on the Law of Laplace, which states that tension in the walls of a container is dependent on both the pressure of the container's content and its radius [77]. This concept translated mathematically into Equation 2.3. As discussed earlier, researchers have expressed their doubts about the model validity and whether it can be used to predict the interface pressure applied by pressure garments. Section 3.2 summarizes the forces that are thought to influence the interface pressure applied by MCBs.

One of the questions which yet has not been answered is whether bandage thickness

affects the interface pressure. Section 3.3 will explore the effect of MCBs' thickness on the interface pressure using an analytical method. This will be followed by a computational simulation for the pressure applied by MCBs to a real leg and experimental validation for the analytical work.

In addition, Thomas [75] modified Equation 2.3 by multiplying the model with a constant that represents the number of MCB layers in order to use the model to estimate the pressure applied by multi-layer MCB. This simple multiplication adjustment was questioned by Wertheim et al. [80]. Section 3.4 tackles the effect of multi-layer bandaging on the interface pressure using mathematical models, which then are assessed using both computational simulation and experimental apparatus.

As reported in Section 2.2.4, Ghosh et al. [73] found MCBs angle application have an impact on the interface pressure. An attempt to mathematically model the application angle effect on interface pressure is reported in Sections 3.5 and 3.6.

Moreover, a mathematical model for the impact of the change in the limb shape on the interface pressure is reported in Section 3.7. This is addressed to inform the problem of bandage classification reviewed in Section 2.2.4.

Finally, the chapter ends with an experimental evaluation for the model proposed by Vinckx et al. [86] to estimate the perturbation in pressure measurement due to sensors' physical dimensions (Section 2.3.3).

3.2 Forces Interaction Between the Compression Bandages and the Lower Limb

Liu et al. [74] summarized the forces (see Section 2.2.4 for details) generated in a pressure stocking garment when it is applied to a human leg. Even though they have reported that thicker bandages are able to apply higher pressures, they have only shown the effect of the biaxial tension forces on the stocking garments and have not modeled the radial direction of the forces. In bandages, tension is applied in mono-axial (circumferential) direction, which results in compression forces both in the other axis of the bandage; longitudinal and radial directions (see Figure 3.1 for definitions).

In addition, the force body diagram for a bandage will also differ from the ones reported by Liu et al. [74], as bandages are applied in multiple of layers and each subsequent layer will apply compressive forces to the previous bandage layers. Figure 3.1 summarizes the above forces and the one identified by Liu et al. [74].

Figure 3.2 illustrates the dynamic modeling for the forces interaction when a bandage is applied to a limb. It is worth mentioning at this stage that even though some of the forces mentioned in Figure 3.1 are believed to play an important role in delivering the pressure like shear forces, friction forces and bending forces, they are not discussed in this chapter and are reserved for future work in this field.

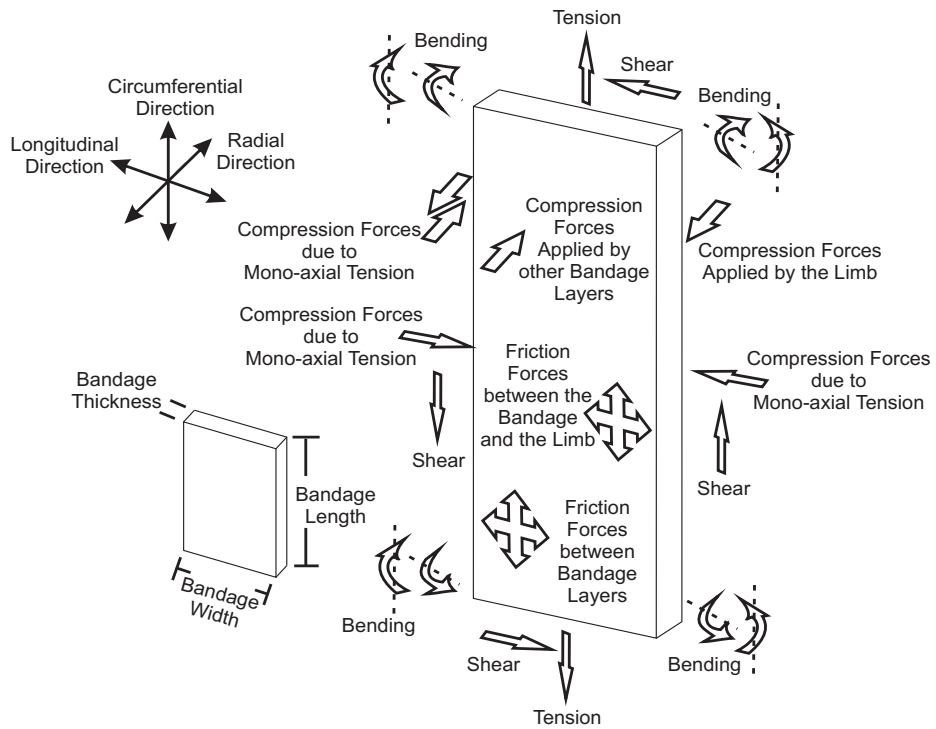


Figure 3.1: Force Body Diagram for the bandage limb interaction

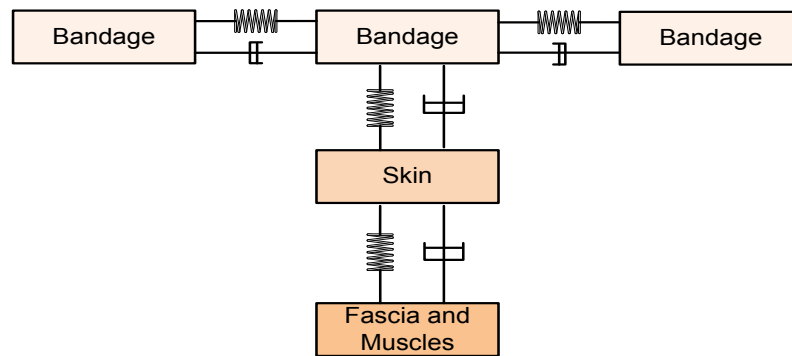


Figure 3.2: Dynamic bandage-limb interaction. This dynamic interaction is for a single-layer bandage

3.3 Effect of Bandage Thickness on the Interface Pressure

In the present section, the formula that describes the sub-bandage pressure for one layer of compression product is re-derived using two different approaches. The first assumes that the bandage thickness is negligible, whereas the second one takes the bandage thickness into consideration. The estimated pressures using the two formulae are then compared. This is followed by an experimental validation for the models derived and illustration for their limits.

3.3.1 Interface Pressure Model Using Thin Wall Cylinder Theory

In this approach, the bandage or stocking is assumed to form a thin-walled cylinder as shown in Figure 3.3. The cylinder wall is subjected to three types of stresses: hoop or circumferential, radial and longitudinal stresses [85] (Figure 3.4). If the ratio of thickness of the cylinder wall to its inside radius is less than 1 : 10, then it can be assumed that the hoop and longitudinal stresses are constant across the wall thickness, and the magnitude of the radial stresses is very small compared to the other stresses; thus, it can be ignored [85].

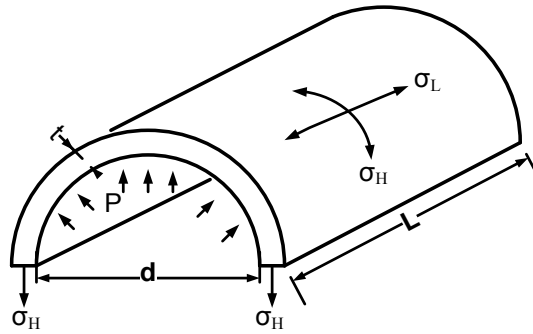


Figure 3.3: Half of a thin cylinder subjected to internal pressure

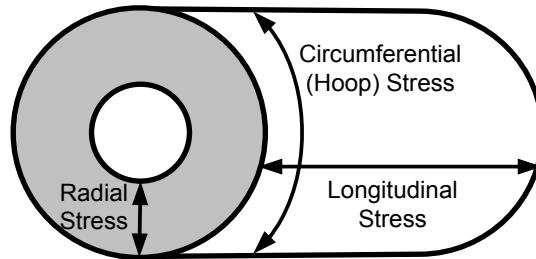


Figure 3.4: Stresses within the cylinder wall

Based on the above assumptions, it can be shown that the hoop stress can be expressed as given in the following equation:

$$\sigma_H = \frac{PD}{2t} \quad (3.1)$$

Where, σ_H is the circumferential or hoop stress in (N/m^2), P is the internal pressure in (N/m^2), D is the cylinder or limb diameter in (m) and t is the bandage thickness in (m).

The hoop stress can be written in terms of the tension in the cylinder wall (T), the length of the cylinder wall (L) and the thickness (t).

$$\sigma_H = \frac{F}{A} = \frac{T}{tL} \quad (3.2)$$

This is true as far as the tension across the cylinder wall is constant. Then, by combining Equation 3.1 and Equation 3.2 the pressure can be described as follows:

$$P = \frac{2T}{DL} \quad (3.3)$$

The length of the cylinder (L) will be the same as the bandage width (w), therefore the equation can be re-written as follows:

$$P = \frac{2T}{Dw} \times 0.0075 \quad (3.4)$$

Where, P is the internal pressure in ($mmHg$), T is the tension force in (N), D is the limb diameter in (m) and w is the bandage width when it is extended in (m).

This model is exactly the same as the model reported by other researchers [76; 83].

3.3.2 Interface Pressure Model Using Thick Wall Cylinder Theory

The assumptions that were held for thin wall cylinder theory are not valid with this theory. The hoop and longitudinal stresses are not constant and the radial stresses are not negligible. In addition, there is a pressure gradient across the cylinder wall (Figure 3.5).

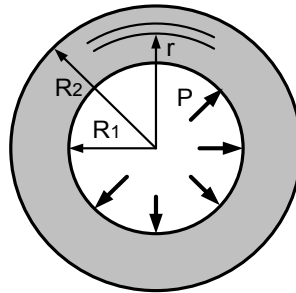


Figure 3.5: Thick cylinder subjected to internal pressure

The derivation of the stresses is out of the scope of this report and can be found in the work of Hearn [85]. The stresses are shown in the following equations:

$$\sigma_L = \frac{P_1 R_1^2 - P_2 R_2^2}{R_2^2 - R_1^2} \quad (3.5)$$

Where, σ_L is the longitudinal stress in (N/m^2), R_1 is the internal radius in (m), R_2 is the external radius in (m), P_1 is the internal pressure in (N/m^2) and P_2 is the external pressure in (N/m^2).

The longitudinal stress is constant as far the pressures are constant.

$$\sigma_r = \frac{P_1 R_1^2}{R_2^2 - R_1^2} \left[1 - \frac{R_2^2}{r^2} \right] \quad (3.6)$$

Where, σ_r is the radial stress in (N/m^2) and r is a variable that describes the radius in (m) across the wall.

$$\sigma_H = \frac{P_1 R_1^2}{R_2^2 - R_1^2} \left[1 + \frac{R_2^2}{r^2} \right] \quad (3.7)$$

Where, σ_H is the hoop stress in (N/m^2).

Equation 3.7 can be re-written in terms of limb or cylinder diameter (D) and bandage thickness (t) by making $D = 2R_1$ and $R_2 = R_1 + t$. The maximum stress will occur at $r = R_1$; thus, the maximum hoop stress can be expressed by the following:

$$\sigma_H = \left[\frac{\frac{1}{2}D^2 + t(D+t)}{t(D+t)} \right] P \quad (3.8)$$

Now equating Equation 3.8 with Equation 3.2 will result in an expression for the sub-bandage interface pressure:

$$P = \frac{T(D+t)}{\frac{1}{2}wD^2 + wt(D+t)} \times 0.0075 \quad (3.9)$$

Where, P is the internal pressure in ($mmHg$), T is the tension force in (N), D is the limb diameter in (m), t is the bandage thickness in (m) when it is extended and w is the bandage width in (m) when it is extended.

3.3.3 Comparison Between Thin and Thick Cylinder Wall Theories

In order to investigate the effect of bandage thickness on the estimated pressure values, the tension/pressure ratio in Equation 3.4 and 3.9 was calculated for a number of diameter/thickness ratios and the difference between the tension/pressure ratio in each situation was calculated and plotted in Figure 3.6. Clearly, the thin cylinder theory is valid as far as the ratio D/t is larger than 20 : 1 (the radius/thickness ratio is larger than 10 : 1).

In order to put this in a medical context, suppose a bandage of 1.2mm thickness and 100mm width (these values were obtained by measuring the thickness and the width for some commercial bandages) is going to be applied with 15N tension to a leg. If the tension in the bandage material is kept constant and the leg local curvature radius is varied from 5mm to 70mm, then the pressure calculated using Equations 3.4 and 3.9 could be plotted against the change in the local curvature radius as shown in Figure 3.7, where it is clear that at limb radius of 35mm, the difference between the pressure estimated by the two models is about 1.8%. The 0.6mmHg difference is medically insignificant.

However, due to the variation in the leg radii, the effect of bandage thickness on the estimation of the interface pressure will be greater on the tendons and bony structures. In order to illustrate this, the pressure applied using the above described bandage when it

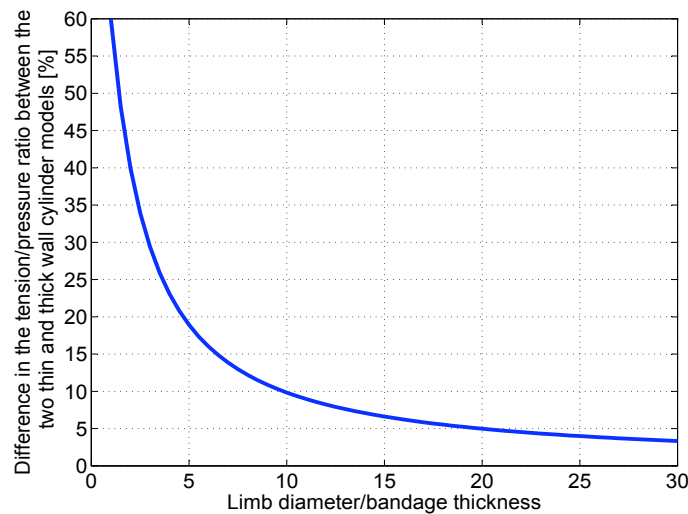


Figure 3.6: Percentage difference in tension/pressure ratio between the thin and thick wall cylinder theories vs. limb diameter/bandage thickness ratio

is applied to a real leg is simulated and the results are shown in Figures 3.8 and 3.9. The leg local radii were measured from a 3D model for a healthy participant at 103 different locations. The simulation was done using LabView2009 (NI, USA).

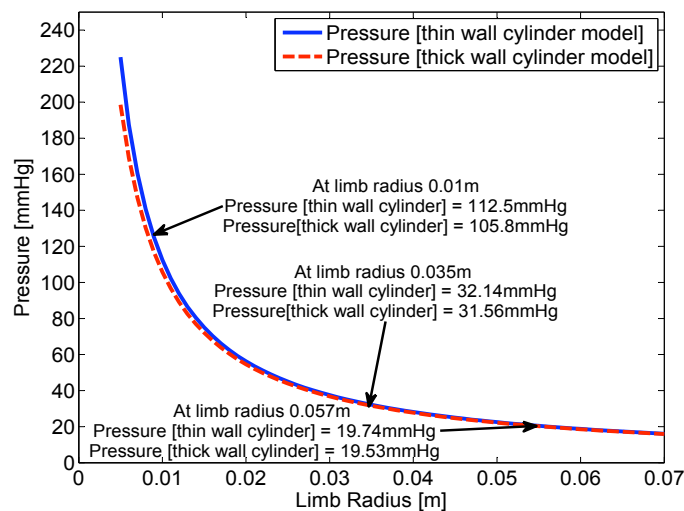


Figure 3.7: Pressure calculated using the models based on thin and thick wall cylinder theory vs. limb radius

The simulations illustrate that neglecting the bandage thickness will result in overestimating the pressure over the bony prominences of the leg compared to the case when bandage thickness is considered in the calculation (see the white area which represents unacceptable levels of pressure). In addition, the simulations show that applying bandage with constant tension will result in graduated pressure for this particular case. Moreover, in spite of the moderate tension used (15N), the pressure peaked over the bony promi-

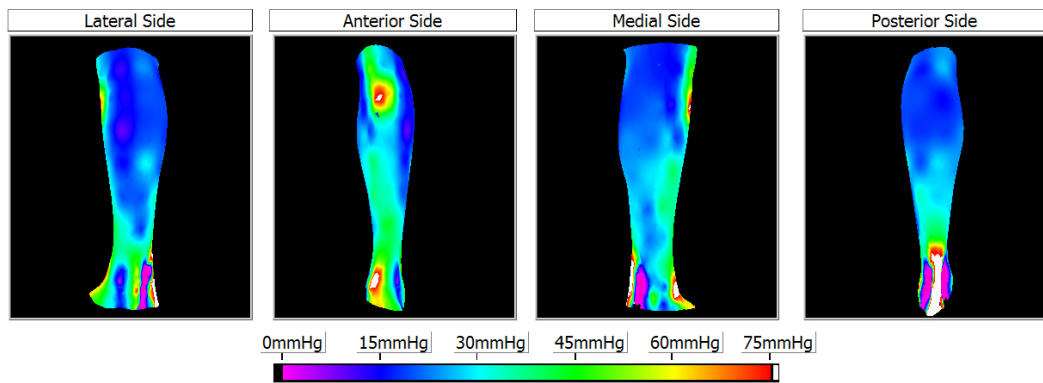


Figure 3.8: The simulated pressure map over a real leg when single-layer bandage is applied to the leg. The pressure calculated using the pressure model derived using thin wall cylinder theory (Equation 3.4)

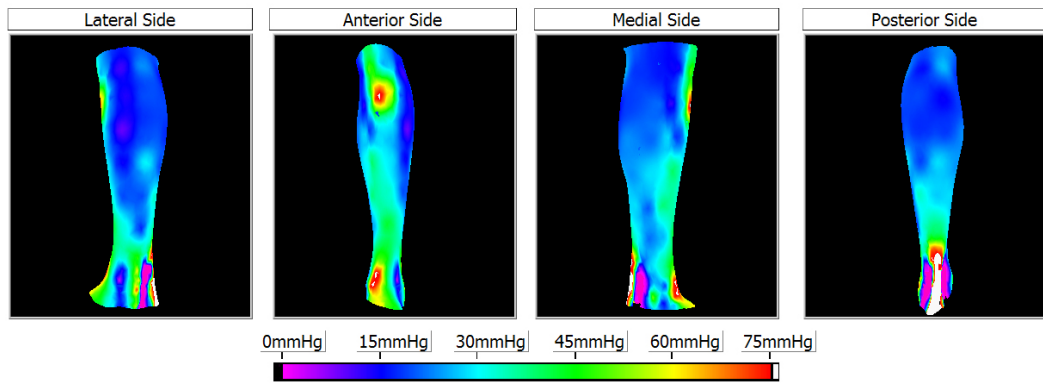


Figure 3.9: The simulated pressure map over a real leg when single-layer bandage is applied to the leg. The pressure calculated using the pressure model derived using thick wall cylinder theory (Equation 3.9)

nences and the Achilles tendon. This provides a support for the current practice to cover these areas with padding layers of bandage. Furthermore, the areas behind the lateral malleolus and medial malleolus are subjected to minimum pressure due to the negative radius which means that the bandage will not be able to apply pressure to these areas without using plastic paddings. Nevertheless, the usage of these plastic paddings needs to be investigated, so that they do not form local high spots of pressure that might cause more harm to the leg. On top of that, extra protection and caution should be considered when applying bandage to the shin bone especially to the area palpable below the knee.

3.3.4 Experimental Validation for the Models

As mentioned in Section 2.2.4, the only experimental work found to compare between the pressures calculated using mathematical models and the pressure measured experimentally is the work reported by Macintyre et al. [78]. However, they calculated the pressure by

estimating the amount of extension in the fabric used; thus, experimental verification of the models developed based on thin and thick wall cylinder is necessary. This section reports the experimental work carried out to validate the models.

Materials and Method

The test rig: A simple test rig was designed (Figure 3.10). The rig is composed of a cylinder of $0.114m$ diameter and $0.55m$ length, a wooden base with a clamp with rubber padding to hold the bandage tightly from one of its two ends, a load carrier to fastened to the other side of the bandage, and a $1.6kg$ load which is hung from the load carrier and used to apply constant known tension to the bandage ($15.97N$).

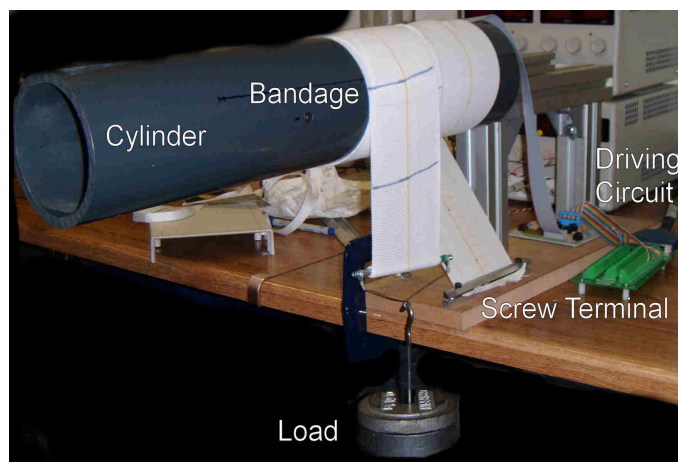


Figure 3.10: Rig used in the experiment

Sensors: Four FlexiForce sensors from the lowest force range ($0-4.4N$) ($0-464mmHg$) were used in this experiment. They were connected to a conditioning circuit that powers up the sensors with $5V$. The conditioning circuit was also designed to amplify and filter out the signal using a first-order low-pass filter with cut-off frequency set to $10Hz$, which was found experimentally to remove most of the noise in the signal (see Section 7.2 for details). The circuit output was connected to a screw terminal board (LPR-68, NI, USA) which in turn was connected to a Mass Term 6225 USB DAQ card (NI, USA).

Due to the curved nature of the cylinder used in this experiment and due to the reported errors linked to bending flexible sensors over curved surfaces [176], the sensors were calibrated using an aneroid sphygmomanometer for the pressure range $0-40mmHg$ ($0-5.3kN/m^2$). The calibration was carried out on the same cylinder used in the experiment. The aneroid sphygmomanometer cuff was inflated by $10mmHg$ ($1.3kN/m^2$) increments from $0mmHg$ to $40mmHg$ and then deflated by $10mmHg$ decrements to $0mmHg$. The inflating and deflating process was used to address the hysteresis problem associated with these sensors and it followed other researchers' recommendations [169]. The process was repeated 15 times to overcome the repeatability error associated with both the sensor

and the aneroid sphygmomanometer. A linear fitting line was used to describe the pressure ($mmHg$) in terms of the measured voltage. The average combined nonlinearity, repeatability and hysteresis errors for the four sensors used in the experiment were found to be $\pm 13.7mmHg$ (details for the assessment method is provided in Section 5.2). However, some of the repeatability errors might have been caused by the calibration method.

The signals for calibration were acquired using a program written in LabView 8.6 (NI, USA) and the fitting lines were obtained using PASW 17 (SPSS Inc., Chicago, USA) and a program written using LabView 2009.

Pressure measurement display program: A program was written in LabView 8.6 to acquire the signals, convert them to the equivalent pressure values, display them using numerical values and store the voltage and pressure values in separate files for further processing. The signals were sampled at $1kHz$ and a software based 2^{nd} order low pass filter with $10Hz$ cut-off frequency was used to filter out the signals.

The four sensors were mounted on top of the cylinder next to one other. Due to the deficiencies associated with FlexiForce sensors, the average of the four sensors pressure output was used in reporting the measured pressure instead of using the values reported by individual sensors. This in theory should reduce the uncertainty of the measurement to $\pm 7mmHg$ for each pressure reading (details are provided in Section 5.7.3).

Computing pressures from the load: If all the load weight attached to the bandage is converted into tension force in the bandage and the effect of friction between the bandage and cylinder surface is ignored, the pressure applied by the bandage can be calculated using Equations 3.4 and 3.9 and they are $19.7mmHg$ and $19.51mmHg$ respectively.

Computing pressures from the levels of extension: The bandage used in the experiment was marked every $50mm$. These marks were used to measure the extension in the bandage material when it was applied to the cylinder using a measurement tape. The extension readings were then used to estimate the tension forces in the bandage which then was used to compute the interface pressures using Equations 3.4 and 3.9. The estimation of tension from extension was found using the fourth loading cycle of the tension extension curves of the bandage which was obtained using Instron 4031 (Instron, High Wycombe, UK). Pressure calculation was done through a routine written in MATLAB R2009b (The MathWorks Inc, Massachusetts, USA).

Experiment protocol: The $1.6kg$ load was hung from the load carrier at the end of the bandage and used to apply pressure to the sensors 20 times. Each time, the sensors' average output was recorded and the extension in the bandages was measured. The reason behind repeating the process 20 times was to reduce the uncertainty in the pressure measurements due to the systematic errors associated with the sensors used in the experiment.

Results, Analysis and Discussion

The summary of the results and the statistical analysis is provided in Table 3.1 and plotted in Figure 3.11. The mean of the averaged measured pressures was 20.15mmHg . However, considering the transducer error after using the averaging ($\pm 7\text{mmHg}$) reported earlier and the variation in the averaged measured pressures, the error of the mean of the averaged measured pressure has been calculated and found to be $\pm 1.86\text{mmHg}$. As the computed pressures from the load using both thin and thick wall cylinder theories (Equations 3.4 and 3.9) are within the 95% confidence intervals of the mean of the averaged measured pressure ($18.28 - 22.01\text{mmHg}$) and the 95% confidence intervals of the mean of the average computed pressures from the extension using the thick wall cylinder theory crosses with the 95% confidence intervals of the mean of the averaged measured pressure ($18.28 - 22.01\text{mmHg}$), then it can be safely concluded that the interface pressure model developed based on thick wall cylinder theory (Equation 3.9) might be able to explain the pressure induced by single-layer MCBs. The interface pressure model based on thin wall cylinder theory (Equation 3.4) might also be equally suitable to estimate the pressures applied by MCBs. However, as the 95% confidence intervals of the mean of the average computed pressures from the extension using the thin wall cylinder theory does not cross with the 95% confidence intervals of the mean of the averaged measured pressure; hence, the model needs further experimental validation. It is worth mentioning that the 95% confidence intervals of the mean of the averaged measured pressure ($18.28 - 22.01\text{mmHg}$) is different to the ones reported in Table 3.1 ($19.14 - 21.16\text{mmHg}$). The ($18.28 - 22.01\text{mmHg}$) has been calculated by considering both the variation in the measurement and the transducers block combined error, while the ones reported in Table 3.1 ($19.14 - 21.16\text{mmHg}$) has been calculated by considering the SE of the mean only.

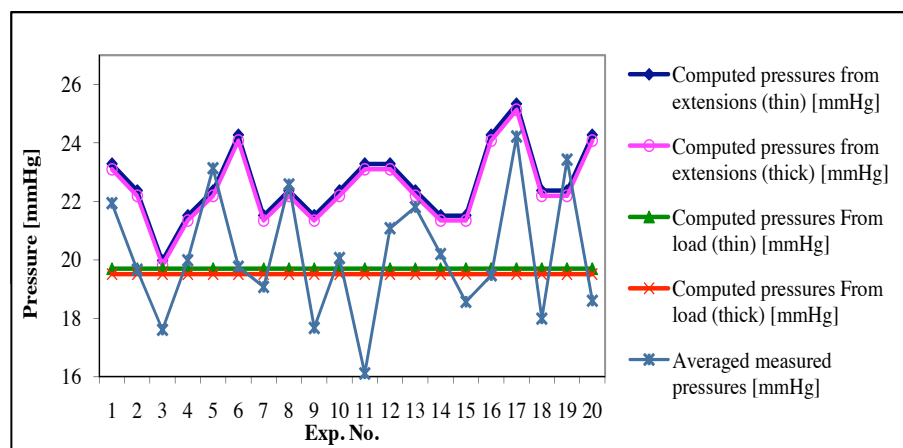


Figure 3.11: The experimental results in validating the model developed to study the effect of bandage thickness on the interface pressure. Lines connecting the pressure values are for illustrative purposes

Table 3.1: Summary of the experimental results in validating the model developed to study the effect of bandage thickness on the interface pressure. The upper and lower 95% $spread = mean \pm (1.96 \times SD)$, and the upper and lower 95% $CI = mean \pm (t \times SE)$, where “ t ” is critical point at 95% for the data degrees of freedom obtained from the student’s t-distribution look-up table [189]

Statistical analysis	Extension [%]	Tension calculated from extension [N]	Tension calculated from load [N]	Computed pressures from extension (thin) [mmHg]	Computed pressures from extensions (thick) [mmHg]	Computed pressures from load (thin) [mmHg]	Computed pressures from load (thick) [mmHg]	Averaged measured pressures [mmHg]
Mean	86.40	18.04	15.97	22.61	22.43	19.70	19.51	20.15
SD	2.80	1.01	0.00	1.27	1.26	0.00	0.00	2.17
SE	0.63	0.23	0.00	0.28	0.28	0.00	0.00	0.49
Upper 95% spread	91.89	20.02	15.97	25.09	24.89	19.70	19.51	24.40
Lower 95% spread	80.91	16.06	15.97	20.13	19.97	19.70	19.51	15.89
Upper 95% CI	87.70	18.51	15.97	23.20	23.01	19.70	19.51	21.16
Lower 95% CI	85.10	17.57	15.97	22.02	21.84	19.70	19.51	19.14

3.4 Interface Pressure Induced by Multi-Layered MCBs

In clinical practice, bandages are applied in the form of overlapping layers which results in multiple layers of fabric that overlay a particular point of the surface of the limb [30]. For example, MCBs applied with spiral 50% overlap technique will overlay the leg with two layers of bandage, MCBs applied with with 33% overlap will result in three layers of bandage and MCBs applied with figure-of-eight technique with 50% overlap will result in four layers of bandage [30; 66]. In addition, many MCB systems involve the use of several layers of different MCB components. Therefore, in many situations researchers need to calculate the pressure applied by several layers of bandage.

Thomas [75] calculated the pressure produced by several layers of bandage by multiplying the pressure applied by one bandage layer with the number of bandage layers, given that the tension is the same in all these bandage layers (see Equation 2.5). The problem with this derivation is that it does not consider the increase in the radius due to additional layers of bandage i.e. the later bandage layers are applied to a larger radius medium with the overall radius equivalent to the sum of the limb radius and the bandage thickness. This section will demonstrate, using the findings from the thin and the thick wall cylinder theories that additional layers cannot be treated with simple multiplication. It will compare the different models, simulate the pressure over a 3D leg and report on some of the clinical issues related to the findings.

3.4.1 Multi-Layer Bandage Interface Pressure Modeled Using Thin Wall Cylinder Theory

Equation 3.4 can be re-written so that it can be used to calculate the interface pressure applied by a multi-layer bandage.

$$P_n = \sum_{i=1}^n \frac{2T_i}{w_i D_i} \times 0.0075 \quad (3.10)$$

Where, $D_i = D + \sum_{i=1}^n 2t_{i-1}$

Where, i is the bandage layer, t_{i-1} is the extended and compressed bandage layer thickness in (m), T_i is the tension in (N), w_i is the extended bandage width in (m), D is the limb diameter in (m), D_i is the combined limb diameter and previous bandage layers thickness in (m), and P_n is the pressure induced by n number of bandage layers in ($mmHg$).

3.4.2 Multi-Layer Bandage Interface Pressure Modeled Using Thick Wall Cylinder Theory

Equation 3.9 can be re-written to estimate the interface pressure applied by a multi-layer bandage.

$$P_n = \sum_{i=1}^n \frac{T_i(D_i + t_i)}{\frac{1}{2}w_i D_i^2 + w_i t_i(D_i + t_i)} \times 0.0075 \quad (3.11)$$

Where, $D_i = D + \sum_{i=1}^n 2t_{i-1}$

Where, i is the bandage layer, t_i is the extended and compressed bandage layer thickness in (m), T_i is the tension in (N), w_i is the extended bandage width in (m), D is the limb diameter in (m), D_i is the combined limb diameter and previous bandage layers thickness in (m), and P_n is the pressure induced by n number of bandage layers in ($mmHg$).

3.4.3 Computational Comparison Between the Multi-Layer Bandage Pressure Models

In order to compare the pressure estimation models for multi-layer MCBs, MATLAB R2009b was used to calculate the bandage pressure when a 100mm wide and 1mm thick MCB is applied with constant 4N tension using figure-of-eight application (4 layers of bandage) to cylinders with various radii 10mm – 75mm. The pressure was calculated using Equations 2.5, 3.10 and 3.11 and results are reported in Figure 3.12, which illustrates that using simple multiplication will result in overestimating the pressure. The difference between the pressures calculated using thin and thick wall cylinder models is small with differences being significant at small radii (pressure difference is > 5%).

The same bandage is now used to simulate pressure maps on the 3D model of a real leg. The pressure values were calculated using MATLAB R2009b. LabView 2009 was used

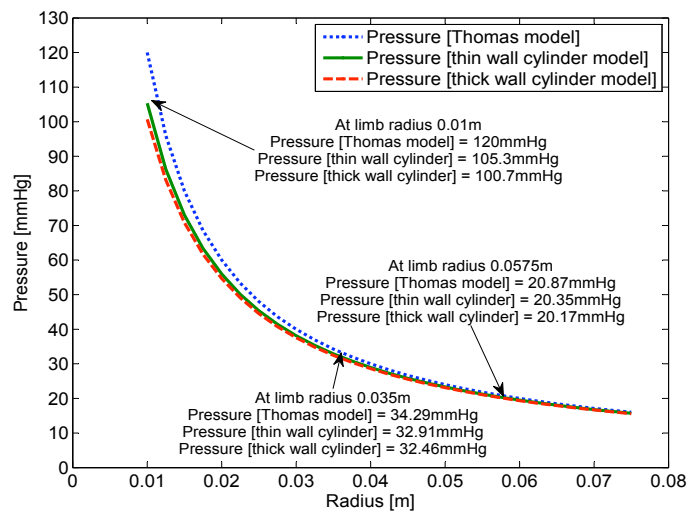


Figure 3.12: Pressure calculated using three models; Thomas [75] model, thin wall cylinder model and thick wall cylinder model vs. radius

to simulate the pressure values estimated using the three models for 103 points on the 3D model. Simulation results are illustrated in Figures 3.13, 3.14 and 3.15. The white areas on the three plots demonstrate that Thomas's model [75] will overestimate the pressure over the bony prominence and indicates that the bandage is applied with dangerous levels of pressure (more than 60mmHg) [71]. The thick cylinder model illustrates also this peak in pressure, however, the areas of dangerous peak pressures are much smaller.

The clinical importance of the new models reported in this section lies in their ability to explain some of the experimental results reported by other researchers. For example Dale et al. [107] reported that when they applied a cohesive bandage as the fourth part of four-component system, the bandage produced only 73.2% of the pressure produced when it was applied directly to the limb at the same extension and overlap. This led some researchers to think that when superimposing stockings the overall pressure is given by simple addition of pressure that these stockings provide when they are applied individually to the leg, whereas applying MCBs on top of each other will result in minor increase in the interface pressure [142]. The above models explain the reason behind the apparent differences in the behavior of bandages and stockings. Superimposing stockings involve the usage of two to three stockings i.e. two to three layers of thin pressure garment. This means that when the sum of the interface pressure applied by individual stockings are compared to the interface pressure, when they are superimposed, there will be very small differences in the pressure. However, when bandages are superimposed, they involve a higher number of bandage layers. This will have an impact on the interface pressure due to the larger increase in limb diameter. This means that superimposing bandages will result in a noticeable reduction in the interface pressure when compared to the sum of their individual pressures when they are applied directly to the limb.

To explain how these new models help, MATLAB R2009b is used to calculate the per-

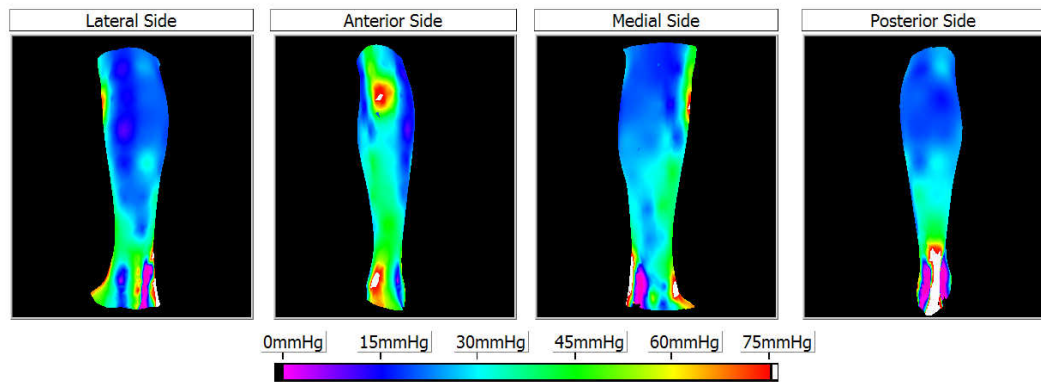


Figure 3.13: The simulated pressure map over a real leg when four layers of bandage are applied to the leg. The pressure calculated using the pressure model reported by Thomas [75] (Equation 2.5)

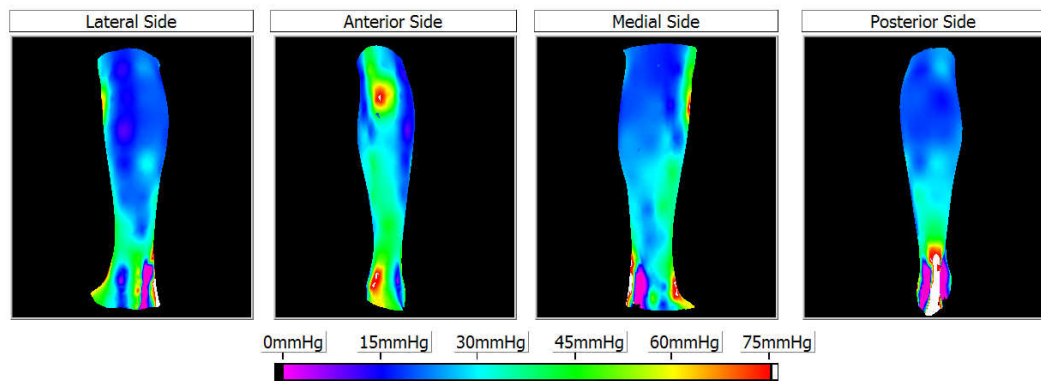


Figure 3.14: The simulated pressure map over a real leg when four layers of bandage are applied to the leg. The pressure calculated using the pressure model based on thin cylinder wall theory (Equation 3.10)

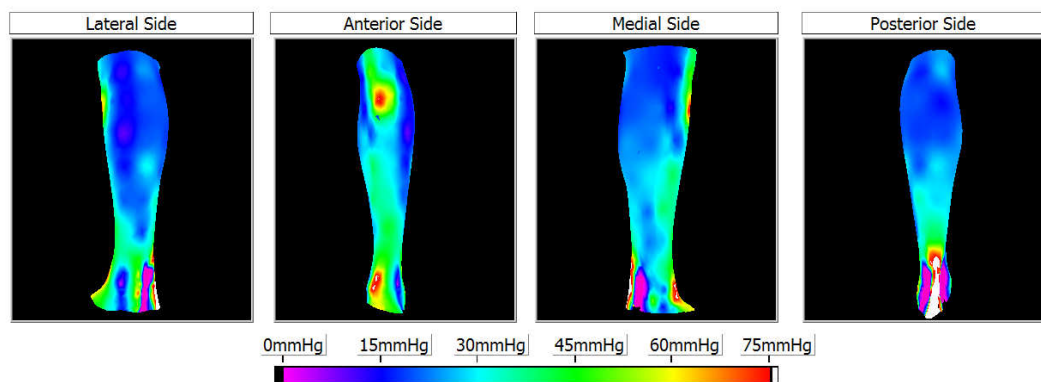


Figure 3.15: The simulated pressure map over a real leg when four layers of bandage are applied to the leg. The pressure calculated using the pressure model based on thick cylinder wall theory (Equation 3.11)

centage of the interface pressure that every single layer of bandage will provide compared to the interface pressure applied by the first layer of the bandage using thick cylinder wall model for different limb circumferences ($150 - 600mm$), with bandage thickness set to $1mm$. The results are shown in Figure 3.16. The cohesive component is normally applied over 8 layers of other bandages [30]. This means if the bandage is applied to a $18cm$ circumference leg, the pressure applied will be about 78% of the pressure that the same bandage will apply when it is applied directly to the leg. This is very close to what Dale et al. [107] have reported. On the other hand, stockings are normally superimposed on one layer of stocking i.e. the superimposed stocking will apply 97% of the pressure that it will apply to the same leg if applied directly. This is again very close to the values reported by Cornu-Thenard et al. [142].

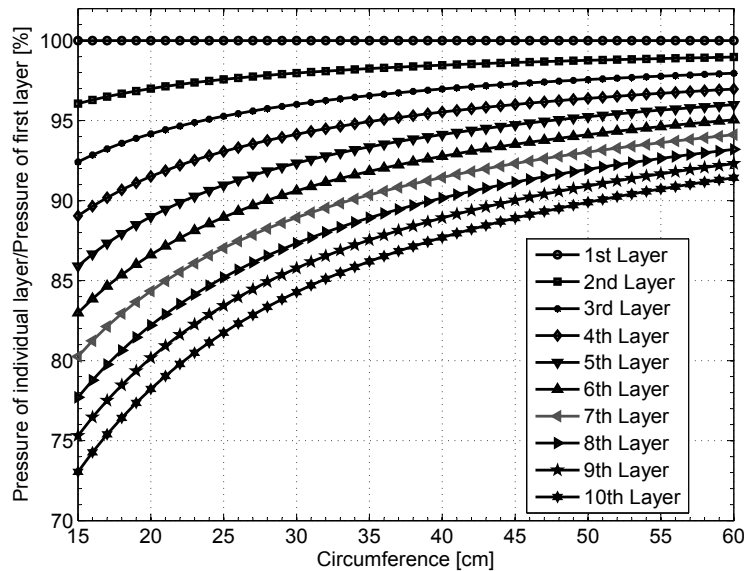


Figure 3.16: The pressure of individual layers as a percentage of the first layer pressure for variable limb circumference

3.4.4 Experimental Validation

The only works found in literature to discuss experimental issues related to multi-layer bandaging application are those published by Dale et al. [107], Cornu-Thenard et al. [142] and Melhuish et al. [84]. Nevertheless, none of these studies compared the theoretical pressure expectation with the measured pressure values. The objective of the following experimental work is to compare the estimated pressure applied by multi-layer MCBs using theoretical models with the ones measured experimentally.

Materials and Method

Experiment hardware and software setup: The same test rig, FlexiForce sensors, pressure measurement display program and method to compute pressures from the levels of

extension in the MCB, which were used in Section 3.3.4 were used in this experiment. The only differences in this experiment are that the interface pressures was computed using Equations 2.5, 3.10 and 3.11 and the sensors were re-calibrated for the pressure range $0 - 80\text{mmHg}$. The average combined nonlinearity, repeatability and hysteresis errors for the four sensors used in the experiment after re-calibration was found to be $\pm 20.86\text{mmHg}$ (details for the assessment method is provided in Section 5.2). However, using the average of the four sensors pressure output to report the measured pressure instead of using the values reported by individual sensors would reduce the uncertainty of the measurement in theory to $\pm 11\text{mmHg}$ for each pressure reading.

Experiment Protocol: Three layers of bandage were applied to the cylinder with mounted pressure sensors, with the 1.6kg load attached to the last bandage layer. The three layer bandage was applied 10 times to reduce the uncertainty in the pressure measurements due to the systematic errors associated with the sensors used in the experiment. In each of these iterations, the extension in the three layers were measured and used to estimate the tension and subsequently calculate the pressure using Thomas', thin wall cylinder and thick wall cylinder models for multi-layer bandages. The pressure calculated was then compared to the measured pressure.

Results, Analysis and Discussion

Table 3.2: Summary of the experimental results in validating the models developed to calculate the pressure applied by multi-layer MCBs. The upper and lower 95% *spread* = $mean \pm (1.96 \times SD)$, and the upper and lower 95% *CI* = $mean \pm (t \times SE)$, where “*t*” is the critical point at 95% for the data degrees of freedom obtained from the student’s t-distribution look-up table [189]

Statistical analysis	Layer extension [%]			Layer Tension [N]			Computed pressures [mmHg]			
	Layer 1 extension [%]	Layer 2 extension [%]	Layer 3 extension [%]	Layer 1 Tension [N]	Layer 2 Tension [N]	Layer 3 Tension [N]	Computed pressures Thomas [mmHg]	Computed pressures thin cylinder [mmHg]	Computed pressures thick cylinder [mmHg]	Averaged measured pressures [mmHg]
Mean	46.40	63.20	73.60	8.53	12.14	14.73	44.36	43.44	43.08	34.70
SD	13.46	14.21	13.46	2.84	3.11	3.48	8.30	8.11	8.04	6.58
SE	3.01	3.18	3.01	0.63	0.69	0.78	1.86	1.81	1.80	1.47
Upper 95% spread	72.78	91.05	99.98	14.09	18.23	21.56	60.63	59.34	58.84	47.60
Lower 95% spread	20.02	35.35	47.22	2.97	6.05	7.90	28.10	27.55	27.32	21.80
Upper 95% CI	53.20	70.38	80.40	9.97	13.71	16.49	48.56	47.54	47.14	38.02
Lower 95% CI	39.60	56.02	66.80	7.10	10.57	12.97	40.17	39.34	39.01	31.37

A summary of the results and analysis is provided in Table 3.2 and plotted in Figure 3.17. The mean of the averaged measured pressure was 34.70mmHg . The combined error of the variation in the measurement and the transducer error was $\pm 4.81\text{mmHg}$. This means that the 95% CI of the mean of the averaged measured pressures ($29.89 - 39.51\text{mmHg}$) will cross the 95% CI of the mean of the computed pressures using the thin and thick wall cylinder theory models (Equations 3.10 and 3.11). This indicates that multiplying the pressures applied by one layer of bandage with the number of bandage layers or ignoring the increase radius of the limb due to former applied bandage layers might result in reporting pressures which are higher than the actual pressures applied to the leg. It is worth mentioning that the 95% confidence intervals of the mean of the averaged measured pressure ($29.89 - 39.51\text{mmHg}$) differs from the ones reported in Table 3.2 ($31.37 - 38.02\text{mmHg}$). The ($29.89 - 39.51\text{mmHg}$) has been calculated by considering both the variation in the measurement and the transducer error, while the ones reported in Table 3.2 ($31.37 - 38.02\text{mmHg}$) has been calculated by considering the SE of the mean only.

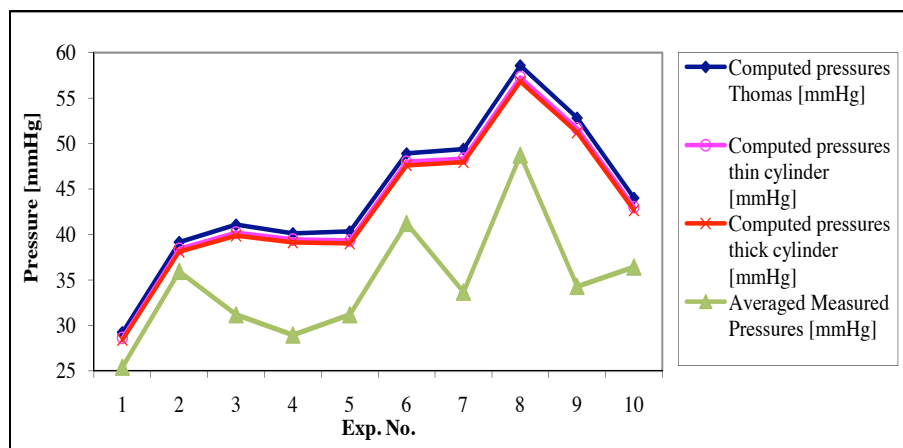


Figure 3.17: The experimental results in validating the models developed to calculate the pressure applied by multi-layer MCBs. Lines connecting the pressure values are for illustrative purposes

The above findings are well demonstrated in Figure 3.17. Figure 3.17 shows that the pressures measured were significantly different from the computed pressures using Equations 2.5, 3.10 and 3.11. Nevertheless, for the first two iterations the calculated and measured values were much closer to each other than the other eight iterations, which might be explained by the fact that the tension was calculated from the fitting loading line for the fourth cycle tension-elongation curve for the bandage; thus, as the bandage was used in the previous experiment (Section 3.3.4 and in this experiment, the fourth cycle might not present a good approximation for the tension elongation relationship, knowing that the bandage performance degrades with usage. In addition, due to the nature of bandage application, the tension applied in the first and second layers might be affected

heavily with the large hysteresis in the tension elongation curves. Other factors might have also contributed to the difference between the measured and calculated pressures (see Section 4.4 for details).

Despite the fact the 95% CI of the mean measured pressures crosses with the 95% CI of the mean of the computed pressures using Equations 3.10 and 3.11, the results illustrated in Figure 3.17 raise doubts about the validity of the models. Therefore, another set of experiments is recommended where every single MCB layer is connected to a hung load. Bandages also need to be changed through the experiment to avoid potential problems of degradation. However, as the single-layer thick wall cylinder model was found to agree with the experimental results, both the thin and thick wall cylinder models for multi-layer MCB were found to be in agreement with the experimental results and the thick wall cylinder model was found to be the most accurate theoretically, the thick wall cylinder theory model for interface pressure was used throughout the thesis to compare the pressure computed from extension to the pressures measured using pressure transducers.

3.5 Effect of Biaxial Tension Forces on the Interface Pressure

3.5.1 Mathematical Modeling

In the previous models for the interface pressure, the leg was treated as a cylinder with curvature changing only in the circumferential direction. In reality, there is a small change in the leg curvature in the longitudinal direction also. These changes are significant at the bony prominence of the ankle. Therefore, the thin cylinder model for single layer (Equation 3.4) was altered to accommodate these curvature changes as shown below:

$$P = P_H + P_L \quad (3.12)$$

Where, P_H is the pressure due to the curvature change in the circumferential direction of the leg in (N/m^2) and P_L is the pressure due to the curvature change in the longitudinal direction of the leg in (N/m^2) . P_H and P_L can be expressed as follows:

$$P_H = \frac{T_H}{R_H} \times 0.0075 \quad (3.13)$$

Where, T_H is the tension per unit length of bandage in the circumferential direction of the leg in (N) and R_H is the radius of curvature in the circumferential direction of the leg in (m) .

$$P_L = \frac{T_L}{R_L} \times 0.0075 \quad (3.14)$$

Where, T_L is the tension per unit length of bandage in the longitudinal direction of the leg in (N) and R_L is the radius of curvature in the longitudinal direction of the leg in

(*m*). Hence,

$$P = \left(\frac{T_H}{R_H} + \frac{T_L}{R_L} \right) \times 0.0075 \quad (3.15)$$

This model is the same as the model proposed by De Bruyne and Dvořák [76] (see Equation 2.4). Instead of expressing the pressure in terms of tension per unit length of bandage it can be expressed in terms of the bandage width and length which the tension is applied to:

$$P = \left(\frac{T_H}{R_H w_W} + \frac{T_L}{R_L w_L} \right) \times 0.0075 \quad (3.16)$$

Where, T_H is the tension in the bandage in the circumferential direction of the leg in (*N*), R_H is the radius of curvature in the circumferential direction of the leg in (*m*), T_L is the tension in the bandage in the longitudinal direction of the leg in (*N*), R_L is the radius of curvature in the longitudinal direction of the leg in (*m*), w_W is the extended bandage width in (*m*) which the tension T_H is applied to and w_L is the extended bandage length in (*m*) which the tension T_L is applied to.

Equation 3.16 shows that the pressure due to the longitudinal change in curvature is dependent on the radius of the curvature which is normally very large and on the tension in the longitudinal direction or across the width of the bandage. In the case of the MCB, the tension is normally applied to the length of the bandage. However, due to the Poisson's effect, a compression force will be generated along the width of the bandage, which is normally small $1 - 2N$ when the bandage is applied by 50% extension (see Section 4.5).

3.5.2 Theoretical Simulation for the Effect

Figure 3.18 shows the effect of the biaxial force in a bandage on the interface pressure. Circumferential tension force and the longitudinal compression force were set to $10N$ and $1N$ respectively and the bandage width and length to which the tension is applied were set to $100mm$. Clearly, the effect of biaxial forces will be significant at bony prominences like the malleolus where the curvature radius in the longitudinal direction is sharp (radius can be as small as $10mm$).

3.6 Effect of Angle of Application on the Interface Pressure

In order to apply bandages all the way from the ankle towards the knee, they need to be applied at an angle which depends on the leg size and technique of application. Ghosh et al. [73] reported that bandages are applied at 50° to the vertical (length of the leg). They demonstrated that as the angle decreased from 90° to 50° the pressure applied by seven different bandages decreased. However, they have commented that the reason behind the decrease in the pressure is that there were fewer layers of bandage covering the sensor when the angle decreased; thus, more work should be carried out to investigate the

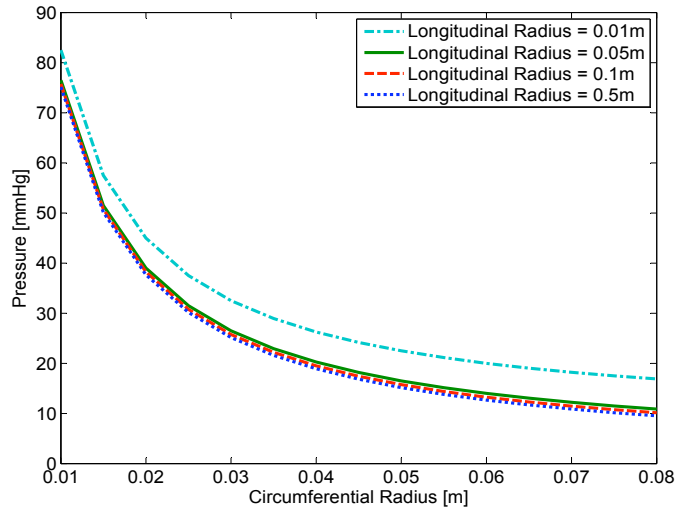


Figure 3.18: The effect of biaxial forces on the interface pressure

effect of angle application on the interface pressure. Nelson [7] addressed the impact of angle of application on the interface pressure theoretically. She reported that due to the change in leg curvature in both the longitudinal and circumferential directions, applying bandages at an angle will result in higher pressures at leg sites with sharp circumferential and longitudinal curvatures than sites with only sharp circumferential curvatures. This section will attempt to model the effect of angle application theoretically.

3.6.1 Mathematical Modeling

Figure 3.19 shows the forces in the bandage when it is applied at an angle. Equation 3.16 can be re-written with the tension force components as shown in Figure 3.19.

$$T_H = T_E \sin(\theta) + T_W \cos(\theta) \quad (3.17)$$

$$T_L = T_E \cos(\theta) + T_W \sin(\theta) \quad (3.18)$$

$$P = \left(\frac{T_E \sin(\theta) + T_W \cos(\theta)}{R_H} + \frac{T_E \cos(\theta) + T_W \sin(\theta)}{R_L} \right) \times 0.0075 \quad (3.19)$$

Where, θ is the angle between the length of the bandage and the limb in degrees, T_E is the tension per unit length in the length direction of the bandage in (N) and T_W is the tension per unit length in the width direction of the bandage in (N).

Instead of expressing the pressure in terms of tension per unit length it can be expressed in terms of the bandage width and length which the tension is applied to:

$$P = \left(\frac{T_E \sin(\theta)}{R_H w_W} + \frac{T_W \cos(\theta)}{R_H w_L} + \frac{T_E \cos(\theta)}{R_L w_W} + \frac{T_W \sin(\theta)}{R_L w_L} \right) \times 0.0075 \quad (3.20)$$

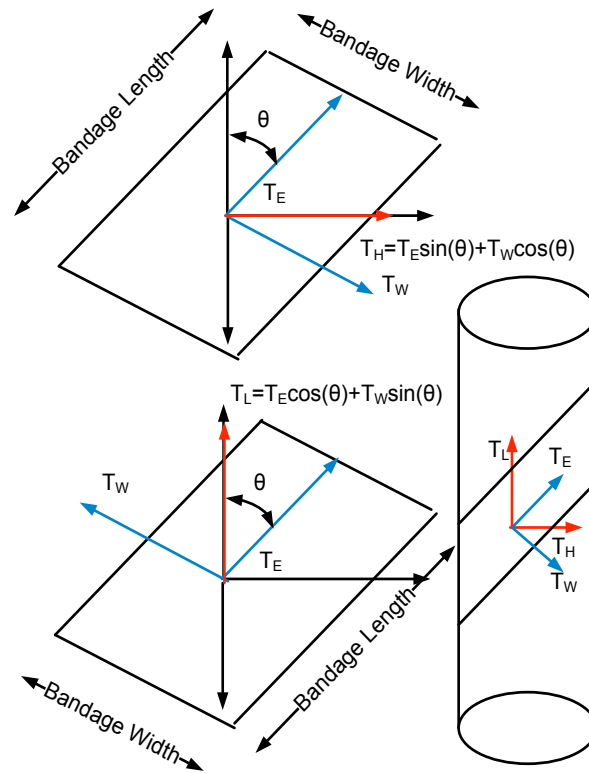


Figure 3.19: Tension forces in bandage when applied in angle

Where, θ is the angle between the length of the bandage and the limb in degrees, T_E is the tension in the length direction of the bandage in (N), T_W is the tension in the width direction of the bandage in (N), R_H is the radius of curvature in the circumferential direction of the leg in (m), R_L is the radius of curvature in the longitudinal direction of the leg in (m), w_W is the extended bandage width in (m) which the tension T_E is applied to and w_L is the extended bandage length in (m) which the tension T_W is applied to.

3.6.2 Theoretical Simulation for the Angle Effect

Figure 3.20 illustrates the effect of applying the bandage in angle on the interface pressure. The plot is for a bandage with tension in the length direction is set to $10N$, tension in the width direction is set to $1N$, circumferential radius is set to $0.05m$, longitudinal radius is set to $0.1m$ and bandage width is set to $0.2m$ and bandage width and length are set to $0.1m$. Figure 3.20 shows that as the angle decreases the pressure applied by the bandage will increase first due to the transverse compression force generated in the bandage. However, this increase will start to diminish and then decreases as the bandage angle of application decreases further. This contradicts with Ghosh et al. [73] experimental findings.

From a clinical point of view, Figure 3.20 might explain why nurses produce reverse gradient pressure profile with pressure higher at knee compared to ankle even when they try to apply bandages with constant extension, which in theory should produce graduated

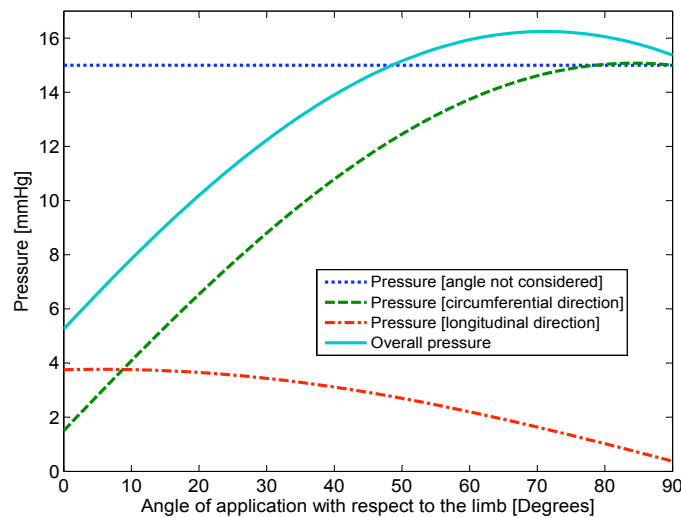


Figure 3.20: The effect of changing the application angle on the interface pressure

pressure. This can be explained by the fact that nurses apply bandages with an angle of $30^\circ - 60^\circ$ at the ankle and with an angle of $80^\circ - 90^\circ$ at the knee. Therefore, even if the ankle has a smaller circumference, which, in theory, will result in higher pressure, if the bandage is applied at small angle ($30^\circ - 50^\circ$) at the ankle and at an angle of 80° at the knee, the pressure at the ankle might be lower than the pressure applied by the same tension to the knee (larger radius of curvature). However, this will depend also on the amount of compressive tension generated in the bandage width direction as it is extended in its length direction, as bandages with small compressive forces will provide smaller window of where pressure is higher than the expected pressure when angle is not considered (see Figure 3.21).

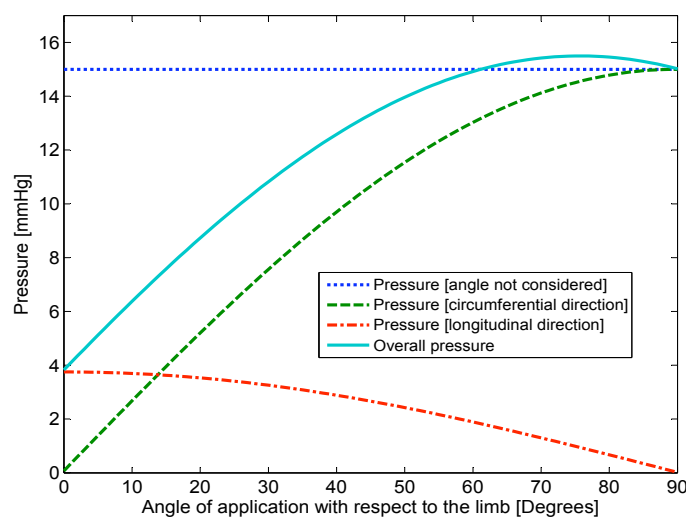


Figure 3.21: The effect of changing the application angle on the interface pressure when the tension in the width direction of the bandage is set to $0.1N$

3.7 Impact of Change in Limb Shape on the Interface Pressure

Many researchers are interested in measuring the change in pressure under the compression devices caused by the interaction of the change in the calf muscles size and MCBs and MCSs [8; 63; 64; 72; 190]. The reason behind this interest is that muscle activity in the leg during movement results in a change in the limb size, which results in a change in the extension in the MCBs and MCSs fabric. This leads to a change in the tension forces in the fabric and hence a change in the interface pressure applied by the pressure garment. This section will study the impact of change in limb shape on the interface pressure using analytical method based on thin and thick wall cylinder theories.

3.7.1 Thin Cylinder Wall Theory Model

The increase in limb size can be assumed to result in a circumferential strain in the MCBs and MCSs. This circumferential strain can be shown to be equal to the diametrical strain [85]. In addition, the thickness of the bandage is assumed to be negligible in this theory; thus, the radial stress can be assumed to be very small and negligible compared to the hoop stress and the longitudinal stress. Therefore, the diametrical strain can be expressed as follows:

$$\frac{\Delta D}{D} = \frac{1}{E}(\sigma_H - \nu\sigma_L) \quad (3.21)$$

Where, ΔD is the change in the limb diameter in (m), D is the original limb diameter in (m), E is the Youngs modulus for the compression material in (N/m^2), σ_H is the hoop stress in (N/m^2), σ_L is the longitudinal stress in (N/m^2) and ν is the Poissons ratio. Poissons ratio is the ratio of the strain (contraction) normal to the applied load, to the strain (extension) in the direction of the applied load [85] (Figure 3.22).

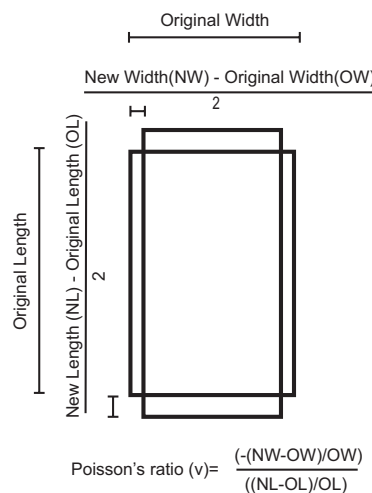


Figure 3.22: Poisson's ratio for a bandage [thin cylinder wall]

Hoop stress can be expressed as Equation 3.1 and longitudinal stress can be expressed as follows [85]:

$$\sigma_L = \frac{PD}{4t} \quad (3.22)$$

Hence, the change in diameter can be expressed as in the following equation:

$$\Delta P = \frac{4\Delta DEt}{D^2(2 - \nu)} \quad (3.23)$$

Where, ΔP is the change in the pressure in (N/m^2) that is caused by the change in limb diameter and E is the dynamic Young's modulus for the bandage 'Chord modulus' in (N/m^2).

By assuming that the strain in the circumferential direction will not result in changes in the width of the bandage or, if any, it will be minimal and can be ignored (i.e. the Poissons ratio is approximately zero), then Equation 3.23 can be simplified to the following:

$$\Delta P = \frac{2\Delta DEt}{D^2} \quad (3.24)$$

The above formula can be used to predict the change in the interface pressure (relative values) due to the change in the limb shape.

3.7.2 Thick Cylinder Wall Theory Model

By assuming that the increase in limb size will result in a circumferential strain in MCB and MCS, and as the diametrical strain can be shown to be equal to the circumferential strain [85]; therefore, diametrical strain can be expressed as follows:

$$\frac{\Delta D}{2R} = \frac{1}{E}(\sigma_H - \nu\sigma_R - \nu\sigma_L) \quad (3.25)$$

Where, σ_R is the radial stress in (N/m^2).

The stresses at the inner radius of the compression material (Figure 3.5) can be shown to be as follows [85]:

$$\begin{aligned} \sigma_H &= \frac{PR^2}{([R+t]^2 - R^2)} \left[1 + \frac{[R+t]^2}{R^2} \right] \\ \sigma_R &= \frac{PR^2}{([R+t]^2 - R^2)} \left[1 - \frac{[R+t]^2}{R^2} \right] \\ \sigma_L &= \frac{PR^2}{([R+t]^2 - R^2)} \left[1 - \frac{[R+t]^2}{R^2} \right] \end{aligned} \quad (3.26)$$

Hence, the change in diameter can be expressed as follows:

$$\Delta D = \frac{2\Delta PR^3}{E([R+t]^2 - R^2)} \left(\left[1 + \frac{[R+t]^2}{R^2} \right] - 2\nu \left[1 - \frac{[R+t]^2}{R^2} \right] \right) \quad (3.27)$$

$$\Delta D = \frac{2\Delta PR^3}{E(2Rt + t^2)} \left(\left[\frac{2R^2 + 2Rt + t^2}{R^2} \right] - 2\nu \left[\frac{-2Rt - t^2}{R^2} \right] \right) \quad (3.28)$$

By assuming now that $t^2 \ll R^2$, then the above equation can be simplified to the following:

$$\Delta D = \frac{2\Delta PR^2}{2Et} \left(\frac{2R}{R} + \frac{2t}{R} + \frac{2\nu t}{R} \right) \quad (3.29)$$

$$\Delta D = \frac{2\Delta PR}{Et} (R + t + \nu t) \quad (3.30)$$

Which can be re-written to describe the change in pressure due to the change in limb size:

$$\Delta P = \frac{\Delta DEt}{2R(R + t + \nu t)} \quad (3.31)$$

If the Poissons ratio is assumed to be very small and the change in the longitudinal and radial directions is assumed to be negligible, then Equation 3.31 can be re-written as follows:

$$\Delta P = \frac{\Delta DEt}{2R(R + t)} \quad (3.32)$$

3.7.3 Comparison between the Two Models and Theoretical Simulation

Equation 3.32 demonstrates that the compression material thickness will be an important factor if the limb radius is small. The difference in the pulsation pressure calculated using Equations 3.24 and Equation 3.32 is plotted in Figure 3.23, which shows clearly that the difference in pulsation pressure increases as the compression material thickness increases and it is more than 3% if the compression material thickness is $2mm$. This is significant as the minimum number of layers that an MCB applied in a spiral with 50% overlap, can have, is two layers which corresponds to $2mm$ wall thickness if the MCB thickness is assumed to be $1mm$. Based on the above discussion, the model based on thick wall cylinder theory (Equation 3.32) will be used through out the rest of this section.

In order to demonstrate how the model can be used, a simulation for the dynamic pressure produced by Mediven 550 (Medi, Bayreuth, Germany) is shown in Figure 3.24. This was achieved by using the Chord modulus for Mediven 550, which was found to be $2.622MN/m^2$. This value was calculated from the data provided by Wegen-Franken et al. [64]. The mean pressure used to plot the graph was also obtained from the data published by Wegen-Franken et al. [64], who found that the mean pressure that Mediven 550 applies to a cylinder with $200mm$ circumference is $39.13 \pm 1.08mmHg$.

Equation 3.32 can be used with Chord modulus to explore dynamic changes in the interface pressure during locomotion. For example, if the information about the detailed change in limb shape during locomotion is available, the model can used to simulate the

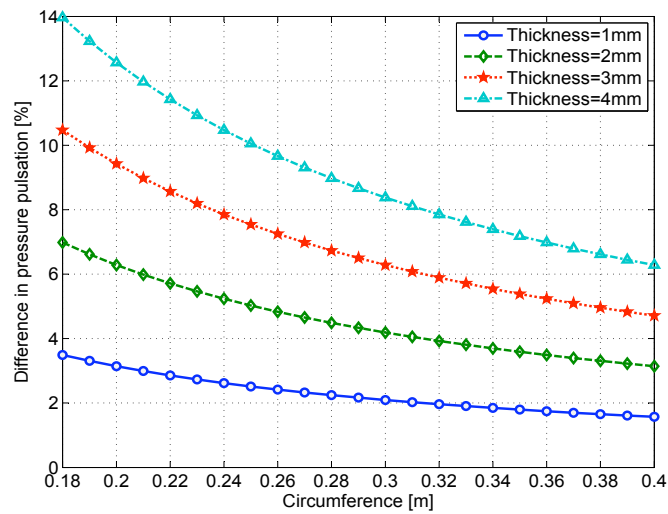


Figure 3.23: The percentage difference in pressure pulsation calculated using thin and thick wall cylinder theories

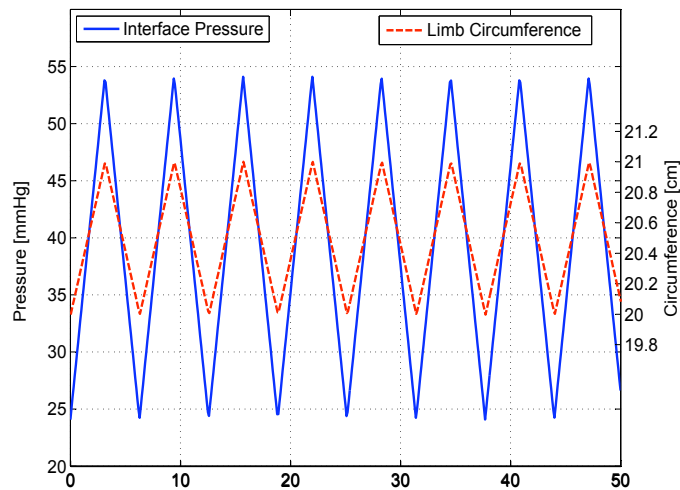


Figure 3.24: Change in interface pressure caused by 10mm change in the limb circumference.

interface pressure and select, for example, exercises that will accelerate ulcer healing.

However, it should be mentioned at this point that the above models are based on the assumption that the change in limb size will result only in a circumferential strain in the compression fabric and all other strains are negligible. This needs to be verified experimentally. Moreover, assuming that the Poissons ratio for a compression bandage is small needs to be verified experimentally.

3.8 The Effect of Sensor's Physical Dimensions on the Interface pressure

As the literature review revealed, some researchers attempted to estimate the perturbation in measured pressure due to sensor's physical dimension (Section 2.3.3). Vinckx et al. [86] have developed a mathematical model to estimate the perturbation effect for thin plate sensors (see Equation 2.8). The model they have developed was not verified experimentally. In fact, no experimental work was found on the effect of sensor aspect ratio or physical dimensions on the interface pressure. Therefore a series of experiments were designed to investigate the effect and test the mathematical model developed by Vinckx et al. [86]. It is worth mentioning that investigating Equation 2.8 derivation showed an error during simplification; thus, the model was kept at its complex form without any simplifications:

$$\begin{aligned}
 C_{pp} &= \frac{\sin(\alpha/2 + \gamma)}{\sin(\alpha/2)} \\
 \alpha &= \frac{D_S}{R} \\
 \gamma &= \arccos\left(\frac{R}{R+d}\right)
 \end{aligned} \tag{3.33}$$

Where, d is the sensor thickness in (m), D_S is the sensor diameter in (m), C_{PP} is the coefficient of pressure perturbation, R is the limb radius in (m).

3.8.1 Experimental Work to Investigate the Effect of Sensor Physical Dimensions on the Interface Pressure

Objectives of the Experiment

- To investigate the effect of sensor thickness and length on the measured pressure.
- To compare the measured perturbation in pressure with the calculated values of perturbation in pressure.

Materials and Method

The test rig: The rig used in this experiment was the same rig used in Section 3.3.4.

Sensors: Four FlexiForce sensors from the lowest force range ($0-4.4N$) were used in this experiment. They were connected to a conditioning circuit that powers up the sensors with $5V$. The conditioning circuit was also designed to amplify and filter out the signal using a low pass filter with cut-off frequency set to $10Hz$. The circuit outputs were connected to a screw terminal board (LPR-68) which in turn was connected to a Mass Term 6225 USB DAQ card.

Each sensor was calibrated using deadweights from 0 – 105g or in terms of pressures 0 – 109mmHg. The calibration process involved stacking 13 loads on top of one another and, then, removing them one by one. The process was repeated five times. The averaged measured voltage values were used to obtain the best linear fitting line that describes the pressure in mmHg obtained by transformation from the measured voltage. The stacking and un-stacking process was used to address the hysteresis problem associated with these sensors and it follows other researchers recommendations [169]. Repetition of the calibration process was conducted in order to reduce the effect of the repeatability error on the calibration process.

However, because of the curved nature of the cylinder used in this experiment and the reported errors linked to bending flexible sensors over curved surfaces [176], the sensors were re-calibrated individually using an aneroid sphygmomanometer between 0 – 120mmHg. The calibration was carried out by inflating the aneroid sphygmomanometer to 120mmHg and then deflating by 10mmHg decrements, where the transducer output was recorded at each of these decrements. The process was repeated ten times to overcome the repeatability error associated with both the sensor and the aneroid sphygmomanometer. The best linear fit was used again to describe the pressure (mmHg) in terms of the measured voltage.

The average combined accuracy, repeatability and hysteresis errors for the sensors used in the experiment was found to be $\pm 18\text{mmHg}$. This was obtained from calibration data using deadweights.

The signals for calibration were acquired in both calibration processes using a program written in LabView 8.6 and the fitting lines were obtained using Excel 2003 (Office 2003, Microsoft, USA).

Pressure Measurement Display Program: A program was written in LabView 8.6 to acquire the signals, convert them into the equivalent pressure values, display them using numerical values and store the voltage and pressure values in separate files for further processing. The signals were sampled at 1kHz and a software based on 2nd order low pass filter with 10Hz cut-off frequency used to filter out the signal.

Experiment Protocol: In order to check the effect of sensor length, the four sensors were placed next to each other in four different configurations as shown in Figure 3.25. In order to alter the thickness of the sensors, rubber pads (1.5mm thick, 14mm wide, length the same as the sensor configurations length) were used. Two pads were used for each configuration to obtain three different thicknesses. For configurations with multiple sensors, the average value of the sensors was obtained and used in the analysis as a representation for the configuration.

A type 3C MCB was used to apply pressure to the cylinder and the transducers in this experiment (Figure 3.26). The 1.6kg load was connected to the bandage and used to apply a constant known tension. This should, theoretically, result in the bandage applying

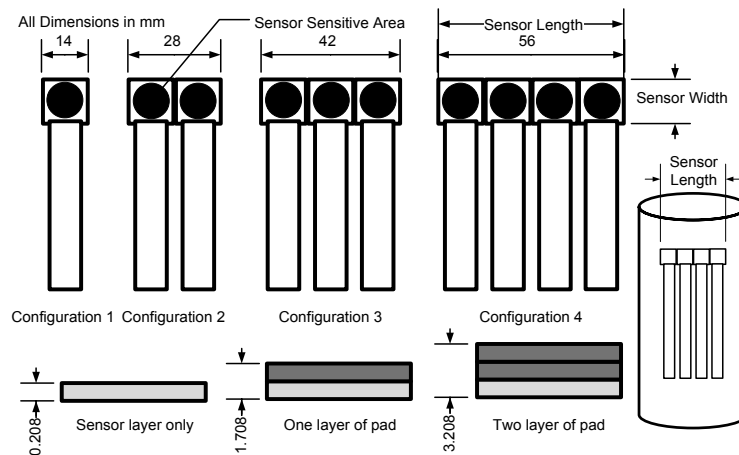


Figure 3.25: FlexiForce sensors' arrangement

19.51mmHg to the cylinder. This was calculated using Equation 3.9. For each sensor-padding configuration, the bandage was applied 10 times, to reduce the uncertainty in the pressure measurements caused by the systematic errors associated with the FlexiForce sensors.

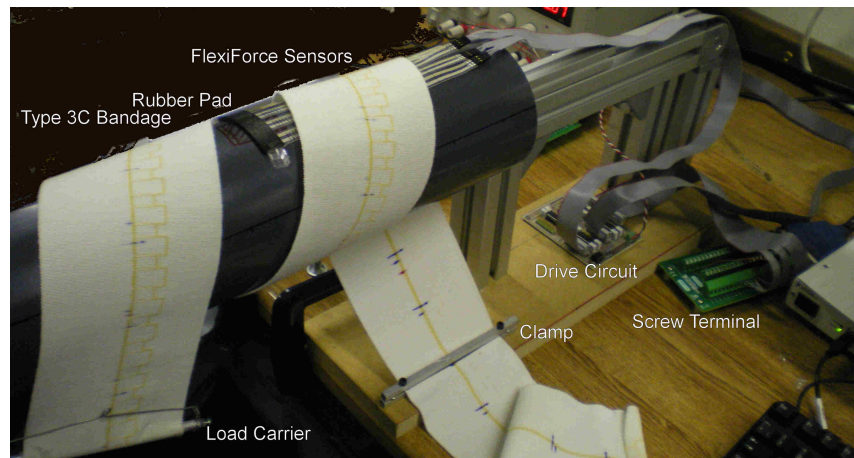


Figure 3.26: Class 3C MCB is used to apply pressure to FlexiForce sensors

In order to check if the results fit with the model proposed by Vinckx et al. [86], the values for transducer thickness and length and the cylinder radius were used to calculate the amount of perturbation in the transducer output for each length-thickness configuration using Equation 3.33. MATLAB R2009b was used to calculate the values of the theoretical perturbation.

Results, Analysis and Discussion

The average value from the ten repeats, the standard error of the mean and the overall combined error of the measurement variation and the sensors accuracy error are sum-

marized in Table 3.3. Figures 3.27 and 3.28 illustrate that as the transducer thickness increases, the transducer reports higher pressure values. However, the effect of the transducer thickness decreases as the transducer length increases.

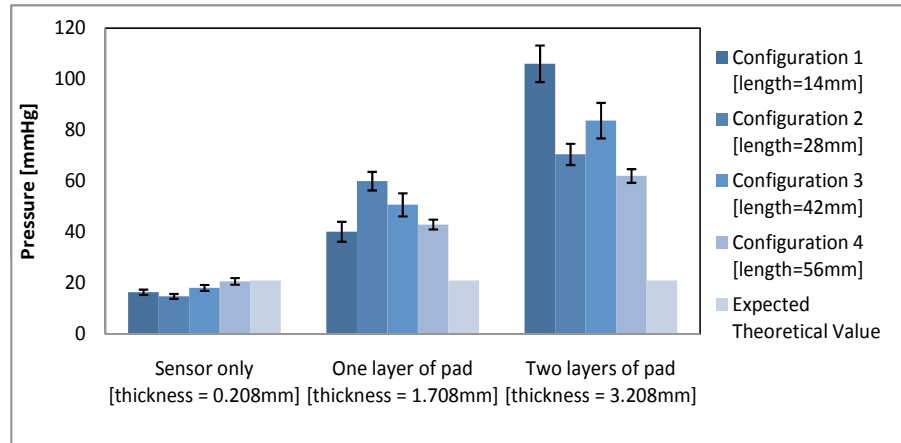


Figure 3.27: The effect of sensor aspect ratio on measured pressure (deadweights calibration). The error bars represent the standard error of the mean

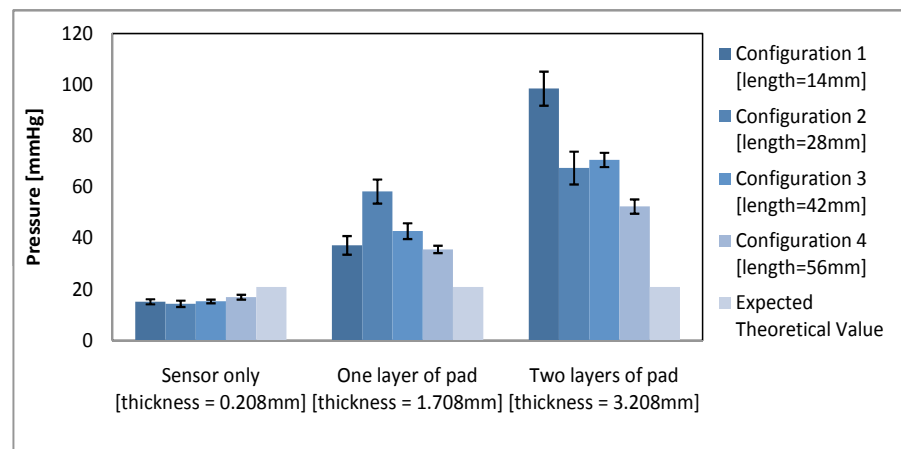


Figure 3.28: The effect of sensor aspect ratio on measured pressure (Aneroid Sphygmomanometer calibration). The error bars represent the standard error of the mean

Table 3.4 summarizes the measured perturbation for each length-thickness configuration. Table 3.5 shows the mean measured perturbation for each configuration \pm the overall error. Clearly, the measured perturbation values do not agree with the perturbation values estimated using Vinckx et al. [86] model. This indicates that the model proposed by Vinckx et al. [86] may not be sufficient to estimate the perturbation in the measured values of pressure due to the sensor physical dimensions.

The results demonstrate that the effect of sensors dimensions on the measured interface pressure over curved objects cannot be neglected and should be addressed. The results suggest that the sensor thickness should be as small as possible. However, most current

Table 3.3: Summary of the average pressure measured at each configuration.

Error = $\sqrt{\text{Overall Sensor Error}^2 + \text{Measurement Error}^2}$.

Overall Sensor Error = Sensor Accuracy Error/ $\sqrt{\text{Number of Repeats}}$.

Measurement Error = $t \times SE$, where “t” is critical point at 95% for the data degrees of freedom obtained from the student's t-distribution look-up table [189]

Deadweights Calibration						
Configuration	Configuration 1 [length=14mm]			Configuration 2 [length=28mm]		
	Average [mmHg]	SE [mmHg]	Error [mmHg]	Average [mmHg]	SE [mmHg]	Error [mmHg]
Sensor only [thickness = 0.208mm]	16.35	1.06	6.17	14.78	1.17	4.82
One layer of pad [thickness = 1.708mm]	40.10	3.91	10.51	60.00	4.54	11.01
Two layers of pad [thickness = 3.208mm]	106.05	7.16	17.15	70.49	6.98	16.28
Configuration	Configuration 3 [length=42mm]			Configuration 4 [length=56mm]		
	Average [mmHg]	SE [mmHg]	Error [mmHg]	Average [mmHg]	SE [mmHg]	Error [mmHg]
Sensor only [thickness = 0.208mm]	18.08	0.94	3.92	20.64	1.30	4.08
One layer of pad [thickness = 1.708mm]	50.70	3.65	8.89	42.95	1.93	5.21
Two layers of pad [thickness = 3.208mm]	83.75	4.17	9.99	62.03	2.70	6.72
Aneroid Sphygmomanometer Calibration						
Configuration	Configuration 1 [Length=14mm]			Configuration 2 [Length=28mm]		
	Average [mmHg]	SE [mmHg]	Error [mmHg]	Average [mmHg]	SE [mmHg]	Error [mmHg]
Sensor only [thickness = 0.208mm]	15.19	0.98	6.11	14.40	1.23	4.89
One layer of pad [thickness = 1.708mm]	37.25	3.63	9.99	58.28	4.71	11.38
Two layers of pad [thickness = 3.208mm]	98.50	6.65	16.07	67.46	6.43	15.07
Configuration	Configuration 3 [Length=42mm]			Configuration 4 [Length=56mm]		
	Average [mmHg]	SE [mmHg]	Error [mmHg]	Average [mmHg]	SE [mmHg]	Error [mmHg]
Sensor only [thickness = 0.208mm]	15.35	0.72	3.67	16.99	0.95	3.56
One layer of pad [thickness = 1.708mm]	42.80	3.08	7.69	35.66	1.45	4.33
Two layers of pad [thickness = 3.208mm]	70.62	2.79	7.12	52.40	2.78	6.90

Table 3.4: Summary of the average perturbation calculated from measured pressures at each configuration. All values are the percentage ratio of the values reported in Table 3.3 to the target pressure (19.51mmHg)

Deadweights Calibration						
Configuration	Configuration 1 [length=14mm]			Configuration 2 [length=28mm]		
	Average	SE	Error	Average	SE	Error
Sensor only [thickness = 0.208mm]	84%	5%	32%	76%	6%	25%
One layer of pad [thickness = 1.708mm]	206%	20%	54%	308%	23%	56%
Two layers of pad [thickness = 3.208mm]	544%	37%	88%	361%	36%	83%
Configuration	Configuration 3 [length=42mm]			Configuration 4 [length=56mm]		
	Average	SE	Error	Average	SE	Error
Sensor only [thickness = 0.208mm]	93%	5%	20%	106%	7%	21%
One layer of pad [thickness = 1.708mm]	260%	19%	46%	220%	10%	27%
Two layers of pad [thickness = 3.208mm]	429%	21%	51%	318%	14%	34%
Aneroid Sphygmomanometer Calibration						
Configuration	Configuration 1 [Length=14mm]			Configuration 2 [Length=28mm]		
	Average	SE	Error	Average	SE	Error
Sensor only [thickness = 0.208mm]	78%	5%	31%	74%	6%	25%
One layer of pad [thickness = 1.708mm]	191%	19%	51%	299%	24%	58%
Two layers of pad [thickness = 3.208mm]	505%	34%	82%	346%	33%	77%
Configuration	Configuration 3 [Length=42mm]			Configuration 4 [Length=56mm]		
	Average	SE	Error	Average	SE	Error
Sensor only [thickness = 0.208mm]	79%	4%	19%	87%	5%	18%
One layer of pad [thickness = 1.708mm]	219%	16%	39%	183%	7%	22%
Two layers of pad [thickness = 3.208mm]	362%	14%	36%	269%	14%	35%

Table 3.5: Comparison between calculated pressure perturbation and the ones found experimentally. The ones found experimentally are reported as mean \pm overall error

Configuration		Theoretical expected perturbation [%]	Deadweights calibration: mean-error [%]	Deadweights calibration: mean+error [%]	Aneroid calibration: mean-error [%]	Aneroid calibration: mean+error [%]
Configuration 1	Sensor only	167%	52%	115%	47%	109%
	One layer of pad	291%	152%	259%	140%	242%
	Two layers of	355%	456%	631%	422%	587%
Configuration 2	Sensor only	133%	51%	100%	49%	99%
	One layer of pad	192%	251%	364%	240%	357%
	Two layers of	223%	278%	445%	269%	423%
Configuration 3	Sensor only	121%	73%	113%	60%	97%
	One layer of pad	159%	214%	305%	180%	259%
	Two layers of	178%	378%	480%	325%	398%
Configuration 4	Sensor only	116%	85%	127%	69%	105%
	One layer of pad	142%	193%	247%	161%	205%
	Two layers of	155%	284%	352%	233%	304%

commercial medical transducers used to measure the interface pressure under compression bandages are a few millimetres thick. For instance, PicoPress is about $50mm$ in diameter and $3mm$ thick when inflated, and the Kikuhime, which is popular among clinicians, is $40mm \times 30mm \times 3mm$. As a consequence of their physical dimensions, both mentioned transducers will overestimate the pressure according to these experimental results.

The high error associated with FlexiForce sensors might have had an effect on the experimental results. which even after repeating the procedure for a few times and using the mean values to report the pressure, might still had an effect. However, the differences between the calculated perturbation and the measured perturbation is much higher than the sensor error. Moreover, applying rubber pads over the sensor might have caused some local stresses under the pads when the compression bandage was applied. Accordingly, the pads might be responsible partly for the huge increase in the measured pressure. This needs to be addressed in future work.

Considering the model studied, some of the Vinckx et al. [86] assumptions might contribute to the model being unsuccessful to estimate the pressure perturbation. For example, the assumption that both bandage curvatures, before placing the sensor and after placing the sensor, will have the same centre might have resulted in underestimating the pressure perturbation, which was visible for one and two layers of pad (Figure 2.16). In addition, Vinckx et al. [86] the decomposition of the tension bandage tension component is only true for small α angles and cannot be extended to situations where the ratio of the length of the sensor to the leg radius is large (Figure 2.16).

To sum up, this section reported experimental work carried out to investigate the effect of sensor thickness and length on the measured interface pressure induced by compression

bandages when they are applied to curved surfaces, and compared the experimental results to the values estimated using the model proposed by Vinckx et al. [86] in order to check their agreement. The experimental results suggest that increasing the thickness of the sensor will result in overestimating the pressure. However, this perturbation in pressure reduces as the sensor length increases. In addition, there was a significant difference between the experimental results of perturbation and the ones calculated using the model proposed by Vinckx et al. [86].

3.9 Summary

This chapter presented the analytical work carried out to understand the underpinning physics of MCBs. It illustrated the forces generated or applied to an MCB when it is applied to a limb.

This chapter also investigated the effect of bandage thickness on the interface pressure. This was achieved by deriving two equations using thin and thick wall cylinder theories. The analytical work showed that the effect of bandage thickness on pressure produced by one layer of bandage is insignificant from medical perspectives. However, it was useful to explain the experimental results reported by other researchers. The impact of bandage thickness was investigated for the first time in this work, according to the literature. In addition, the theoretical pressure produced by a bandage when it is applied with a constant tension was simulated over a 3D model representing a real leg, and the areas with peak pressures were identified. The simulation, which is a novel contribution of this chapter, showed that pressure peaked on the Achilles tendon and upper parts of the shin bone, close to the tibial tuberosity. Nevertheless, these peaks of pressure were not found over other crucial places like the lateral and medial malleolus. This might be due to the fact that the simulation was done for the circumferential curvature of the leg. Moreover, the models developed were compared to data obtained using experimental setup which confirmed the validity of the mathematical model for the interface pressure applied by single layer MCB based on thick wall cylinder theory.

Furthermore, two derived models based on thin and thick wall cylinder theories to calculate the pressure applied by multi-layer MCBs were compared to a model reported by Thomas [75]. Results from the analytical and experimental analysis confirmed that the Thomas [75] approach to use simple multiplication of the number of MCB layers with the pressure applied with one layer to estimate the overall pressure will result in pressure estimation error, with significant error even for few small numbers of bandage layers over sharp edges. The results explained some of the so called pressure damping effect when bandages are applied within multi-component MCB compared to their performance when applied directly to the leg. The experimental results confirmed any the validity of the models based on thin and thick wall cylinder theories. However, the results might be questioned due to the big differences in pressures between the computed and measured pressures in some of the experiment iterations which might be affected by MCB hysteresis

and degradation and deficiencies in sensors performances. The model based on thick wall cylinder theory was used throughout the rest of the thesis to analyze and compute the interface pressures because it was found theoretically and experimentally to provide more accurate pressure estimations than the model based on thin wall cylinder theory or the model proposed by Thomas [75].

Moreover, the effect of biaxial tension-compression forces in the bandage on the interface pressure was introduced in this chapter. Even when the compression force in the width direction of the bandage is small, it might have a significant effect on the interface pressure at sites with sharp longitudinal curvatures like the malleolus for example. This, when combined with the impact of the MCB application angle, might explain why nurses apply a reverse gradient pressure profile even when they apply MCBs with constant tension over a leg with ankle circumference smaller than below knee circumference. This was attributed to nurses applying bandages with small angle ($30^\circ - 50^\circ$) at the ankle and at an angle of 80° at the knee to secure bandage in position. In addition, modeling the application angle effect on the interface pressure illustrated that as the angle between the MCB and the limb vertical axis, parallel to the median plane, decreases the pressure applied by the bandage increases first and then decreases. The amount of increase will depend on the amount of tension forces developed in the transverse direction of the bandage, if all other variables were kept constant.

Additionally, the impact of change in limb shape secondary to calf muscle contraction on the interface pressure was explored. The result of exploration was in the form of two mathematical models; one based on thin wall cylinder theory and the other based on thick wall cylinder theory. The latter was found to be more accurate using analytical work and was recommended to be used in conjunction with Chord modulus to simulate bandage performances in dynamic situation, for example during locomotion.

On top of that, the chapter detailed the material, method, results, analysis and discussion of sets of experiments to validate a model proposed by Vinckx et al. [86] to estimate the pressure perturbation caused by sensors physical dimensions, when used to measure the interface pressure over curved surfaces. Experimental results were not in agreement with the theoretical results calculated using the model proposed by Vinckx et al. [86]. However, the results confirmed that increasing the sensor thickness will result in overestimating the pressure, which can be reduced by increasing its length (diameter) accordingly. Therefore, the chapter ended with the recommendation for future work to re-explore the impact of sensors physical dimensions on the interface pressure.

Chapter 4

Medical Compression Bandages: Selection and Experimental Evaluation

This chapter addresses issues related to MCBs selection and their performance evaluation. It reports on the experimental work carried out to measure the bandage thickness and width under extension and compression. It also presents graphs describing the tension-elongation relationship for the selected MCBs and analysis of their performance with respect to tension. The method to compute the interface pressure is detailed in this chapter. Furthermore, forces developed in the width direction of the bandage are studied and measured experimentally. Moreover, the chapter illustrates how the Chord modulus for an MCB can be obtained experimentally and it demonstrates its usefulness in MCBs classification. Some of the work reported in this chapter has been presented at the 12th Mechatronics Forum Biennial International Conference (“Relationship between extension and pressure in compression bandages used in leg ulcers for the control of interface pressure” and “Comparison between sub-bandage interface computed and measured pressure when bandages are applied to a mannequin leg”), and has been accepted for publication in Phlebology (“Impact of Multi-Layered Compression Bandages on Sub-Bandage Interface Pressure: a Model”) and (“Impact of Variation in Limb Shape on Sub-Bandage Interface Pressure”).

4.1 Introduction

The main aim of this project is to develop pressure measurement systems that can be used as reference to evaluate subsequent pressure-mapping bandages. However, these pressure measurement systems need to be evaluated for their accuracy and reliability. As a part of the evaluation process, pressures measured when MCBs are applied are going to be compared to the pressures computed from the levels of extension in the bandage using Equation 3.11. However, in order to use Equation 3.11, a few MCB related parameters are needed which are the width and thickness of the MCB and the tension developed

in the MCB. Section 4.2 describes the selection of MCBs for the current investigation. Section 4.3 reports on experiments to measure MCB width and thickness. Section 4.4 presents tension-elongation relationships for the selected bandages. It also outlines some other important findings which are useful to explain some of the experimental findings in other chapters.

As the importance of biaxial forces on the interface pressure was introduced in Section 3.5, this chapter will report on an experimental setup to measure the tension induced in the width direction of the bandage when tension is applied to its length (Section 4.5).

Many researchers in the field are interested in the change in the interface pressure under MCBs secondary to the changes in limb shape due to muscle contraction during locomotion or exercise [8; 63; 64; 190]. They have used the information they have obtained for the change in the interface pressure under MCBs to introduce a newer classification methods for MCBs (Section 2.2.4). Section 4.6 introduces a new method to classify MCBs based on a parameter that can be obtained using in-vitro methods.

The chapter ends with illustrating how measured extension levels from the applied MCBs can be used to compute the pressures applied by these MCBs, given that the radius of the curvature to which these MCBs are applied is known (Section 4.7).

4.2 MCB Selection

Various types of medical bandages are used in the treatment of venous leg ulcers. These bandages differ in a number of ways (see Section 2.2.4). MCBs used in this study are selected based on their ability to apply high levels of pressure with minimum stretch. In order to design pressure-mapping bandages, the stretch in the bandage should be minimized as much as possible to reduce the design challenges with respect to methods of sensor's attachments and wiring. Two bandages have been selected for this study:



Figure 4.1: Comprilan Bandage

Comprilan (BSN Medical Inc, Charlotte, North Carolina, USA) (Figure 4.1) is a low-stretch bandage that provides high compression for leg ulcers and venous disease.

The open woven fabric is made completely from cotton. On the Drug Tariff, this bandage is classified as type 2 support bandage.

SurePress (ConvaTec Ltd, Deeside, UK) (Figure 4.2) is a type 3C MCB and it is capable to provide high, sustained levels of pressure. The bandage has an overlap indicator in the form of a centre yellow line and an extension indicator in the shape of two rectangles, which are deformed to become square at the manufacturer's recommended levels of extension.



Figure 4.2: SurePress Bandage

4.3 MCB Width and Thickness Measurement

Objectives

To measure the thickness and width of the two selected bandages at four different situations: not stretched and not compressed, not stretched and compressed, stretched and not compressed, and stretched and compressed.

Materials and Method

Bandages: Three samples of Comprilan and SurePress bandages were used.

The test rig: The test rig used in this experiment is shown in Figure 4.3. It consists of two clamps: one is fixed and the other one can be moved in a sliding uni-direction motion using a fixed sliding guide.

Thickness, width and extension measurements: Thickness was measured using a Shirly Thickness Gauge (Shirly Development Ltd, Manchester, UK) (Figure 4.3). Width was measured using a ruler. The bandage samples were marked at constant intervals of 50mm. When extended, the new length was measured using a ruler and extension was then calculated using the following equation:

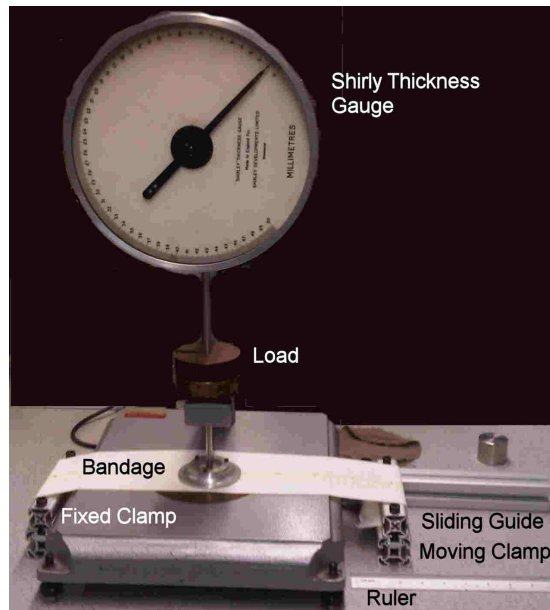


Figure 4.3: Shirly thickness gauge and the mechanical arrangement used in the experiment

$$Extension[\%] = \frac{\text{New Length} - \text{Old Length}}{\text{Old length}} \quad (4.1)$$

Experiment protocol: Bandage sample is first clamped to the test rig and both its initial width and thickness are measured. Then, two deadweights of 1 kg and 2 kg were used to apply a pressure of 14.64 mmHg and 29.27 mmHg respectively to the bandage sample. Each time, the bandage thickness under compression was measured. The bandage was then extended to approximately 50% extension using the sliding clamp, where the width and the extension in the bandage were measured using a ruler. Next, the thickness of the bandage was measured using Shirly Thickness Gauge with and without pressure being applied to the bandage. After that, the clamp was returned to its original position, where the width and the distance between the marks were measured again, as bandages did not return to their original size due to the plastic behavior of some of the bandage threads. The thickness of the bandage was also measured again with and without applying compression pressure to the bandage. The process repeated for three bandage samples.

Results, Analysis and Discussion

Results are shown in Tables 4.1 and 4.2. The results indicate that when the selected bandages are compressed, they become thinner by 20%. Hence, when applied in spiral 50% overlap, for example, the inner bandage layer will be thinner than the outer bandage layer due to the additional compression. This should be considered when estimating the interface pressure.

Table 4.1: Summary of the experimental results to measure the thickness and width of Comprilan bandage

Comprilan bandage thickness and width when it is not extended						
Weight [g]	Pressure [N/m]	Pressure [mmHg]	Thickness [m]			Average [m]
			1st Reading	2nd Reading	3rd Reading	
0	0.00	0.00	0.00110	0.00120	0.00120	0.0012
1000	1951.64	14.64	0.00090	0.00100	0.00100	0.0010
2000	3903.27	29.27	0.00090	0.00100	0.00095	0.0010
			Width [m]			Average [m]
			1st Reading	2nd Reading	3rd Reading	
			0.0990	0.0990	0.0995	0.0992
			Extension [%]			Average [%]
			1st Reading	2nd Reading	3rd Reading	
			0%	0%	0%	0%

Comprilan bandage thickness and width when it is extended						
Weight [g]	Pressure [N/m]	Pressure [mmHg]	Thickness [m]			Average [m]
			1st Reading	2nd Reading	3rd Reading	
0	0.00	0.00	0.00110	0.00110	0.00110	0.0011
1000	1951.64	14.64	0.00080	0.00080	0.00090	0.0008
2000	3903.27	29.27	0.00080	0.00080	0.00080	0.0008
			Width [m]			Average [m]
			1st Reading	2nd Reading	3rd Reading	
			0.0950	0.0980	0.0985	0.097
			Extension [%]			Average [%]
			1st Reading	2nd Reading	3rd Reading	
			50%	53%	48%	50%

Comprilan bandage thickness and width when it is relaxed post extension						
Weight [g]	Pressure [N/m]	Pressure [mmHg]	Thickness [m]			Average [m]
			1st Reading	2nd Reading	3rd Reading	
0	0.00	0.00	0.00110	0.00115	0.00120	0.0012
1000	1951.64	14.64	0.00090	0.00095	0.00100	0.0010
2000	3903.27	29.27	0.00090	0.00090	0.00095	0.0009
			Width [m]			Average [m]
			1st Reading	2nd Reading	3rd Reading	
			0.0980	0.0990	0.0995	0.099
			Extension [%]			Average [%]
			1st Reading	2nd Reading	3rd Reading	
			20%	16%	18%	18%

Table 4.2: Summary of the experimental results to measure the thickness and width of SurePress bandage

SurePress bandage thickness and width when it is not extended						
Weight [g]	Pressure [N/m]	Pressure [mmHg]	Thickness [m]			Average [m]
			1st Reading	2nd Reading	3rd Reading	
0	0.00	0.00	0.00130	0.00130	0.00140	0.0013
1000	1951.64	14.64	0.00110	0.00110	0.00120	0.0011
2000	3903.27	29.27	0.00105	0.00105	0.00110	0.0011
			Width [m]			Average [m]
			1st Reading	2nd Reading	3rd Reading	
			0.1050	0.1050	0.1050	0.1050
			Extension [%]			Average [%]
			1st Reading	2nd Reading	3rd Reading	
			0%	0%	0%	0%

SurePress bandage thickness and width when it is extended						
Weight [g]	Pressure [N/m]	Pressure [mmHg]	Thickness [m]			Average [m]
			1st Reading	2nd Reading	3rd Reading	
0	0.00	0.00	0.00110	0.00110	0.00120	0.0011
1000	1951.64	14.64	0.00085	0.00090	0.00090	0.0009
2000	3903.27	29.27	0.00080	0.00085	0.00090	0.0009
			Width [m]			Average [m]
			1st Reading	2nd Reading	3rd Reading	
			0.1050	0.1050	0.1050	0.105
			Extension [%]			Average [%]
			1st Reading	2nd Reading	3rd Reading	
			56%	51%	51%	53%

SurePress bandage thickness and width when it is relaxed post extension						
Weight [g]	Pressure [N/m]	Pressure [mmHg]	Thickness [m]			Average [m]
			1st Reading	2nd Reading	3rd Reading	
0	0.00	0.00	0.00130	0.00130	0.00150	0.0014
1000	1951.64	14.64	0.00110	0.00110	0.00120	0.0011
2000	3903.27	29.27	0.00105	0.00105	0.00150	0.0012
			Width [m]			Average [m]
			1st Reading	2nd Reading	3rd Reading	
			0.1050	0.1050	0.1050	0.105
			Extension [%]			Average [%]
			1st Reading	2nd Reading	3rd Reading	
			4%	4%	4%	4%

In addition, the data in Tables 4.1 and 4.2 illustrate that when Comprilan is extended, the width of the bandage decreases, which is a clear indication for a compression force in the width direction of the bandage. The amount of this force might impact the interface pressure specially when bandages are applied at an angle to the limb or applied to a limb with sharp longitudinal curvatures. Furthermore, data in Table 4.1 illustrates that that when Comprilan was relaxed, the bandage did not return to its original length, indicating a delayed recovery for the bandage. This is due to the fact that the bandage is made completely from cotton. With regards to SurePress, there is no measured decrease in its width when extended and the delayed recovery is much smaller compared to Comprilan.

4.4 Evaluation of MCB Tension-Elongation Interconnection

Objectives

To obtain tension-elongation curves for Comprilan and SurePress bandages for different extension ranges for multiple of cycles.

Materials and Method

Bandages: Eight samples of Comprilan and ten samples of SurePress bandages were used in the apparatus. All samples were 200mm in length, with all samples being taken from the middle of the bandage roll to minimize the error.

Constant Transverse Machine: Instron 4301 (Instron, High Wycombe, UK) (Figure 4.4) was used to measure the tension developed in the bandage while it was extended at constant speed of $100\text{mm}/\text{min}$. A 100N load cell was used to measure the tension in the MCB. The load cell output signal was acquired using an Oscilloscope program that was available in the computer connected to the device in the School of Design in the University of Leeds. The load cell output signal was sampled at 5Hz . The device gauge length was set to 100mm . Custom-made jaws with 100mm width were used, as the largest jaws supplied with Instron 4301 were of 75mm width.

Experiment protocol: Bandage sample was first clamped in the custom made jaws. The device was set to do a cyclic test for the required extension range for at least 5 cycles. The sample was then changed and the process was repeated with another extension range. The following extension ranges were obtained for Comprilan bandage: 0 – 10%, 0 – 20%, 0 – 30%, 0 – 40%, 0 – 50%, 0 – 60%, 0 – 70% and 0 – 80%. For SurePress, an additional two extension ranges were also obtained 0 – 90% and 0 – 100%. All data was post processed using Excel 2003 and Excel 2007.

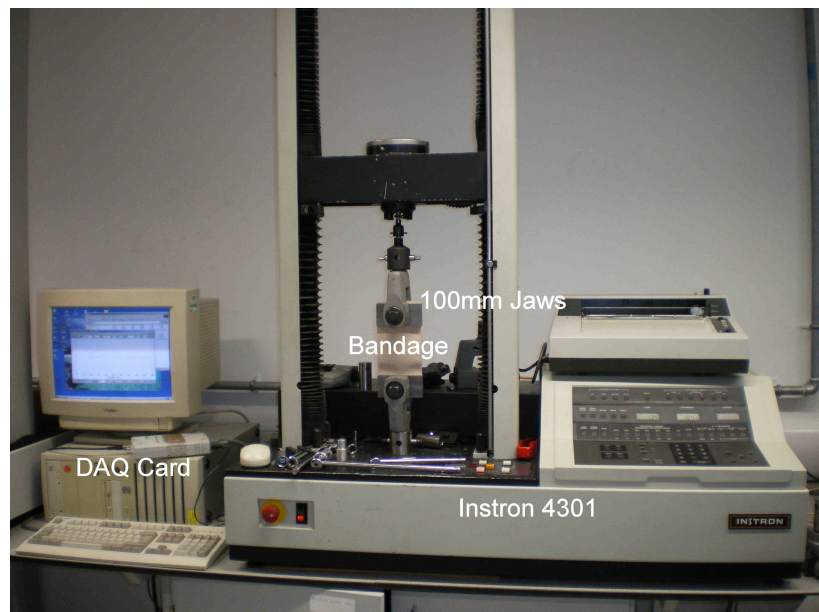


Figure 4.4: Instron 4301

Results, Analysis and Discussion

Figure 4.5 illustrates typical tension-elongation cyclic curves for Comprilan and SurePress bandages. In this case, they are for the 0 – 60% elongation range as a typical range. Clearly from the figures, Comprilan has higher hysteresis compared to SurePress. This is due to the fact that SurePress is an elastic bandage with elastomeric yarns interconnecting its non-elastomeric yarns, whereas, Comprilan is made of cotton entirely. In addition, the first cycle of both bandages is quite different from the rest of the cycles. As in the first cycle, some of the forces are consumed in removing all the 'kinks' in the MCB material [71].

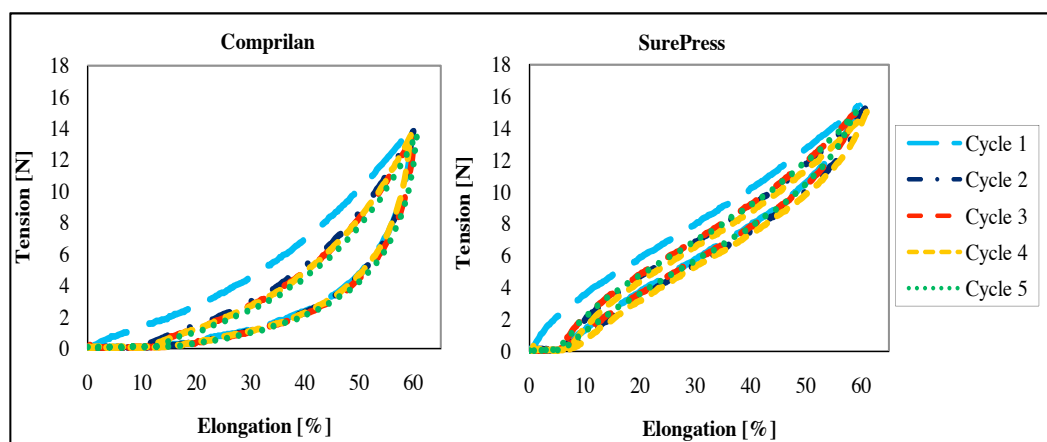


Figure 4.5: Tension-elongation curves for Comprilan and SurePress bandages for the 0 – 60% elongation range. Left: comprilan. Right: SurePress.

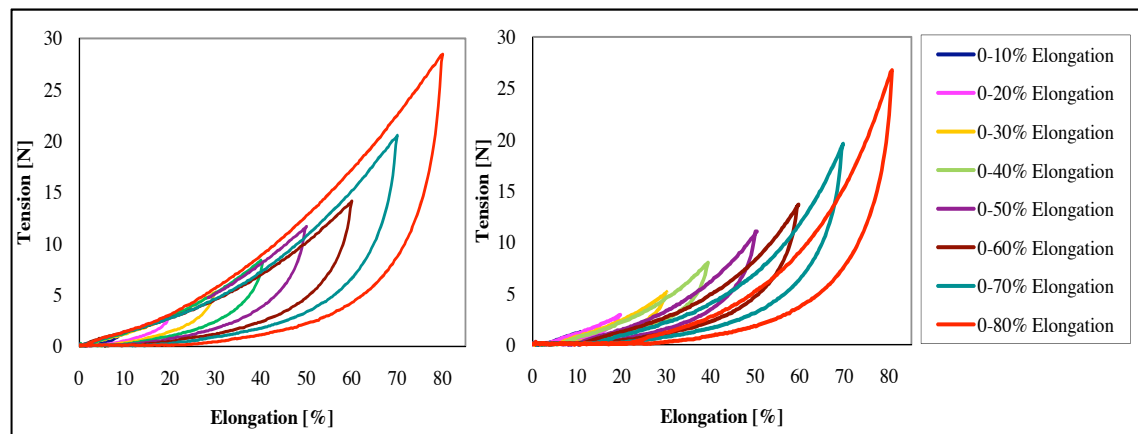


Figure 4.6: 1st and 5th cycles tension-elongation curves for Comprilan bandage of different elongation ranges. Left: 1st cycle. Right: 5th cycle

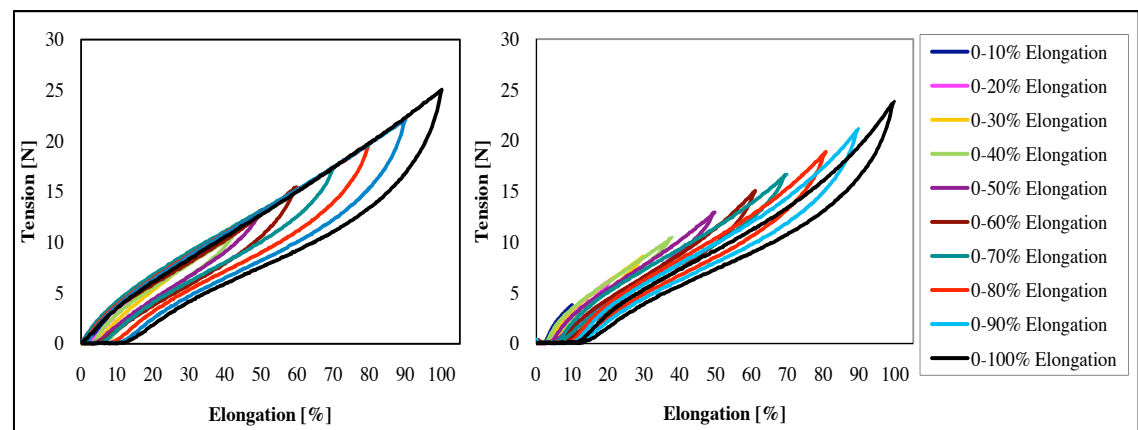


Figure 4.7: 1st and 5th cycles tension-elongation curves for Comprilan SurePress of different elongation ranges. Left: 1st cycle. Right: 5th cycle

Figures 4.6 and 4.7 show the 1st cycle of the tension-elongation curves for the different ranges of elongation for Comprilan and SurePress respectively. The graphs show that the SurePress bandage has more linear loading curve compared to Comprilan. In addition, the loading line seems to be more consistent from one sample to another, while clearly, Comprilan loading curve changes from one sample to another. Moreover, hysteresis is quite large in Comprilan bandage compared to SurePress. Furthermore, while SurePress bandage needs higher forces to extend the bandage to a specific extension in the elongation range 0 – 70%, Comprilan develops much higher tension forces when the bandage is extended beyond 70%. These forces are even higher than the tension forces in the SurePress bandage at 100% elongation. This suggests that applying Comprilan beyond 70% elongation will need much more effort from the user. Furthermore, it implies that applying Comprilan with extensions higher than 70% will result in a very high pressure being applied to the patient’s leg.

Figures 4.6 and 4.7 also show the 5th cycle tension-elongation curves for the different ranges of elongation for Comprilan and SurePress respectively. The figures show that the SurePress, even at the 5th cycle, keeps its linear loading shape with much smaller hysteresis compared to 1st cycle. However, the linear line is shifting horizontally with an offset due to the delayed recovery and plastic deformation effect. This effect is more visible in the case of Comprilan, where tension starts to build up in the bandage in the 0 – 80% elongation cycle at approximately 20% elongation. This is quite significant and helps explain why short-stretch bandages like Comprilan, get loose easily and do not keep their pressure for a long time when applied [37].

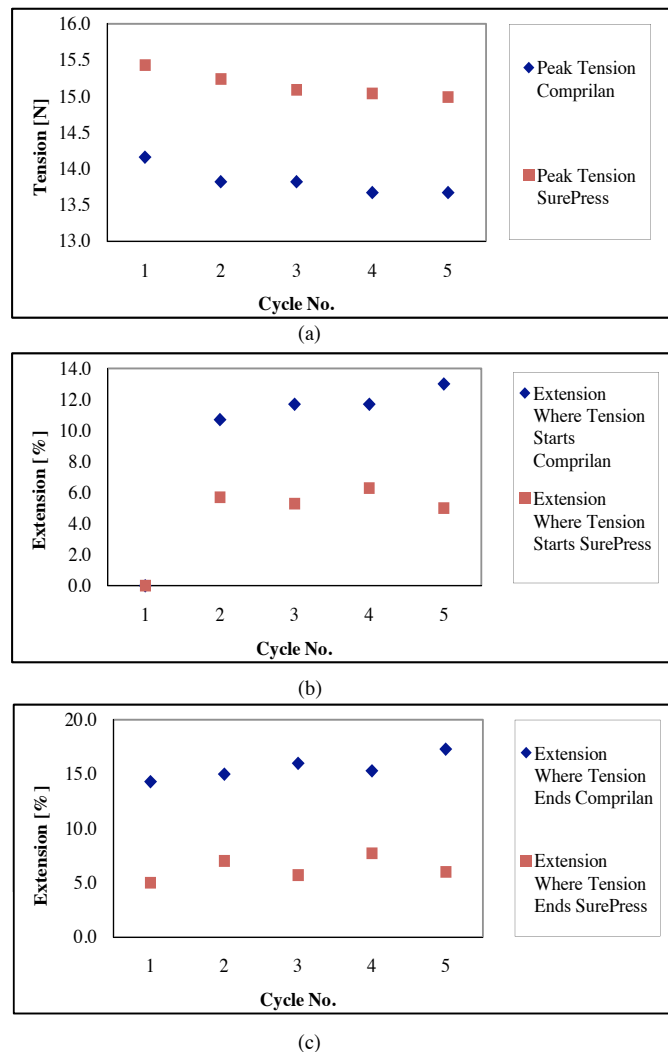


Figure 4.8: (a) Change in peak tension over 5 cycles for Comprilan and SurePress bandages for the elongation range 0 – 60%. (b) Change in elongation value where tension starts over 5 cycles for Comprilan and SurePress bandages for the elongation range 0 – 60%. (c) Change in elongation value where tension ends over 5 cycles for Comprilan and SurePress bandages for the elongation range 0 – 60%

Figure 4.8 illustrates the drop in peak tension and the increase in the elongation value

where tension starts and ends for both Comprilan and SurePress bandages for the 0 – 60% elongation range. In both bandages, the peak tension in the bandage drops linearly with the number of cycles. The extension at which tension starts or ends in Comprilan is higher than SurePress.

The above results were true for all elongation ranges for both bandages. The summary of the peak tension and elongation where tension starts or ends for the 5th cycle of all elongation ranges and the rate of drop in tension by cycle and the rate of increase in the elongation by cycle where tension starts or ends for all elongation ranges for both bandages is provided in Table 4.3. The rate of drop in tension or increase in extension by cycle was obtained by fitting the data with a linear line and using the slope of the line to report the rate.

Table 4.3: Summary of the peak tension and elongation where tension starts or ends for the 5th cycle of all elongation ranges, the rate of drop in tension and the rate of increase in the elongation values where tension starts or ends for all elongation ranges for Comprilan and SurePress

Comprilan						
Elongation cycle range	Tension		Elongation where tension starts		Elongation where tension ends	
	Peak [N]	Rate of change [N/cycle]	Elongation [%]	Rate of change [%/cycle]	Elongation [%]	Rate of change [%/cycle]
0-10%	1.22	-0.003	3.27	-0.043	4.61	0.109
0-20%	2.92	-0.027	3.85	0.157	6.3	0.085
0-30%	5.05	-0.041	6.62	0.178	8.65	0.176
0-40%	7.94	-0.043	7.51	0.197	10.72	0.173
0-50%	11.18	-0.096	10.24	0.307	13.46	0.373
0-60%	13.83	-0.113	11.78	0.690	15.58	0.630
0-70%	19.86	-0.283	13.43	0.910	19.14	0.660
0-80%	27.28	-0.435	20.18	0.850	26.72	0.750
SurePress						
Elongation cycle range	Tension		Elongation where tension starts		Elongation where tension ends	
	Peak [N]	Rate of change [N/cycle]	Elongation [%]	Rate of change [%/cycle]	Elongation [%]	Rate of change [%/cycle]
0-10%	3.83	-0.005	2.58	0.013	2.91	0.039
0-20%	6.37	-0.004	2.68	0.082	3.21	0.156
0-30%	8.53	-0.016	4.49	0.072	4.85	0.095
0-40%	10.45	-0.011	4.23	0.023	5.83	-0.019
0-50%	12.96	-0.037	4.20	0.104	5.18	0.079
0-60%	15.13	-0.086	6.00	0.370	6.62	0.443
0-70%	16.87	-0.176	6.00	0.540	6.80	0.500
0-80%	19.18	-0.230	8.93	0.310	9.86	0.390
0-90%	21.52	-0.304	10.43	0.500	11.83	0.330
0-100%	24.32	-0.393	11.47	0.500	13.43	0.210

4.5 MCB Biaxial Force Evaluation

In Section 3.5, the effect of the compression forces, developed in the width (transverse) direction of the MCBs when MCBs are extended due to tension applied in their length direction, on the interface pressure was illustrated. However, in order to measure these tension forces in the transverse direction of the bandage, Drapier and Gaied [191] used a transverse machine to apply tension forces to a stocking sample in the circumferential direction and, then, compared them to the tension developed in the bandage when the same tensions were applied to the same side of the bandage, while maintaining the transverse direction dimension, preventing, therefore, the bandage from shrinkage. The additional forces measured are assumed to be caused by the compression forces developed in the bandage. However, the method they used was complex as they used image processing to measure the strain, a load cell to measure the tension and FEA to simulate of the forces. The objective of this section is to show how the compression forces developed in the bandage can impact on the interface pressure; therefore, a simpler method is used in this section to evaluate these forces. This method is based on the same assumption that is used to evaluate the formability of a fabric, the ability of the fabric to be compressed in a plane without buckling [192]. The assumption used is for small strains around zero on the force extension curve, the slope of the curve is the same at positive and negative stresses [192]. Hence, for small strains like the one in the transverse direction of the bandage, as it was found in Section 4.3, the tension-elongation curves for the transverse direction of the bandage might be a good representation for the compression-elongation curves.

Objectives

To obtain the tension-elongation curves for Comprilan and SurePress bandages in the width direction.

Materials and Method

Bandages: Two samples of Comprilan and SurePress bandages were used. All samples were nominally 50mm in length and 100mm in width, with all samples taken from the middle of the bandage roll, to minimize any inconsistencies might present at the end of the bandage role.

Constant Transverse Machine: Instron 4301 was used to measure the tension. The system setup was exactly as described in Section 4.4 except that the device gauge length was set to 50mm and the jaws used were of 50mm in width.

Experiment protocol: Bandage sample was clamped in the jaws, such that tension was applied to the width direction of the bandage. The device was then set to do a cyclic test for 0–10% elongation range for Comprilan and 0–4% elongation range for SurePress.

This was repeated for two bandage samples. All data was post processed using Excel 2003 and Excel 2007.

Results, Analysis and Discussion

Figures 4.9 and 4.10 illustrate the tension-elongation cyclic curves for the transverse direction for Comprilan and SurePress bandages respectively. Results from the 1st loading cycle of Comprilan indicate that at 2% elongation, there is about 1N tension force per 50mm bandage length. This value is almost about the same for SurePress bandage. However, as it was reported in Section 4.3, at 50% extension in the length direction of the bandage, Comprilan and SurePress bandages shrank by 2% and 0%. These values indicate that the effect of biaxial forces on the interface pressure might be higher with Comprilan than SurePress. However, this is true only if the assumption proposed is true. In addition, as the load cell used in the apparatus has a full scale force range of 100N, small values like 1N might not be accurate as they are within the lower end of the force range.

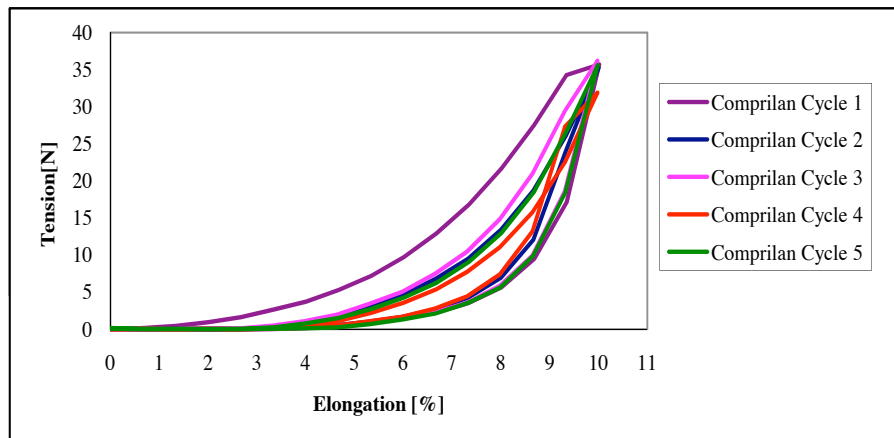


Figure 4.9: Tension-elongation curves for Comprilan bandage in the transverse direction for 0 – 10% elongation range

4.6 New Method to Classify MCB

Some researchers are interested in measuring the change in pressure under the compression devices caused by the interaction of the change in the calf muscle size and the MCBs and MCSs [8; 63; 64; 190]. This is due to the fact that the muscle activity in the leg during movement results in a change in the limb size, causing a change in the extension in the MCB and MCS fabric. This will lead to a change in the tension in the fabric and hence a change in the interface pressure. According to the European Committee of Normalization, the increase in pressure if the circumference of the leg increases by 1cm is called the stiffness index [62]. In fact, once MCBs and MCSs are applied to a leg, stiffness of the compression material plays the greatest role in producing the difference between the resting pressure

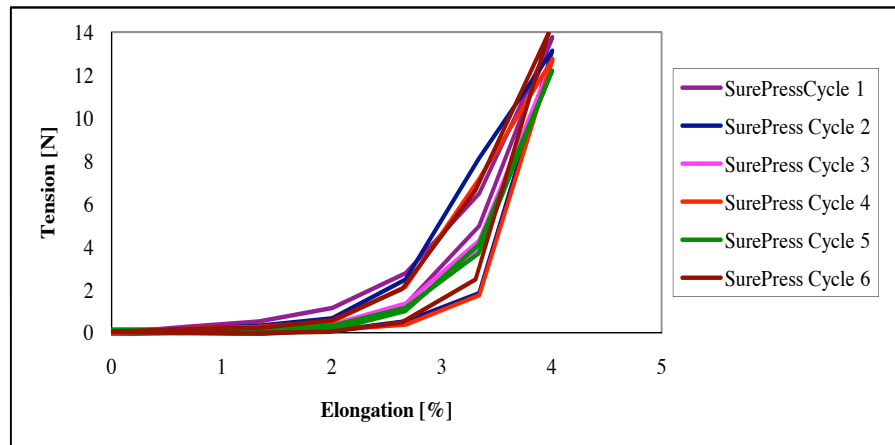


Figure 4.10: Tension-elongation curves for Comprilan bandage in the transverse direction for 0 – 4% elongation range

and working pressure [39; 190]. This difference underlies the beneficial hemodynamic effects of MCBs and MCSs [39; 72].

Tension-elongation curves for MCBs and MCSs under static conditions, where MCBs and MCSs are stretched to a certain extent, will be different to the ones generated under dynamic conditions, where MCBs and MCSs are stretched to a certain extent and small cyclic changes in the compression material take place. Under dynamic conditions such as walking the circumferential change of the leg will result in small elongation increments. However, because of the steep slope in the tension-elongation curves for small elongation increments, the change in the tension will be much higher than what is suggested by the slope of the static tension-elongation curves. It follows that dynamic situations will result in higher differences between the maximum and minimum tension forces compared to static situations. This, in turn, means that the differences between maximum and minimum pressure generated under dynamic conditions will be much higher than the differences between maximum and minimum predicted pressure under static conditions.

Researchers have proposed several terms and indices to describe this dynamic behaviour of the MCBs and MCSs like SSI and the DSI (Section 2.2.4). Researchers have concluded that these indices are important in classifying MCBs and MCSs and they have proposed that these indices will help clinicians in prescribing MCBs and MCSs for their patients [61]. This arises from different preferences for compression systems across countries. Some practitioners prefer bandages with high resting pressure and minimal change in pressure on exercise (hence effectiveness having less dependent on patient activity); others, on the other hand, prefer bandages with moderate resting pressures and large increases in pressure on movement (hence high safety margin as skin is not subjected to constant high pressure).

Both SSI and DSI relate the amount of pressure applied by MCBs and MCSs to the amount of elongation secondary to the change in limb shape due to muscle activity.

However, the interface pressure is directly proportional to the tension in the compression fabric. Engineering constants like the Young's modulus and the Chord modulus relate the stress or the tension force in the material to the elongation that caused this tension force. These moduli are used to describe the slope of the force elongation curves. Generally, the slope of the tension-elongation curve for a fabric is called the Young's modulus [192].

Young's modulus for a fabric is more specifically defined in some textile measurement reference works as the slope value of the straight line made through the steepest linear region of the curve using the least square fit method [192] (Figure 4.11). However, MCBs and MCSs are not always applied within the linear region of the tension-elongation curve and very few compression products are applied within the steepest region of the curve. Chord modulus or tangent modulus, is defined as the slope of the straight line drawn between any two points on the force elongation curve [192] (Figure 4.11). This modulus can be described as the dynamic Young's modulus. The advantage of using this modulus is that it depends only on measuring the difference in the force between two given values of extension or the difference in extension between two given values of force [192]. In this way, Chord modulus can be used to describe the stiffness of a compression product in dynamic situations like the situation generated during muscle activity.

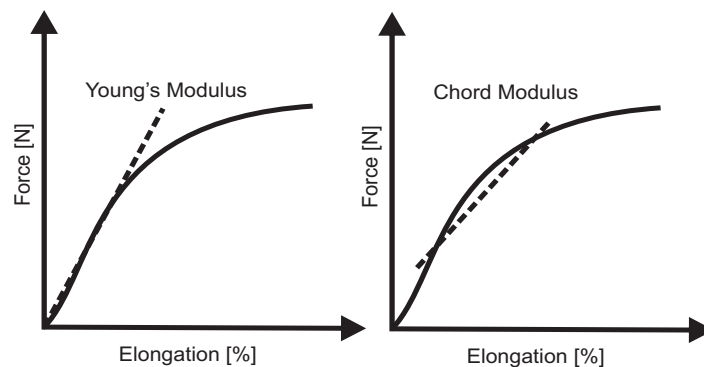


Figure 4.11: Young's modulus and Chord modulus

Some researchers have suggested that the maximum change in the circumference of a limb occurs at level B1 and it is approximately $18mm$ [65]. Others have found that it is less than $10mm$ [8]. This means that a standard cyclic tensile test can be used to measure Chord modulus for a compression material, which then can be used to classify this product. The only difference is that the cyclic test should be performed between two extensions that represent the dynamic change in extension once the compression product is applied to the lower limb. In order to show how Chord modulus can be obtained and used to classify MCBs, an experiment was designed and conducted.

Materials and Method

Bandages: Comprilan and SurePress bandages were used. Samples used were 200mm in length.

Constant Transverse Machine: Instron 4301 was used to measure the tension again. The system setup was exactly as described in Section 4.4.

Experiment protocol: Bandage sample was first clamped in the jaws. Then, the device was set to apply a cyclic test for the elongation range 45 – 55% to the bandage. These values were selected as they represent $50 \pm 5\%$ gauge length, where 50% is normally what manufacturers recommend to use when applying MCBs and the $\pm 5\%$ gauge length is equivalent to the maximum 20mm change in the circumference of a leg with 200mm circumference. The stress-strain curve for one of the cycles was, then, plotted and the gradient of the slope of the line between the maximum and the minimum values of stresses was measured. The gradient of the slope represented the Chord modulus for this specific compression material. Data was post-processed using Excel 2003 and Excel 2007.

4.6.1 Results, Analysis and Discussion

Figure 4.12 illustrates the Chord modulus obtained for both bandages. From the Chord moduli one can classify MCBs into two categories, bandages with high pressure pulsation and bandages with low pressure pulsation. These are related to more familiar terms like elastic and non-elastic bandages.

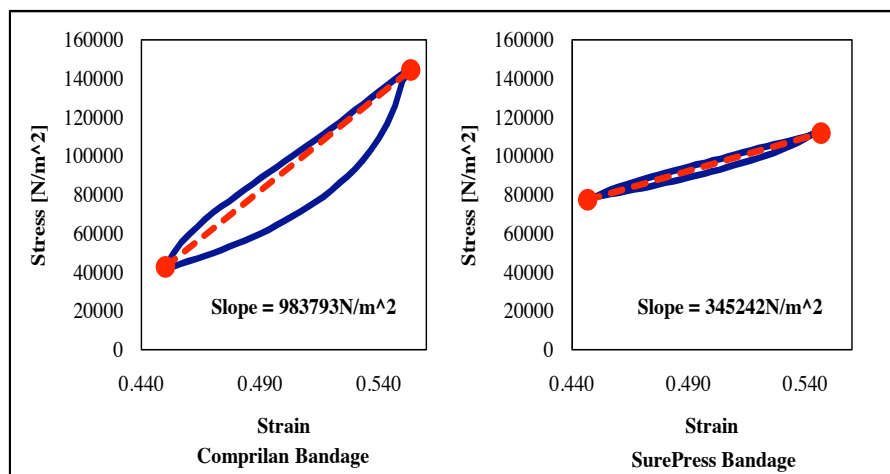


Figure 4.12: Chord modulus for both bandages for the elongation range 45 – 55%

The data gathered during the experiment was used to check the impact of a change in limb shape on the tension developed at specific elongation values and peak-peak tension of the bandage. Figures 4.13, 4.14 and 4.15 demonstrate the change in the tension developed at 45% elongation, the tension developed at 55% elongation and the peak-peak tension

respectively, when cyclic load is applied to the two bandages. The results show that Comprilan will lose approximately $2N$ of its tension within 38 cycles, with peak-peak tension decaying slightly also. These findings are true also for SurePress but with lower decay. Note, the decaying process due to dynamic force is not linear as treated by other researchers [109], it is rather a logarithmic decay.

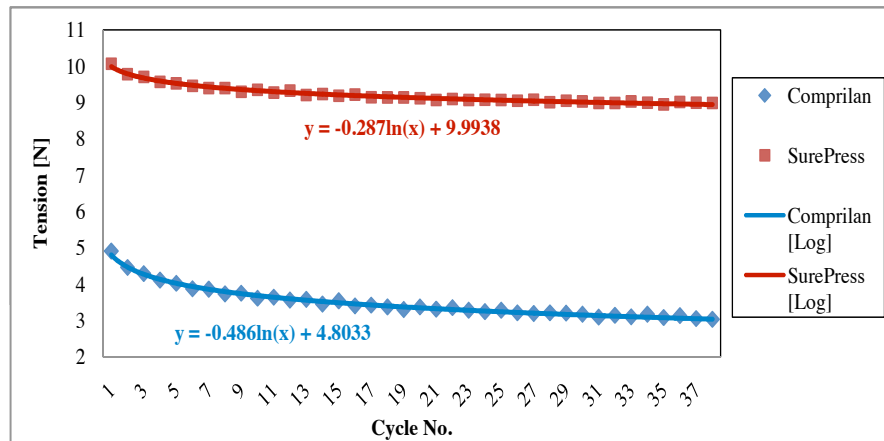


Figure 4.13: Change in tension at 45% elongation when cyclic load is applied to the two bandages

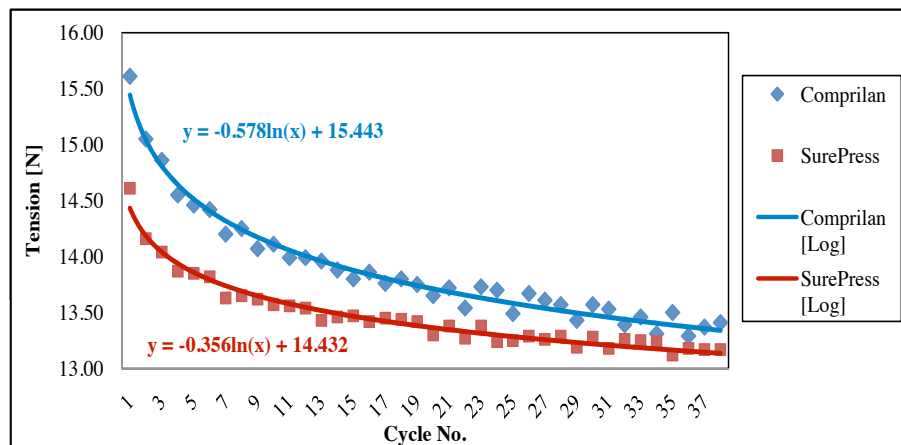


Figure 4.14: Change in tension at 55% elongation when cyclic load is applied to the two bandages

4.7 Computing Pressure from Extension in MCBs

The amount of extension in the bandage was used to estimate the amount of tension using the data gathered in Section 4.4. This was done by getting the 4^{th} power polynomial fitting-line for the 1^{st} and 5^{th} cycles loading sides of the tension-elongation curves for both Comprilan and SurePress using MATLAB R2009b (see Figure 4.16 as an example). In

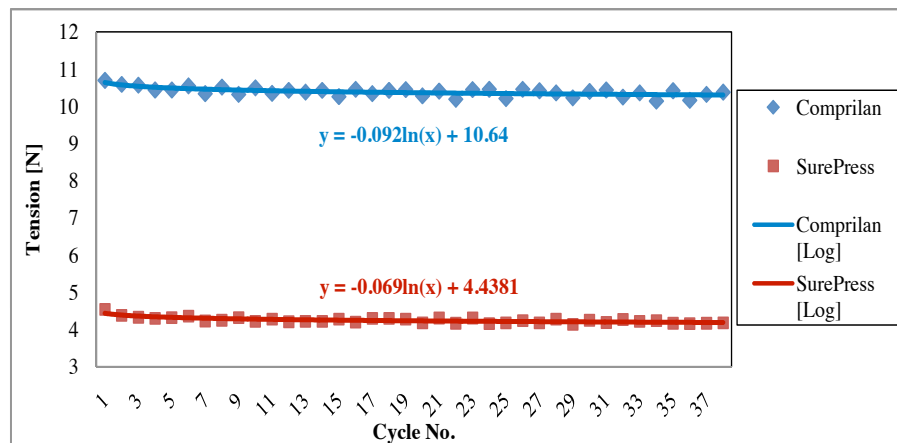


Figure 4.15: Change in peak-peak tension when cyclic load is applied to the two bandages

situations where new or unused MCBs for a long time were utilized to apply the pressure, the fitting-line obtained for the loading side of the 1st cycle of the tension-elongation curve was used to estimate the tension. When recently used bandages are used (within the last day or so) the fitting-line for the 5th cycle was used to estimate the tension. In addition, care was taken during applying the bandage so that bandages were applied using the loading cycle of the tension-elongation curve i.e. applying the bandage without removing the force or allowing to relax. The tension values were then converted to the equivalent pressures using Equation 3.11 and the data obtained experimentally about the physical dimensions of the selected bandages (Section 4.3).

4.8 Summary

For this current research work, two bandages were selected and their physical dimensions were measured at different extension and compression cases. The bandages' tension-elongation relationship was explored and it was concluded that SurePress had better linearity, more consistent loading tension curves, smaller hysteresis, higher static forces at low extensions and more durable pressure than Comprilan.

Tension forces developed in the transverse direction of the bandage extension were measured. These measurements were based on the assumption that for low elongations, both tension and compression forces from the transverse direction of the bandage will be the same. Results indicated that at even low extensions (2%), 1 – 2N of tension force per 100mm of bandage will be developed in the bandage to shrink the width side of the bandage.

A new method to classify compression bandages based on Chord modulus was presented and the experimental setup to obtain the chord modulus corresponding values for the two selected bandages was detailed. The outcomes suggest that Chord modulus can be used to

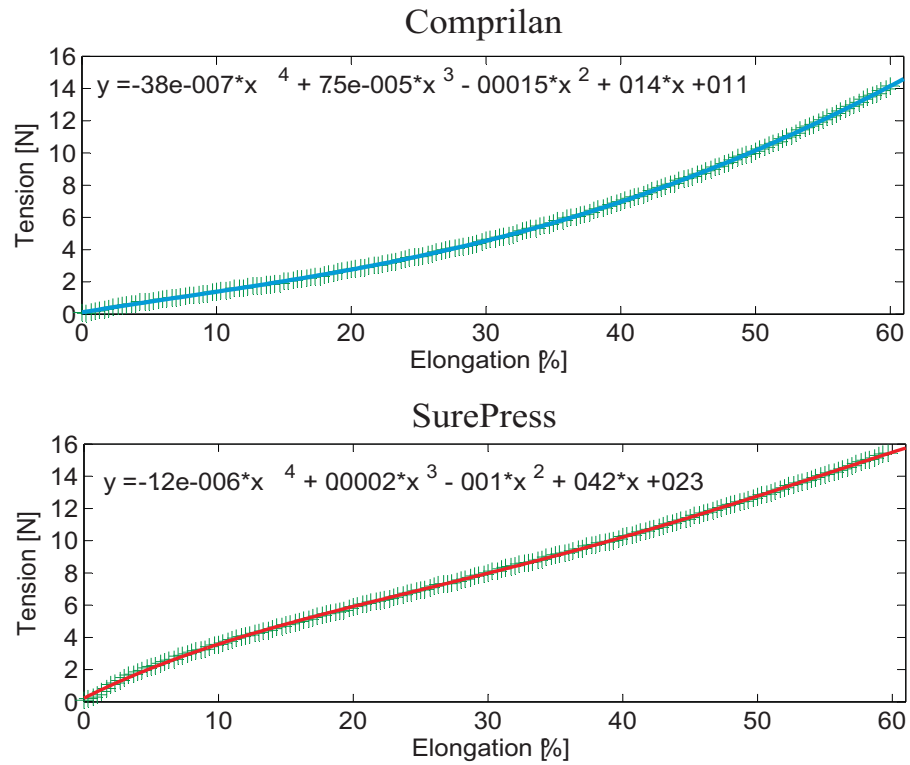


Figure 4.16: 4th order polynomial fitting-lines for the 1st loading cycle for the tension-elongation curves for the range 0 – 60% elongation for Comprilan [top] and SurePress [bottom] bandages

classify compression bandages instead of creating new types of indices based on expensive in-vivo experiments. In addition, the data illustrates that while Comprilan has higher dynamic forces and higher pressure pulsation than SurePress. Comprilan is less durable to dynamic forces and loses both tension and the pulsation power with time at higher rate than SurePress. Furthermore, decay rate for both bandages is not linear as proposed by other researchers.

Finally, the chapter presented a method to estimate the pressure from extension using fitting-lines describing the tension developed in the bandage at a given elongation and then converting the estimated tension into pressure using Equation 3.11, given that all other variables are known.

Chapter 5

Sensors Characteristics

This chapter addresses questions about the static performance of the sensors selected for this project. It provides an evaluation for PicoPress transducer in terms of nonlinearity, repeatability, hysteresis and accuracy, and the effect of physical dimensions on the measured pressure. It presents a static assessment for MEMS FS01 force sensor with regards to its nonlinearity, repeatability, hysteresis and drift on flat and curved surfaces and compares the assessment with the manufacturer's specifications. In addition, it details the experimental setup to characterize FlexiForce, Tactilus and two sizes of FSR sensors, compare their performance and select one of them to develop a pressure measurement system and pressure-mapping bandage.

5.1 Introduction

This chapter details assessments for the sensors used in this project in static mode. Pressure measurements under compression bandages are normally taken after applying the bandage, hence users are normally interested in static pressure measurements. However, researchers will be interested in a measurement system capable of providing dynamic pressure readings, to enable them to study the change in pressure when bandages are applied or removed from the leg, and the changes in pressure during motion. Elderly people walk on average 1.8 steps per second at comfortable walking pace [193] i.e. the calf muscle will change its shape with $1.8Hz$; therefore, the frequency of the dynamic forces applied to any sensor to be used under compression bandages will be roughly $2Hz$ which can be considered as a low frequency. With regards to bandage application, the frequency of applying successive layers of bandages is about $1Hz$ or less. Therefore, any pressure measurement system that is developed for dynamic measurements under compression bandages should be able to stand low frequency forces without any degradation. As dynamic tests are normally required for a very short period, and they can be represented with static postures if needed; thus, dynamic performance of the selected sensors will not be evaluated in this work.

The chapter starts with defining sensors' characteristics like nonlinearity, repeatability,

hysteresis etc. and the way they are derived and the way they are calculated in this thesis (Section 5.2). This is followed with a small section on sensors selected for this project and reasons behind these selection (Section 5.3).

Section 5.4 reports the evaluation of a commercial medical pressure sensor; PicoPress, in terms of static characterization of nonlinearity, repeatability and hysteresis, theoretical calculation for pressure overestimation due to its probe physical dimensions and experimental validation for these theoretical calculations.

The chapter then details the experimental evaluation for FS01 force sensor (Honeywell International Inc, New Jersey, USA) in Section 5.5 on both flat and curved surfaces and compares the experimental results to the manufacturer's specifications. In addition the chapter compares the calibration line obtained from the sensor on a flat surface and when embedded in a curved surface to select the calibration method that will provide more accurate measurement readings.

Section 5.6 presents in depth an evaluation and comparison of nonlinearity, repeatability, hysteresis and accuracy of FlexiForce, Tactilus and two FSR sensors using two calibration methods. This is followed by a comparison of drift for the four sensors on flat surfaces.

Section 5.7 reports FlexiForce's dynamic response to a step input and its sensitivity to temperature. It discusses issues related to FlexiForce sensor accuracy and methods used to increase the accuracy and reduce the uncertainty associated with these flexible sensors.

5.2 Instrumentation Specification Terms: Background Information

As mentioned in Sections 2.3 and 2.4, researchers use different methods and terminologies to describe measurement systems and flexible sensors performance. This section defines terminologies used to describe sensors, the mathematical translation for these terminologies and how these methods were combined with statistical methods to describe sensors performances.

5.2.1 Calibration

This is the process of comparing the output of a measurement system against standards of known accuracy [189].

5.2.2 Span or Full Scale (FS)

This represents the highest possible input value that can be applied to the sensor without causing unacceptable inaccuracies [123]. In this work, full scale refers to the maximum input value used during the calibration rather than the highest possible input value. Therefore, the value of FS will always be declared before it is used in any paragraph. In addition, FS is also used to describe the span of the output measured for the input span.

5.2.3 Nonlinearity Error

This is the error that occurs as a result of assuming a linear relationship between the input and the output over the working range [189]. Nonlinearity error is often quantified in terms of maximum nonlinearity and expressed as a percentage of FS [194].

$$\text{max nonlinearity} = \text{max} \left(\frac{\text{actual output} - \text{ideal output}}{\text{FS output}} \times 100 \right) \quad (5.1)$$

In this thesis, this was slightly altered as the usage of maximum value might result in a biased evaluation, as the maximum value might be caused by an outlier in the data set. Thus, the following method was adopted. During calibration, sensors are exposed to between 5 and 15 input values for at least 10 times for each input. The absolute difference between the actual output [input pressure to the sensor] and the ideal output (pressure calculated from the average sensor output signal using linear fitting-line) was then divided by the sensor FS calibration output signal. The average of the absolute difference in FS percentage plus the 95% confidence interval (CI) of the average is used to quantify the nonlinearity error. The 95% CI is calculated using the 't' value from the t-distribution look-up table with the assumption that the absolute differences between the actual output and the ideal output will follow a normal distribution. The 't' value for a large data set will be 1.96, however, it is larger than 1.96 for small size samples [189]. This is translated into a mathematical expression:

$$\begin{aligned} \text{nonlinearity} = \text{average} \left(\frac{|\text{actual output} - \text{ideal output}|}{\text{FS output}} \times 100 \right) \\ + \left[t \times SE \left(\frac{|\text{actual output} - \text{ideal output}|}{\text{FS output}} \times 100 \right) \right] \end{aligned} \quad (5.2)$$

Where, SE is an abbreviation of the standard error.

5.2.4 Hysteresis Error

This is the term used to refer to the difference in the output given for the same value of the quantity being measured according to whether that value has been reached by continuously increasing change or decreasing change [189]. Hysteresis error is also often quantified in terms of maximum hysteresis and expressed as a percentage of FS [195].

$$\text{max hysteresis} = \text{max} \left(\frac{|\text{loading output} - \text{unloading output}|}{\text{FS output}} \times 100 \right) \quad (5.3)$$

In this thesis, this was slightly altered as the maximum value might be caused by an outlier in the data set, which will result in a biased evaluation for the error. Therefore, the following method was adopted. During calibration, sensors were loaded by between 5 and 15 input values with 10 times for each input; 5 times for loading the sensor and 5

times for unloading the sensor. The absolute difference between the loading sensor output and the unloading sensor output was divided by the sensor FS calibration output signal. The average of the absolute difference in FS percentage plus the 95% CI of the average was used to quantify the hysteresis error. The 95% CI was calculated using the 't' value from the t-distribution look up table with the assumption that the differences between the loading and unloading sensor output will follow a normal distribution. This is translated into a mathematical expression, as follows:

$$\begin{aligned} \text{hysteresis} = & \text{average} \left(\frac{|\text{loading output} - \text{unloading output}|}{FS \text{ output}} \times 100 \right) \\ & + \left[t \times SE \left(\frac{|\text{loading output} - \text{unloading output}|}{FS \text{ output}} \times 100 \right) \right] \end{aligned} \quad (5.4)$$

5.2.5 Repeatability Error

This term is used to quantify the ability of the measurement system to give the same value for repeated measurements for the same value of input variable [189]. Repeatability error is often quantified in terms of maximum differences between two calibration cycles and expressed as a percentage of FS [123] (Equation 5.5) or using the 95% of the deviation range [195] (Equation 5.6).

$$\text{max repeatability} = \text{max} \left(\frac{\text{output run 1} - \text{output run 2}}{FS \text{ output}} \times 100 \right) \quad (5.5)$$

$$\text{repeatability} = \frac{2SD(\text{output})}{FS \text{ output}} \times 100 \quad (5.6)$$

In this thesis, the latter was adopted with a small change. Instead of quantifying repeatability at one measurement point, the average repeatability over the sensor full span plus the 95% CI of the mean was used to quantify the repeatability error of the sensor. The 95% CI was calculated using the 't' value from the t-distribution look up table with the assumption that the 95% deviation at any input point will follow a normal distribution. This was translated into a mathematical expression, as follows:

$$\begin{aligned} \text{repeatability} = & \text{average} \left(\frac{1.96SD(\text{output})}{FS \text{ output}} \times 100 \right) \\ & + \left[t \times SE \left(\frac{1.96SD(\text{output})}{FS \text{ output}} \times 100 \right) \right] \end{aligned} \quad (5.7)$$

5.2.6 Drift

This term is used to describe the change in output when used to measure a constant input over a period of time [189]. It can be expressed in terms of FS or relative to the output at time where the load is first applied [189].

$$Drift = \frac{output(t = T) - output(t = 0)}{output(t = 0)} \times 100 \quad (5.8)$$

In this thesis, drift was measured over various time slots. Therefore, drift is always reported relative to the output at the time where the load is first applied and the time ($t = T$) where the drift is measured.

5.2.7 Calibration Fitting Line Error

In many cases, linear fitting-lines do not describe accurately the relationship between the input stimulus and the sensor output. Therefore, polynomial fitting-lines are used in these cases. The difference between the actual output (input stimulus) and the ideal output (calculated using sensor output and the calibration fitting-line) is described in this thesis as the calibration fitting-line error. Similar to nonlinearity error, it is expressed in percentage FS. The average of the absolute difference percentage FS plus the 95% CI of the average is used to quantify the calibration fitting-line error. The 95% CI is calculated using the 't' value from the t-distribution look up table with the assumption that the absolute differences between the actual output and the ideal output will follow a normal distribution. This is translated into a mathematical expression, as follows:

$$\begin{aligned} fitting\ line\ error = & average \left(\frac{|actual\ output - ideal\ output|}{FS\ output} \times 100 \right) \\ & + \left[t \times SE \left(\frac{|actual\ output - ideal\ output|}{FS\ output} \times 100 \right) \right] \end{aligned} \quad (5.9)$$

5.2.8 Accuracy

The accuracy of a system is the extent to which the reading it gives might be wrong and it can be quantified by summing all the possible errors that are likely to occur [189]. Error can be summed using the following general equation [189]:

$$\Delta Z = \sqrt{\Delta A^2 + \Delta B^2} \quad (5.10)$$

In this thesis, accuracy always represents the combined errors of nonlinearity or calibration fitting-line, hysteresis and repeatability.

5.2.9 Uncertainty

Uncertainty in the measurements is normally caused by systematic errors and can be quantified, like sensor's accuracy, and by other means, like operator error [123]. In this thesis, if uncertainty is used with any averaged reading, then it refers to the summation of the accuracy of the sensors used to obtain the average reading and the 95% CI of that average. Equation 5.10 is used to carry out the summation.

5.2.10 Response Time

Response time is the time taken for the output to reach 63% of its steady-state value or in the case of oscillation, the time taken to reach its first peak of the oscillation, when a step input is applied to the sensor [189].

5.3 Sensor Selection

5.3.1 Commercial Medical Pressure Sensor

Section 2.3 reviewed the current commercial medical pressure sensors used to measure the pressure under compression bandages. PicoPress was selected among them for the following reasons:

1. Mosti and Rossari [122] illustrated that the sensor outperformed Kikuhime and the SIGaT, with Kikuhime being very popular among clinicians.
2. The sensor can be calibrated under the bandage. This means one PicoPress transducer and array of PicoPress balloons can be used under MCBs to map the pressure. Every time a sensor balloon is connected to the transducer, the transducer can be calibrated and used directly to read the pressure, without the need for calibrating using external devices.
3. The transducer can be used for dynamic measurements.

5.3.2 MEMS Force Sensor

There are various types of these sensors which are available in the market. FS01 force sensor (Figure 5.1) was selected as it can measure low forces $0 - 0.68kg$ with typical FS is $3V$, nonlinearity $\pm 1\%FS$, maximum hysteresis $\pm 0.5\%FS$, drift $0.5\%FS$ at full scale load in 20 minutes and $1\%FS$ difference after 1 million force cycles [196]. The sensor also has low physical profile. In addition, the sensor is relatively cheap compared to other low profile load cells, priced at about £65. Moreover, the sensor has its onboard amplification circuit and can be powered by $5V$ [196].

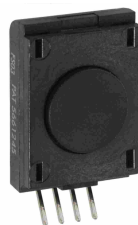


Figure 5.1: FS01 force sensor from Honeywell [196]

5.3.3 Flexible Sensors

Resistive-based flexible sensors were considered for this project as capacitive sensors are expensive. FlexiForce, Tactilus and two sizes of FSR: $5mm$ active sensing diameter and $12mm$ active sensing diameter sensors were selected for this project. From the resistive-based, FSA and QTC were not considered as no FSA or QTC single point sensor could be allocated. Indeed, single point QTC sensors can be made from QTC sheets; however, as found by Komi et al. [169] this did not result in a robust sensor. Furthermore, there is another size from the freeform FSR sensors which was not selected due to its large size, $38 \times 38mm$ active sensing area.

5.4 Evaluation of PicoPress Sensor

5.4.1 Static Characteristics of PicoPress Sensor

Objective

To evaluate the nonlinearity, hysteresis and repeatability errors of the PicoPress sensor and quantify its accuracy.

Materials and Method

The sensor was tested on a rigid cylinder using an aneroid sphygmomanometer (Figure 5.2). Pressure was applied to the transducer with $10mmHg$ pressure increments from $0mmHg$ to $120mmHg$ and then with $10mmHg$ decrements from $120mmHg$ to $0mmHg$. The process was repeated five times and the recorded data was analyzed using Excel 2007.

Results, Analysis and Discussion

Table 5.1 summarizes the nonlinearity, repeatability and hysteresis errors for the sensor. The overall accuracy for the sensor is $\pm 2.81\%FS$, where FS here is $120mmHg$. This means that the sensor accuracy is $\pm 3.4mmHg$. Figure 5.3 illustrates the sensor output over 5 repeats.

Table 5.1: Summary of PicoPress sensor's static characteristics. Accuracy is calculated by using Equation 5.10 and the upper 95% CI, which takes in consideration some of the uncertainty due to the measurement variation

Statistics	Nonlinearity error	Repeatability error	Hysteresis error
Max	3.33%	2.00%	2.83%
Mean	1.09%	0.90%	1.77%
Upper 95% CI	1.27%	1.09%	2.26%
Lower 95% CI	0.91%	0.72%	1.28%
Accuracy	2.81%		



Figure 5.2: PicoPress sensor, the aneroid sphygmomanometer and the cylinder used to evaluate the sensor

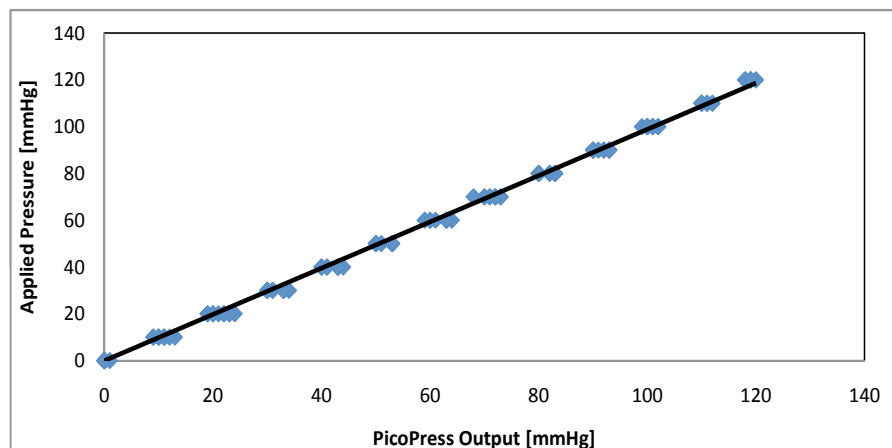


Figure 5.3: PicoPress sensor output for five repeats when tested with aneroid sphygmomanometer

5.4.2 Evaluation of the effect of PicoPress Physical Dimensions on the Measured Interface Pressure

Objective

To evaluate the impact of PicoPress balloon's physical dimensions on the interface pressure.

Materials and Method

The sensor was tested on the same rig used in Section 3.3.4 (Figure 5.4). The pressure was applied to the transducer using a SurePress bandage with 1.6kg attached load. The pressure was applied to the transducer probe 20 times. Each time both the pressure applied and the extension in the bandage were measured. The extension in the bandage was converted into the equivalent tension using the 4th order polynomial fitting-line for the 5th cycle tension elongation curve (0 – 80% elongation) for SurePress. These tension values and the ones estimated from the load were converted into the equivalent theoretical pressures using Equation 3.9. A correction to the pressures measured using the PicoPress transducer was also obtained using Equation 3.33. MATLAB R2009b and Excel 2007 were used to process and display the data.

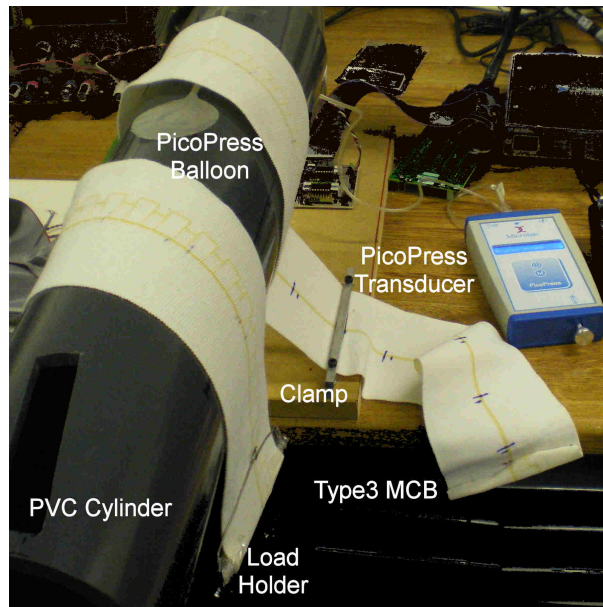


Figure 5.4: Rig used to evaluate the impact of PicoPress probe's physical dimensions on the interface pressure

Results, Analysis and Discussion

Table 5.2 provides a statistical summary of the extensions and pressures measured and the tensions, computed pressures from load, computed pressures from extension and the corrected measured pressures. Figure 5.5 illustrates the theoretical, measured and corrected pressures. The PicoPress transducer will overestimate the pressure applied by a bandage due to the formation of local sharp curvature secondary to the sensor's physical dimensions. Using the equation model proposed by Vinckx et al. [86] (Equation 2.8) resulted in pressures which are slightly smaller than the pressures expected theoretically. This indicates that using devices like PicoPress to study compression bandages will result in overestimating the pressures applied by compression bandages. In this particular

case where the cylinder diameter is large the PicoPress was expected to overestimate the pressure by 61% and data measured showed that it overestimated the pressure by approximately 48%, which is a significant value.

Table 5.2: Summary of the experimental results for the impact of PicoPress probe's physical dimension on the interface pressure. The correction factor used was 0.62

Statistical Analysis	Extension [%]	Tension calculated from extension [N]	Tension calculated from load [N]	Computed pressures from extension [mmHg]	Computed pressures from load [mmHg]	Measured pressures [mmHg]	Corrected measured pressures [mmHg]
Mean	73%	16.58	15.97	20.61	19.51	28.85	17.89
SD	4%	1.41	0.00	1.76	0.00	3.10	1.92
SE	1%	0.32	0.00	0.39	0.00	0.69	0.43
Upper 95% Range	81%	19.35	15.97	24.06	19.51	34.93	21.65
Lower 95% Range	66%	19.52	15.97	24.27	19.51	35.30	21.88
Upper 95% CI	75%	19.52	15.97	24.27	19.51	35.30	21.88
Lower 95% CI	71%	15.92	15.97	19.80	19.51	27.41	16.99

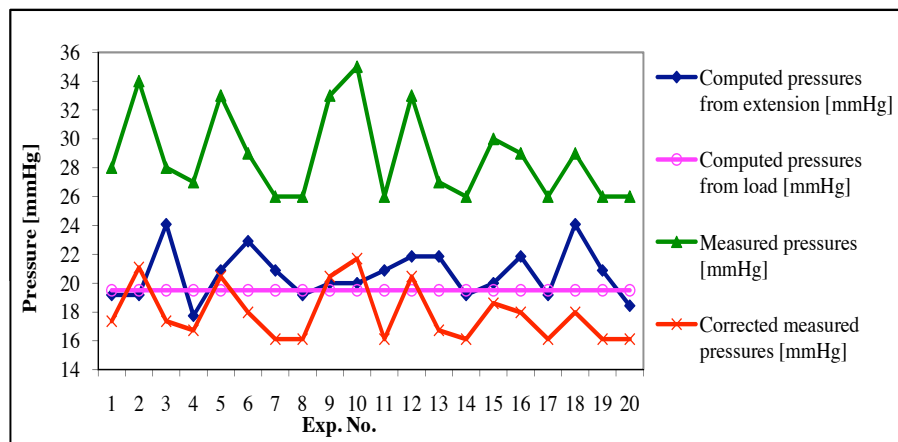


Figure 5.5: The pressures measured, estimated and corrected during the experimental setup to study the impact of PicoPress probe's physical dimension on the interface pressure. Lines connecting the pressure points are for illustrative purposes

5.5 Evaluation of MEMS FS01 Force Sensor

From FS01 specification sheet [196], the sensor can be used to measure forces up to $0.68kg$. The overall sensor accuracy is calculated to be $\pm 1.1\%FS$ (approximately $\pm 4.7mmHg$) [196]. However, no information is available about sensor repeatability error. This section will demonstrate in-house testing for the sensor both on flat surfaces and curved surfaces.

5.5.1 Evaluation of FS01 Force Sensor over Flat Surface

Objective

To evaluate nonlinearity, hysteresis, repeatability and drift errors of the FS01 sensor and quantify its accuracy on a flat surface.

Materials and Method

The test rig: A special rig was designed to carry out the testing (Figure 5.6). Eleven loads were used in the experiment to apply pressures from 0 – 109 $mmHg$.

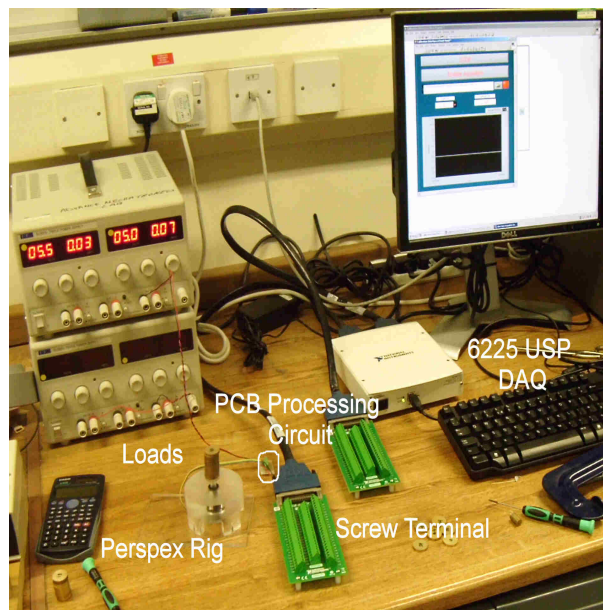


Figure 5.6: The test rig and the arrangement used to test the FS01 force sensor

Processing circuit: A conditioning circuit was designed and fabricated over a printed circuit board (PCB) to power up the sensor and pass the output signal to a screw terminal which in turn was connected to a Mass Term 6225 USB DAQ card.

Signal acquisition: The data acquired through a differential I/O on the 6225 USB DAQ card was sampled at 1 kHz and filtered using a program written in LabView 8.6. The filter used was a low-pass filter with cut-off frequency of 10 Hz . This was selected to remove the noise due to the main (50 Hz). The program was also used to save only one data point per load for the calibration process. For the drift test, the program was modified to take the average of every 1000 samples and save them into a file for 10 minutes.

Protocol: The loads were applied to the transducer with 10 $mmHg$ pressure increments from 0 $mmHg$ to 109 $mmHg$ and then with 10 $mmHg$ decrements from 109 $mmHg$ to

0mmHg (the first load applied only 9mmHg). The process was repeated five times and the recorded data was analyzed using Excel 2007.

For the drift test, 59mmHg was applied to the sensor for 10 minutes and the data was processed using Excel 2007.

Results, Analysis and Discussion

Table 5.3 summarizes the nonlinearity, repeatability and hysteresis errors of the sensor. The overall accuracy of the sensor is $\pm 1.9\%FS$, where FS here is 109mmHg. This means the sensor's accuracy error is $\pm 2.07mmHg$, which is about half the accuracy that is reported by the manufacturer. This can be explained by the fact that only 1/4 of the sensor range was used in this calibration process. Figure 5.7 illustrates the sensor output over 5 repeats. The sensor drift error was -0.68% after 10 minutes of applying 59mmHg pressure to the sensor (less than 1mmHg).

Table 5.3: Summary of FS01 sensor's static characteristics on flat surface. Accuracy is calculated by using Equation 5.10 and the upper 95% CI, which takes in consideration some of the uncertainty due to the measurement variation

Statistics	Nonlinearity error	Repeatability error	Hysteresis error
Max	1.69%	1.92%	1.56%
Mean	0.71%	0.78%	1.06%
Upper 95% CI	0.79%	0.98%	1.42%
Lower 95% CI	0.62%	0.59%	0.71%
Accuracy	1.90%		

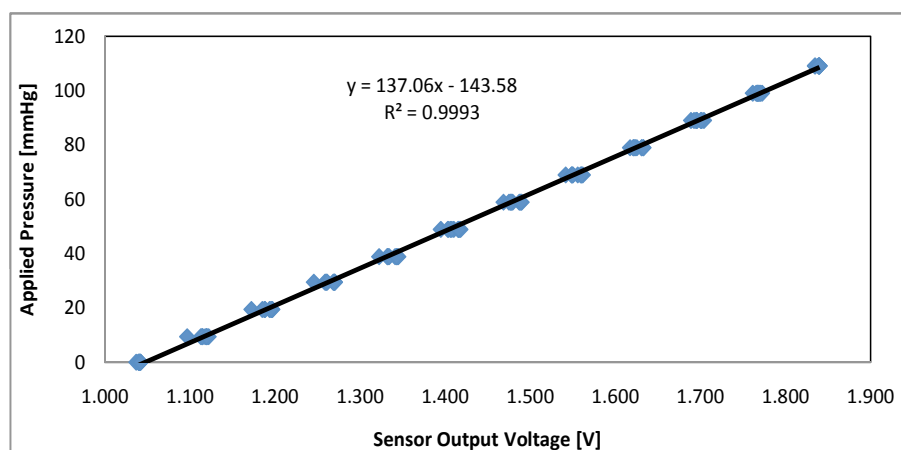


Figure 5.7: FS01 force sensor output for five repeats when tested with deadweights

5.5.2 Evaluation of FS01 Force Sensor Over Curved Surface

As it was demonstrated in the last section, FS01 force sensor has good accuracy over flat surfaces. However, the sensor will be embedded during the project within a curved surface, which even in the case where the sensor is flashed with the cylinder wall, it will still produce an edge that may overestimate the pressure. Therefore, this section will evaluate the sensor's performance when embedded in a curved surface.

Objective

To evaluate the nonlinearity, hysteresis and repeatability errors of the FS01 sensor and quantify its accuracy on a curved surface.

Materials and Method

The test rig: A rectangular hole was drilled in the wall of a cylinder with $0.14m$ diameter. The sensor was pushed through the tight fit hole and secured in place with cellular tapes. An aneroid sphygmomanometer was used to apply pressure from $0 - 120mmHg$ to the sensor (Figure 5.8).

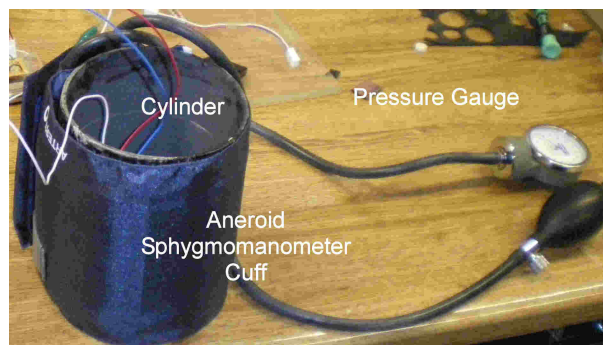


Figure 5.8: The test rig and arrangement used to test FS01 over a curved surface

Signal acquisition: The data was acquired through a differential I/O on 6225 USB DAQ card, sampled at $1kHz$ and filtered using a program written in LabView 8.6. The filter used was a low-pass filter with cut-off frequency of $10Hz$. The program saved one data point per load for the calibration process.

Protocol: The pressure was applied to the transducer with $10mmHg$ pressure increments from $0mmHg$ to $120mmHg$ and then with $10mmHg$ decrements from $120mmHg$ to $0mmHg$. The process was repeated four times and the recorded data was analyzed using Excel 2007.

Results, Analysis and Discussion

Table 5.4 summarizes the nonlinearity, repeatability and hysteresis errors of the sensor. The overall accuracy error of the sensor was $\pm 6.43\%FS$, where FS is $120mmHg$. This means the sensor accuracy error is $\pm 7.61mmHg$, which is about four times of its accuracy on flat surface. Calibration errors due to the usage of aneroid sphygmomanometer might be the main source of this increase in the error.

Table 5.4: Summary of FS01 sensor's static characteristics on a curve surface. Accuracy is calculated by using Equation 5.10 and the upper 95% CI, which takes in consideration some of the uncertainty due to the measurement variation

Statistics	Nonlinearity error	Repeatability error	Hysteresis error	2nd order poly fitting line error
Max	7.72%	6.94%	1.55%	5.21%
Mean	2.89%	4.65%	0.97%	2.08%
Upper 95% CI	3.32%	5.36%	1.23%	2.34%
Lower 95% CI	2.47%	3.93%	0.72%	1.82%
Accuracy	6.43%			5.98%

Comparing Figure 5.9 and Figure 5.7 it can be seen that the FS output over a curved surface is more than twice as much as the the FS output over a flat surface (FS over flat surface is $0.85V$ and over cylinder is $2.2V$). This indicates that the sensor's plunger sharp edges might be creating local high forces. In addition, the nonlinearity of the sensor did increase specially at low pressures. Using polynomial fitting will result in further improvements of the sensor's accuracy as can be seen in Table 5.4

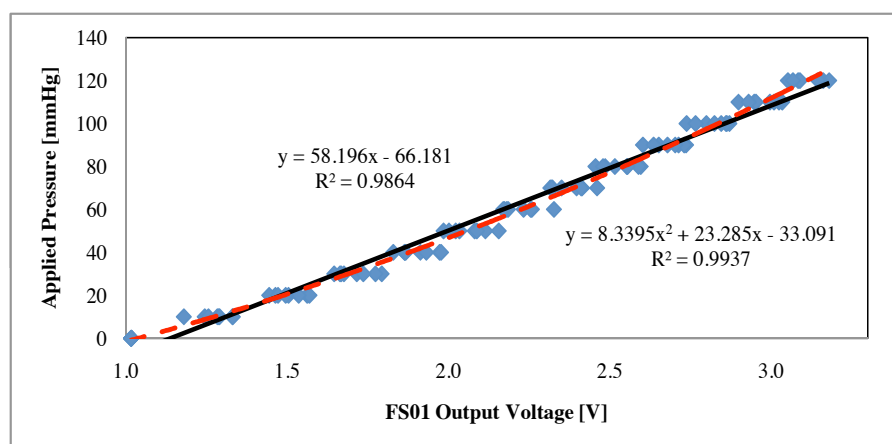


Figure 5.9: FS01 force sensor output for five repeats when tested with aneroid sphygmomanometer

5.6 Evaluation and Comparison of Flexible Resistive-Based Sensors

The resistive-based flexible sensors were identified through the literature review with the potential to be used within the interface pressure measurement system and within the pressure-mapping bandage. The identified sensors were: FlexiForce, Tactilus and FSR (Figure 5.10). As FSR sensors come in multiple of sizes and shapes, two of their standard shapes were selected for this project: 5mm and 12mm active sensing diameter. The current section will provide a comparison of these sensors using two calibration techniques and will select one of them to be further used.

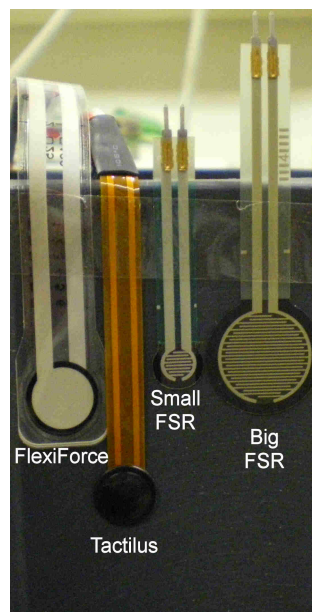


Figure 5.10: FlexiForce, Tactilus, big FSR and small FSR sensors

5.6.1 Evaluation of Flexible Resistive-Based Sensors Using Deadweights

Objective

To evaluate and compare the selected sensors nonlinearity, hysteresis, repeatability and drift errors and quantify their accuracy using deadweights.

Materials and Method

The test rig: A special rig was designed to carry out the testing for Tactilus sensor (Figure 5.11). For the other three sensors, a puck was used between the sensor and deadweights to direct the force towards the sensing area of the sensor. Dead weights were selected so they produced 0 – 110mmHg of pressure on the sensitive area of the sensor.

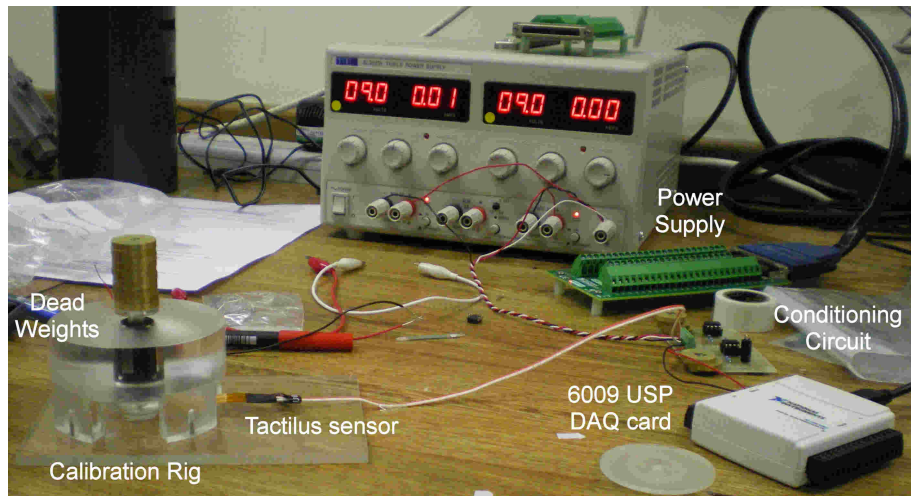


Figure 5.11: The test rig and the arrangement used to test Tactilus force sensor

Processing Circuit: Resistance of samples from the selected sensors was measured at 120mmHg pressure. The resistance values were used to design and fabricate a processing circuit on a PCB for each sensor. The processing circuit consisted of a voltage follower that provided a constant -5V for the sensors, a variable gain op-amp circuit and a low-pass filter with cut-off frequency of 10Hz to remove the noise. The gain was set so that the transducer output provided approximately 7V at 120mmHg . The circuit was powered with $\pm 9\text{V}$ via voltage generator.

Signal Acquisition: 6009 USB DAQ card was used to acquire the output signal from the processing circuits. The output signal sampled at 1kHz using a program written in LabView 8.6. The acquired signal was filtered using a software based low-pass filter with cut-off frequency of 10Hz .

Protocol: The loads were applied to the transducer with increasing pressure increments from 0mmHg to approximately 110mmHg and then with decreasing pressure decrements from approximately 110mmHg to 0mmHg . The process was repeated five times for two sensors of each type and the recorded data was analyzed using Excel 2007.

For the drift test, 60mmHg equivalent load was applied to the sensor for 20 minutes. The test was repeated three times for two sensors from each type. The data was processed using MATLAB R2009b and Excel 2007.

Results, Analysis and Discussion

The two FSR sensors did not respond to pressures lower than 30mmHg . Therefore, they were excluded from the test. Table 5.5 summarizes the nonlinearity, repeatability and hysteresis errors of FlexiForce and Tactilus sensors. FlexiForce sensor outperforms Tactilus sensor. The overall accuracy is $\pm 11.52\%FS$ and $\pm 14.76\%FS$ of FlexiForce sensors 1 and

2 respectively, where FS here is 106mmHg . This means the sensor accuracy is about $\pm 12.21\text{mmHg}$ and $\pm 15.65\text{mmHg}$ respectively, which is about half the accuracy reported by the manufacturer $\pm 6\%FS$, where FS is $4.4N$ or 462mmHg (accuracy 28mmHg). Figures 5.12 and 5.13 illustrate the two sensors output over 5 repeats.

Table 5.5: Summary of FlexiForce and Tactilus sensor's static characteristics using deadweights. Accuracy is calculated by using Equation 5.10 and the upper 95% CI, which takes in consideration some of the uncertainty due to the measurement variation

Statistics	Nonlinearity error			Repeatability error			Hysteresis error			Accuracy
	Mean	Upper 95% CI	Lower 95% CI	Mean	Upper 95% CI	Lower 95% CI	Mean	Upper 95% CI	Lower 95% CI	
FlexiForce Sensor 1	4.17%	4.70%	3.64%	8.07%	9.69%	6.44%	3.27%	4.08%	2.46%	11.52%
FlexiForce Sensor 2	4.84%	5.50%	4.18%	10.59%	13.04%	8.14%	3.17%	4.19%	2.15%	14.76%
Tactilus Sensor 1	3.97%	4.71%	3.23%	9.05%	11.61%	6.50%	4.04%	5.61%	2.46%	13.73%
Tactilus Sensor 2	7.07%	8.30%	5.85%	17.85%	21.64%	14.06%	4.39%	6.32%	2.46%	24.02%

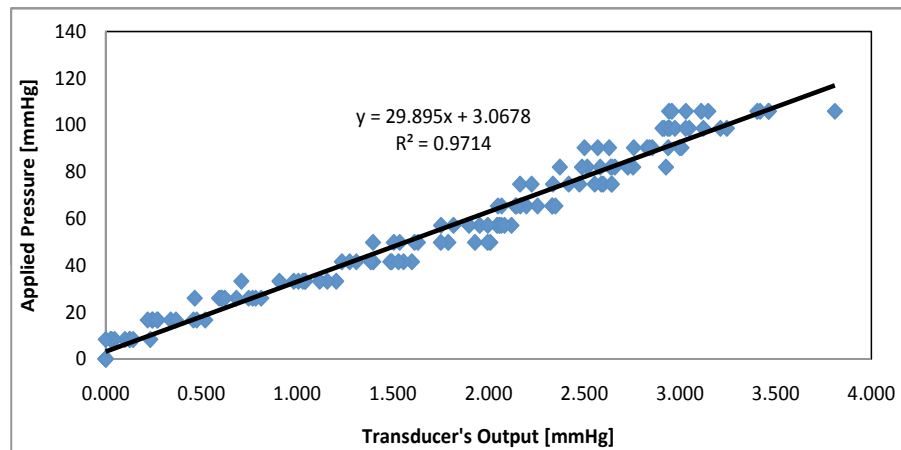


Figure 5.12: FlexiForce sensor output for five repeats when tested with deadweights

The four sensors drift error after 10 minutes from applying approximately 60mmHg is reported in Table 5.6. The results demonstrate that FlexiForce was the most stable sensor at low pressures. The high drift values for both FSR sensors can be explained by the fact that the loads used were less than $1N$ which is less than the $1/100$ of the sensor span. However, no reason was found to explain the high drift presented in Tactilus performance.

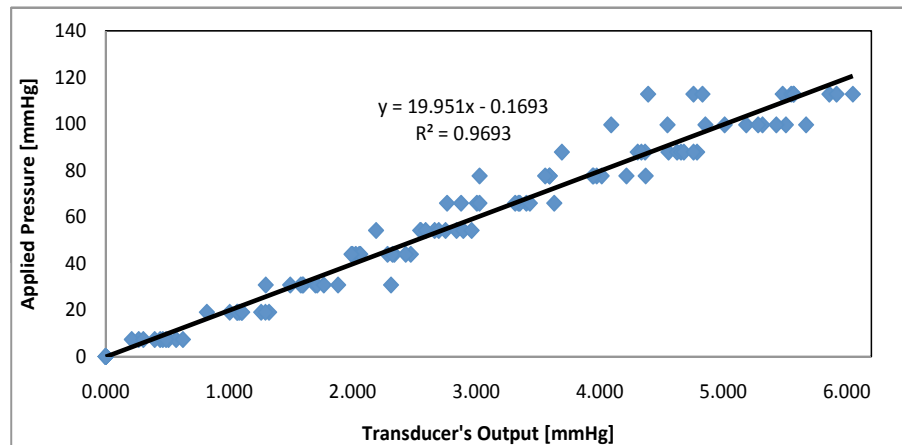


Figure 5.13: Tactilus sensor output for five repeats when tested with deadweights

Table 5.6: Summary of FlexiForce, Tactilus, big FSR and small FSR sensor's drift error after applying 60mmHg on a flat surface

	FlexiForce		Tactilus		Big FSR		Small FSR	
	Sensor 1	Sensor 2	Sensor 1	Sensor 2	Sensor 1	Sensor 2	Sensor 1	Sensor 2
Mean	-6.35%	3.79%	34.15%	22.40%	53.12%	53.26%	47.04%	41.74%
SD	4.79%	2.03%	17.59%	11.32%	35.13%	50.97%	24.97%	19.51%

5.6.2 Evaluation of Flexible Resistive-Based Sensors Using Aneroid Sphygmomanometer

During the preliminary tests of these sensors, FlexiForce and the FSR sensors were found to be more sensitive when an aneroid sphygmomanometer was used. Therefore another experiment was designed to test these sensors using aneroid sphygmomanometer to apply pressures to these sensors and check their performances accordingly.

Objective

To evaluate and compare the selected sensors nonlinearity and repeatability errors and quantify their accuracy using an aneroid sphygmomanometer.

Materials and Method

The test rig: Due to these sensors being sensitive to bending, a cylinder with flattened side (Figure 5.14) was used to test them. The sensors were tested using an aneroid sphygmomanometer for the pressure range $100 - 0\text{mmHg}$.

Processing circuit: The same circuits used in Section 5.6.1 were used in this experiment.

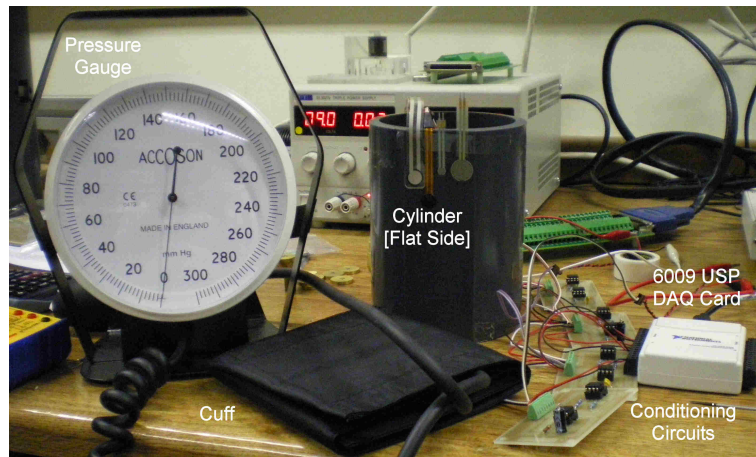


Figure 5.14: The arrangement to test nonlinearity and repeatability of FlexiForce, Tactilus, big FSR and small FSR sensors using aneroid sphygmomanometer

Signal acquisition: The arrangement of the data acquisition from Section 5.6.1 was used in this experiment. Only the program used was changed to acquire the signal from the four sensors simultaneously.

Protocol: The sphygmomanometer cuff was inflated to 100mmHg first and then deflated with 10mmHg decrements until 0mmHg . The process was repeated 20 times. Two sensors from each type were tested. Data was analyzed using Excel 2007.

Results, Analysis and Discussion

The two small FSR sensors did not respond to pressures lower than 50mmHg . Therefore, they were excluded from the test. The two big FSR sensors did not respond to pressures as low as 10mmHg , which means that they cannot be used in the pressure measurement system and pressure-mapping bandages. Table 5.7 summarizes the nonlinearity and repeatability errors of FlexiForce, Tactilus and big FSR sensors. As other researchers found [162], FSR sensors have better repeatability than FlexiForce sensors, while, FlexiForce sensors have better linearity than FSR sensors. Overall, combining both linearity and repeatability errors, FSR shows slightly better performance than FlexiForce sensors. However, as they are not sensitive at low pressures (10mmHg) and as their drift error at low pressures is very high, FlexiForce seems to be a better sensing solution than FSR for this particular project.

Figures 5.15, 5.16 and 5.17 illustrate the three sensors output over 20 repeats. Comparing the performance of FlexiForce using both deadweights and aneroid calibration technique, the two sensors show similar nonlinearity and repeatability errors. However, comparing the two FlexiForce sensors output using the two calibration techniques shows that FlexiForce transducer output voltage at any pressure is larger when an aneroid sphygmomanometer is used than when deadweights are used. This indicates a potential calibra-

Table 5.7: Summary of FlexiForce, Tactilus and big FSR sensors' static characteristics using aneroid sphygmomanometer. Accuracy is calculated by using Equation 5.10 and the upper 95% CI, which takes in consideration some of the uncertainty due to the measurement variation

Statistics	Nonlinearity error			Repeatability error			Accuracy
	Mean	Upper 95% CI	Lower 95% CI	Mean	Upper 95% CI	Lower 95% CI	
FlexiForce Sensor 1	2.11%	2.92%	1.31%	7.86%	10.13%	5.60%	10.54%
FlexiForce Sensor 2	4.30%	6.42%	2.18%	8.10%	10.83%	5.37%	12.59%
Tactilus Sensor 1	8.57%	11.63%	5.50%	11.15%	15.07%	7.23%	19.04%
Tactilus Sensor 2	12.96%	17.53%	8.39%	16.61%	20.40%	12.83%	26.89%
Big FSR 1	2.29%	3.93%	0.64%	3.60%	4.86%	2.34%	6.26%
Big FSR 2	4.18%	7.26%	1.11%	4.99%	7.78%	4.99%	10.64%

tion problem. Interestingly, Tactilus sensors showed higher sensitivity when an aneroid sphygmomanometer was used than when deadweights were used.

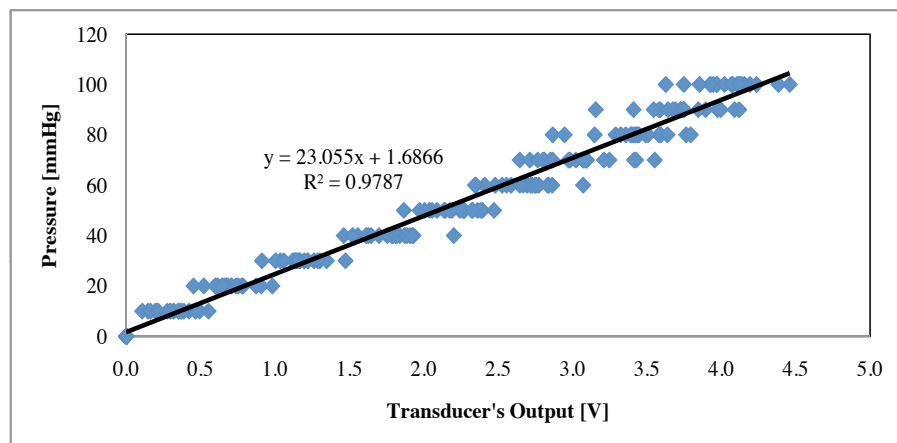


Figure 5.15: FlexiForce sensor output for twenty repeats when tested with aneroid sphygmomanometer

5.7 FlexiForce Sensors: Other Issues

5.7.1 FlexiForce Dynamic Response to Step Input

Tekscan claims that their sensor time response is less than $5\mu s$ [174]. Lebosse et al. [162] reported that FlexiForce sensor can be identified as a first-order system with a time constant of $30ms$, which corresponds to a cut-off frequency around $30Hz$. They also reported a significant degradation in the sensor output even at very low frequencies, when the sensor is excited for long time. However, they have not reported how they arrived at

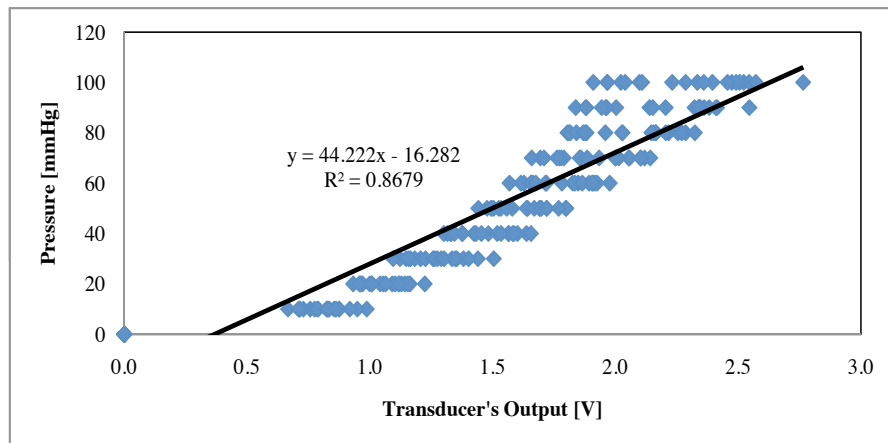


Figure 5.16: Tactilus sensor output for twenty repeats when tested with aneroid sphygmomanometer

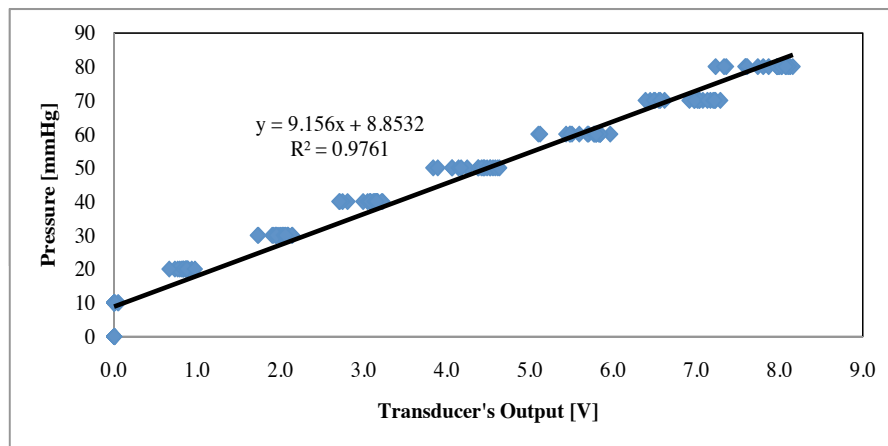


Figure 5.17: Big FSR sensor output for twenty repeats when tested with aneroid sphygmomanometer

the $30ms$ figure for the time constant. This section will present the work carried out to study the sensor's response to step input and estimate its time constant and bandwidth.

Objectives

- To study the sensor's response to a step input.
- To study the transducer (sensor + gain and low-pass filter circuit) response to a step input.

Materials and Method

In order to study the dynamic response to a step input, it is necessary to identify first the first-order model for the system, which can be obtained by using MATLAB R2009b

system identification toolbox or LabView signal express. However, these softwares need to have both the excitation signal and output signal from the sensor to produce the required model, which can be achieved, in this case, by measuring the forces applied to a FlexiForce sensor using another high performance load cell which has better static and dynamic characteristics than FlexiForce sensors. A LCAE-600G load cell (Omega, Connecticut, USA) was used in this experiment (Figure 5.18). The sensor was calibrated in-house and found to have an accuracy of $0.9\%FS$, where FS here is $112g$, which if applied to FlexiForce sensor will result in $106mmHg$ of pressure. According to the load cell manufacturer, the time response of the load cell is better than $10ms$.

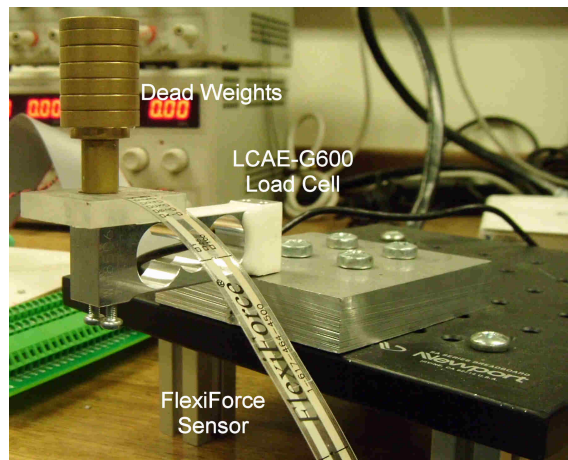


Figure 5.18: LCAE-600G load cell used to study the FlexiForce step response to a step input

A load equivalent to $77mmHg$ was applied to two FlexiForce sensors 10 times. This was repeated for the sensors when they were connected in a potential divider arrangement with a $100k\Omega$ resistor and when they were connected to the gain and low-pass filter circuit used in Section 5.6.1 . The reason behind repeating the test on two different circuits is to identify whether the low-pass filter had any effect on the sensor response. A Mass term 6225 USB DAQ card was used to acquire the load cell and the FlexiForce signals at a sampling rate of $10kHz$. A LabView routine was written to handle the acquired signals and MATLAB R2009b system identification toolbox was used to post process them.

Results, Analysis and Discussion

Figures 5.19 and 5.20 show the excitation pressures applied to a FlexiForce sensor and its output for both potential divider arrangement and gain-low-pass-filter circuit. The first-order autoregressive model with exogenous input (ARX) was not always able to provide a good approximation for the output signal of the FlexiForce sensor. Only the model of sensor 1 with gain-filter circuit showed low errors in estimation during model validation. However, using higher orders of ARX model or using autoregressive moving average model with exogenous input (ARMAX) did not result in any improvement. MATLAB LTI

viewer was used to examine the response of the model estimated for the two conditioning arrangement for the two sensors. The time constant was $1265ms$ for sensor 1 with a resistor circuit, $268ms$ for sensor 1 with a gain-filter circuit, $662ms$ for sensor 2 with resistor circuit and $696ms$ for sensor 2 with gain-filter circuit. If these models are an accurate representation of the sensor, then it is very clear that the time constant of the sensor is much higher than the $30ms$ reported earlier. This means that the sensor bandwidth is in the range of $0.126 - 0.594Hz$. Indeed, this explains why Lebosse et al. [162] found that applying low forces with $0.5Hz$ for 20 minutes results in a significant reduction in the sensor's output.

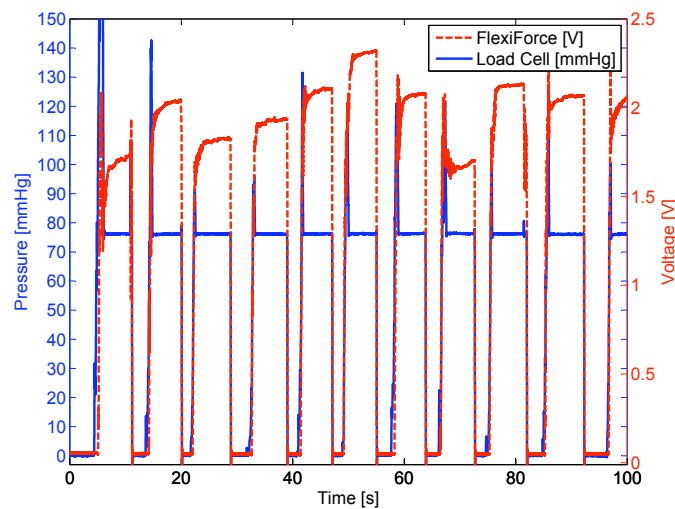


Figure 5.19: The output of the load cell and the FlexiForce sensor 1, when connected in a potential divider arrangement

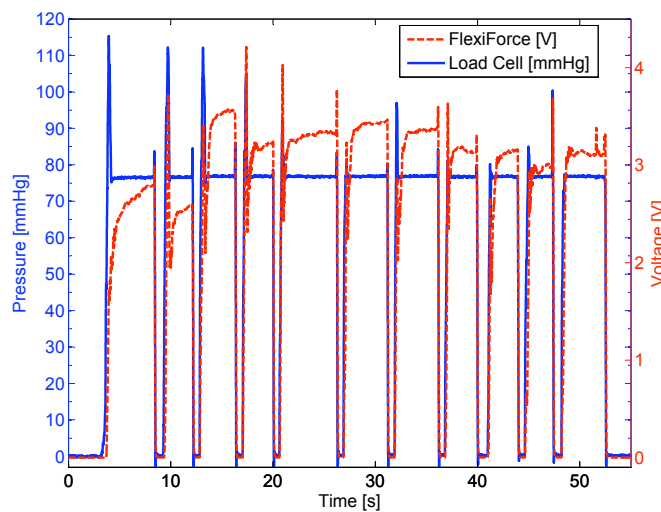


Figure 5.20: The output of the load cell and the FlexiForce sensor 1, when connected in a gain-filter circuit arrangement

In addition, from the time constant of sensor 2, it can be seen that there is no significant difference in the sensor's response when a capacitor is introduced to form a low-pass filter. Figures 5.21 and 5.22 illustrate that FlexiForce sensor output signal lags the input signal measured by the load cell, which explains some of the above findings. These results might be explained by the capacitive behavior for FlexiForce sensors reported by Paredes-Madrid et al. [182]. Additionally, these results challenge Tekscan claims of $5\mu s$ time response.

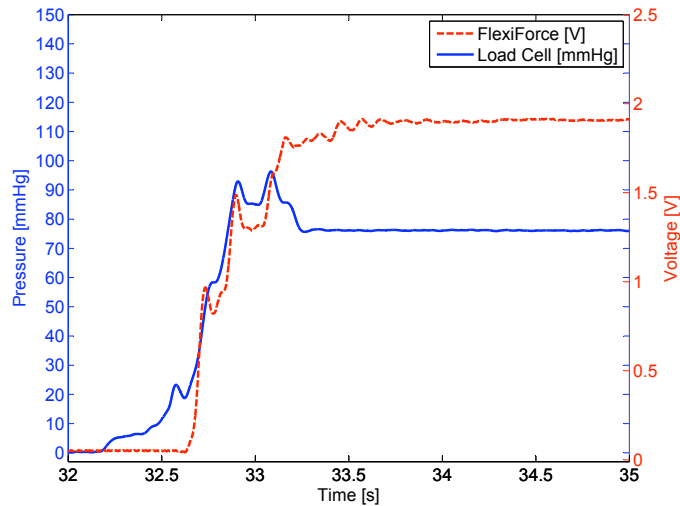


Figure 5.21: The time difference in response time of the output of the load cell and the FlexiForce sensor 1, when connected in a potential divider arrangement.

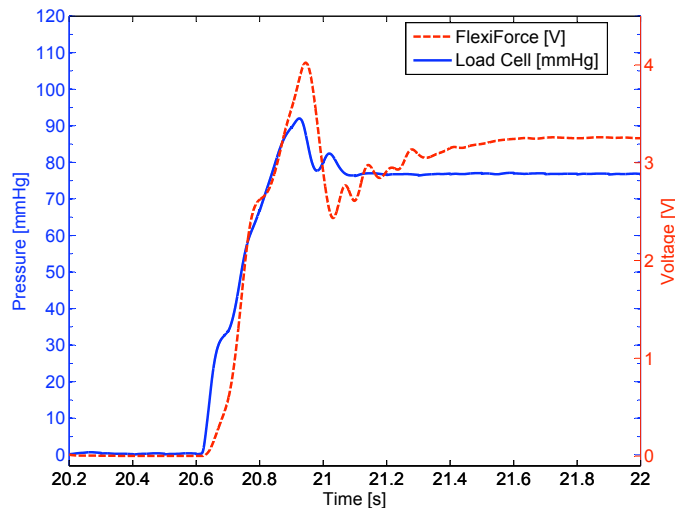


Figure 5.22: The time difference in response time of the output of the load cell and the FlexiForce sensor 1, when connected in a gain-filter circuit arrangement [one cycle]

5.7.2 FlexiForce Temperature Sensitivity

According to Tekscan [174], FlexiForce sensors temperature sensitivity is about $0.36\%/^{\circ}C$. Wertheim et al. [134] reported that a median of $1.9^{\circ}C$ in temperature was recorded under compression bandages at the medial aspect of the leg after applying the bandage for 12 minutes (range $1.5 - 4.3^{\circ}C$). Taking into account that the surface temperature of the leg is about $37^{\circ}C$, then, a sensor calibrated at $25^{\circ}C$ may be affected by the additional $12^{\circ}C$ change in temperature. However, Tekscan specifications were not clear whether this temperature sensitivity is for the full span or not. Therefore, a simple experiment was conducted to check the impact of temperature change from $22^{\circ}C$ to $42^{\circ}C$ on the sensor's performance.

Objective

To study the impact of temperature change from $22^{\circ}C$ to $42^{\circ}C$ on the sensor's performance, when subjected to low pressures.

Materials and Method

A controllable temperature oven (Figure 5.23) was used to increase the temperature from $22^{\circ}C$ to $42^{\circ}C$, while a constant pressure of $37mmHg$ was applied to a FlexiForce sensor. The change in the sensor's output and temperature was recorded manually, with voltage being monitored using a multimeter. The process was repeated three times. Both the correlation and linear regression between the temperature and sensor's output voltage were tested using PASW 17.

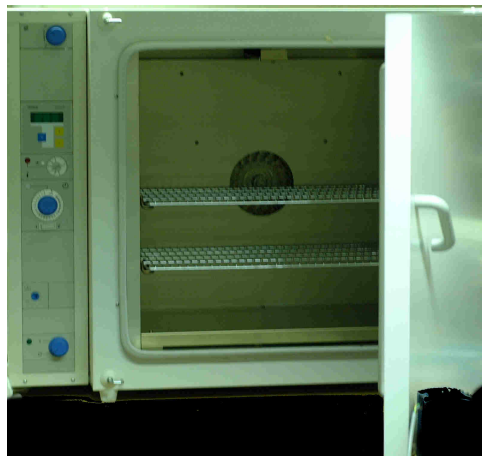


Figure 5.23: Oven used in the experiment

Results, Analysis and Discussion

Figure 5.24 illustrates the measured voltages and temperatures. The correlation between temperature and voltage when low pressures were applied to the sensor was found to be

statistically insignificant. The linear fitting-line in Figure 5.24 was statistically insignificant when tested using ANOVA. These results suggests that temperature effect on the sensors output at low pressures and temperature might be insignificant. Therefore, there is no need to build a controlled temperature chambers to calibrate these sensors at $37^{\circ}C$ to use them over human subjects. Nevertheless, the fan inside the oven used in the experiment might have had an impact on the experiment; thus, further work is required in order to explore fully the effect of temperature on the sensor performance.

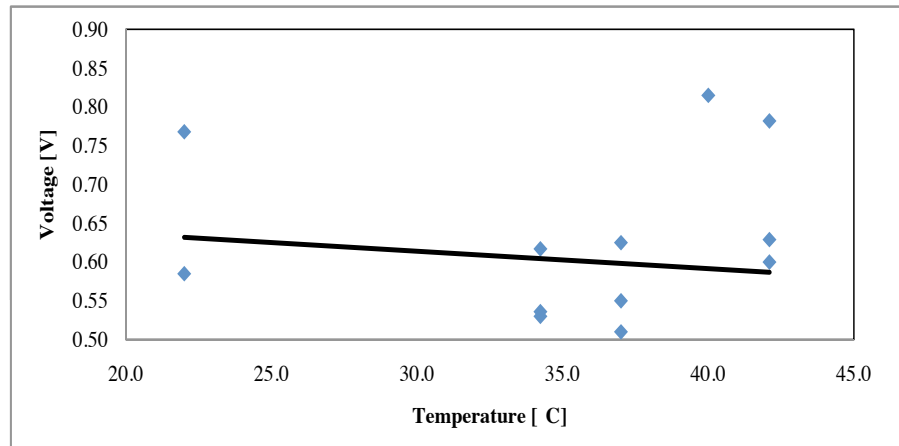


Figure 5.24: The output voltage of the FlexiForce sensor vs. change in temperature

5.7.3 FlexiForce Averaging Technique

The FlexiForce sensor's accuracy was found to be between $\pm 10 - 15mmHg$. This means if the output of four FlexiForce sensors is averaged, the accuracy of the combined block in theory will be the sums of the four sensors accuracy (using Equation 5.10) divided by 4. To put in numbers, if the accuracy of each of the sensors used is $\pm 14mmHg$, then the accuracy of average of the combined block of the four sensors will be $\pm 7mmHg$. Indeed, using more sensors will result in an increase in accuracy. Nevertheless, the uncertainty will not be reduced by increasing the accuracy, as the uncertainty will also be influenced by the confidence intervals of the mean due to the deviation in the output of the four or more sensors.

Table 5.8 shows an example where a bandage is applied to four FlexiForce sensors with pressure readings expected to be in theory $19.51mmHg$. It is clear that the probability of having one sensor producing a very low or high pressure value is likely. However, this effect is attenuated when averaging is used.

In this work, averaging four sensors is adopted because FlexiForce sensors can be arranged in matrix arrangement, enabling window averaging for adjacent sensors easily. However, using window averaging means that if 16 FlexiForce sensors are arranged in the form of a matrix of 4×4 over a cylinder, then, the pressure map resulted by applying

Table 5.8: An example of the averaging technique for FlexiForce sensor. All values reported are for pressure in *mmHg*. The theoretical pressure is 19.51mmHg

Sensor No.	1st Reading	2nd Reading	3rd Reading	4th Reading	5th Reading	6th Reading	7th Reading	8th Reading	9th Reading	10th Reading
Sensor 1	21.35	20.75	21.80	31.78	27.03	23.23	19.70	39.04	22.39	21.47
Sensor 2	8.87	16.04	13.63	24.46	17.72	9.13	18.62	21.63	13.96	13.91
Sensor 3	18.70	20.22	24.32	18.54	16.76	21.63	10.61	17.65	18.53	19.04
Sensor 4	17.93	14.69	22.57	14.42	26.68	15.71	16.34	21.18	19.96	14.55
Average	16.71	17.92	20.58	22.30	22.05	17.43	16.32	24.87	18.71	17.24

window averaging will be a 3×4 matrix due to the circular nature of the cylinder cross section (Figure 5.25).

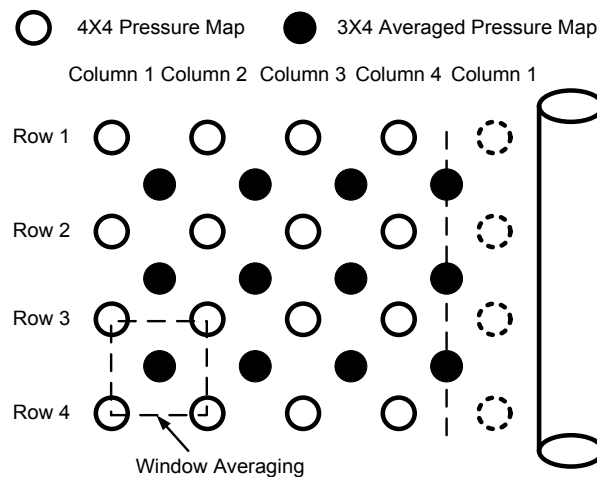


Figure 5.25: The size of pressure map before and after using window averaging, when 16 FlexiForce sensors are arranged in 4×4 matrix over a cylinder. The white circles represent the 16 FlexiForce sensors in 4×4 matrix. The black circles represent the 3×4 pressure map matrix after applying window averaging

5.8 Summary

This chapter presented the first work to assess the nonlinearity, repeatability and hysteresis of the PicoPress sensor. It also demonstrated the impact of its physical dimensions on the interface pressure, which suggested that PicoPress sensors and similar medical transducers overestimate the pressure applied by compression bandages. This was found to be an overestimation by 48% when PicoPress sensors were used to measure the pressure applied by compression bandages to a cylinder with 0.114m diameter.

The FS01 force sensor was also evaluated and found to have a good level of accuracy

when tested over a flat surface ($2\%FS$). However, experimental results showed that sensor sensitivity to pressure when embedded in a cylinder and pressure was applied with an aneroid sphygmomanometer is more than twice as much as when pressure is applied with deadweights on a flat surface. This suggests that these sensors, if used, should be calibrated by applying pressure to them over a curved surface using material that is conformable like a sphygmomanometer cuff.

Despite having more repeatability error compared to $12mm$ diameter active-sensing-area FSR, the FlexiForce sensor was selected over Tactilus and the two sizes of FSR, mainly because it showed better linearity, good sensitivity to low pressure values and the lowest drift errors among the selected sensors. FSR sensors were not sensitive at low pressure values and had high drift error at low pressures too. Tactilus sensors suffered from significant stability deficiencies.

Dynamic response to a step input for a 1^{st} order system model for FlexiForce sensors suggests that the sensor time constant is much higher than $30ms$ reported by other researchers and certainly higher than the $5\mu s$ response time claimed by the manufacturer. Results suggests that FlexiForce bandwidth is in the range of $0.126 - 0.594Hz$, which explains the degradation in its output when subjected to long-duration, low-frequency and high-force. Temperature variation had an insignificant effect on sensor output for low pressure inputs, when temperature and temperature variation are low ($22 - 42^{\circ}C$). Calibration of sensors at room temperature will be sufficient to use FlexiForce sensors in contact with human skin. Furthermore, the chapter demonstrated how averaging can be used to increase the accuracy of the pressure measurement using arrays of FlexiForce sensors.

Chapter 6

Pressure-Mapping Reference Systems

This chapter presents the development of a number of pressure-mapping measurement reference systems. Each answers some research questions and helps in developing a pressure-mapping measurement system with custom arrays of flexible sensors that can be used to map pressures applied by MCBs to the leg. The chapter first describes three systems developed to map the pressure applied to a rigid cylinder. These cylinders aimed to address two main key aspects: the usage of extension to provide reliable feedback information about the pressure applied, and the reliability of using PicoPress, FS01 and FlexiForce sensors for pressure-mapping. The chapter then addresses the same two key aspects by detailing experiments to map pressures applied to a mannequin leg and to measure the leg dimensions. Finally, the chapter addresses the effect of skin softness on the measurement of pressure using a leg model with soft exterior. Some of the work reported in this chapter has been presented at the 12th Mechatronics Forum Biennial International Conference (“Relationship between extension and pressure in compression bandages used in leg ulcers for the control of interface pressure” and “Comparison between sub-bandage interface computed and measured pressure when bandages are applied to a mannequin leg”).

6.1 Introduction

This chapter describes the development of various pressure-mapping measurement systems (reference systems) and reports on the usage of these systems to investigate the reliability of using extension to provide feedback about the pressures applied by MCBs. The chapter starts with describing the pressure-mapping systems built over rigid cylinders using arrays of PicoPress sensors, FS01 force sensors and FlexiForce sensors. It also reports on the experimental work carried out to compare the pressure maps obtained by these systems to each other and to the ones computed from bandage extension. Moreover, it reports on experiments, where the three sensing technologies were used at the same time on the same cylinder to map the pressure applied by MCBs. The pressure readings reported were used

to compare the three sensing technologies and explore the pros and cons of each of these technologies.

The chapter then describes the development, construction and evaluation of three pressure-mapping systems on mannequin leg. It also compares the pressures obtained by these different systems to each other, and to the pressures computed from extensions by using leg dimensions from a 3D model of a mannequin leg.

Furthermore, the chapter describes the usage of arrays of PicoPress and FlexiForce sensors to map the pressure under MCBs when applied to a leg model with a soft exterior. It compares the pressure maps obtained using each system. additionally, it compares the pressure maps obtained by each system with the ones estimated from extension.

6.2 Pressure-Mapping Systems Over Rigid Cylinders

In Section 3.3 and 3.4 the interface pressure mathematical models were derived and validated. Tensions in bandages calculated from extensions and loads attached to the end of the bandage were used to compute the interface pressure, which, in turn, was compared to the measured pressures. However, in both Section 3.3 and 3.4 bandages were not applied as they would normally be applied in clinical situations. This section will evaluate the reliability of using visual feedback from bandages in terms of extension as a method for prescription control of pressure, by using arrays of PicoPress probes, FS01 force sensors and FlexiForce sensors to map the pressures applied by MCBs to PVC cylinders and comparing these maps to the ones computed from the extension in MCBs. In addition, the section will compare the mentioned three sensing technologies and explore the pros and cons of each of these technologies.

6.2.1 Pressure-Mapping Cylinder Using PicoPress Sensors

This section will compare the pressures computed from extension for two bandages to the pressures measured using arrays of PicoPress sensors. The computed pressure will be compared to the measured pressure after applying a correction factor to the measured pressures. This correction factor is based on pressure perturbation due to the physical dimensions of the sensor and change in local bandage extension due to calibrating the sensors under compression bandages.

Materials and Methods

The rig used and PicoPress balloons arrangement: The rig used in the apparatus was composed of a cylinder, $0.114m$ diameter and $0.55m$ length, supported with a fixed joint making 45° with the horizontal and a wooden base clamped to a table (Figure 6.1). A slot, with an angle of 8° to the vertical axis of the cylinder was designed to enable bandage application using a spiral technique with 50% overlap between bandage layers. Fifteen PicoPress balloons were attached to the cylinder in 5×3 array format. The three

columns were separated by $0.12m$ centre-to-centre and the five rows separated by $0.08m$ centre-to-centre. The cylinder was treated as a left leg and the three columns were treated as medial-anterior, posterior and lateral-anterior sides of the leg.

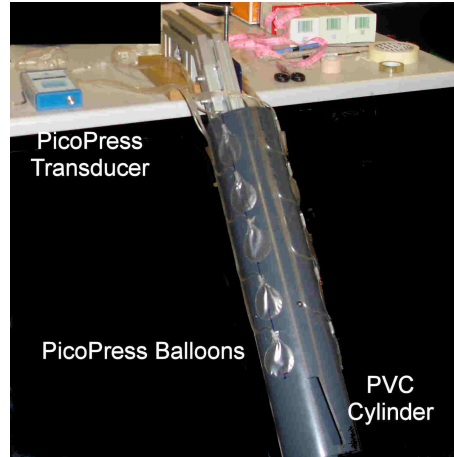


Figure 6.1: PVC cylinder with PicoPress sensors in a 5×3 array

Bandages: Two types of bandages were used in the apparatus: Comprilan and Sure-Press bandages. Each bandage was marked every $5cm$.

Measuring the extension and pressure: Prof. E.A. Nelson (a qualified nurse and an experienced bandager) applied the two types of bandages to the cylinder once. She was asked to apply the bandages at a pressure of $40mmHg$. The pressures at the 15 different points were measured using PicoPress transducer after calibrating each sensor under the bandage. The extension at the outer (2^{nd}) layer of the bandage was measured using a measurement tape at the fifteen points where the PicoPress sensors were placed.

Computing the pressure: MATLAB R2009a was used to calculate the tension in the two bandages at the fifteen different points from the extension measurement. The tension was calculated using the 4^{th} order polynomial fitting-lines for the loading side of the 1^{st} cycle of the tension-elongation curves for both bandages (Section 4.4). By assuming that the tension in the inner bandage layer equals the tension in the outer bandage layer, and by using the thickness and width measured values of the two bandages reported in Section 4.3 and Equation 3.11, the interface pressure at the 15 different points was calculated.

Correction for the measured pressures: As discussed in Sections 3.8 and 5.4.2, PicoPress balloon physical dimensions will result in PicoPress overestimating the pressure. Therefore, the pressure readings reported by PicoPress need to be multiplied with a correction factor. However, calibrating the sensors under the bandage means that the pressure perturbation is not only caused by the physical dimensions of the sensors only, as inflating

the balloons under bandages will result in a local stretch for the bandage i.e. local increase in tension; thus, increasing the pressure.

By assuming that the small local increase in bandage elongation will result in a linear increase in tension, the perturbation due to the local stretch can be shown to be the following:

$$C_{TP} = \frac{\alpha(R + d) + 2((R + d)^2 - R^2)}{\alpha R} \quad (6.1)$$

where, $\alpha = \frac{D_S}{R}$

Where, d is the sensor thickness in (m), D_S is the sensor diameter in (m), C_{TP} is the coefficient of pressure perturbation due to local stretch, R is the limb radius in (m).

However, the assumption that tension varies linearly with extension for small values of extension might only be applicable for elastic bandages and the pressure perturbation for inelastic bandages might be higher than reported by Equation 6.1.

The total pressure perturbation then can be calculated by the following expression:

$$\text{Total Pressure Perturbation} = C_{PP} \times C_{TP} \quad (6.2)$$

Where, C_{PP} is the coefficient of perturbation due to the sensor dimension (Equation 3.33).

The correction factor for the measured pressure values can be obtained using:

$$\text{Correction Factor} = \frac{1}{\text{Total Pressure Perturbation}} \quad (6.3)$$

Equation 2.8, Equation 6.1, Equation 6.2 and Equation 6.3 were used to calculate the correction factor for using PicoPress sensors over a cylinder with 0.114m diameter.

Statistical analysis: Bland-Altman plots [197] and frequency percentage counts were used to check the levels of agreement between the computed and the measured pressures for the two bandages and between the computed and the corrected measured pressures for the two bandages. The pressures were considered to be in agreement when the difference between the computed and measured pressures was within $\pm 5mmHg$. PASW 17 and Excel 2007 were used to carry out the statistical analysis.

Results, Analysis and Discussion

Table 6.1 and Figures 6.2 and 6.3 summarize the measured extensions and pressures, and the calculated tensions and pressures. The correction factor used was 0.58 where the combined perturbation due to the local stretch and the sensors physical dimensions was 172% i.e. PicoPress will overestimate the pressure by 72%. The results plotted in Figures 6.2 and 6.3 clearly illustrate the perturbation problem. The results also show that

using a correction for PicoPress readings leads to pressure values which are much closer to ones calculated theoretically particularly in the case of SurePress.

Table 6.1: Summary of Comprilan and SurePress measured extensions, calculated tensions and pressures, measured pressures and corrected pressures. The upper and lower 95% *spread* = $mean \pm (1.96 \times SD)$, and the upper and lower 95% *CI* = $mean \pm (t \times SE)$, where “*t*” is critical point at 95% for the data degrees of freedom obtained from the student’s t-distribution look-up table [189]

Comprilan Bandage							
Statistical Analysis	Extension [%]	Tension [N]	Computed pressure [mmHg]	Measured pressure [mmHg]	Corrected measured pressure [mmHg]	Measured pressure / computed pressure	Corrected measured pressure / computed pressure
Mean	49.20	10.47	27.27	63.13	36.62	2.35	1.36
SD	3.19	1.22	3.17	4.82	2.80	0.34	0.20
SE	0.82	0.31	0.82	1.25	0.72	0.09	0.05
Upper 95% spread	55.45	12.86	33.49	72.59	42.10	3.01	1.74
Lower 95% spread	42.95	8.08	21.05	53.68	31.13	1.69	0.98
Upper 95% CI	50.96	11.15	29.02	65.80	38.16	2.53	1.47
Lower 95% CI	47.44	9.80	25.51	60.47	35.07	2.16	1.25

SurePress Bandage							
Statistical Analysis	Extension [%]	Tension [N]	Computed pressure [mmHg]	Measured pressure [mmHg]	Corrected measured pressure [mmHg]	Measured pressure / computed pressure	Corrected measured pressure / computed pressure
Mean	50.27	13.21	33.09	52.40	30.39	1.58	0.92
SD	6.41	1.34	3.35	8.21	4.76	0.17	0.10
SE	1.65	0.35	0.87	2.12	1.23	0.04	0.03
Upper 95% spread	62.83	15.83	39.66	68.49	39.72	1.92	1.11
Lower 95% spread	37.71	10.58	26.51	36.31	21.06	1.25	0.72
Upper 95% CI	53.81	13.95	34.94	56.94	33.02	1.68	0.97
Lower 95% CI	46.73	12.47	31.23	47.86	27.76	1.49	0.86

In addition, despite the target pressure being $40mmHg$, the pressure applied was not constant, with the theoretical mean pressure being lower than $40mmHg$ and the mean measured pressures being higher than $40mmHg$. Furthermore, the mean of the ratio of the corrected measure pressures to the computed pressure for Comprilan is > 1 and for SurePress is < 1 for SurePress. This might be explained by the the following:

- The correction model assumes linear relationship between the extension and the tension. In the case of Comprilan, this is not true as it is shown in Section 4.4.
- The expected ratio was < 1 for both bandages as friction forces and combined effect of low compression forces in the transverse direction of the bandage and angle of application would result in attenuating some of the pressure applied. Therefore,

SurePress pressure ratio of < 1 was expected. However, Comprilan bandage had higher inter-variation in its tension-elongation characteristics than SurePress (Section 4.4). In this particular experiment, Comprilan bandage might produced higher tensions than the bandage used to obtain the tension-elongation fitting-line for the same amount of extension. In addition, Comprilan generates higher compression forces in the transverse direction compared to SurePress. Combining this with the effect of angle of application might result in applying higher levels of pressures compared to the pressure levels expected without considering these variables.

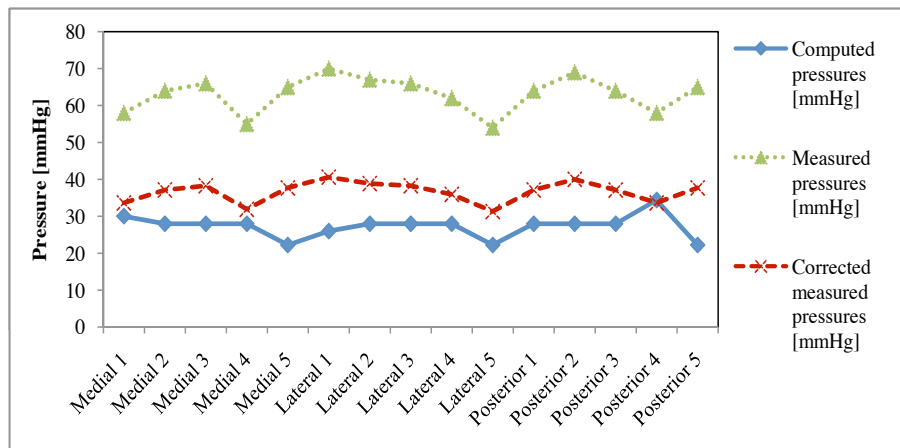


Figure 6.2: Comprilan: computed, measured and corrected measured pressures. Lines connecting the pressure points are for illustrative purposes

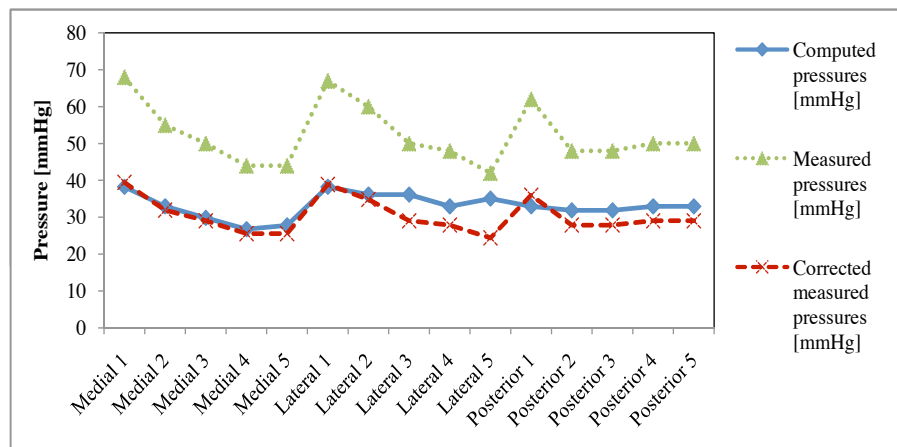


Figure 6.3: SurePress: computed, measured and corrected measured pressures. Lines connecting the pressure points are for illustrative purposes

Table 6.2 and Figures 6.4 and 6.5 demonstrate that pressures computed theoretically and the corrected measured pressures in the case of SurePress is within the tolerance values for agreement $\pm 5mmHg$. However, in the case of Comprilan this is only true for 20% of

the cases, with corrected measured pressures higher than the ones estimated theoretically. This might indicate that using extension as a feedback to control the pressure applied by MCBs might only be a good method for elastic bandages like SurePress. However, the same method might result in applying much higher pressure values in the case of inelastic bandages like Comprilan.

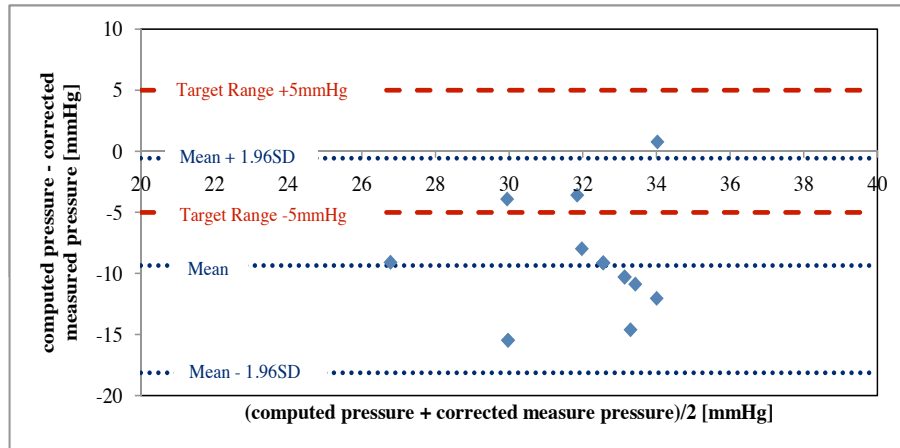


Figure 6.4: Bland-Altman plot for computed pressures and corrected measured pressures for Comprilan

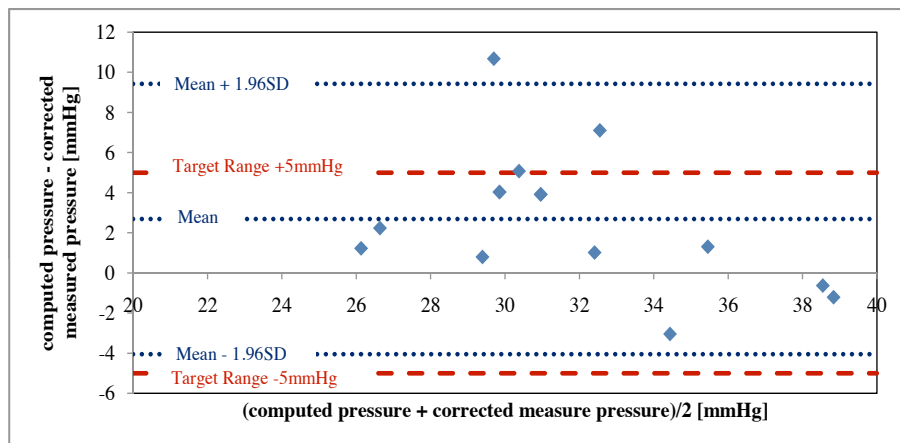


Figure 6.5: Bland-Altman plot for computed pressures and corrected measured pressures for SurePress

6.2.2 Pressure-Mapping Cylinder Using FS01 Force Sensors

The aim of the reported work in this section was to compare the pressures measured experimentally using FS01 force sensors when bandages were applied to a cylinder with constant radius with the pressures computed indirectly from the level of extension in the MCB.

Table 6.2: The percentage of cases where the difference between the computed and the measured and corrected measured pressures being within $\pm 5mmHg$ for Comprilan and SurePress

Statistical Analysis	Percentage of cases where the difference is within $\pm 5mmHg$
Comprilan computed pressures and measured pressures	0%
Comprilan computed pressures and corrected measured pressures	20%
SurePress computed pressures and measured pressures	0%
SurePress computed pressures and corrected measured pressures	87%

Materials and Methods

The rig used and FS01 force sensors arrangement: The rig was composed of a cylinder, with a $0.114m$ diameter and $0.55m$ length, a support with adjustable rotating joint, to mimic the knee motion and a wooden base (Figure 6.6). A slot, oriented 8° with the vertical axis of the cylinder, was designed in the cylinder wall. The slot was used to fix the bandage to the cylinder using medical textile based tapes and to enable applying the bandage using a spiral wrapping technique with 50% bandage layers overlap. Twelve rectangular slots were made in the cylinder wall to house the force sensors (Figure 6.7). The arrangement was selected to enable the study of interface pressure both in the longitudinal and circumferential directions of the cylinder.

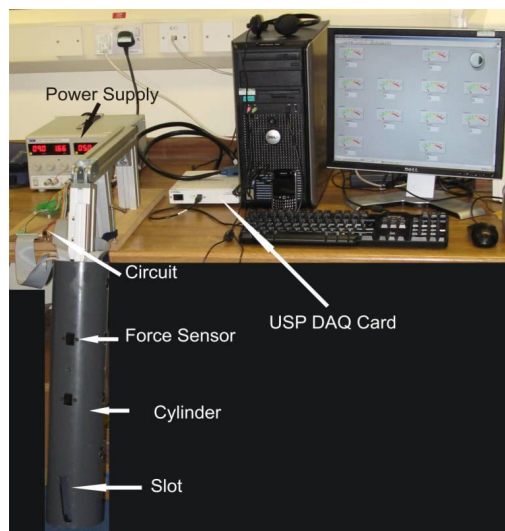


Figure 6.6: PVC cylinder with FS01 force sensors embedded in its wall

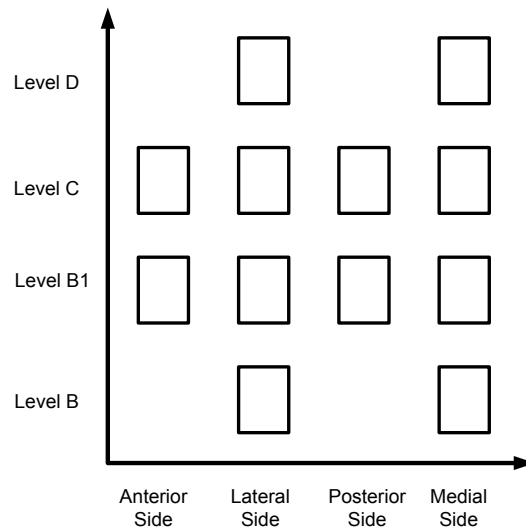


Figure 6.7: The arrangement of FS01 force sensors

Conditioning circuit, data acquisition and sensor calibration: The sensors were powered with $5V$ through a processing circuit. The sensors output signals were passed to the processing circuit and then to a DAQ card through a screw terminal board (LPR-68). The DAQ card used in this experiment was a Mass Term 6225 USB DAQ card.

Due to the curved nature of the cylinder, the force sensors were calibrated individually using an aneroid sphygmomanometer after the sensors were attached to the cylinder (Figure 6.8). The sensors were calibrated for the pressure range $0 - 120mmHg$ by inflating the aneroid sphygmomanometer cuff to $120mmHg$ and then deflating the cuff at $10mmHg$ intervals. The process was repeated 10 times to reduce the repeatability error of the aneroid sphygmomanometer. A 3rd order polynomial fitting-line was used to fit the averaged data points of the 10 repeats. A program written in LabView 8.6 was used to acquire the sensor signals in the calibration process. Excel 2003 was used to obtain the fitting-lines and calculate the “R” squared regression values for the sensors.

The pressure measurement display program: A program was written in LabView 8.6 to acquire and display the signals, convert them to the equivalent pressure values, display the values numerically and via colour gauges, and store the voltages and pressure values for further processing. The signals were sampled at $100Hz$ and a software based 2^{nd} order low-pass filter with $10Hz$ cut-off frequency was used to filter out the signal. Figures 6.9 and 6.10 show the front panel of the program and the flow chart of the program respectively.

Computing pressures: This is the same as the ones reported in Section 6.2.1.

Measuring the extension and pressure: Prof. E.A. Nelson (a trained bandager) was asked to apply four pre-marked Comprilan bandages and four pre-marked SurePress

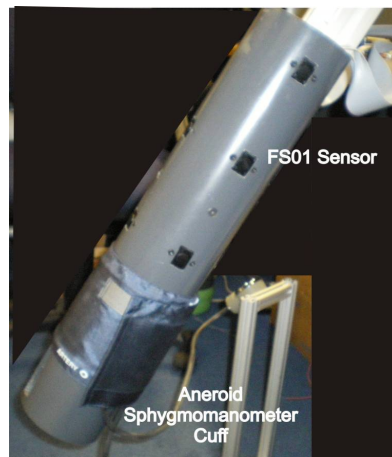


Figure 6.8: Calibration of FS01 force sensors using aneroid sphygmomanometer



Figure 6.9: The front panel of the display program

bandages to the cylinder with a constant pressure of 40mmHg . Pressure measurements were acquired throughout the bandage application. After applying the MCBs, the extension was recorded using a measurement tape. MATLAB R2009a was used to compute the theoretical pressures from the measured extension values. Excel 2007 was used to compare the theoretical and measured pressure values.

Statistical analysis: Bland-Altman plots [197] and frequency percentage counts were used to check the levels of agreement between the computed and measured pressures for the

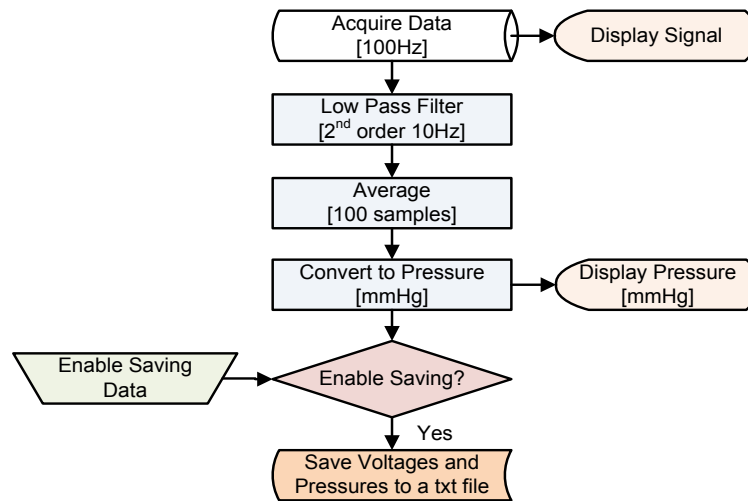


Figure 6.10: The flow chart of the display program

two bandages. The computed and measured pressures were considered to be in agreement if the difference between the computed and measured pressures was within $\pm 5mmHg$. PASW 17 and Excel 2007 were used to carry out the statistical analysis.

Results, Analysis and Discussion

Table 6.3 and Figures 6.11 and 6.12 summarize the measured extensions and pressures and the calculated tensions and pressures.

Despite the target pressure being constant ($40mmHg$), the pressures applied were not constant, with the mean of the theoretical pressure being $31.77mmHg$ for Comprilan and $28.12mmHg$ for SurePress and the mean of the measured pressures being $32.31mmHg$ for Comprilan and $25.6mmHg$ for SurePress.

The ratio of the measured pressure over the computed pressures shows similar results to those reported for PicoPress sensors, with the mean of the pressure ratio being > 1 for Comprilan and < 1 for SurePress. Friction forces between MCB layers and MCB angle of application, in theory, should result in damping the pressure applied, especially in the case of SurePress, i.e. the ratio should be < 1 . However, the sharp edges of the FS01 sensors will result in generating local pressure, which in theory will result in higher pressures than anticipated theoretically. Having only Comprilan showing an average pressure ratio of > 1 might be explained by the variation in the tension-elongation characteristics of Comprilan bandage than SurePress bandage (Section 4.4) and the higher compression forces generated in the transverse direction of Comprilan bandage than SurePress bandage. Combining this with the effect of angle of application might result in applying higher levels of pressures compared to the pressure levels expected without considering these variables.

Figures 6.13 and 6.14 demonstrate that SurePress computed and measured pressures are within $\pm 5mmHg$ for 63% of the cases. However, for Comprilan this is only true for

Table 6.3: Summary of Comprilan and SurePress measured extensions, calculated tensions and pressures and measured pressures. The upper and lower 95% *spread* = $mean \pm (1.96 \times SD)$, and the upper and lower 95% *CI* = $mean \pm (t \times SE)$, where “*t*” is critical point at 95% for the data degrees of freedom obtained from the student’s t-distribution look-up table [189]

Comprilan Bandage					
Statistical Analysis	Extension [%]	Tension [N]	Computed pressure [mmHg]	Measured pressure [mmHg]	Measured pressure / computed pressure
Mean	51.21	12.20	31.77	32.31	1.15
SD	10.18	4.83	12.57	9.48	0.47
SE	1.47	0.70	1.81	1.37	0.07
Upper 95% spread	71.16	21.66	56.40	50.89	2.07
Lower 95% spread	31.26	2.74	7.14	13.72	0.23
Upper 95% CI	54.09	13.57	35.33	34.99	1.29
Lower 95% CI	48.33	10.84	28.21	29.62	1.02

SurePress Bandage					
Statistical Analysis	Extension [%]	Tension [N]	Computed pressure [mmHg]	Measured pressure [mmHg]	Measured pressure / computed pressure
Mean	40.67	11.22	28.12	25.60	0.91
SD	7.20	1.48	3.70	6.76	0.20
SE	1.04	0.21	0.53	0.98	0.03
Upper 95% spread	54.77	14.12	35.38	38.85	1.30
Lower 95% spread	26.56	8.33	20.87	12.35	0.52
Upper 95% CI	42.70	11.64	29.17	27.51	0.97
Lower 95% CI	38.63	10.81	27.08	23.69	0.85

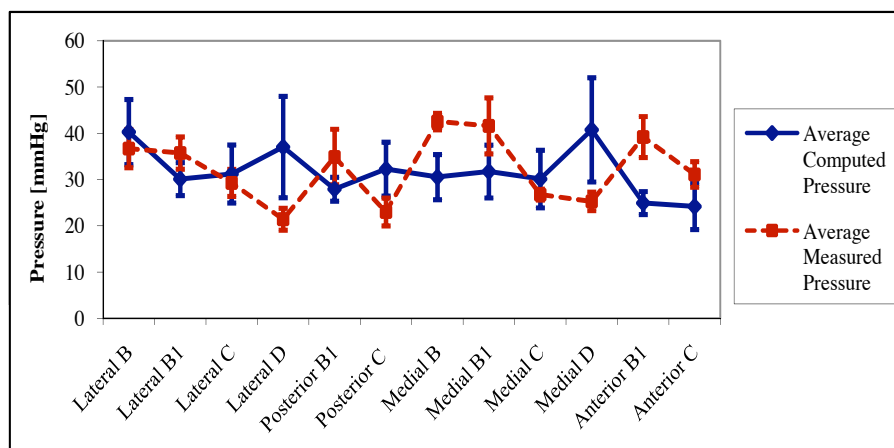


Figure 6.11: Comprilan: computed and measured pressures. Error bars represent the SE of the mean for four bandage applications. Lines connecting the pressure points are for illustrative purposes

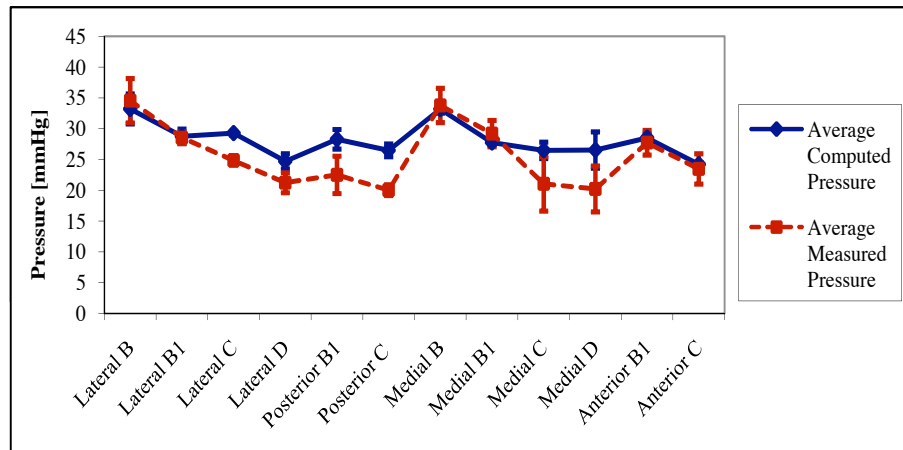


Figure 6.12: SurePress: computed and measured pressures. Error bars represent the SE of the mean for four bandage applications. Lines connecting the pressure points are for illustrative purposes

21% of the cases. This is about the same percentage of agreement found when PicoPress with correction factor was used (Section 6.2.1). This might indicate that using extension as a feedback to control the pressure applied by MCBs might only be a good feedback method for elastic bandages like SurePress.

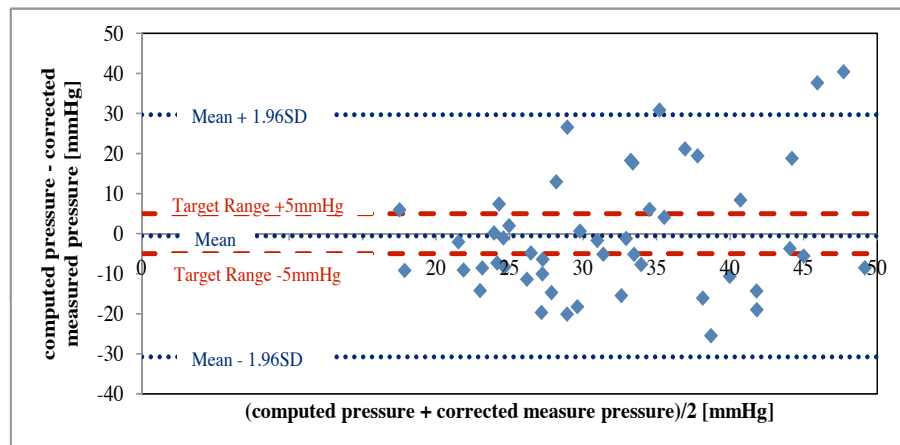


Figure 6.13: Bland-Altman plot for computed pressures and measured pressures for Comprilan

6.2.3 Pressure-Mapping Cylinder Using FlexiForce Sensors

The aim of the reported work in this section was to compare the pressures measured experimentally using arrays of FlexiForce sensors when MCBs were applied to a cylinder with constant radius against the pressures computed indirectly from the extension in the MCB.

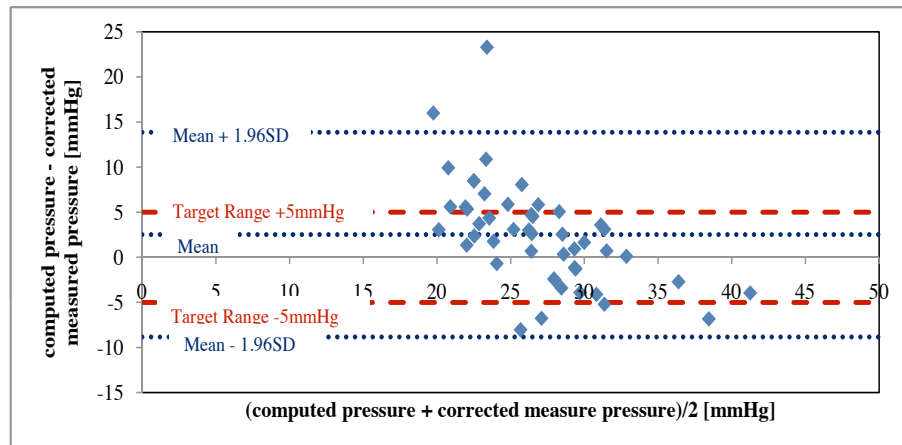


Figure 6.14: Bland-Altman plot for computed pressures and measured pressures for SurePress

Materials and Methods

The rig used and FlexiForce sensors arrangement: The rig was composed of a cylinder, 0.114m diameter and 0.55m length, a support with adjustable rotating joint, to mimic the knee motion and a wooden base (Figure 6.15). A slot, oriented at 8° with the vertical axis of the cylinder, was designed in the cylinder wall, to fix the bandage to the cylinder using medical tapes and to enable application of the bandage with a spiral wrapping technique with 50% bandage layers overlap. Fifty-six FlexiForce sensors were mounted on top of the cylinder in a 8×7 matrix. This provided the highest resolution map possible without having overlapped sensors.

Conditioning circuit, data acquisition and sensors calibration: The sensors were powered with a constant 3V through four processing circuits. Each circuit was consisted of a voltage follower to maintain the input voltages to 16 sensors and 4 quad operational amplifiers to amplify and filter the sensors output signals using low-pass filters with cut-off frequency of 10Hz to filter out the signal and remove the noise (Figure 6.16). The output signals from the four processing circuits were passed to a Mass Term 6225 USB DAQ card through a screw terminal board (LPR-68).

Due to the curved nature of the cylinder, the FlexiForce sensors were calibrated individually using an aneroid sphygmomanometer after the sensors were been attached to the cylinder. The sensors were calibrated for the pressure range 0 – 120mmHg by inflating the aneroid sphygmomanometer cuff to 120mmHg and then deflating the cuff at 10mmHg intervals. The process was repeated 20 times to reduce the repeatability error of the aneroid sphygmomanometer. A 3rd order polynomial fitting-line was used to fit the averaged data points of the 20 repeats. A program written in LabView 8.6 was used to acquire the sensors signals in the calibration process. Excel 2003 was used to obtain the fitting-lines and calculate the “R” squared regression values for the sensors.

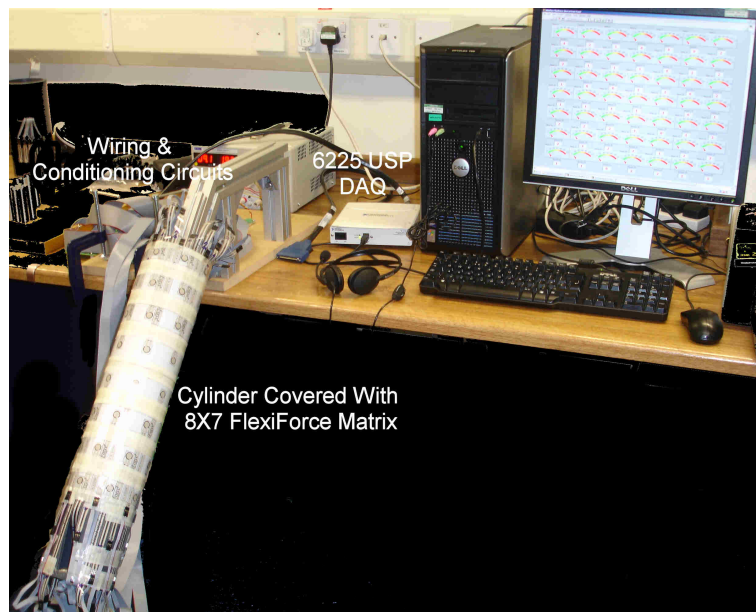


Figure 6.15: PVC cylinder with FlexiForce sensors mounted in the form of 8×7 matrix

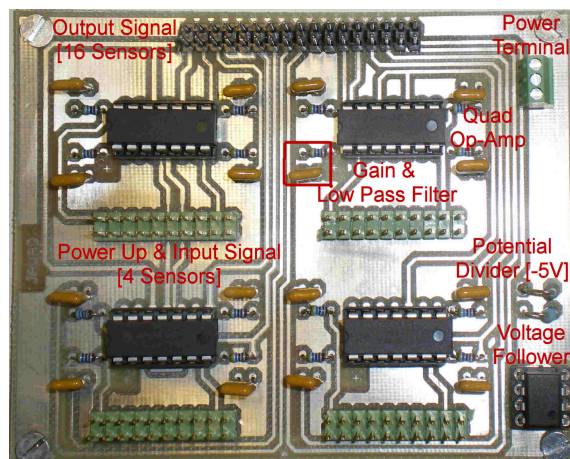


Figure 6.16: The conditioning circuit used to power up and process the output signals of 16 FlexiForce sensors

The pressure measurement display program: A program was written in LabView 8.6 to acquire and display the signals, convert them to the equivalent pressure values, perform window averaging for the pressure values, display the average pressure values numerically and via colour gauges and store the voltages, the measured pressures and the average pressures for further processing. The signals were sampled at 100Hz and a software based 2^{nd} order low-pass filter with 1Hz cut-off frequency was used to filter out the signal. Figures 6.17 and 6.18 show the front panel of the program and the flow chart of the program respectively.

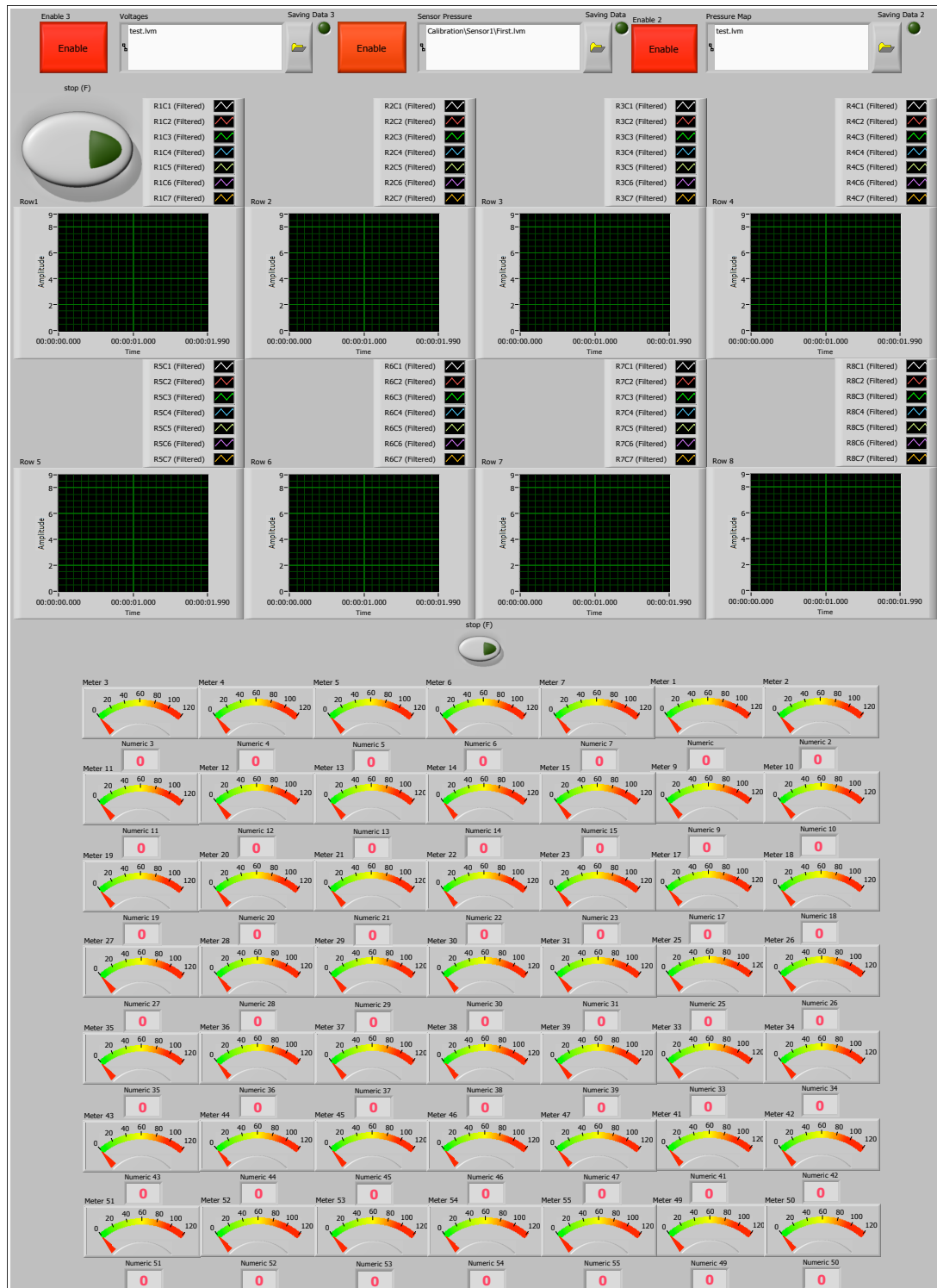


Figure 6.17: The front panel of the display program for FlexiForce cylindrical pressure-mapping system

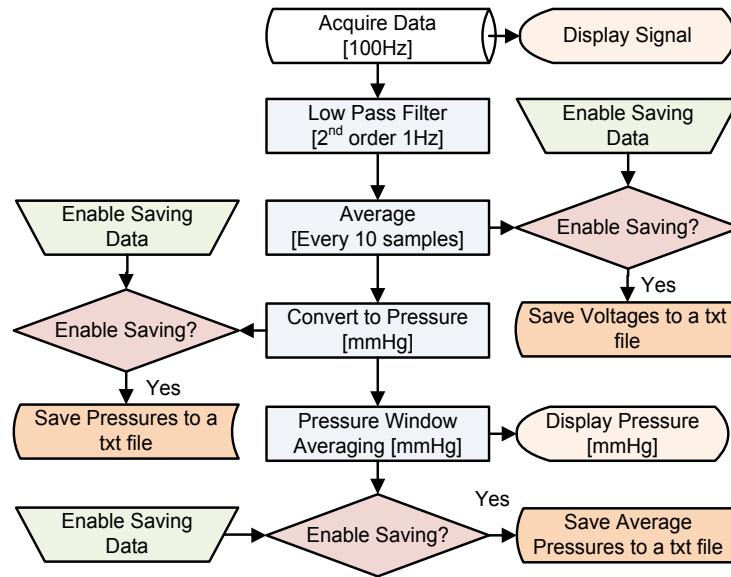


Figure 6.18: The flow chart of the display program for FlexiForce cylindrical pressure-mapping system

Computing pressures: This is as reported in Section 6.2.1.

Measuring the extension and pressure: Prof. E.A. Nelson (a trained bandager) was asked to apply two pre-marked Comprilan bandages and two pre-marked SurePress bandages to the cylinder with a constant pressure of 40mmHg . Pressure measurements were acquired throughout the bandage application. After applying the MCB, the amount of extension was recorded using a measurement tape at 16 points (4×4 matrix). MATLAB R2009b was used to compute the theoretical pressures from the measured extensions. MATLAB R2009b and Excel 2007 were used to compare the computed pressure values with the measured pressure values.

Statistical analysis: Bland-Altman plots [197] and frequency percentage counts were used to check the levels of agreement between the computed and measured pressures for the two bandages. The computed and measured pressures were considered to be in agreement if the difference between the computed and measured pressures was within $\pm 5\text{mmHg}$. PASW 17 and Excel 2007 were used to carry out the statistical analysis.

Results, Analysis and Discussion

Figure 6.19 shows the computed pressure map, measured pressure map and the average pressure map obtained for Comprilan and SurePress (the first application for both bandages). Despite the computed maps showing that SurePress was applied with a constant pressure, both the measured and average pressure maps show variation in the pressure at the top of the cylinder (top two rows of sensors), reporting rather low pressure values.

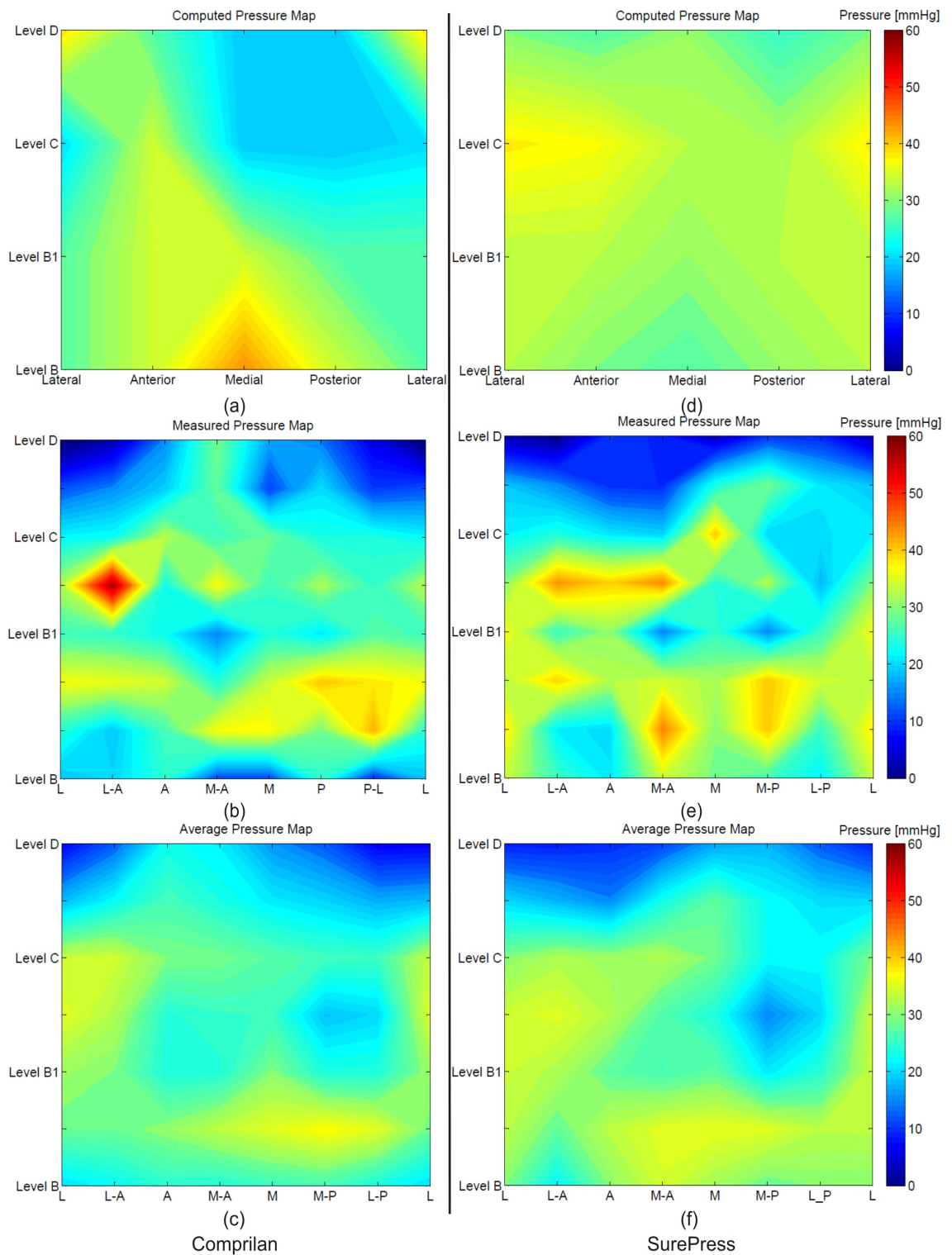


Figure 6.19: Comprilan and SurePress pressure maps: (a) Comprilan computed pressure map, (b) Comprilan measured pressure map, (c) Comprilan averaged pressure map, (d) SurePress computed pressure map, (e) SurePress measured pressure map and (f) SurePress averaged pressure map. The maps are shown with the first column “Lateral” being repeated at the start and end for better clarity. ‘L’ = Lateral, ‘A’ = Anterior, ‘M’ = Medial and ‘P’ = Posterior

It is also clear from the maps that using the measured pressures directly might result in reporting pressure peaks due to the deficiencies associated with the FlexiForce sensors. However, these peaks were smoothed out when averaging techniques were used.

In order to compare the computed pressures with the averaged measured pressures, the averaged measured pressures map was re-sampled from a 7×7 matrix to a 4×4 matrix with the elements of the new map being the ones corresponding to the same places where the extensions were measured. Table 6.4 and Figures 6.20 and 6.21 summarize the measured extensions, averaged pressures and the calculated tensions and pressures for the two samples of the two bandages. Despite the target pressure being constant 40mmHg , the pressures applied were not constant, with theoretical mean pressure being 30.67mmHg for Comprilan and 32.21mmHg for SurePress and the mean measured pressures being 32.70mmHg for Comprilan and 25.26mmHg for SurePress.

Table 6.4: Summary of Comprilan and SurePress measured extensions, calculated tensions and pressures and measured pressures. The upper and lower 95% *spread* = $mean \pm (1.96 \times SD)$, and the upper and lower 95% *CI* = $mean \pm (t \times SE)$, where “*t*” is critical point at 95% for the data degrees of freedom obtained from the student’s t-distribution look-up table [189]

Comprilan Bandage					
Statistical Analysis	Extension [%]	Tension [N]	Computed pressure [mmHg]	Averaged measured pressure [mmHg]	Averaged pressure / computed pressure
Mean	52.00	11.85	30.67	32.70	1.08
SD	7.82	3.26	8.29	14.54	0.41
SE	1.38	0.58	1.47	2.57	0.07
Upper 95% spread	67.33	18.23	46.92	61.20	1.88
Lower 95% spread	36.67	5.46	14.41	4.20	0.28
Upper 95% CI	54.82	13.02	33.66	37.94	1.23
Lower 95% CI	49.18	10.67	27.68	27.46	0.93

SurePress Bandage					
Statistical Analysis	Extension [%]	Tension [N]	Computed pressure [mmHg]	Averaged measured pressure [mmHg]	Averaged pressure / computed pressure
Mean	50.69	13.28	33.21	25.56	0.77
SD	8.57	1.76	4.57	8.55	0.25
SE	1.52	0.31	0.81	1.51	0.04
Upper 95% spread	67.49	16.73	42.18	42.31	1.25
Lower 95% spread	33.89	9.83	24.25	8.81	0.28
Upper 95% CI	53.78	13.91	34.86	28.64	0.86
Lower 95% CI	47.60	12.65	31.56	22.48	0.68

The ratio of the measured pressure over the computed pressures again shows similar results to those reported for PicoPress sensors and FS01 sensors (Sections 6.2.1 and 6.2.2), with the average pressure ratio being > 1 for Comprilan and < 1 for SurePress. However, in this case Comprilan pressure ratio is close to one while SurePress is much less than one when compared to PicoPress pressure-mapping cylinder and FS01 pressure-mapping

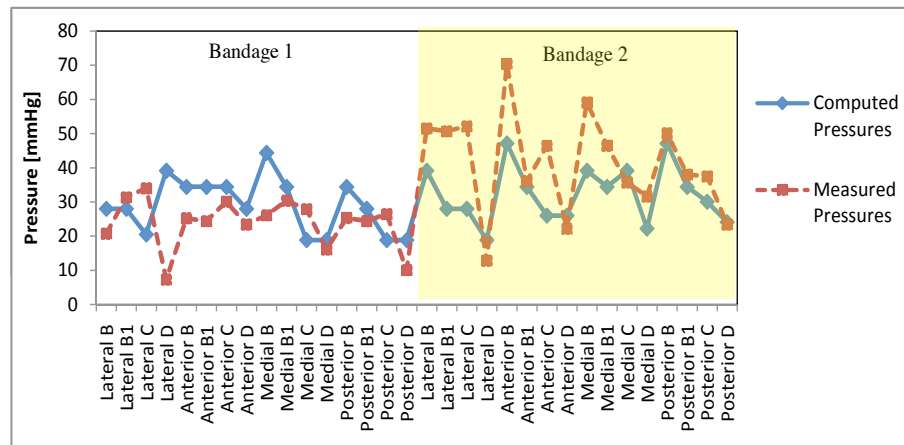


Figure 6.20: Comprilan: computed and measured pressures. Lines connecting the pressure points are for illustrative purposes

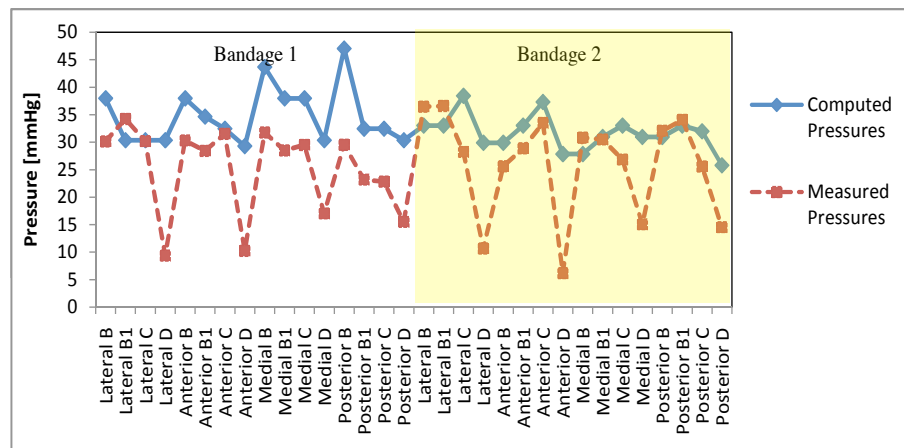


Figure 6.21: SurePress: computed and measured pressures. Lines connecting the pressure points are for illustrative purposes

cylinder. Friction forces between bandage layers and bandage angle of application, in theory, should result in damping the pressures applied, especially in the case of SurePress, i.e. ratio should be < 1 . A closer look at Figure 6.20 explains why Comprilan showed higher ratio, as the averaged measured pressures reported for the second Comprilan bandage are higher than the pressures applied by the first Comprilan bandage, which, in turn, can be explained by the inter-variation in the tension-elongation characteristics of Comprilan bandage (Section 4.4). The lower pressure ratios found for SurePress might be explained by the fact that the sensors used are very low in profile which, in turn, will overcome the problem of overestimation due to thickness (PicoPress and FS01) or sharp edges (FS01). However, Figure 6.21 shows that the high difference mainly occurs at level D (close to the knee). This might indicate that the extension recorded next to the knee might not represent the 1st tension-elongation cycle or even the loading cycle, as nurses will tend at

that point to relax the bandage to secure the bandage from falling by using a tape. This also was visible in the case of Comprilan.

Figures 6.22 and 6.23 demonstrate that pressures computed theoretically and the averaged measured pressures in the case of both SurePress and Comprilan are within the tolerance values for agreement $\pm 5\text{mmHg}$ for 37.5% of the cases.

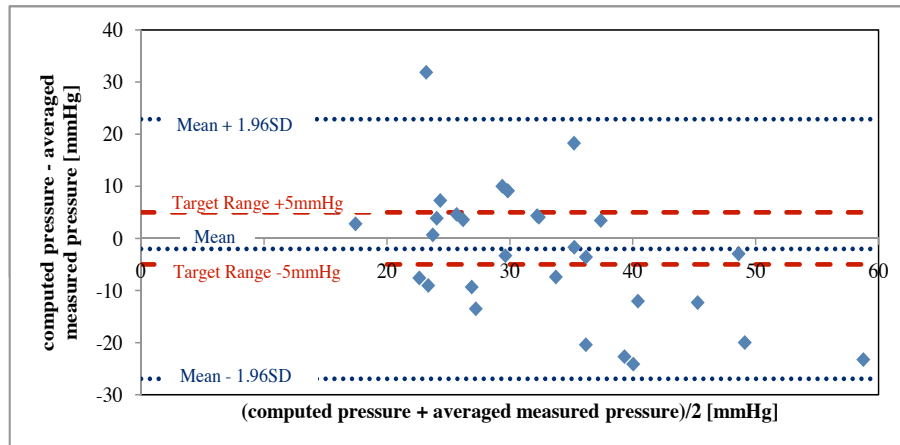


Figure 6.22: Bland-Altman plot for computed pressures and measured pressures for Comprilan

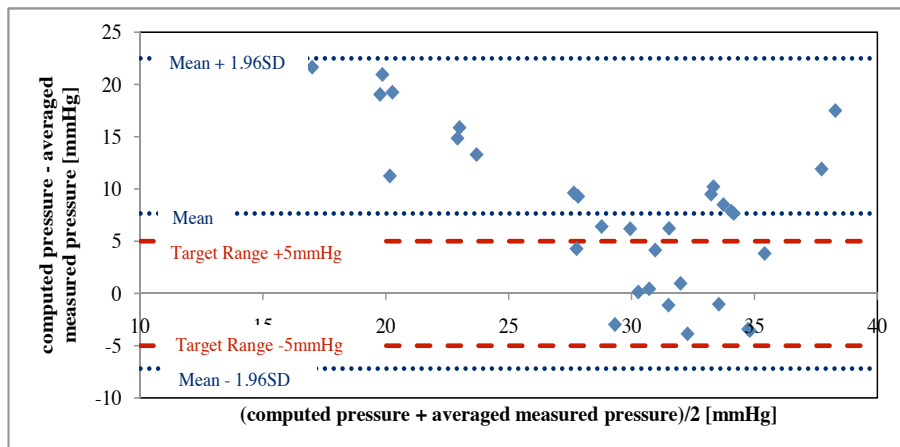


Figure 6.23: Bland-Altman plot for computed pressures and measured pressures for SurePress

6.2.4 Comparison Between the Different Pressure-Mapping Cylinders

Comprilan was applied in the three experiments with an average extension of 50%. SurePress was applied with an average of 50% extension on PicoPress and FlexiForce cylindrical measurement systems and with an average of 40% on FS01 cylindrical measurement system.

Comprilan averaged measured pressures were 63.13mmHg , 36.63mmHg , 32.31mmHg and 32.70mmHg for PicoPress, corrected PicoPress, FS01 and FlexiForce sensors respectively. These values indicate that both FlexiForce and FS01 sensors reported very similar results. The averaged measured pressures for SurePress were 52.40mmHg , 30.39mmHg , 25.60mmHg and 25.56mmHg for PicoPress, corrected PicoPress, FS01 and FlexiForce sensors respectively.

In all three systems SurePress average pressure ratio for measured pressure over computed pressures was < 1 and for Comprilan the average pressure ratio was always > 1 . Levels of agreements between measured and computed pressures are higher for SurePress than Comprilan for both PicoPress and FS01. This might be explained by the variation in the tension-elongation characteristics of Comprilan bandage (Section 4.4).

6.2.5 Comparison Between the Different Pressure Sensing Technologies on the Same Cylinder

The comparison in Section 6.2.4 is not sufficient to give a complete answer about the performance of the different sensing systems. It suggested that PicoPress sensors will overestimate the pressure. It also showed that the levels of agreement between the computed and measured pressures are better for SurePress than Comprilan and overall there is no high agreement between the computed and measured pressures. However, it did not provide conclusive information about the levels of agreement between the measured pressures using different systems. Therefore, the following experiment was conducted to check the levels of agreement between the measured pressures using the three different technologies. The experiment also studied the impact of calibration method: deadweights and aneroid sphygmomanometer, on the pressure readings obtained using FlexiForce sensors.

Materials and Methods

The rig used and FlexiForce sensors arrangement: The same rig used in Section 6.2.2 was used in this experiment (Figure 6.24). Twelve FS01 sensors were plugged into the 12 holes in the cylinder wall. Sixteen FlexiForce sensors were distributed over the cylinder at 4 locations: anterior B, posterior B, anterior D and posterior D. Four FlexiForce sensors were mounted at each of these locations and the average of their readings was used to report the pressure. Two PicoPress sensors were allocated at lateral-anterior B and medial-anterior D.

Conditioning circuit, data acquisition and sensor calibration: FS01 sensors were powered using the processing circuit described in Section 6.2.2 and the FlexiForce sensors were powered using the condition circuit reported in Section 6.2.3. The output signals from the two processing circuits were passed to Mass Term 6225 USB DAQ card through a screw terminal board (LPR-68).



Figure 6.24: PVC cylinder with FlexiForce sensors mounted in the form of 8×7 matrix

FS01 sensors and FlexiForce sensors were calibrated both using the same technique described in Sections 6.2.2 and 6.2.3. In addition, FlexiForce sensors were also calibrated using deadweights as described in Section 3.8.1. A 3^{rd} polynomial fitting-line was used to describe the calibration in all cases. A program written in LabView 8.6 was used to acquire the sensors' signals in the calibration process. Excel 2003 was used to obtain the fitting-lines and calculate the "R" squared regression values for the sensors.

The pressure measurement display program: A program was written in LabView 8.6 to acquire and display the signals, convert them to the equivalent pressure values, perform averaging for FlexiForce pressure values, display the measured pressure values for FS01 and FlexiForce sensors and the averaged pressure values for FlexiForce sensors numerically and store the voltages, the measured pressures and the average pressures for further processing. The signals were sampled at $1kHz$ and a software based 2^{nd} order low-pass filter with $10Hz$ cut-off frequency was used to filter out the signals. The program used is similar to the ones reported in Sections 6.2.2 and 6.2.3.

Computing pressures: This is the same as the ones reported in Section 6.2.1.

Measuring the extension and pressure: Prof. E.A. Nelson (a trained bandager) was asked to apply four pre-marked Comprilan and four pre-marked SurePress to the cylinder with a constant pressure of $40mmHg$. Pressure measurements were acquired throughout the bandage application. After applying the MCB, PicoPress transducer was used to obtain the pressure at lateral-anterior B and medial-anterior D. Pressure readings

for each PicoPress measurement point was obtained three times and then averaged to report the pressure. The amount of extension was recorded using a measurement tape at 8 points: lateral, anterior, medial and posterior, of the two levels B (ankle) and D (knee) (Figure 6.24). MATLAB R2009b was used then to compute the theoretical pressures from the measured extension values. MATLAB R2009b and Excel 2007 were used to compare the theoretical and measured pressure values.

Statistical analysis: The average computed pressure for the four sides at levels B and D was used to report the computed pressure for each bandage. The average of the three subsequent measurements for each PicoPress transducer was used to report the PicoPress measured pressure. A correction factor of 0.58 was also applied to the PicoPress averaged pressure (Section 6.2.1). The average of two FS01 sensors located laterally and medially at each level was used to report the pressure measured by FS01 for that particular level. The average of the two sets of 4 FlexiForce sensors at level B and level D was used to report the pressure measured by FlexiForce sensors for that level. In the case of FlexiForce sensors the pressures were reported using both deadweights and aneroid sphygmomanometer calibration fitting-lines.

Bland-Altman plots [197] and frequency percentage counts were used to check the levels of agreement between:

- the pressures measured using PicoPress sensors and the pressures measured using FlexiForce sensors (deadweight calibration),
- the pressures measured using PicoPress sensors plus correction factor and the pressures measured using FlexiForce sensors (aneroid sphygmomanometer calibration),
- the pressures measured using PicoPress sensors plus correction factor and the pressures measured using FS01 sensors,
- and the pressures measured using FS01 sensors and the pressures measured using FlexiForce sensors (aneroid sphygmomanometer).

In each test the measured pressures were said to be in agreement if the difference between them were within $\pm 5mmHg$. PASW 17 and Excel 2007 were used to carry out the statistical analysis.

Results, Analysis and Discussion

Figures 6.25 and 6.26 illustrate the computed pressures, PicoPress measured pressures, PicoPress corrected measured pressures, FS01 sensors measured pressures and FlexiForce sensors measured pressures for both deadweight and aneroid sphygmomanometer calibration fitting-lines for the two bandages. Table 6.5 and 6.6 summarize the measured extensions, averaged pressures and the calculated tensions and pressures for the two samples of the two bandages.

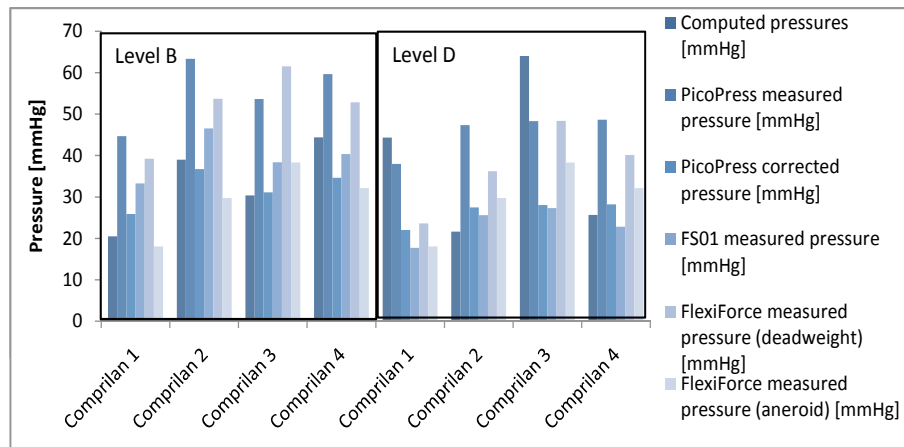


Figure 6.25: Summary of computed pressures, measured pressures using PicoPress sensors, FS01 sensors and FlexiForce sensors using fitting-lines obtained from two calibration methods and the PicoPress corrected pressures at two levels for four Comprilan bandages.

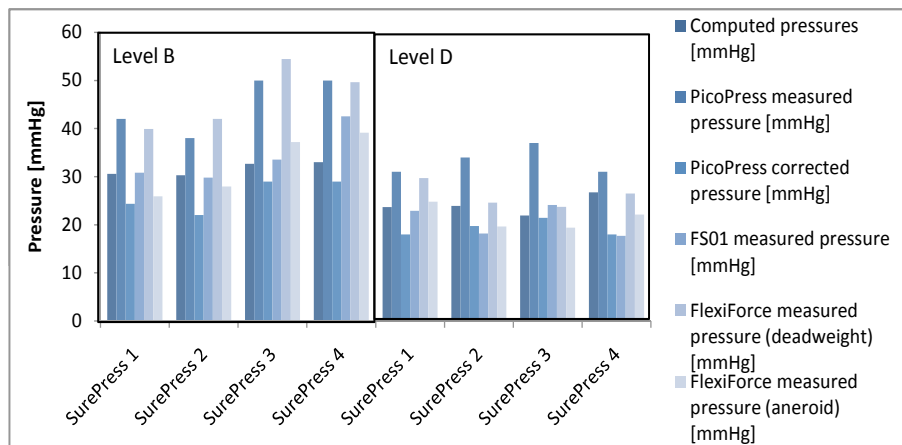


Figure 6.26: Summary of computed pressures, measured pressures using PicoPress sensors, FS01 sensors and FlexiForce sensors using fitting-lines obtained from two calibration methods and the PicoPress corrected pressures at two levels for four SurePress bandages.

Results shows that at level B, computed pressures, corrected PicoPress measured pressures, FS01 measured pressures and FlexiForce measured pressures using aneroid sphygmomanometer calibration are close to each other for both bandages. This is also true for SurePress level D with one difference; pressures measured using FlexiForce sensors using deadweights calibration are also close to the mentioned pressure measurement methods. The PicoPress measured pressures (without correction) are close to ones reported by FlexiForce using deadweights calibration fitting-lines. This indicates that pressures reported by PicoPress sensors should be treated with a correction factor. In addition, these results suggest that calibrating FlexiForce sensors using deadweights will result in overestimating

Table 6.5: Summary of computed pressures, measured pressures using PicoPress sensors, FS01 sensors and FlexiForce sensors using fitting-lines obtained from two calibration methods and the PicoPress corrected pressures at two levels for four Comprilan bandages' applications. The upper and lower 95% *spread* = $mean \pm (1.96 \times SD)$, and the upper and lower 95% *CI* = $mean \pm (t \times SE)$, where “*t*” is critical point at 95% for the data degrees of freedom obtained from the student's t-distribution look-up table [189]

Comprilan Bandage						
Level B						
Statistical Analysis	Computed pressures [mmHg]	PicoPress measured pressure [mmHg]	PicoPress corrected pressure [mmHg]	FS01 measured pressure [mmHg]	FlexiForce measured pressure (dead weight) [mmHg]	FlexiForce measured pressure (aneroid) [mmHg]
Mean	33.58	55.33	32.09	39.64	51.84	29.58
SD	10.46	8.15	4.73	5.49	9.25	8.49
SE	5.23	4.08	2.36	2.74	4.62	4.25
Upper 95% spread	54.07	71.31	41.36	50.39	69.96	46.23
Lower 95% spread	13.08	39.36	22.83	28.89	33.71	12.93
Upper 95% CI	50.20	68.29	39.61	48.36	66.54	43.08
Lower 95% CI	16.95	42.37	24.58	30.91	37.13	16.07
Level D						
Statistical Analysis	Computed pressures [mmHg]	PicoPress measured pressure [mmHg]	PicoPress corrected pressure [mmHg]	FS01 measured pressure [mmHg]	FlexiForce measured pressure (dead weight) [mmHg]	FlexiForce measured pressure (aneroid) [mmHg]
Mean	38.91	45.58	26.44	23.36	37.09	29.58
SD	19.44	5.09	2.95	4.20	10.31	8.49
SE	9.72	2.54	1.48	2.10	5.16	4.25
Upper 95% spread	77.01	55.55	32.22	31.60	57.30	46.23
Lower 95% spread	0.82	35.61	20.66	15.13	16.88	12.93
Upper 95% CI	69.82	53.67	31.13	30.05	53.49	43.08
Lower 95% CI	8.01	37.49	21.75	16.68	20.69	16.07

the pressure when used over a curved surface.

Figures 6.27, 6.28, 6.29 and 6.30 demonstrate that the pressures measured using PicoPress sensors and the pressures measured using FlexiForce sensors (deadweight calibration) are within the tolerance values for agreement $\pm 5mmHg$ for 43.75% of the cases. They also demonstrate that the PicoPress corrected measured pressures and the pressures measured using FlexiForce sensors (aneroid sphygmomanometer calibration) are within the tolerance values for agreement $\pm 5mmHg$ for 50% of the cases. The agreement is higher between the corrected PicoPress sensors measured pressures and FS01 sensors measured pressures, 56.25% of the cases. The highest levels of agreement found to be between FS01 and FlexiForce sensors using aneroid calibration, 68.75% of the cases.

These values indicate that even though FlexiForce sensors suffer from low accuracy, they not only report less error in pressure readings than PicoPress sensors, they also

Table 6.6: Summary of computed pressures, measured pressures using PicoPress sensors, FS01 sensors and FlexiForce sensors using fitting-lines obtained from two calibration methods and the PicoPress corrected pressures at two levels for four SurePress bandages' applications. The upper and lower 95% *spread* = $mean \pm (1.96 \times SD)$, and the upper and lower 95% *CI* = $mean \pm (t \times SE)$, where “*t*” is critical point at 95% for the data degrees of freedom obtained from the student's t-distribution look-up table [189]

SurePress Bandage						
Level B						
Statistical Analysis	Computed pressures [mmHg]	PicoPress measured pressure [mmHg]	PicoPress corrected pressure [mmHg]	FS01 measured pressure [mmHg]	FlexiForce measured pressure (dead weight) [mmHg]	FlexiForce measured pressure (aneroid) [mmHg]
Mean	31.64	45.00	26.10	34.17	46.52	32.56
SD	1.39	6.00	3.48	5.80	6.76	6.58
SE	0.70	3.00	1.74	2.90	3.38	3.29
Upper 95% spread	34.36	56.76	32.92	45.54	59.78	45.46
Lower 95% spread	28.91	33.24	19.28	22.81	33.26	19.66
Upper 95% CI	33.85	54.54	31.63	43.39	57.27	43.02
Lower 95% CI	29.43	35.46	20.57	24.95	35.76	22.10
Level D						
Statistical Analysis	Computed pressures [mmHg]	PicoPress measured pressure [mmHg]	PicoPress corrected pressure [mmHg]	FS01 measured pressure [mmHg]	FlexiForce measured pressure (dead weight) [mmHg]	FlexiForce measured pressure (aneroid) [mmHg]
Mean	24.07	33.25	19.29	20.73	26.13	21.49
SD	1.99	2.87	1.67	3.26	2.64	2.52
SE	1.00	1.44	0.83	1.63	1.32	1.26
Upper 95% spread	27.97	38.88	22.55	27.12	31.31	26.43
Lower 95% spread	20.16	27.62	16.02	14.33	20.96	16.55
Upper 95% CI	27.23	37.82	21.93	25.91	30.33	25.50
Lower 95% CI	20.90	28.68	16.64	15.54	21.94	17.48

produce pressure values that are more in agreement with FS01 than PicoPress sensors even after applying the correction values.

It might be argued that in the absence of a gold standard, there is no proof that FS01 force sensors provide more accurate pressure measurements than PicoPress for example. The counter argument is that having computational pressures, measured pressures using FS01 and FlexiForce sensors, both calibrated using aneroid sphygmomanometer, and corrected PicoPress measured pressures all close to each other, and all much lower than the pressures measured using PicoPress sensors without correction, suggests that those values who are in agreement are much likely to report the actual pressures than PicoPress sensor without correction.

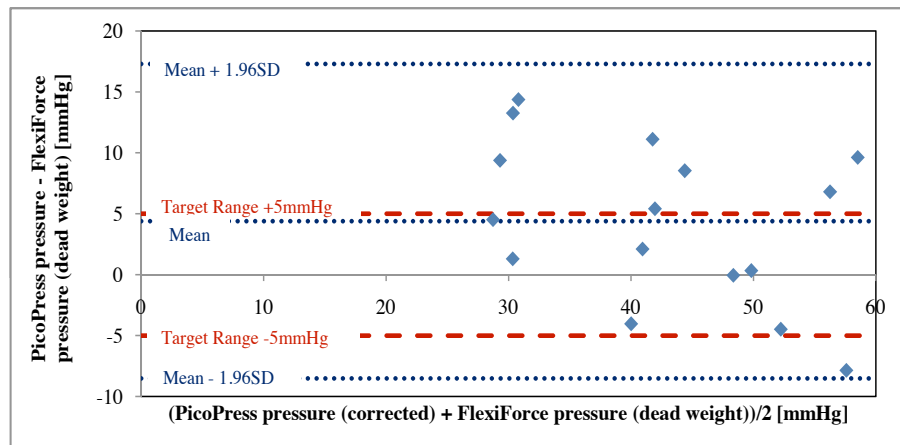


Figure 6.27: Bland-Altman plot for PicoPress sensors vs. FlexiForce deadweights calibration

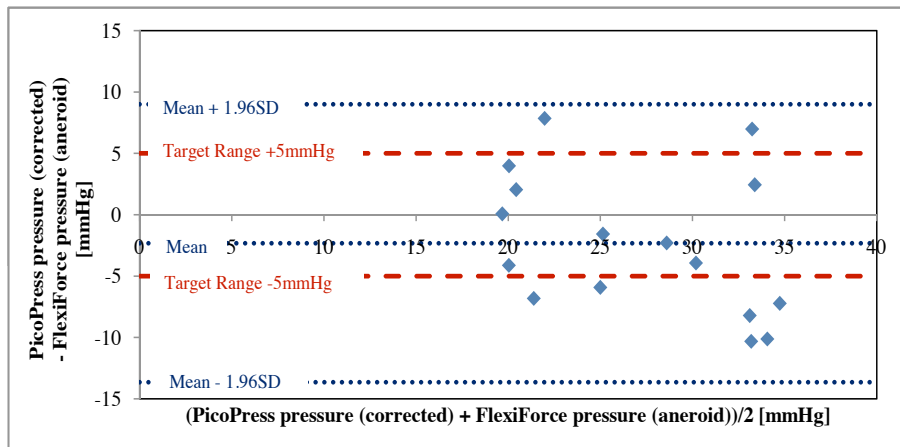


Figure 6.28: Bland-Altman plot for PicoPress sensors with correction vs. FlexiForce aneroid sphygmomanometer calibration

6.3 Pressure-Mapping Systems Over Rigid Mannequin Leg

In Sections 3.3 and 3.4 the interface pressure mathematical models were derived and validated. Tensions in bandages calculated from extensions and loads attached to the end of the bandage were used to compute the interface pressure, which, in turn, was compared to the measured pressures. However, in both Sections 3.3 and 3.4 bandages were not applied as they would normally be applied in clinical situations. Section 6.2 addressed this by comparing the computed and measured pressures when bandages were applied to a cylinder with constant radius and found a good agreement between the computed pressures and the measured pressures, particularly in the case of SurePress bandage. However, the curvature of the leg is not constant, therefore, this section will study if the bandage extension provides reliable feedback to nurses to control the applied pressure by MCBs

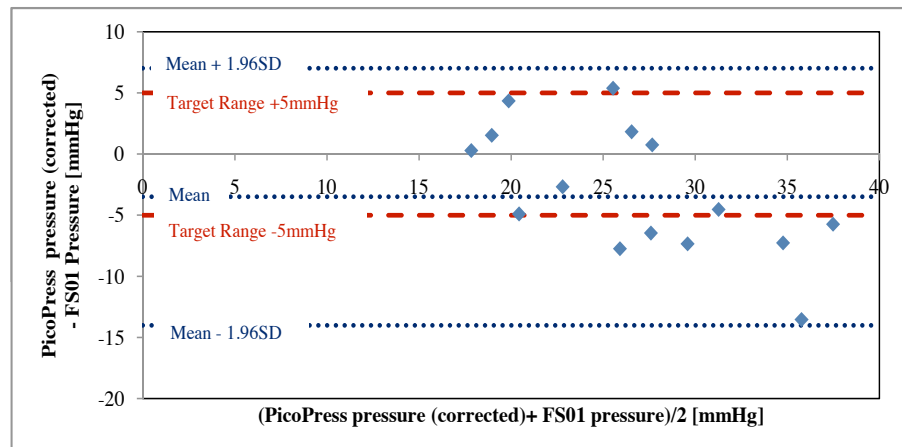


Figure 6.29: Bland-Altman plot for PicoPress sensors with correction vs. FS01 force sensors

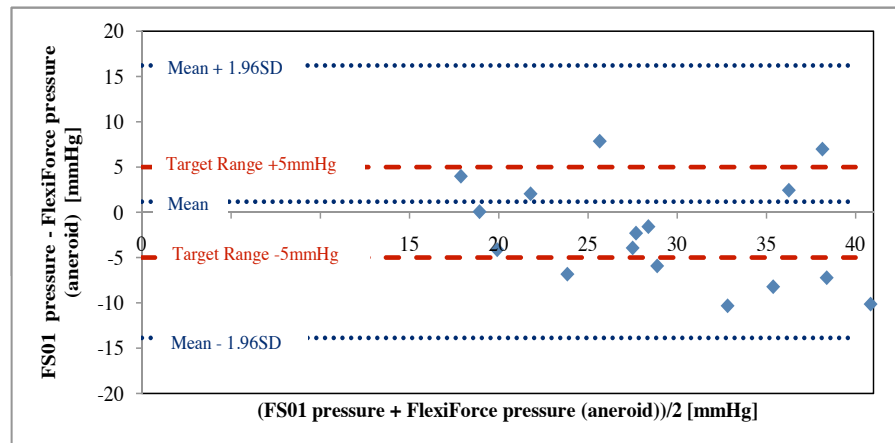


Figure 6.30: Bland-Altman plot for FS01 force sensors vs. FlexiForce aneroid calibration

when they apply MCBs to a solid leg. This section will also compare the three sensing technologies when used over a rigid mannequin leg.

6.3.1 3D Scan and Curvature Measurements for Rigid mannequin Leg

In order to calculate the pressures applied by MCB to a leg, the leg radii of curvatures need to be measured. Nelson [7] measured the curvature using a plaster cast, tracing the plaster cast curves onto paper and measuring the transformed drawing by dissecting the arcs of the curve. Gaied et al. [81] scanned their rigid leg into a 3D, which then was used to obtain the digital profile of the required cross sections of the leg. However, they have not published the details of their method.

Plastic mannequin legs, used to display hosiery in shops, were obtained. One of these legs was painted in white and marked with a red marker. This leg was scanned using Nex-

tEngine 3D scanner (model 2020i, NextEngine, California, USA) (Figure 6.31). 3D Scan Studio (NextEngine, California, USA) was used to attach, trim, fuse and generate mesh data from the 3D scans (Figure 6.32). The mesh file was then imported into SolidWorks 2009 (Dassault Systemes SolidWorks Corp, Massachusetts, USA) to create a solid model of the leg mannequin. SolidWorks 2009 then was used to measure the radii of curvature of the required cross sections of the leg (Figure 6.33). This was done via the next few steps:

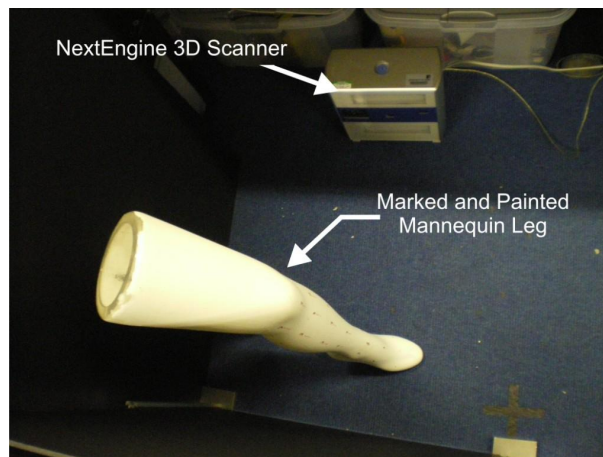


Figure 6.31: NextEngine's 3D scanner and the mannequin leg. The mannequin leg is painted in white for scanning purposes

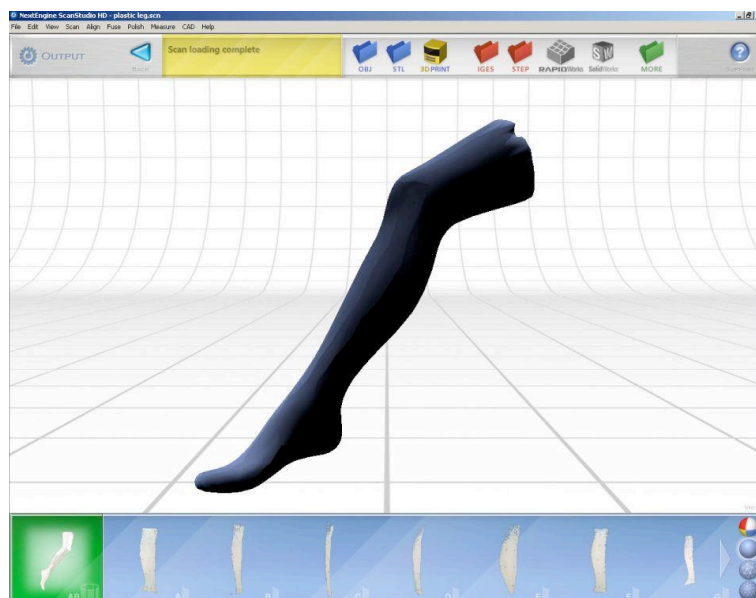


Figure 6.32: The mannequin leg's mesh data as displayed in 3D Scan Studio

- First: defining a plane
- Second: creating 3-point curves that follow the intersection line between the defined

plane and the leg at the interested cross section. This is done manually and by visual tracking for the intersection line.

- Third: converting the new plane into a sketch.
- Fourth: re-draw each two adjacent curves into one curve using again 3-point curve, this reduces the errors that might occur as a result of visual manual tracking for the intersection line.
- Finally: the radius of these new curvatures were then measured using the measurement tools available in the SolidWorks Software.

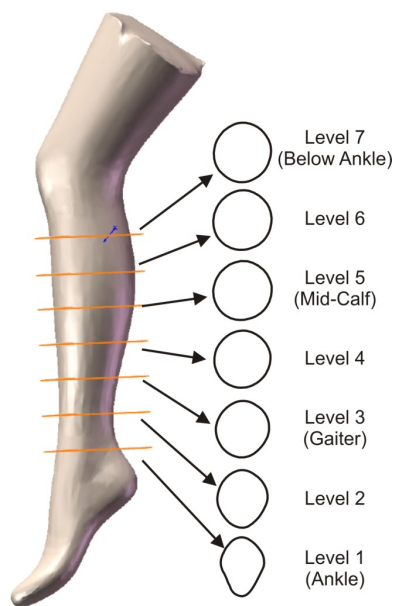


Figure 6.33: The 3D mannequin leg solid model with the cross sectional digital profiles at seven levels

6.3.2 Pressure-Mapping Mannequin Leg Using PicoPress Sensors

This section will compare the pressures computed from extension for two bandages to the pressures measured using arrays of PicoPress probes. The computed pressures also compared with the corrected measured pressure. This correction factor was based on the pressure perturbation due to the physical dimensions of the sensor and the change in local bandage extension due to calibrating the sensors under compression bandages.

Materials and Methods

The rig used and PicoPress balloons arrangement: The rig used was composed of a plastic mannequin leg, with a $0.2m$ ankle circumference, $0.34m$ circumference at the widest part of the calf and $0.35m$ ankle-knee length and a wooden base clamped to a table

(Figure 6.34). Fourteen PicoPress balloons were attached as per Figure 6.35. No balloons were attached to anterior side level B (ankle) and level B1 (gaiter) as there was not enough area to accommodate four PicoPress balloons next to each other. The mannequin leg was treated as a left leg.

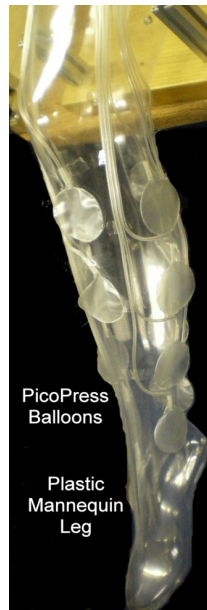


Figure 6.34: Plastic mannequin leg with PicoPress sensors mounted

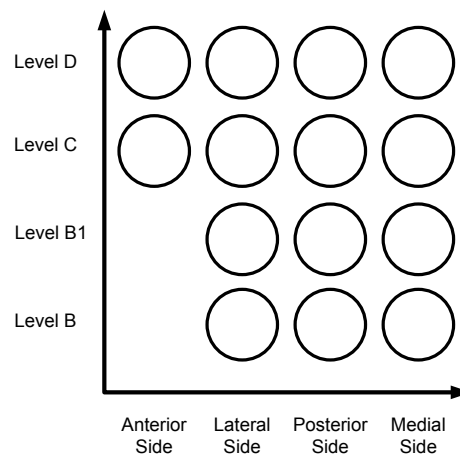


Figure 6.35: The arrangement of the PicoPress sensors on the mannequin leg

Testing the system: All PicoPress balloons were tested after they were attached to the leg with an aneroid sphygmomanometer for the pressure range $0-120\text{mmHg}$. The aneroid sphygmomanometer was inflated to 120mmHg and the pressure then was decreased at 10mmHg intervals. Each time the pressure readings reported by each tested balloon was recorded into a spreadsheet. The process was repeated for three times. The nonlinearity,

repeatability and accuracy of each of PicoPress balloons was assessed. The purpose was to investigate if the location and the change in the radius of the curvature of the leg had an impact on the sensor performance.

Measuring the extension and pressure: Prof. E.A. Nelson applied three pre-marked Comprilan bandages and three pre-marked SurePress bandages to the mannequin. She was asked to apply the bandages with target pressure of 40mmHg at the ankle and 20mmHg at the knee. The pressures at the 14 different points were measured using PicoPress transducers after calibrating each sensor under the bandage. The extension at the outer 2nd layer of the bandage was measured using a measurement tape at the same 14 different points where the PicoPress balloons were placed.

Computing the pressure: The procedure used here is as reported in Section 6.2.1, but the radius of curvature in this case was not constant. The radii used were those obtained in Section 6.3.1. The computational pressure was obtained using a routine written in MATLAB R2009b.

Correction for the measured pressures: Equations 3.33, 6.1, 6.2 and 6.3 were used to calculate the correction factor for PicoPress sensors over the mannequin leg. The radii of curvature were obtained as per Section 6.3.1. The correction factors for each measurement site was calculated using a routine written in MATLAB R2009b.

Statistical analysis: Bland-Altman plots [197] and frequency percentage counts were used to check the levels of agreement between the computed and measured pressures for the two bandages and between the computed and the corrected measured pressures for the two bandages. The computed and measured pressures were considered to be in agreement if the difference between the computed and measured pressures were within $\pm 5\text{mmHg}$. PASW 17 and Excel 2007 were used to carry out the statistical analysis.

Results, Analysis and Discussion

Accuracy testing showed that the median accuracy for the 14 sensors was $5.48\%FS$, where FS is 120mmHg . During testing, the PicoPress probe located at lateral B underestimated the pressure applied via an aneroid sphygmomanometer. For example, when 60mmHg was applied the sensor, the sensor pressure reading was on average 30mmHg . The overall accuracy error for this particular probe was $28\%FS$. This underestimation problem is thought to be caused by the sensor being located just behind the malleolus, which means that, there will be less contact between the sphygmomanometer cuff and the PicoPress probe.

Table 6.7 summarizes the measured extensions and pressures and the calculated tensions and pressures. Figures 6.36 and 6.37 illustrates the computed, measured and corrected measured pressures for both bandages.

Table 6.7: Summary of Comprilan and SurePress measured extensions, calculated tensions and pressures, measured pressures and corrected pressures. The upper and lower 95% *spread* = $mean \pm (1.96 \times SD)$, and the upper and lower 95% *CI* = $mean \pm (t \times SE)$, where “*t*” is critical point at 95% for the data degrees of freedom obtained from the student’s t-distribution look-up table [189]

Comprilan Bandage							
Statistical Analysis	Extension [%]	Tension [N]	Computed pressure [mmHg]	Measured pressure [mmHg]	Corrected measured pressure [mmHg]	Measured pressure / computed pressure	Corrected measured pressure / computed pressure
Mean	36.71	6.57	27.73	56.43	35.73	2.18	1.45
SD	8.13	2.37	11.60	21.70	16.32	0.76	0.58
SE	1.23	0.36	1.75	3.27	2.55	0.11	0.09
Upper 95% spread	52.65	11.21	50.46	98.96	67.72	3.66	2.58
Lower 95% spread	20.78	1.94	5.00	13.90	3.74	0.70	0.32
Upper 95% CI	39.12	7.27	31.15	62.84	40.73	2.40	1.62
Lower 95% CI	34.31	5.88	24.30	50.02	30.73	1.96	1.27

SurePress Bandage							
Statistical Analysis	Extension [%]	Tension [N]	Computed pressure [mmHg]	Measured pressure [mmHg]	Corrected measured pressure [mmHg]	Measured pressure / computed pressure	Corrected measured pressure / computed pressure
Mean	36.95	6.26	25.43	43.56	27.75	1.87	1.24
SD	5.50	1.50	11.22	12.76	10.15	0.56	0.35
SE	0.83	0.23	1.69	1.92	1.59	0.08	0.05
Upper 95% spread	47.74	9.20	47.42	68.57	47.65	2.96	1.93
Lower 95% spread	26.17	3.33	3.44	18.55	7.86	0.78	0.56
Upper 95% CI	38.58	6.70	28.74	47.33	30.86	2.04	1.35
Lower 95% CI	35.33	5.82	22.11	39.79	24.65	1.71	1.14

Due to the small radii of curvature at the posterior B level (ankle), Equation 2.8 was reporting a perturbation coefficient that is smaller than one. This is due to the fact that the radius of the sensor is larger than the radius of curvature at posterior B i.e. if the the radius at posterior B level was for a cylinder, PicoPress sensor would be wrapped around the cylinder. This is one of the limitations of the Vinckx model (Equation 3.33); thus, the perturbation was not calculated for this point.

The results illustrate the perturbation problem. It also shows that applying a correction factor to PicoPress readings results in pressure values much closer to the ones computed from extension especially in the case of SurePress. Unlike the experiment on the cylinder, the ratio of the corrected measured pressures over the computed pressure ratio for both Comprilan and SurePress bandages were > 1 .

Furthermore, there is a clear pressure gradient on the measured pressure profile for both Comprilan and SurePress for the lateral and posterior sides of the leg and for the

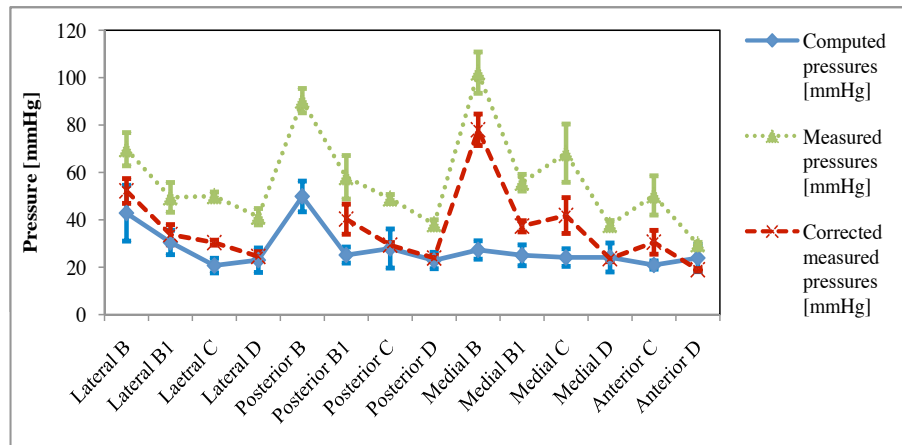


Figure 6.36: Comprilan: computed, measured and corrected measured pressures. The error bars are for the standard error of the mean. Lines connecting the pressure points are used for illustrative purposes

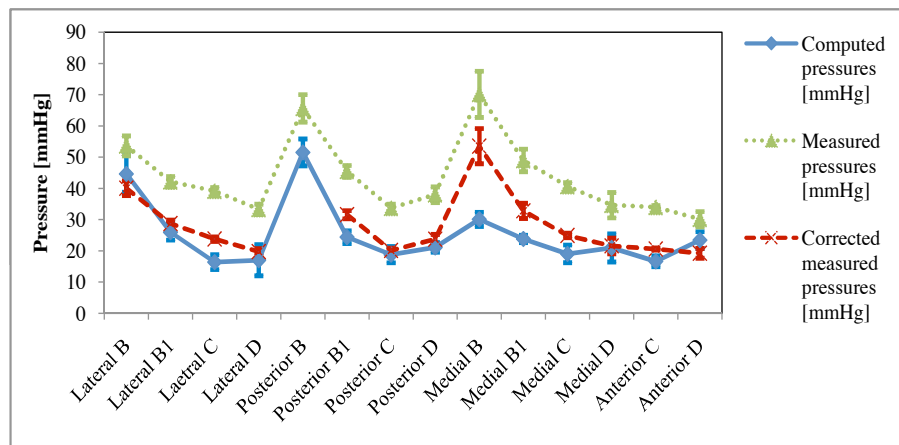


Figure 6.37: SurePress: computed, measured and corrected measured pressures. The error bars are for the standard error of the mean. Lines connecting the pressure points are for illustrative purposes

medial side in the case of SurePress. However, the measured pressure values are much higher than the target pressure values. Also, from Figures 6.36 and 6.37 it is clear that the measured pressure at lateral B is lower than the measured pressures at posterior B and medial B. This might be due to the fact that the bandage was applied with a right hand and lateral B is the point where the nurse starts to apply tension to the bandage when she is applying the bandage to the leg if she is right handed. This also might be caused by the nature of the placement site of the sensor.

Additionally, the effect of the leg radii of curvature on the computed pressures is clear. In fact, the computed pressures shows a good gradient over the lateral and posterior sides of the plastic leg. However, this gradient is reduced medially. This might be explained

by the larger radius of curvature at the medial side of ankle compared with the lateral and posterior sides where both the lateral malleolus and Achilles tendon, have a sharper profile than the medial malleolus for the plastic leg used.

Table 6.8 and Figures 6.38 and 6.39 report the levels of agreements between the pressures computed theoretically from extension and the measured and corrected measured pressures. SurePress computed pressures show again higher levels of agreement with the corrected measured pressures than Comprilan. Nevertheless, the percentage of cases in agreement, this time, is less than the one found when the same test was carried out over a PVC cylinder (Section 6.2.1). These results might indicate that using extension as a feedback to control the pressures applied by MCBs is not a reliable source of feedback.

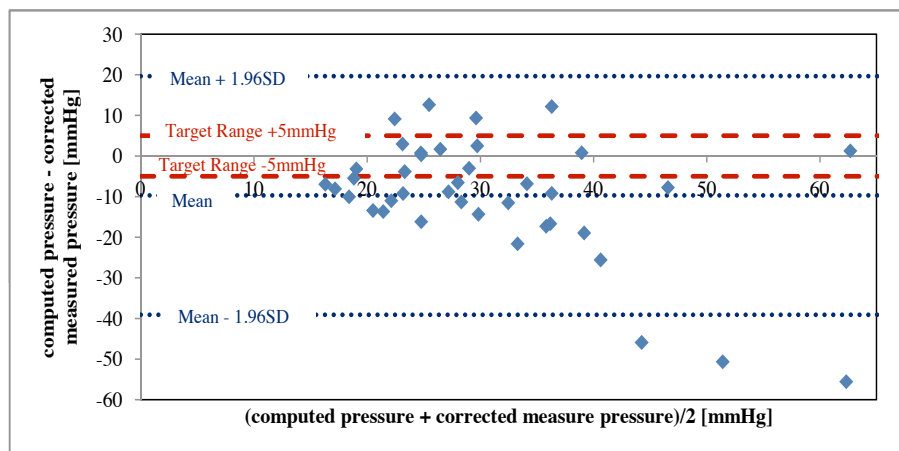


Figure 6.38: Bland-Altman plot for computed pressures and corrected measured pressures for Comprilan

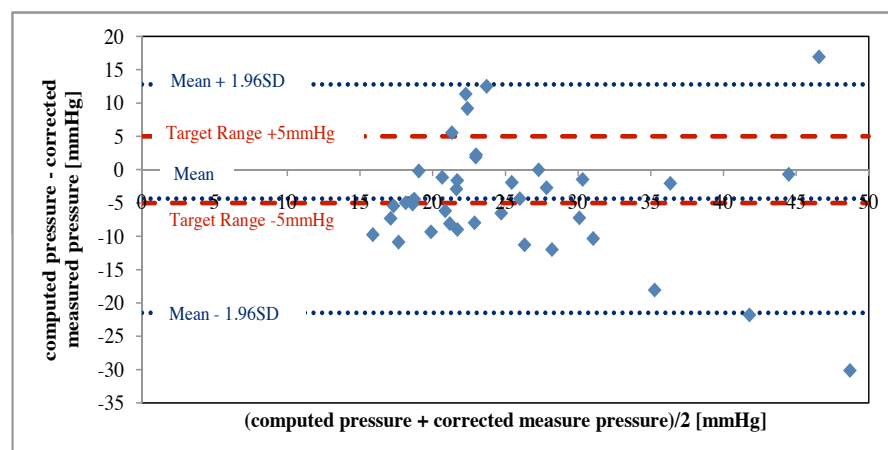


Figure 6.39: Bland-Altman plot for computed pressures and corrected measured pressures for SurePress

Table 6.8: Percentage of the cases where the difference between the computed and measured and corrected measured pressures being within $\pm 5mmHg$ for Comprilan and SurePress

Statistical Analysis	Percentage of cases where the difference is within $\pm 5mmHg$
Comprilan computed pressures and measured pressures	5%
Comprilan computed pressures and corrected measured pressures	26%
SurePress computed pressures and measured pressures	12%
SurePress computed pressures and corrected measured pressures	41%

6.3.3 Pressure-Mapping Mannequin Leg Using FS01 Force Sensors

This section will present the experimental work carried out to compare between the pressures computed from extensions in two MCBs with the pressures measured using arrays of FS01 sensors embedded in the wall of a plastic mannequin leg.

Materials and Methods

The rig used and FS01 force sensors arrangement: The rig used composed of a plastic mannequin leg, with a $0.2m$ ankle circumference, $0.34m$ circumference at the widest part of the calf and $0.35m$ ankle-knee length (Figure 6.40). Sixteen rectangular slots were drilled into the mannequin leg structure to form a 4×4 matrix (Figure 6.41).

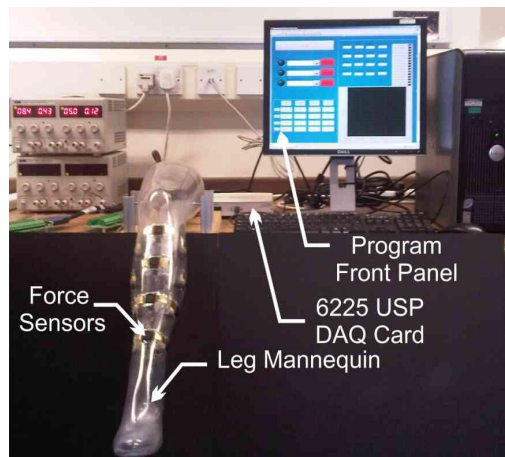


Figure 6.40: Plastic mannequin leg with FS01 force sensors embedded in its wall

Conditioning circuit, data acquisition and sensor calibration: The sensors were powered with constant $5V$ through a processing circuit. The sensors output signals were

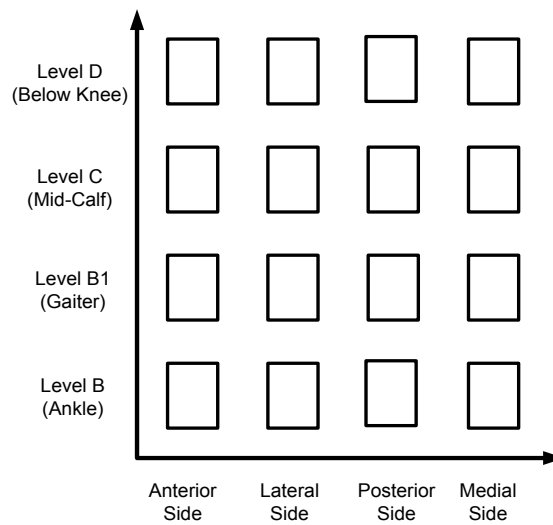


Figure 6.41: The arrangement of FS01 force sensors

passed to the processing circuit and then to a Mass Term 6225 USB DAQ card through a screw terminal board (LPR-68).

Due to the curved nature of the leg, the force sensors were calibrated individually using an aneroid sphygmomanometer after the sensors being attached to the mannequin leg. The sensors were calibrated for the pressure range $0 - 120\text{mmHg}$ by inflating the aneroid sphygmomanometer cuff to 120mmHg and then deflating the cuff with 10mmHg intervals. The process was repeated 10 times to reduce the repeatability error of the aneroid sphygmomanometer. A 3^{rd} order polynomial fitting-line was used to fit the averaged data points of the 10 repeats. A program written in LabView 8.6 was used to acquire the sensors signals in the calibration process. Excel 2003 was used to obtain the fitting-lines and calculate the “R” squared regression values for the sensors.

The pressure measurement display program: A program was written in LabView 8.6 to acquire and display the signals, convert them to the equivalent pressure values, display the pressure values numerically and store the voltages and pressures for further processing. The signals were sampled at 100Hz and a software based 2^{nd} order low-pass filter with 10Hz cut-off frequency was used to filter out the signal. Figures 6.42 and 6.43 show the front panel of the program and the flow chart of the program respectively.

Computing pressures: This is the same as the ones reported in Section 6.3.2.

Measuring the extension and pressure: Prof. E.A. Nelson (a trained bandager) applied three pre-marked Comprilan bandages and three pre-marked SurePress bandages to the mannequin leg. She was asked to apply the bandages with a target pressure of 40mmHg at the ankle and 20mmHg at the knee. Pressure values were acquired throughout the bandage application. After applying the bandage, the extension at the outer 2^{nd}

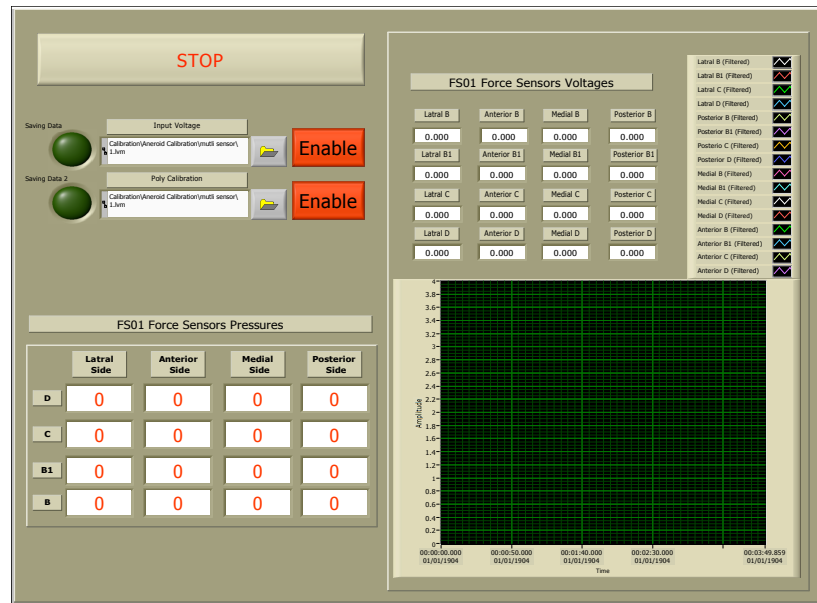


Figure 6.42: The front panel of the display program

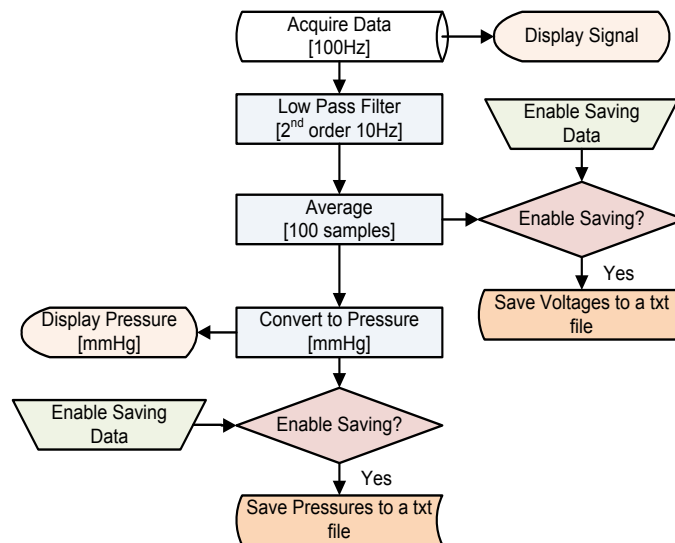


Figure 6.43: The flow chart of the display program

layer of the bandage was recorded using a measurement tape at the same 16 different points where the FS01 sensors are placed.

Statistical analysis: Bland-Altman plots [197] and frequency percentage counts were used to check the levels of agreement between the computed and measured pressures for the two bandages. The computed and measured pressures were considered to be in agreement if the difference between the computed and measured pressures were within $\pm 5\text{mmHg}$. PASW 17 and Excel 2007 were used to carry out the statistical analysis.

Results, Analysis and Discussion

The median accuracy for the sensors used found to be $2.43\%FS$, where FS here is $120mmHg$ and the accuracy is the combined error of the calibration fitting-line and the repeatability of both the sensor and the calibration device used. Table 6.7 summarizes the measured extensions and pressures, and the calculated tensions and pressures. Figures 6.44 and 6.45 illustrates the computed and measured pressures for both bandages.

Table 6.9: Summary of Comprilan and SurePress measured extensions, calculated tensions and pressures and measured pressures. The upper and lower 95% *spread* = $mean \pm (1.96 \times SD)$, and the upper and lower 95% *CI* = $mean \pm (t \times SE)$, where “*t*” is critical point at 95% for the data degrees of freedom obtained from the student’s t-distribution look-up table [189]

Comprilan Bandage					
Statistical Analysis	Extension [%]	Tension [N]	Computed pressure [mmHg]	Measured pressure [mmHg]	Measured pressure / computed pressure
Mean	34.92	6.00	27.01	36.52	1.52
SD	6.74	1.78	10.53	10.89	0.72
SE	0.97	0.26	1.52	1.57	0.10
Upper 95% spread	48.13	9.50	47.65	57.86	2.94
Lower 95% spread	21.70	2.50	6.36	15.18	0.10
Upper 95% CI	36.82	6.51	29.99	39.60	1.73
Lower 95% CI	33.01	5.50	24.03	33.44	1.32

SurePress Bandage					
Statistical Analysis	Extension [%]	Tension [N]	Computed pressure [mmHg]	Measured pressure [mmHg]	Measured pressure / computed pressure
Mean	43.75	8.29	35.23	30.51	1.01
SD	7.69	2.34	18.08	8.87	0.43
SE	1.11	0.34	2.61	1.28	0.06
Upper 95% spread	58.83	12.87	70.65	47.89	1.86
Lower 95% spread	28.67	3.71	-0.20	13.12	0.16
Upper 95% CI	45.93	8.95	40.34	33.02	1.13
Lower 95% CI	41.57	7.63	30.11	28.00	0.88

The average of the ratio of the corrected measured pressures over the computed pressure for Comprilan was > 1 and for SurePress was close to 1. The expected pressure ratio was < 1 as it has been mentioned in Section 6.2.2.

Furthermore, there is a no progressive measured pressure gradient on any of the leg sides for both Comprilan and SurePress. On the contrary, computed pressures shows graduated pressure on the lateral and the anterior sides of the leg for Comprilan, and

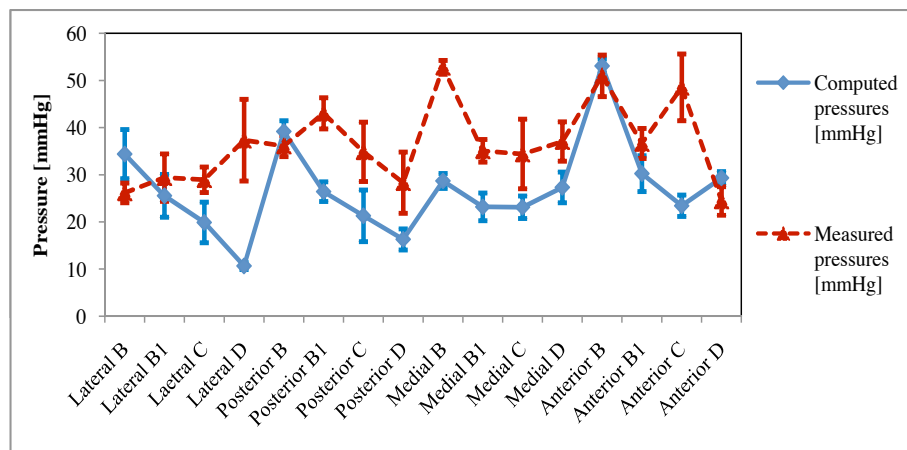


Figure 6.44: Comprilan: computed and measured pressures. The error bars are for the standard error of the mean. Lines connecting the pressure points are for illustrative purposes

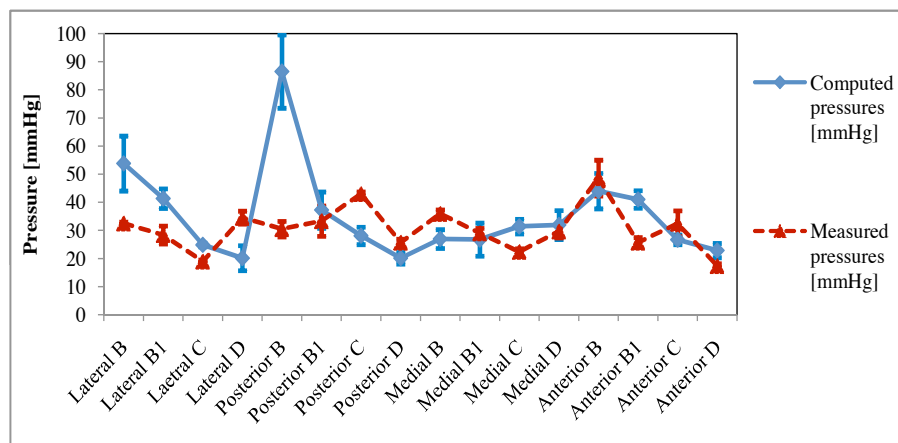


Figure 6.45: SurePress: computed and measured pressures. The error bars are for the standard error of the mean. Lines connecting the pressure points are for illustrative purposes

the lateral, the posterior and the anterior sides of the leg for SurePress. This can be explained by the fact that the radius of curvature of the leg at the ankle level for example has changed due to the presence of the FS01 sensors. This also explains the difference between the computed and the measured pressures at the lateral B and the posterior B for SurePress bandage. The change in radius might have affected other measurement sites also.

Figures 6.46 and 6.47 demonstrate the levels of agreements between the computed and the measured pressures for Comprilan and SurePress bandages. Comprilan computed pressures found to be in agreement with the measured pressures in 29% of the cases, while SurePress computed pressure found to be in agreement with measured pressures in 25%

of the cases. These results might indicate that using extension as a feedback to control the pressure applied by MCBs is not reliable. However, other causes like the change in the curvature of the leg when FS01 sensors were introduced and using extension values measured at the outer bandage layer might have also affected the computed pressure reliability. Furthermore, the presence of FS01 sensors and the way they were integrated to the leg wall might had an impact on the measured pressures.

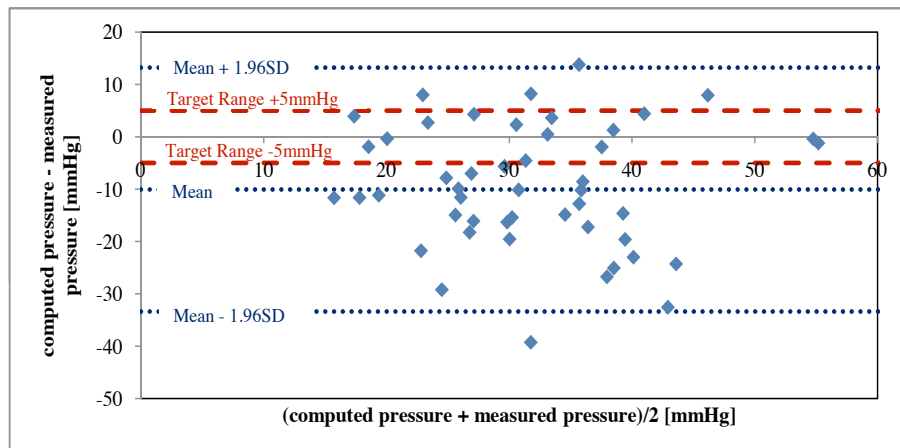


Figure 6.46: Bland-Altman plot for computed pressures and corrected measured pressures for Comprilan

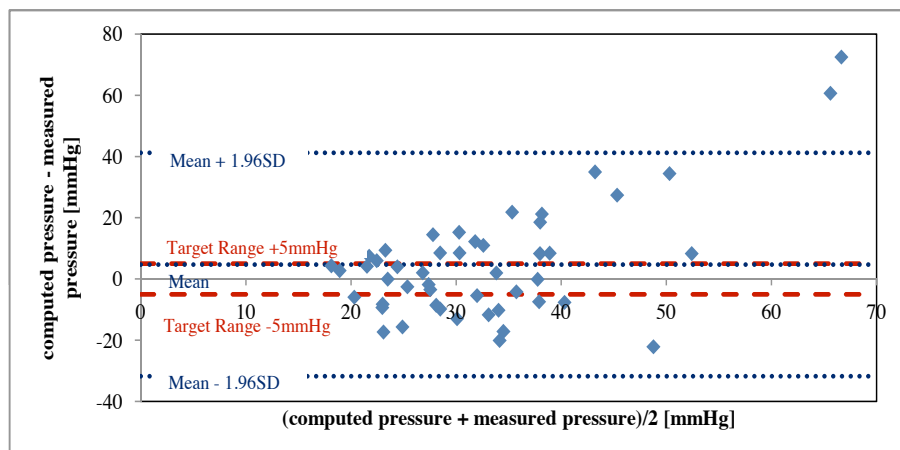


Figure 6.47: Bland-Altman plot for computed pressures and corrected measured pressures for SurePress

6.3.4 Pressure-Mapping Mannequin Leg Using FlexiForce Sensors

The aim of this section is to compare the pressures measured experimentally using arrays of FlexiForce sensors when bandages were applied to a plastic mannequin leg against the pressures computed indirectly from the extension in the MCBs.

Materials and Methods

The rig used and FlexiForce sensors arrangement: The rig used in the apparatus composed of a plastic mannequin leg with a $0.2m$ ankle circumference, $0.34m$ circumference at the widest part of the calf and $0.35m$ ankle-knee length (Figure 6.48). Forty FlexiForce sensors were mounted on top of the plastic leg in 8×5 matrix. This provided the highest resolution map possible without having overlapped sensors.

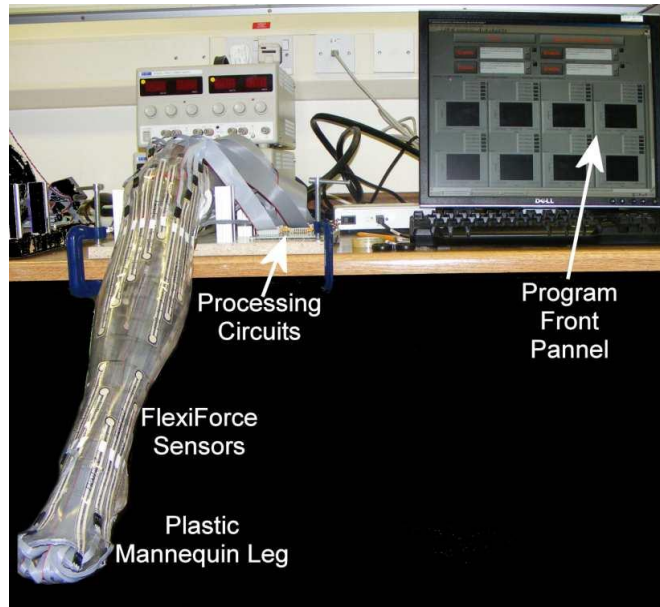


Figure 6.48: Plastic mannequin leg with FlexiForce sensors mounted in the form of 8×5 matrix

Conditioning circuit, data acquisition and sensor calibration: The sensors were powered with constant $5V$ through three conditioning circuits, which were the same as the circuits used in Section 6.2.3. The output signals from the three processing circuits were passed to a Mass Term 6225 USB DAQ card through a screw terminal board (LPR-68).

Due to the curved nature of the mannequin leg, the force sensors were calibrated individually using an aneroid sphygmomanometer. The sensors were calibrated for the pressure range $0 - 120mmHg$ by inflating the aneroid sphygmomanometer cuff to $120mmHg$ and then deflating the cuff at $10mmHg$ intervals. The process was repeated 20 times to reduce the repeatability error of the aneroid sphygmomanometer. A 3^{rd} order polynomial fitting-line was used to fit the averaged data points of the 20 repeats. A program written in LabView 8.6 was used to acquire the sensors signals in the calibration process. Excel 2003 was used to obtain the fitting-lines and calculate the “R” squared regression values for the sensors.

The pressure measurement display program: A program was written in LabView 8.6 to acquire and display the signals, convert them to the equivalent pressure values,

perform window averaging for the pressure values, display the average pressure values numerically and store the voltages, the measured pressures and the average pressures for further processing. The signals were sampled at $100Hz$ and a software based 2^{nd} order low-pass filter with $1Hz$ cut-off frequency was used to filter out the acquired signals. Figures 6.49 and 6.50 show the front panel of the program and the flow chart of the program respectively.



Figure 6.49: The front panel of the display program for FlexiForce mannequin leg pressure-mapping system

Computing pressures: This is as reported in Section 6.3.2.

Measuring the extension and pressure: Prof. E.A. Nelson applied three pre-marked Comprilan bandages and three pre-marked SurePress bandages to the mannequin leg. She was asked to apply the bandages with a target pressure of $40mmHg$ at the ankle and $20mmHg$ at the knee. After applying the MCB, the amount of extension was recorded using a measurement tape at 28 points (7×4 matrix), which corresponds to the spaces between sensor rows and the four sides of the leg. MATLAB R2009b was used to compute the theoretical pressures from the measured extension values. MATLAB R2009b and Excel were used to compare the theoretical and measured pressure values.

Statistical analysis: Bland-Altman plots [197] and frequency percentage counts were used to check the levels of agreement between the computed and measured pressures for the

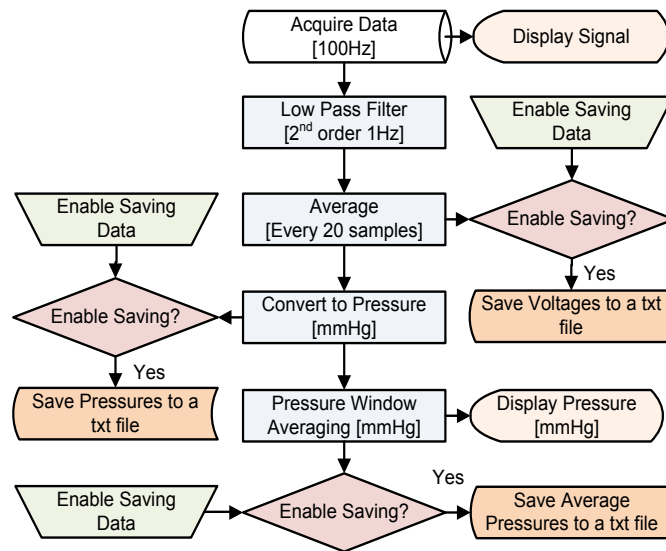


Figure 6.50: The flow chart of the display program for FlexiForce mannequin leg pressure-mapping system

two bandages. The computed and measured pressures were considered to be in agreement if the difference between the computed and measured pressures were within $\pm 5\text{mmHg}$. PASW 17 and Excel 2007 were used to carry out the statistical analysis.

Results, Analysis and Discussion

The median accuracy for the sensors used found to be $\pm 12.17\%FS$, where FS here is 120mmHg and the accuracy is the combined error of the calibration fitting-line and the repeatability of both the sensor and the calibration device used. This means that the median accuracy in terms of pressure for each sensor is $\pm 14.6\text{mmHg}$ and after window averaging the accuracy will be, in theory, $\pm 7.3\text{mmHg}$ for each element of the averaged pressure map. However, the averaged pressures were re-sampled from 7×5 matrix to 7×4 matrix in order to compare the averaged pressures with the computed pressures. This results in further reduction in the accuracy error, in theory, to $\pm 5.2\text{mmHg}$ for each reported measured pressure value.

Figure 6.51 shows the computed pressure map, measured pressure map and the average pressure map obtained for Comprilan and SurePress (the maps are for the third of the three bandage applications for both bandages). The computed pressure map shows that both bandages are applied with pressure gradient. However, the pressure profile particularly in the SurePress bandage case is higher than the target pressure profile. Both the measured and averaged pressure maps differs from the computed pressure maps.

The maps illustrate pressure peak at the anterior ankle (level B), which was expected theoretically. However, the posterior side of the leg reports very low measured pressures for both bandages. When a bandage is applied to this rigid leg, it will need to conform to

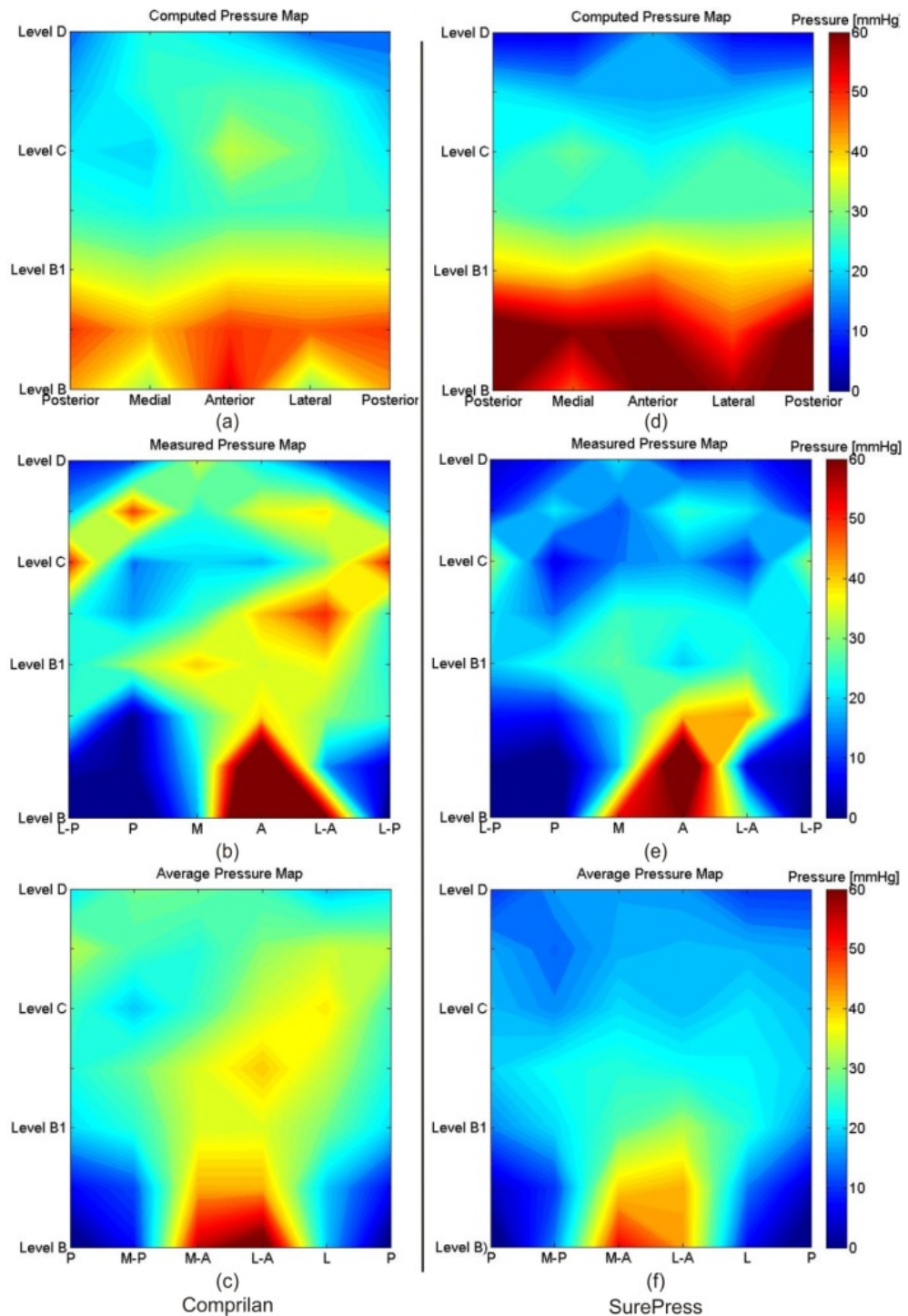


Figure 6.51: Comprilan and SurePress pressure maps: (a) Comprilan computed pressure map, (b) Comprilan measured pressure map, (c) Comprilan averaged pressure map, (d) SurePress computed pressure map, (e) SurePress measured pressure map and (f) SurePress averaged pressure map. The maps are shown with the first column “Posterior” being repeated at the start and end for better clarity. ‘L’ = Lateral, ‘A’= Anterior, ‘M’ = Medial and ‘P’ = Posterior

apply pressure to the sensors located at posterior level B (see levels 1 and 2 in Figure 6.33). This implies that very little pressure will be applied to this tricky site of the leg model, which explains the low pressures reported by FlexiForce sensors at posterior level B.

It is also clear from the maps that using the measured pressures directly might result in reporting pressure peaks due to the deficiencies associated with the FlexiForce sensors. However, these peaks were smoothed out when averaging techniques were used.

In order to compare between the computed pressures and the averaged measured pressures, the averaged measured pressures map was re-sampled from 7×5 matrix to a 7×4 matrix with elements of the new map being the ones corresponding to the same places where the extensions were measured. Table 6.10 summarizes the measured extensions and window averaging pressures and the calculated tensions and pressures for the three samples of the two bandages. Figures 6.52 and 6.53 show the computed and averaged pressures for both bandages.

Table 6.10: Summary of Comprilan and SurePress measured extensions, calculated tensions and pressures and measured pressures. The upper and lower 95% *spread* = $mean \pm (1.96 \times SD)$, and the upper and lower 95% *CI* = $mean \pm (t \times SE)$, where “*t*” is critical point at 95% for the data degrees of freedom obtained from the student’s t-distribution look-up table [189]

Comprilan Bandage					
Statistical Analysis	Extension [%]	Tension [N]	Computed pressure [mmHg]	Averaged measured pressure	Averaged pressure / computed pressure
Median	40.00	7.25	27.19	28.63	1.15
Mean	38.90	7.01	30.71	30.25	1.15
SD	4.43	1.28	11.71	13.79	0.39
SE	0.48	0.14	1.28	1.35	0.04
Upper 95% spread	47.58	9.51	53.66	57.27	1.91
Lower 95% spread	30.23	4.50	7.76	3.23	0.38
Upper 95% CI	39.85	7.28	33.21	32.89	1.23
Lower 95% CI	37.96	6.73	28.20	27.61	1.06

SurePress Bandage					
Statistical Analysis	Extension [%]	Tension [N]	Computed pressures [mmHg]	Averaged measured pressures	Averaged pressure / computed pressure
Median	46.00	8.78	29.50	20.00	0.78
Mean	41.45	7.95	33.92	22.29	0.92
SD	12.87	3.28	20.84	11.03	0.59
SE	1.40	0.36	2.27	1.08	0.06
Upper 95% spread	66.67	14.38	74.77	43.91	2.09
Lower 95% spread	16.24	1.51	-6.93	0.66	-0.25
Upper 95% CI	44.20	8.65	38.38	24.40	1.05
Lower 95% CI	38.70	7.25	29.46	20.18	0.79

The ratio of the measured pressure over the computed pressures shows similar results to the one found when FlexiForce sensors were tested over a cylinder (Section 6.2.3). The average ratio for Comprilan and SurePress were found to be > 1 and < 1 respectively.

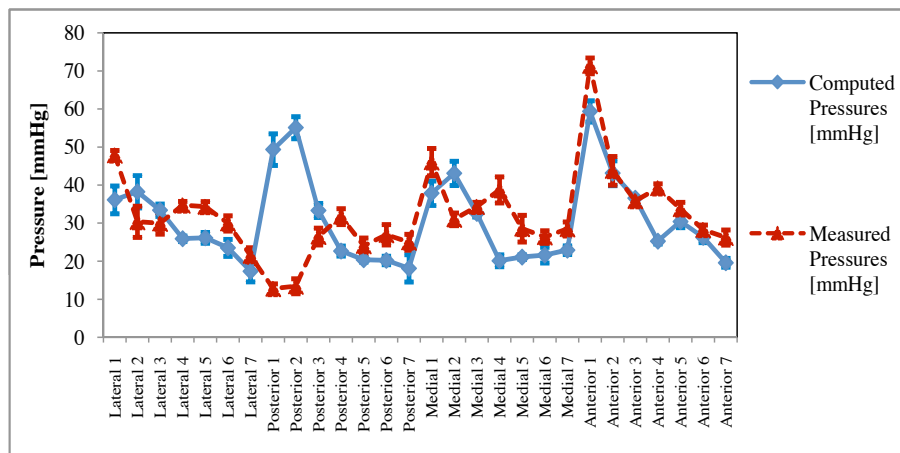


Figure 6.52: SurePress: computed and measured pressures. The error bars are for the standard error of the mean. Lines connecting the pressure points are for illustrative purposes

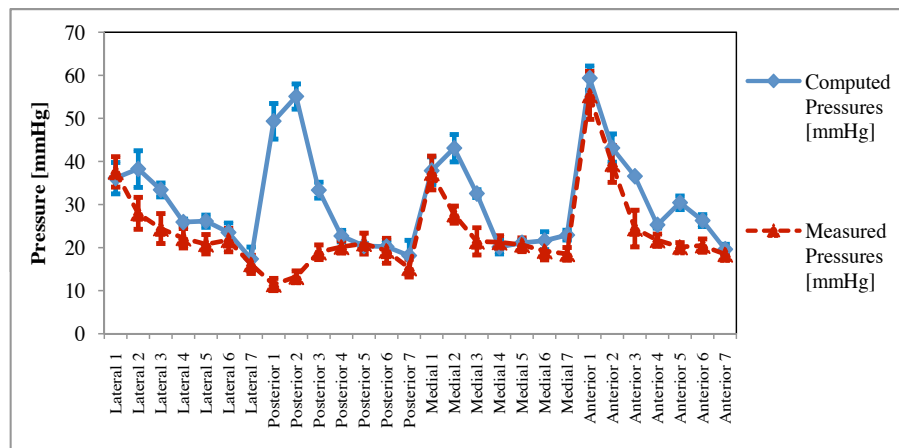


Figure 6.53: SurePress: computed and measured pressures. The error bars are for the standard error of the mean. Lines connecting the pressure points are for illustrative purposes

In the case of Comprilan, pressure ratio is close to one; while in the case of SurePress, it is much less than one. Friction forces between bandage layers and bandage angle of application, in theory, should result in damping the pressures applied, especially in the case of SurePress, i.e. the pressure ratio should be < 1 . On the other hand, the inter-variation in the tension-elongation curves and the high compression forces generated in the transverse direction of Comprilan bandage might result in applying higher pressure than anticipated theoretically.

The results found for FlexiForce pressure-mapping mannequin leg are different to the ones reported by FS01 and PicoPress pressure-mapping mannequin legs. The lower pressure ratios found for SurePress might be explained by the fact that the sensors used are

very low in profile which in turn will overcome the problem of overestimation due to the thickness (PicoPress and FS01 sensors) or sharp edges (FS01 sensors).

Figures 6.54 and 6.55 demonstrate the levels of agreements between the pressures computed and the averaged measured pressures in the case of both SurePress and Comprilan. In the case of Comprilan the computed and averaged measured pressures were found to be in agreement in 33% of the cases and in the case of SurePress they were found to be in agreement in 54% of the cases. This might indicate that using extension as a feedback to control the pressure applied by MCB might only be a good feedback method for elastic bandages like SurePress.

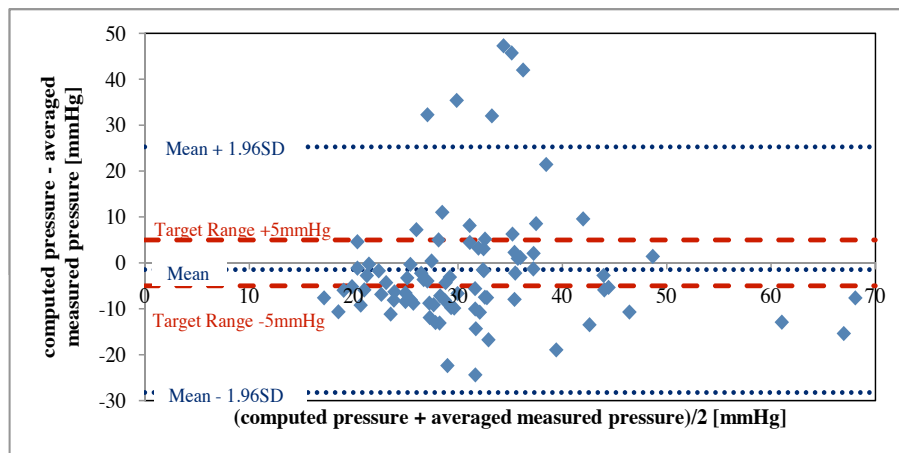


Figure 6.54: Bland-Altman plot for computed pressures and measured pressures for Comprilan

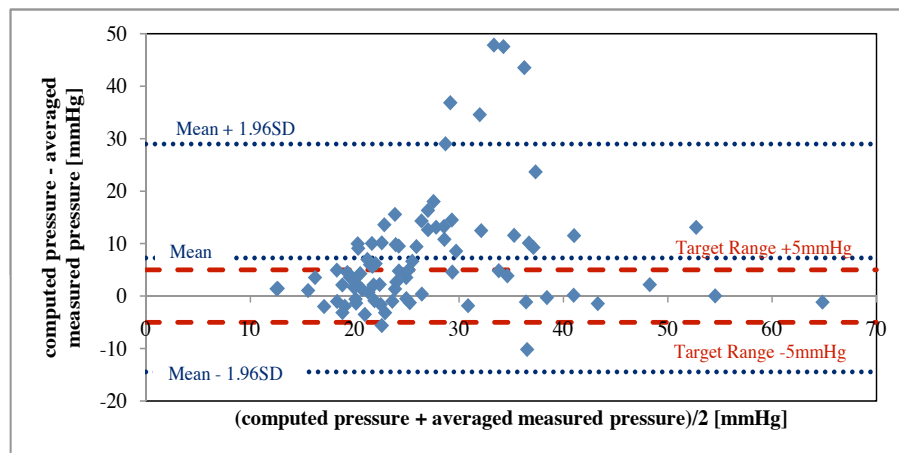


Figure 6.55: Bland-Altman plot for computed pressures and measured pressures for SurePress

6.3.5 Comparison Between the Different Pressure-Mapping Mannequin Legs

Comprilan was applied to the PicoPress, FS01 and FlexiForce mannequin legs with average extensions of 36.71%, 34.92% and 38.0% respectively. In the case of the SurePress, the average extensions were 36.95%, 43.75% and 41.45% respectively. The variation in both the extension and the pressures applied make it very difficult to compare the three sensing technologies. However, in order to carry out this comparison, the average 4×4 computed pressure map for both PicoPress and FS01 and the average 7×4 computed map for FlexiForce for both Comprilan and SurePress were obtained. In addition, the average 4×4 measured pressure map for PicoPress, PicoPress with correction factor and FS01, and the average 7×4 averaged measured map for FlexiForce for both Comprilan and SurePress were also produced. The missing elements for PicoPress and PicoPress correction factors were estimated by assuming it is equal to the average of the adjacent elements in the matrix. The percentage ratio of the measured pressures to the computed pressure was then plotted using counter filled plot for each measurement system for each bandage. These maps were used, then, to compare the different sensing technologies.

The principle behind this comparison method is that if the type of the bandage, the extension in the bandage, the number of bandage layers and the radius of the curvature to which the bandage is applied are kept constant, then, the only main variable that affects the measured pressure will be the sensing technology used. Using the ratio of the measured pressures over the computed pressures implies that any changes in the ratio from one sensing technology to the other will be caused by the nature of the sensing technology. This added to the fact that all the sensors used in these experiments were tested and calibrated using an aneroid sphygmomanometer and all bandages were applied by the same nurse. The only other variables which might still have contributed are the angle of bandage application, hysteresis and the friction forces. The latter can be assumed to be small. Prof. E.A. Nelson was asked always to try to apply the bandages using the loading cycle of the bandage to reduce the hysteresis impact. The impact of angle application can be assumed also to be negligible, as all bandages were applied with Spiral 50% overlap to the same size mannequin leg, which means that the bandage were applied with small angle variation between one bandage to the other in order to maintain the 50% bandage overlap. However, one limitation to this approach is that the extension was recored for the outer layer of the bandage only, which means that if the inner bandage layer was applied with a different extension, than the pressures computed will be different to the ones calculated. Nevertheless, measuring the bandage extension in practice showed that the variation, if existed, is small. Furthermore, using three different bandages for each measurement point will result in reducing farther the effect of the above mentioned variables on the overall conclusion particularly if the differences between the percentage pressure ratios of the different technologies is big.

Figures 6.56 and 6.57 illustrate the percentage pressure ratio maps for PicoPress,

PicoPress with correction factor, FS01 and FlexiForce sensors for both Comprilan and SurePress bandages.

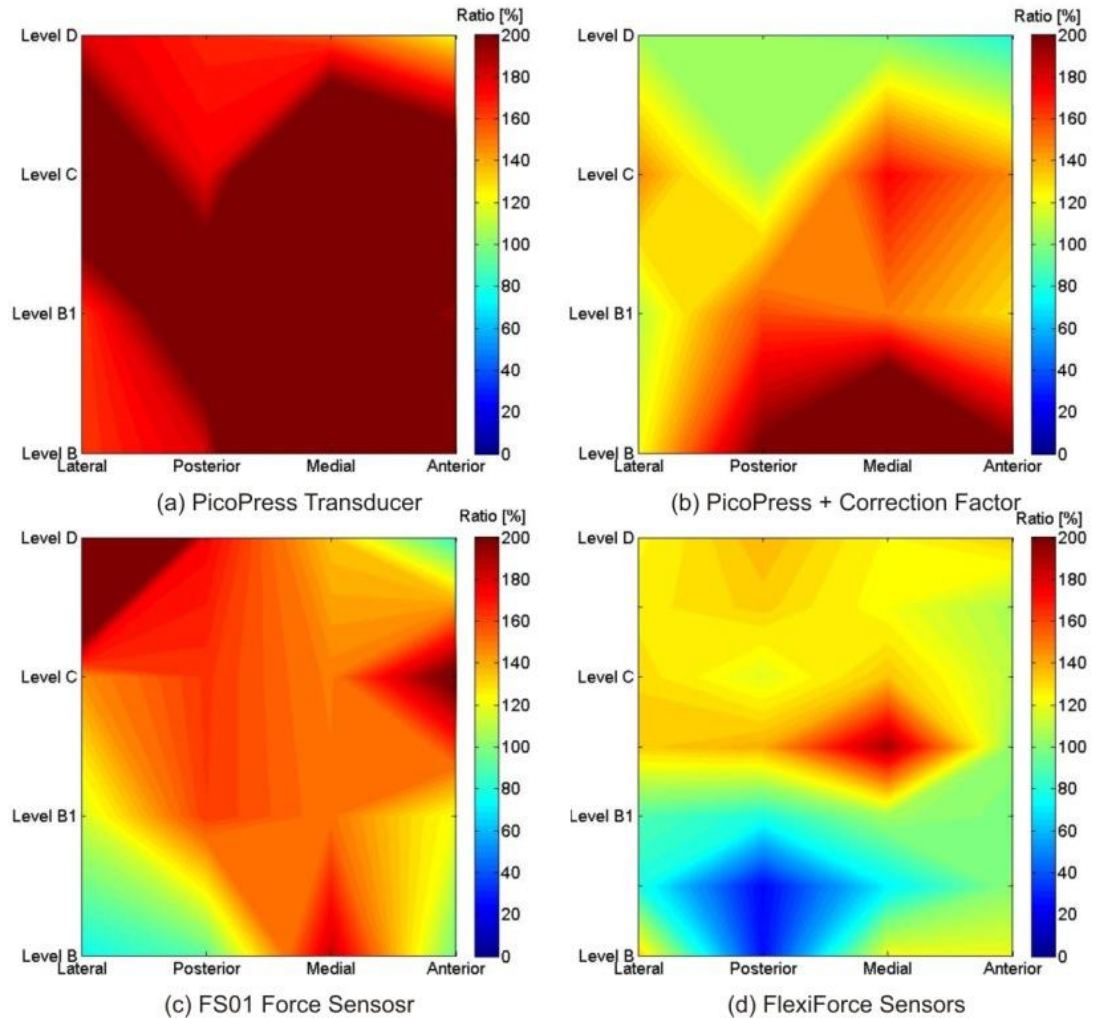


Figure 6.56: Comprilan measured over computed pressure ratio maps: (a) PicoPress, (b) PicoPress plus correction factor, (c) FS01 force sensors, (d) FlexiForce sensors

Comparing Comprilan pressure ratio maps shows that, the measured pressures were higher than the computed pressures in all systems used, with FlexiForce showing the lowest pressure ratios. The results clearly indicate that PicoPress reporting very high pressure values, which can be explained by the impact of the probes physical dimension on the interface pressure and the perturbation in the interface pressure caused by inflating the probe after applying the bandage to the leg. These results suggests that using PicoPress sensors without a correction factor will result in overestimating the pressure. However, using the correction factor implies that the radii of curvature should always be known and the correction model is a reliable model. However, Section 3.8 illustrated that Vinckx et al.'s model [86] had some problems and the values of the perturbation estimated using this model did not fit with the ones found experimentally.

Furthermore, the ratio map obtained using FS01 sensors reported higher pressures than expected theoretically. This can be explained by the sharp edges caused by the presence of the sensor. Despite the poor accuracy for FlexiForce sensors, using window averaging technique resulted in pressures measured being slightly higher than the pressure computed except at the posterior B level. This could be explained by physical change in the rigid leg curvature, which implies that there will be a little contact, if any, between the bandage and the sensors.

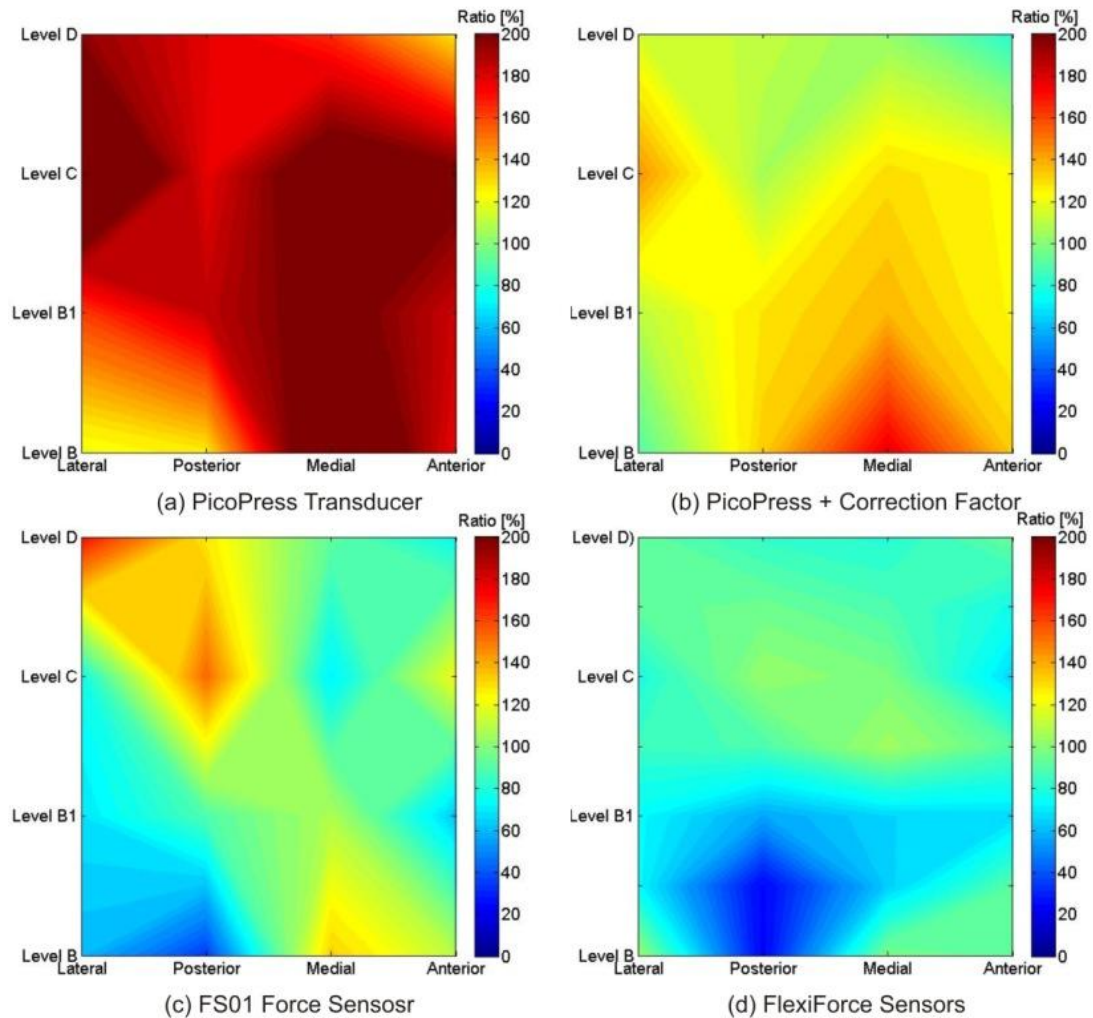


Figure 6.57: SurePress measured over computed pressure ratio maps: (a) PicoPress, (b) PicoPress plus correction factor, (c) FS01 force sensors, (d) FlexiForce sensors

Comparing the SurePress pressure ratio maps shows that the measured pressures were higher than the computed pressures in the case of PicoPress and PicoPress plus the correction factor. FS01 pressure map shows segments where the measured pressures are lower than the ones computed. In the case of FlexiForce, the pressure ratio map is a mixture of the ratio being close to one or smaller than one. As in the case of Comprilan, the results indicates that PicoPress will overestimate the pressure.

Furthermore, the ratio map obtained using FS01 sensors has a mixed picture, where some parts reporting ratios larger than one and others reporting ratios smaller than one. The larger than one pressure ratio values can be explained using the argument used to explain the ratio profile for Comprilan. The lower than one ratios occurs sometimes at where the radii of curvature of the original leg before introducing the FS01 sensor were small and sharp. When the sensor were introduced, the radii of curvature at these locations are less sharper. This means that the bandage will follow a different curve to the one anticipated for the computed pressures.

Despite the poor accuracy for FlexiForce sensors, using window averaging technique resulted in pressures measured being close to the pressure computed or smaller. At the posterior B level, the low ratio can be explained by the physical change in the leg curvature, which implies that there will be a little contact, if any, between the bandage and the sensors. The lower ratio at other sites can be explained by pressure attenuation due to the friction forces between bandage layers and the combined effect of bandage angle of application and the compression forces generated in the transverse direction of the bandage secondary to extending it along its length.

6.4 Pressure-Mapping Systems Over Soft Leg Model

In Section 3.3 and 3.4 the interface pressure mathematical models were derived and validated. Tensions in bandages calculated from extensions and loads attached to the end of the bandage were used to compute the interface pressure, which, in turn, was compared to the measured pressures. However, in both Sections 3.3 and 3.4 bandages were not applied as they would normally be applied in clinical situations. Section 6.2 addressed this by comparing the computed and measured pressures when bandages were applied to a cylinder with a constant radius and found a good agreement between the computed pressures and the measured pressures particularly in the case of SurePress bandage. However, the curvature of the leg is not constant. This was addressed in the work reported in Section 6.3 where pressure calculated from elongation in the bandage were compared to ones measured using arrays of PicoPress probes, arrays of FS01 sensors and arrays of FlexiForce sensors. The computed pressures did not agree with the measured pressure in most cases particularly in the case of Comprilan bandage.

In addition, the work reported in both Sections 6.2 and 6.3 showed that FlexiForce sensors have the potential to be used to map the pressures under MCBs. In the case of both the cylinder and the mannequin leg, arrays of FlexiForce sensors provided pressure maps which were much closer to the theoretical calculation than PicoPress probes. In the case of the mannequin leg, the pressure maps reported by FlexiForce sensors were much closer to the theoretical pressures than the ones reported by FS01. However, both the cylinders and the mannequin legs used were rigid, while the human skin is soft and deformable. Therefore, this section will address this issue by comparing the computed pressures from extension in the bandage and the measured pressures using arrays of PicoPress probes

and arrays of FlexiForce sensors when MCBs are applied to a leg model with soft skin. It will also compare the pressure maps obtained by arrays of PicoPress probes and arrays of FlexiForce sensors.

6.4.1 3D scan and Curvature Measurements for Leg Model

To calculate the pressure applied by MCBs to a leg, the leg radii of curvature needs to be measured. The leg model, which was used to compare the performance of PicoPress and FlexiForce sensors, was scanned using NextEngine 3D scanner (Figure 6.58) from ankle to knee with the same procedure explained in Section 6.3.1.



Figure 6.58: NextEngine's 3D scanner and the soft leg model. The white stickers with red marks were used for scanning purposes

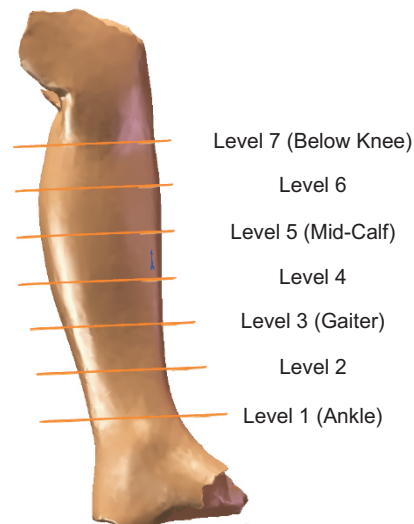


Figure 6.59: The 3D ankle-to-knee solid model of the soft leg showing the planes where the cross sectional digital profiles were obtained

6.4.2 Pressure-Mapping Leg Using PicoPress Sensors

This section will compare the pressures computed from extension for two bandages to the pressures measured using arrays of PicoPress sensors when the two bandages were applied to a leg model with soft skin. The computed pressures were also compared with the PicoPress measured pressures after applying correction factors. These correction factors were based on the pressure perturbation caused by the physical dimensions of the probes and the pressure perturbation due to the change in local bandage extension caused by calibrating PicoPress balloons under MCBs.

Materials and Methods

The rig used and PicoPress balloons arrangement: The rig used was composed of a leg model with a soft skin, with a $0.26m$ ankle circumference, $0.4m$ circumference at the widest part of the calf and $0.4m$ ankle-knee length and a wooden base clamped to a table (Figure 6.60). Twelve PicoPress balloons were attached to the leg as per Figure 6.61. No balloons were attached to anterior side of the leg. The leg used was a model for an average European male left leg.



Figure 6.60: The leg model with PicoPress sensors mounted

Testing the system: All PicoPress balloons were tested after they were attached to the leg with an aneroid sphygmomanometer for the pressure range $0 - 60mmHg$. The aneroid sphygmomanometer was inflated to $60mmHg$ and the pressure then was decreases at $10mmHg$ intervals. The pressure readings reported by each tested balloon was recorded into a spreadsheet. The process was repeated for three times. The nonlinearity, repeatability and accuracy of each of PicoPress balloon was assessed. The purpose was to investigate

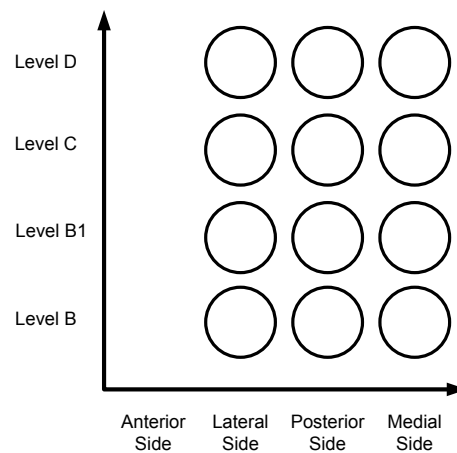


Figure 6.61: The arrangement of the PicoPress sensors on the leg model

the effect of location, the change in the radius of the curvature of the leg and the skin softness on the sensor performance.

Measuring the extension and pressure: Prof. E.A. Nelson applied three pre-marked Comprilan bandages and three pre-marked SurePress bandage to the leg model. She was asked to apply the bandages with a target pressure of 40mmHg at the ankle and 20mmHg at the knee. The pressures at the 12 different points were measured using PicoPress probes after calibrating each sensor under the bandage. The extension at the outer 2^{nd} layer of the bandage was measured using a measurement tape at the same 12 different points where the PicoPress balloons were placed.

Computing the pressure: The procedure used here is the same as reported in Section 6.3.2, but the radii of curvature in this case were obtained from the scanned 3D model of the ankle-to-knee region of the leg model (Section 6.4.1). The computational pressures were obtained using a routine written in MATLAB R2009b.

Correction for the measured pressures: Equations 3.33, 6.1, 6.2 and 6.3 were used to calculate the correction factor for PicoPress probes over the leg model. The radii of curvature were obtained as per Section 6.4.1. The correction factors for each measurement site was calculated using a routine written in MATLAB R2009b.

Statistical analysis: Bland-Altman plots [197] and frequency percentage counts were used to check the levels of agreement between the computed and measured pressures for the two bandages and between the computed and the corrected measured pressures for the two bandages. The computed and measured pressures were considered to be in agreement if the difference between the computed and measured pressures were within $\pm 5\text{mmHg}$. PASW 17 and Excel 2007 were used to carry out the statistical analysis.

Results, Analysis and Discussion

Accuracy testing showed that the median accuracy for the 12 probes was $\pm 6.98\%FS$, where FS is $60mmHg$. In terms of pressures the median accuracy was $\pm 4.2mmHg$, which indicates that the probes accuracy increased compared to the rigid leg, where the median accuracy was found to be $\pm 6.6mmHg$.

Table 6.11 summarizes the measured extensions and pressures and the calculated tensions and pressures. Figures 6.62 and 6.63 illustrate the computed pressures, the PicoPress measured pressures and the PicoPress corrected measured pressures for both Comprilan and SurePress when they were applied to the leg model.

Table 6.11: Summary of Comprilan and SurePress measured extensions, calculated tensions and pressures, measured pressures and corrected pressures. The upper and lower 95% spread = $mean \pm (1.96 \times SD)$, and the upper and lower 95% CI = $mean \pm (t \times SE)$, where “ t ” is critical point at 95% for the data degrees of freedom obtained from the student’s t-distribution look-up table [189]

Comprilan Bandage							
Statistical Analysis	Extension [%]	Tension [N]	Computed pressure [mmHg]	Measured pressure [mmHg]	Corrected measured pressure [mmHg]	Measured pressure / computed pressure	Corrected measured pressure / computed pressure
Mean	50.33	11.91	29.24	34.08	21.57	1.24	0.73
SD	9.54	4.17	12.70	17.58	17.90	0.56	0.40
SE	1.44	0.63	1.91	2.65	2.70	0.08	0.06
Upper 95% spread	69.04	20.09	54.12	68.53	56.66	2.33	1.51
Lower 95% spread	31.63	3.74	4.35	-0.37	-13.52	0.14	-0.04
Upper 95% CI	53.21	13.17	33.07	39.38	26.97	1.40	0.85
Lower 95% CI	47.46	10.66	25.41	28.78	16.17	1.07	0.61

SurePress Bandage							
Statistical Analysis	Extension [%]	Tension [N]	Computed pressure [mmHg]	Measured pressure [mmHg]	Corrected measured pressure [mmHg]	Measured pressure / computed pressure	Corrected measured pressure / computed pressure
Mean	27.39	4.15	10.74	26.56	16.73	2.92	1.63
SD	6.76	1.26	8.35	12.24	13.11	1.03	0.54
SE	1.02	0.19	1.26	1.85	1.98	0.16	0.08
Upper 95% spread	40.63	6.62	27.10	50.55	42.42	4.95	2.68
Lower 95% spread	14.14	1.68	-5.62	2.56	-8.97	0.89	0.59
Upper 95% CI	29.43	4.53	13.25	30.25	20.68	3.23	1.80
Lower 95% CI	25.35	3.77	8.22	22.86	12.77	2.61	1.47

The results illustrate that the perturbation problem is still existed even when a leg with soft exterior was used, with pressure measured being higher than the ones computed. However, comparing to the rigid cylinder and the rigid leg, the picture is totally different. For example, the average of the ratio of the corrected measured pressures to the computed

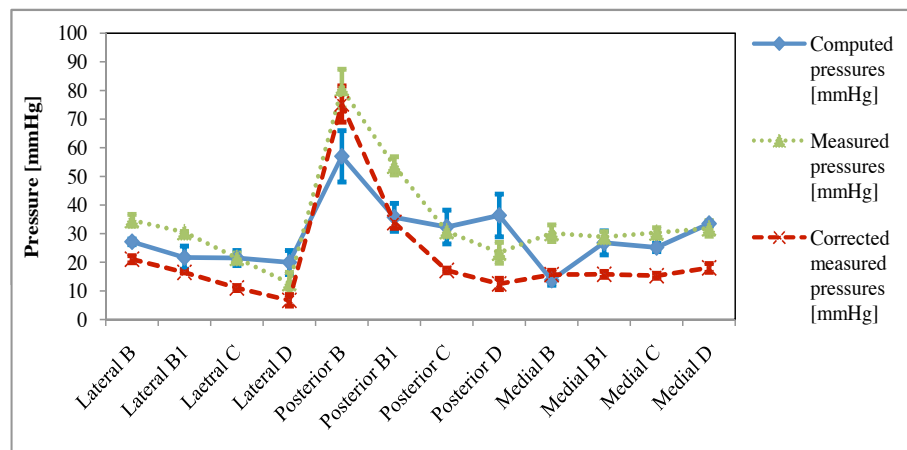


Figure 6.62: Comprilan: computed, measured and corrected measured pressures. The error bars are for the standard error of the mean. The lines connecting the measurement points are for illustrative purposes

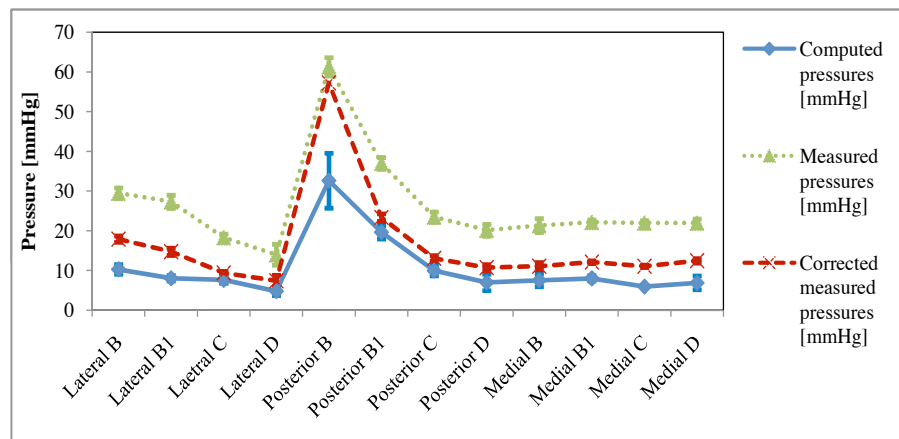


Figure 6.63: SurePress: computed, measured and corrected measured pressures. The error bars are for the standard error of the mean. The lines connecting the measurement points are for illustrative purposes

pressures for Comprilan is for the first time less than one. On the other hand, the SurePress results show much higher pressure perturbation than any other experiment. These results can be explained by the amount of pressure applied to the leg in the two cases. For example, the computed and measured pressures show Comprilan was applied with an average pressure of 29.24mmHg and 34.08mmHg respectively. For SurePress bandage the average computed and measured pressures were 10.74mmHg and 26.56mmHg . This implies that as the leg model exterior was made of a soft material, Comprilan will push the PicoPress balloons into the leg skin, much further than what SurePress bandage will do, as Comprilan bandages were applied with higher pressures. As some of the balloon thickness will be indented in the skin, both sensors physical dimension and inflating the

sensor under the bandage will result in smaller pressure perturbation. This reduction in the pressure perturbation will be higher for Comprilan than SurePress.

Moreover, there was a clear pressure gradient in the computed and measured pressures profiles for both Comprilan and SurePress at the lateral and the posterior sides of the leg. However, the medial side of the leg showed reverse gradient for both bandages for both computed and measured pressures. Furthermore, SurePress bandages were applied with smaller extensions compared to when they were applied to the rigid cylinder and the mannequin leg.

Table 6.12 and Figures 6.64 and 6.65 demonstrate the levels of agreements between pressures computed theoretically and PicoPress measured and corrected measured pressures. SurePress computed pressures show again higher levels of agreement with the corrected measured pressures than Comprilan. The number of cases where the computed and measured pressures for Comprilan were in agreement were higher than the number of cases for the computed and corrected measured pressures. This can be explained again by the fact that applying bandage with higher pressures will force the PicoPress sensors to indent in the deformable soft skin, resulting in a smaller pressure perturbation.

Table 6.12: The percentage of cases where the difference between the computed and the measured and corrected measured pressures being within $\pm 5mmHg$ for Comprilan and SurePress

Statistical Analysis	Percentage of cases where the difference is within $\pm 5mmHg$
Comprilan computed pressures and measured pressures	33%
Comprilan computed pressures and corrected measured pressures	22%
SurePress computed pressures and measured pressures	0%
SurePress computed pressures and corrected measured pressures	61%

6.4.3 Pressure-Mapping Leg Using FlexiForce Sensors

This section will compare the pressures computed from extension for two bandages to the pressures measured using arrays of FlexiForce sensors when MCBs were applied to a leg model with soft skin. It will also investigate the effect of using silicon rubber pads, which were used to direct the force applied into the sensitive area of the sensor, on the pressures measured by FlexiForce sensors and compare the sensors readings to the sensors readings when these pads were not used. The usage of a puck or circular disc to direct the force towards the sensitive area of the Flexible sensors is widely used by researchers to reduce measurement errors and increase accuracy (Section 2.4.2).

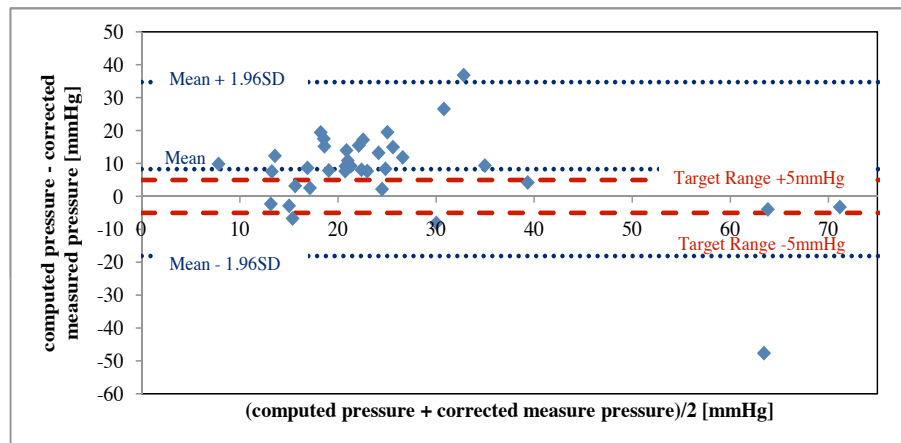


Figure 6.64: Bland-Altman plot for computed pressures and corrected measured pressures for Comprilan

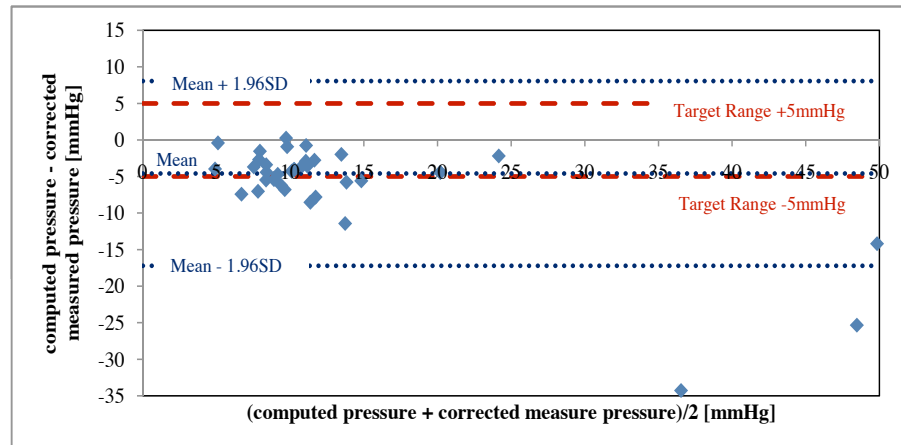


Figure 6.65: Bland-Altman plot for computed pressures and corrected measured pressures for SurePress

Materials and Methods

The rig used and FlexiForce sensors arrangement: The rig used was composed of a leg model with a soft skin, with a $0.26m$ ankle circumference, $0.4m$ circumference at the widest part of the calf and $0.4m$ ankle-knee length (Figure 6.66). Forty-eight sensors were mounted on top of soft leg in the ankle-knee region in 8×6 matrix format.

Conditioning circuit, data acquisition and sensor calibration: The sensors were powered with constant $5V$ through three conditioning circuits. The conditioning circuits used were per reported in Section 6.2.3. The output signals from the three processing circuits were passed to a Mass Term 6225 USB DAQ card through a screw terminal board (LPR-68).

Due to the soft nature of the leg mode, aneroid sphygmomanometer could not be used

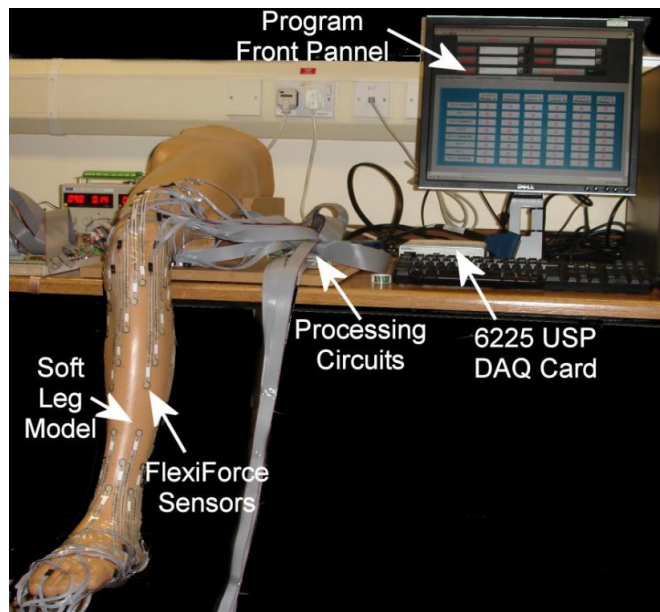


Figure 6.66: Soft leg model with FlexiForce sensors mounted in the form of 8×6 matrix

to calibrate the sensors. Instead, deadweights were used to calibrate the sensors over a flat surface for the pressure range $0 - 136\text{mmHg}$ by stacking 10 different loads on top of each other over the sensitive area of the sensor and then removing these loads one by one. The process was repeated 5 times. A program written in LabView 8.6 was used to obtain the calibration data. A 3^{rd} order polynomial fitting-line was used to fit the averaged data points for the ten readings: five for the loading direction and five for the unloading, for each load. Excel 2003 was used to obtain the fitting-lines and calculate the “R” squared regression values for the sensors. Each sensors accuracy was assessed individually, where accuracy here is the combined error due to calibration fitting-line, repeatability and hysteresis.

The system accuracy was tested by applying 40mmHg to the leg using an aneroid sphygmomanometer after the sensors being attached to the leg. The 40mmHg pressure was applied to each sensor 5 times. Each sensor pressure output was compared to the input pressure 40mmHg and the average deviation for all sensors was used to determine the average accuracy of the sensors used at 40mmHg input pressure. In addition, window averaging was performed over the output of each adjacent 4 sensors. The averaged pressures were then compared to the input pressure of 40mmHg and the average deviation of the 7×6 pressure map matrix (42 clusters or windows) was used to evaluated the the average accuracy of the measurement system at 40mmHg input pressure.

The pressure measurement display program: A program was written in LabView 8.6 to acquire and display the signals, convert them to pressure values, perform window averaging for the pressure values, display the measured and averaged pressure values nu-

merically and store the voltages, the measured pressures and the average pressures for further processing. The signals were sampled at $1kHz$ and a software based 2^{nd} order low-pass filter with $1Hz$ cut-off frequency was used to filter out the signals. The program also had a new feature, when compared to the programs used for the cylinder and mannequin leg, which enable the user to zero the acquired voltages and remove any DC offset. This was introduced in order to reduce the effect of the quad op-amps used in the processing circuits on the pressure measurement. Those quad op-amp were introducing DC offset to the acquired signal and were showing some temperature and humidity dependencies. Figures 6.67 and 6.68 show the front panel of the program and the flow chart of the program respectively.



Figure 6.67: The front panel of the display program for FlexiForce soft leg pressure-mapping system

Computing pressures: This is as reported in Section 6.4.2.

Measuring the extension and pressure: Prof. E.A. Nelson applied three pre-marked Comprilan bandages and three pre-marked SurePress bandages to the soft leg. She was asked to apply the bandages with a target pressure of $40mmHg$ at the ankle and $20mmHg$ at the knee. After applying the third MCB from each bandage type, the amount of extension for the outer bandage layer was recorded using a measurement tape at 28 points (7×4 matrix), which corresponds to the spaces between sensor rows and the four sides of

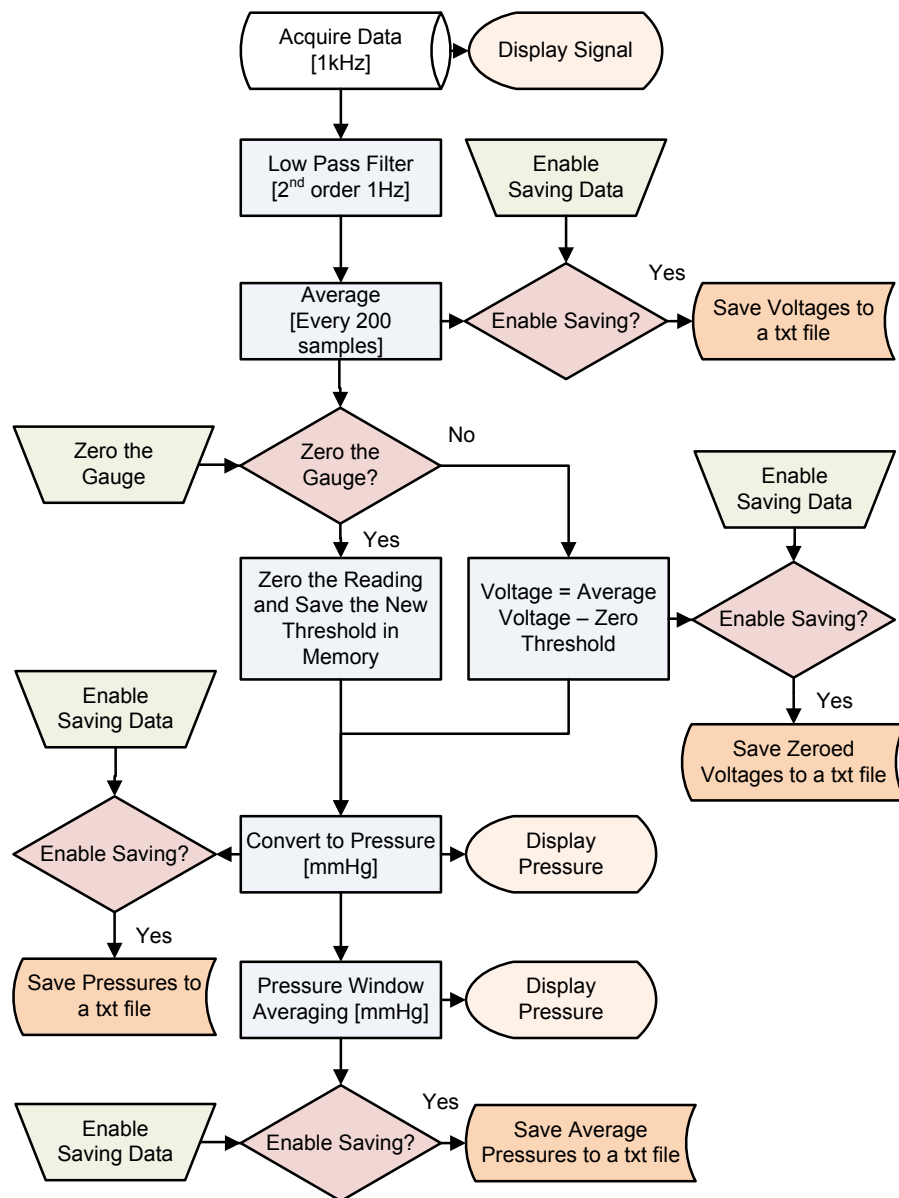


Figure 6.68: The flow chart of the display program for FlexiForce soft leg pressure-mapping system

the leg. The radii of curvature were obtained as per Section 6.4.1. MATLAB R2009b was used to compute the theoretical pressures from the measured extension values. MATLAB R2009b and Excel 2007 were used to compare the theoretical and measured pressure values.

Padding effect: After applying bandages as mentioned above, each sensor sensitive area was covered with an adhesive silicon rubber padding disc with 1.5mm thickness and 10mm diameter (Figure 6.69). Prof. E.A. Nelson applied then the third SurePress bandage to the leg with a target pressure of 40mmHg at the ankle and 20mmHg at the knee. The amount of extension was recorded using a measurement tape at 28 points (7×4 matrix).

After that, the bandage was removed and the silicon rubber discs were removed from half of the sensors and were placed on top of the existing discs on the other 24 sensors. Then, the same SurePress bandage was applied again to the leg and both pressures and extensions were measured. MATLAB R2009b was used to compute the pressures from the measured extension values. MATLAB R2009b and Excel 2007 were used to compare the computed and measured pressures.



Figure 6.69: Silicon rubber adhesive padding disc attached to the sensitive area of the FlexiForce sensor.

Statistical analysis: Bland-Altman plots [197] and frequency percentage counts were used to check the levels of agreement between the computed and measured pressures for the two bandages. The computed and measured pressures were considered to be in agreement if the difference between the computed and measured pressures were within $\pm 5mmHg$. PASW 17 and Excel 2007 were used to carry out the statistical analysis.

Results, Analysis and Discussion

From the calibration process, the median accuracy of the sensors used was found to be $\pm 17.75\%FS$, where FS here is $136mmHg$ and the accuracy is the combined error of the calibration fitting-line, the repeatability and the hysteresis errors of the sensor. This means that the median accuracy in terms of pressure was $\pm 24.14mmHg$. Window averaging will reduce, in theory, the accuracy error to $\pm 12.07mmHg$. In order to compare the computed and the averaged measured pressures, the averaged pressures were re-sampled from 7×6 matrix to 7×4 matrix (to have the same pressure matrix sizes for both computed and averaged measured pressures). This means that the accuracy error for the averaged measured pressures used in the comparison should be, in theory, $\pm 8.53mmHg$.

When tested with an aneroid sphygmomanometer, the average accuracy for the individ-

ual sensor at 40mmHg input pressure was found to be $\pm 16.15\text{mmHg}$ ($SE = 1.66\text{mmHg}$). For the window averaging clusters, this was found to be $\pm 7.25\text{mmHg}$ ($SE = 0.96\text{mmHg}$). These values are lower than the ones calculated from the calibration process.

Figure 6.70 shows the computed pressure map, measured pressure map and the average pressure map obtained for Comprilan and SurePress (the maps are for the third of the three bandage applications for both bandages). The computed maps show that both bandages were not applied with pressure gradient. However, the pressure profile for Comprilan shows that the bandage was applied with high pressures, while the computed pressure map for SurePress shows that it was applied with low pressures. Both the measured pressure and the averaged pressure maps show rather a different pressure map to the ones theoretically computed for SurePress. As both of them reports that the bandage was applied with much higher pressure than the ones estimated from extension.

The averaged pressure map for both SurePress and Comprilan reported high pressures at Anterior level C. By inspecting this area on the leg, it was identified that it corresponds to a palpable area of the shin bone, which is normally covered with cotton wool padding in clinical practice.

It is also clear from the maps that using the measured pressures directly might result in reporting pressure peaks due to the deficiencies associated with the FlexiForce sensors. However, these peaks were smoothed out when averaging techniques were used.

To compare between the computed pressures and the averaged measured pressures, the averaged measured pressures map was re-sampled from 7×6 matrix to a 7×4 matrix with elements of the new map being the ones corresponding to the same sites where the extensions were measured. Table 6.13 summarize the measured extensions and the calculated tensions, pressures and measured over computed pressure ratios for the third sample of each of the two bandages and the and the measured pressures after applying window averaging for all three bandage samples of each bandage type. Figures 6.71 and 6.72 show the computed pressures and the averaged pressures for the third sample of both Comprilan and SurePress.

The ratios of the measured pressure over the computed pressures again show similar results to the ones reported for PicoPress arrays, when tested over the leg model, where the average pressure ratio for Comprilan being smaller than SurePress. As FlexiForce sensors are very thin, the lower pressure ratio for Comprilan compared to SurePress cannot be explained by the impact of the sensors thickness as in the PicoPress case. However, the higher pressure ratio for SurePress in this case compared to SurePress pressure ratios for the mannequin leg and the cylinder was expected, as it was reported previously that using deadweights for calibration will result in reporting higher pressures than if aneroid sphygmomanometer was used to calibrate the sensors (Section 6.2.5). Nevertheless, no explanation can be provided for why Comprilan reported lower pressure ratio than SurePress, except that the inter-variation in the tension-elongation relationship for Comprilan. It is also possible that the SurePress bandages used in this case have different tension-elongation curves to the ones used to obtain the tension-elongation fitting-line.

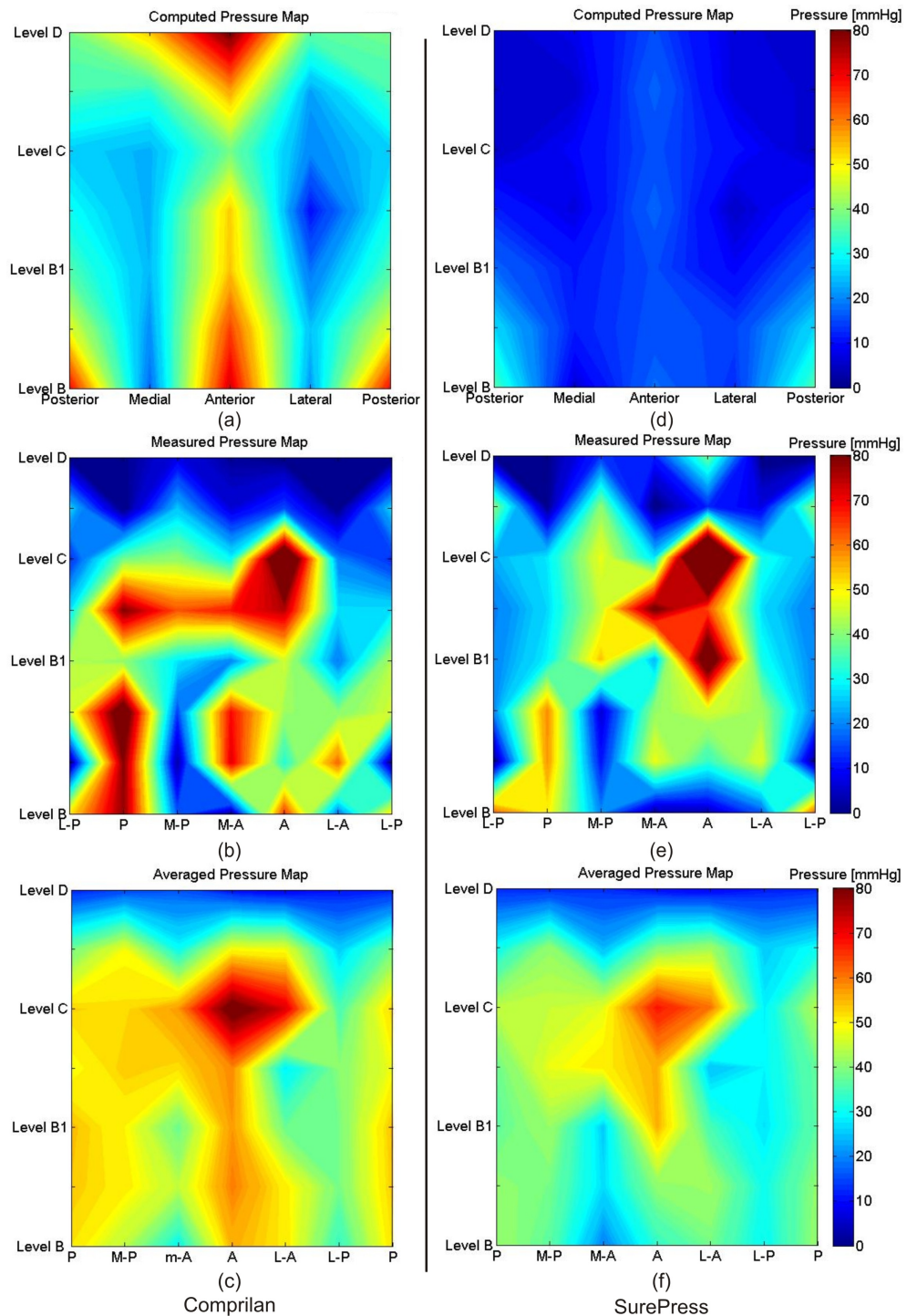


Figure 6.70: Comprilan and SurePress pressure maps: (a) Comprilan computed pressure map, (b) Comprilan measured pressure map, (c) Comprilan averaged pressure map, (d) SurePress computed pressure map, (e) SurePress measured pressure map and (f) SurePress averaged pressure map. The maps are shown with the first column “Posterior” being repeated at the start and end for better clarity. ‘L’ = Lateral, ‘A’ = Anterior, ‘M’ = Medial and ‘P’ = Posterior

Table 6.13: Summary of Comprilan and SurePress measured extensions, calculated tensions and pressures and measured pressures. The upper and lower 95% *spread* = $mean \pm (1.96 \times SD)$, and the upper and lower 95% *CI* = $mean \pm (t \times SE)$, where “*t*” is critical point at 95% for the data degrees of freedom obtained from the student’s *t*-distribution look-up table [189]

Comprilan Bandage					
Statistical Analysis	Extension [%]	Tension [N]	Computed pressure [mmHg]	Averaged measured pressure	Averaged pressure / computed pressure
Median	46.00	11.06	33.88	44.31	1.27
Mean	50.79	13.45	37.76	42.96	1.25
SD	11.16	5.04	18.91	18.45	0.74
SE	2.11	0.95	3.57	1.64	0.14
Upper 95% spread	72.66	23.33	74.83	79.12	2.70
Lower 95% spread	28.91	3.57	0.68	6.79	-0.20
Upper 95% CI	55.11	15.40	44.76	46.18	1.54
Lower 95% CI	46.46	11.50	30.75	39.73	0.97

SurePress Bandage					
Statistical Analysis	Extension [%]	Tension [N]	Computed pressure [mmHg]	Averaged measured pressure	Averaged pressure / computed pressure
Median	30.00	4.55	11.95	34.15	2.61
Mean	29.50	4.54	12.84	34.83	3.23
SD	5.51	1.17	6.82	14.96	1.88
SE	1.04	0.22	1.29	1.33	0.35
Upper 95% spread	40.31	6.83	26.21	64.14	6.91
Lower 95% spread	18.69	2.25	-0.53	5.51	-0.44
Upper 95% CI	31.64	4.99	15.37	37.44	3.96
Lower 95% CI	27.36	4.08	10.31	32.21	2.50

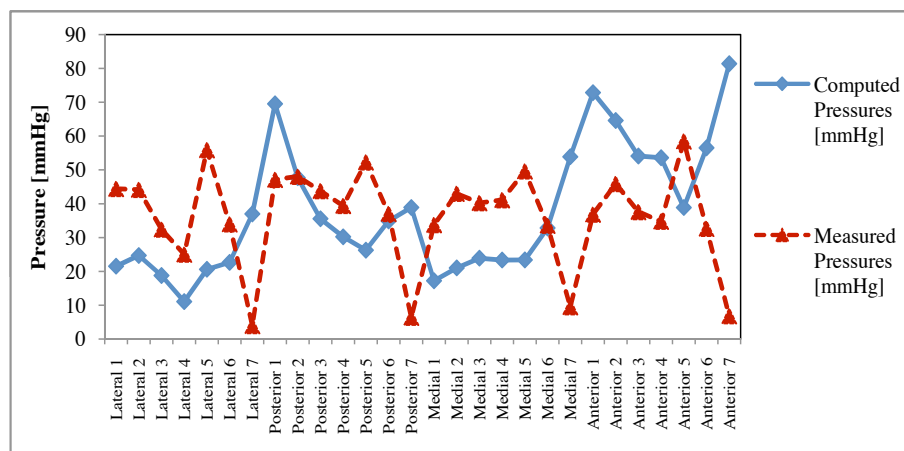


Figure 6.71: Comprilan: computed and measured pressures. The lines connecting the measurement points are for illustrative purposes

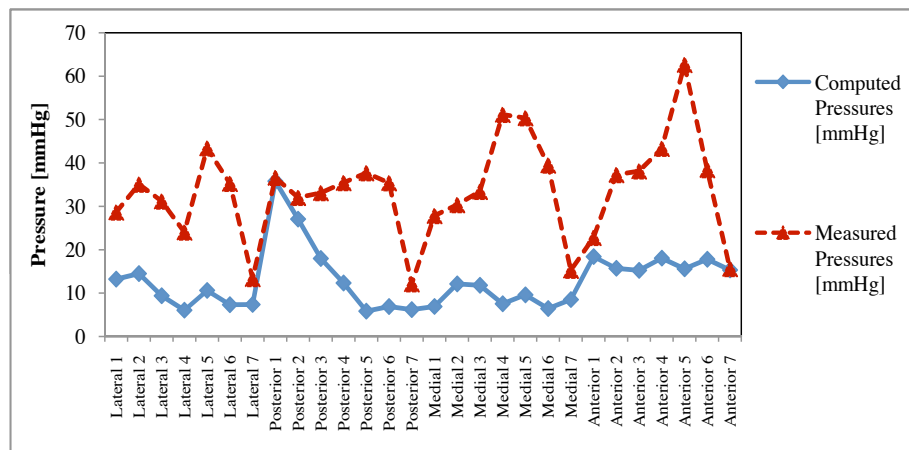


Figure 6.72: SurePress: computed and measured pressures. The lines connecting the measurement points are for illustrative purposes

This might be counter argued by the fact that the bandages used were from the same bunch of bandages which were used before and all of them were purchased together.

Figures 6.73 and 6.74 demonstrate the levels of agreement between the pressures computed and the averaged measured pressures. In the case of Comprilan the computed and averaged measured pressures agreed in 11% of the cases and in the case of SurePress they were found to be in agreement in 14% of the cases. This fit with results reported in Sections 6.2 and 6.3 which shows that using extension as a feedback method to control the pressures applied by MCBs might not be a reliable and adequate method.

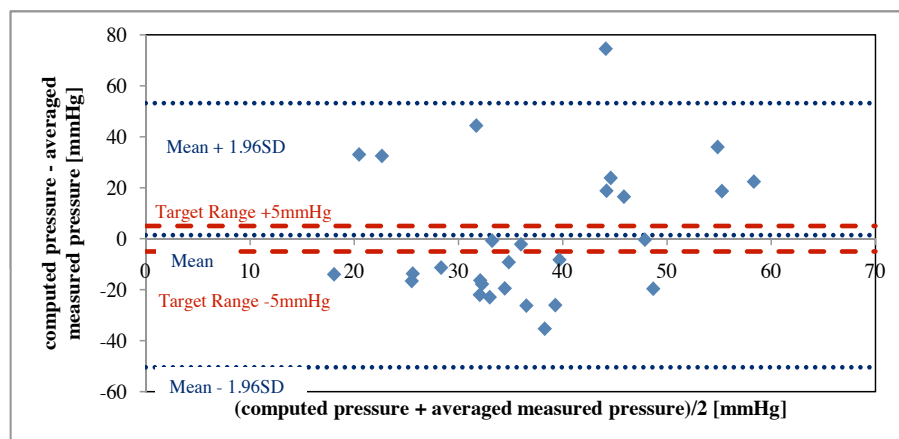


Figure 6.73: Bland-Altman plot for computed pressures and measured pressures for Comprilan

Figure 6.75 demonstrates the impact of padding on the pressure measurement. Clearly, adding silicon soft disks resulted in reporting much higher pressures than anticipated theoretically. This can be easily explained by the impact of sensor thickness on the interface pressure which has been discussed in Section 3.8. The median increase in the pressure

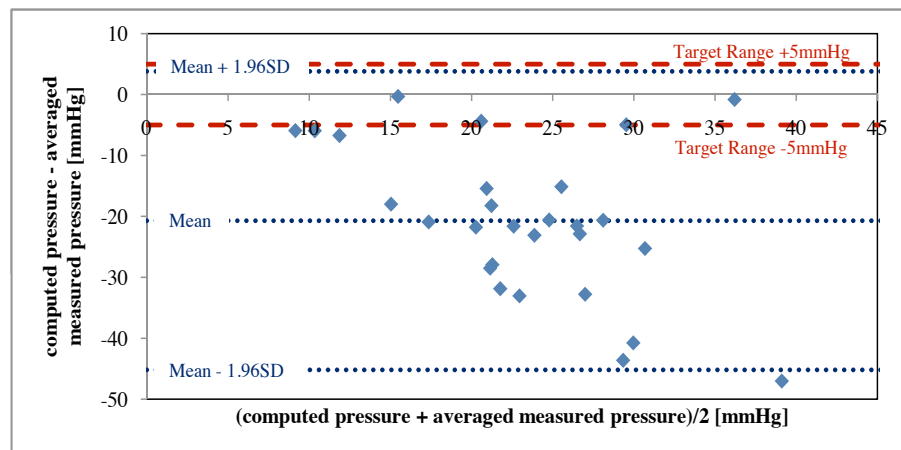


Figure 6.74: Bland-Altman plot for computed pressures and measured pressures for SurePress

reported by individual sensors when one layer of silicon rubber discs were introduced was 274%. This increased to 309% for two layers of silicon pads.

6.4.4 Comparison Between the Different Pressure-Mapping Legs

Comprilan bandages were applied to the soft leg when it was covered with arrays of PicoPress balloons and arrays of FlexiForce sensors with an average extension of 50.33% and 50.79% respectively. In the case of the SurePress, the average extensions applied to the soft leg when it was covered with arrays of PicoPress balloons and arrays of FlexiForce sensors were 27.39% and 29.5% respectively. As in the case of the mannequin leg, the variation in both the extension and pressures applied made it very difficult to compare the two sensing technologies. In order to carry out this comparison, the average 4×3 computed pressure map for PicoPress and the average 7×4 computed pressure map for FlexiForce for both Comprilan and SurePress were obtained. In addition, the average 4×3 measured pressure map for PicoPress and PicoPress with correction factor, and the average 7×4 averaged measured map for FlexiForce for both Comprilan and SurePress were also obtained. The ratios of the measured pressures to the computed pressure in percentage were then plotted using counter filled plot for each measurement system for each bandage. These plots were then used to compare the two sensing technologies. The principles behind this comparison method is explained in Section 6.3.5).

Figures 6.76 and 6.77 illustrate the ratio of the measured to the computed pressure maps for PicoPress, PicoPress with correction factor and FlexiForce sensors for both Comprilan and SurePress bandages.

Comparing the Comprilan pressure ratio maps shows that both PicoPress and FlexiForce sensors tend to report higher pressures than computed pressures. On the other hand, using correction factor for PicoPress resulted in rather pressure ratios that were smaller than one except at the posterior level B, which can be explained by the fact that

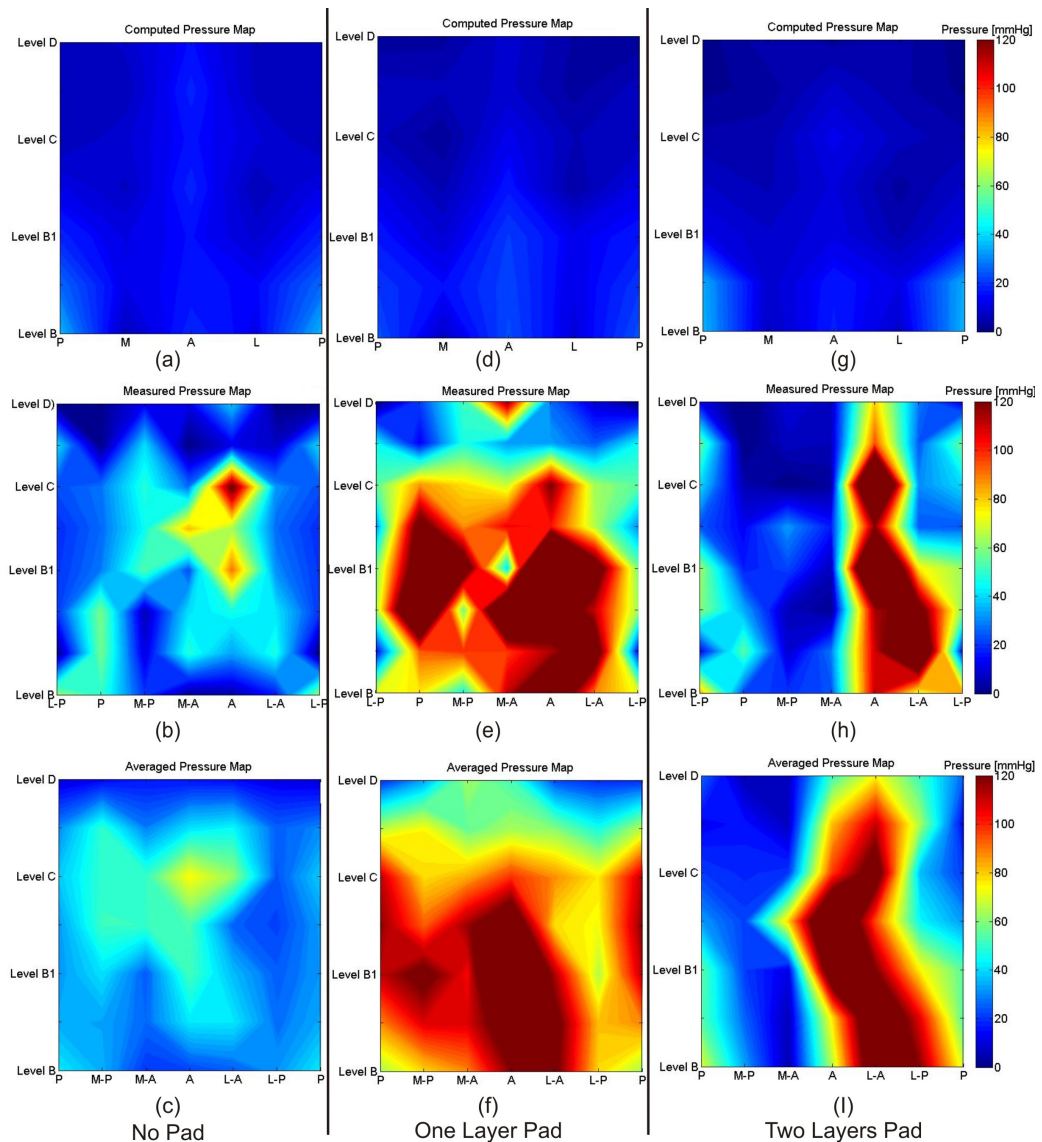


Figure 6.75: SurePress pressure maps: (a) SurePress computed pressure map with sensors not covered with any pads, (b) SurePress measured pressure map with sensors not covered with any pads, (c) SurePress averaged pressure map with sensors not covered with any pads, (d) SurePress computed pressure map with sensors covered with one layer of pad, (e) SurePress measured pressure map with sensors covered with one layer of pad, (f) SurePress averaged pressure map with sensors covered with one layer of pad, (g) SurePress computed pressure map with half of the sensors covered with two layers of pad, (h) SurePress measured pressure map with half the sensors covered with two layers of pad and (i) SurePress averaged pressure map with half the sensors covered with two layers of pad. The maps are shown with the first column “Posterior” being repeated at the start and end for better clarity. ‘L’ = Lateral, ‘A’ = Anterior, ‘M’ = Medial and ‘P’ = Posterior

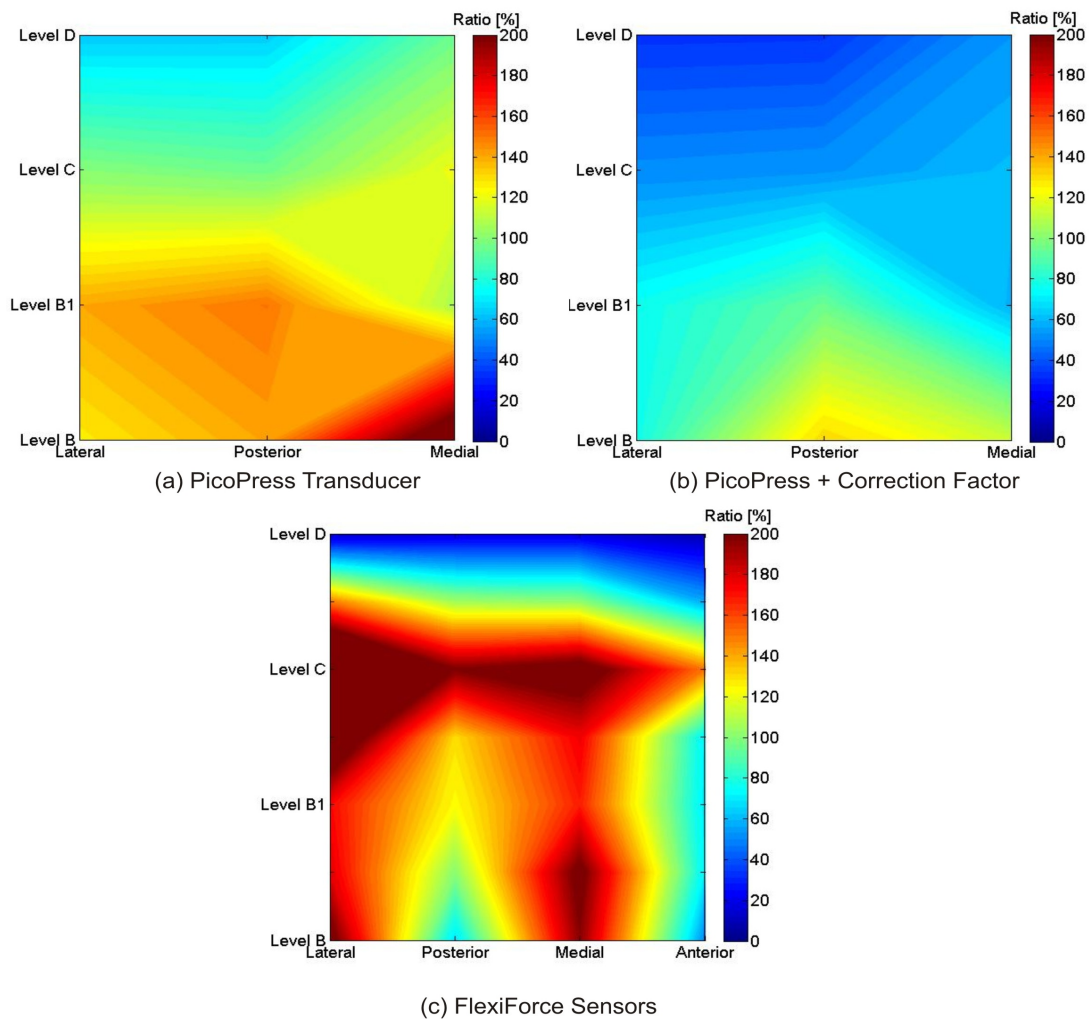


Figure 6.76: Comprilan measured over computed pressure ratio maps: (a) PicoPress, (b) PicoPress plus correction factor and (c) FlexiForce sensors

Vinckx et al. [86] model is not suitable for small radii of curvatures (Section 6.3.5).

Comparing the SurePress pressure ratio maps illustrates that in all cases the measured pressures were much higher than the computed pressures. This was not the case for the mannequin leg and the cylinder. PicoPress and PicoPress plus correction factor in the case of SurePress reported higher pressure ratio than Comprilan. This can be explained by the fact that the MCBs were applied with low pressures, resulting in much higher perturbation problem (less of the sensor thickness was indented into the soft skin). However, this does not explain why FlexiForce arrays showed similar higher pressure ratios for SurePress compared with Comprilan.

FlexiForce pressure ratios for both Comprilan and SurePress are higher than ones reported for the mannequin leg and the cylinder. The only variable which was changed this time was the usage of deadweights to calibrate the sensors on a flat surface rather than calibrating the sensor using aneroid sphygmomanometer over the curved surface of

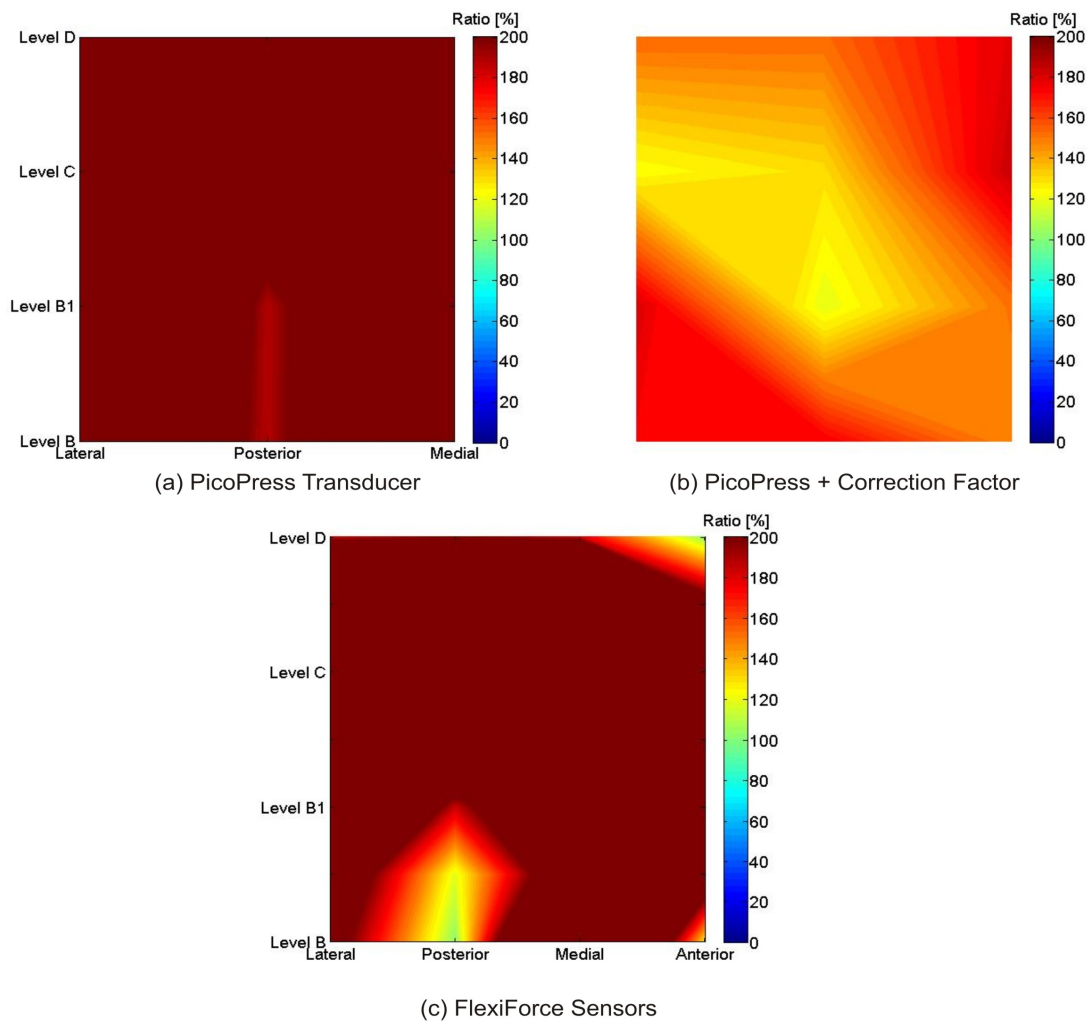


Figure 6.77: SurePress measured over computed pressure ratio maps: (a) PicoPress, (b) PicoPress plus correction factor and (c) FlexiForce sensors

the leg or the cylinder. It has already been demonstrated in Section 6.2.5 that using deadweights calibration fitting-lines will result in reporting higher pressure values compared to the ones reported by aneroid sphygmomanometer calibration fitting-lines. Indeed, testing the system with aneroid sphygmomanometer with 40mmHg did show some deviation ($\pm 7.25\text{mmHg}$). However, the average of this deviation if the sign is considered was 0.26mmHg i.e. no evidence for the sensors to report higher pressures when tested with aneroid sphygmomanometer at low pressures.

6.5 Summary

This chapter reported the development of a number of pressure-mapping reference systems which can be used to study MCBs and be used as a bench mark to evaluate new pressure measurement systems. The chapter demonstrated that elongation cannot be used as an

adequate and reliable feedback method to control the interface pressure applied by MCBs. The differences between the measured and computed pressures was found to be much more significant in the case of Comprilan bandage which is an example of bandages with no elasticity (tension-elongation curves show large hysteresis).

The chapter also showed that FlexiForce sensor arrays, when calibrated on a curved surface using aneroid sphygmomanometer and window averaging, have outperformed PicoPress transducer, which is a typical example of medical pressure transducers used to measure the pressure applied by MCBs to the patient leg. Even after window averaging of FlexiForce sensor arrays, the accuracy error is still higher than the target maximum error of $\pm 5mmHg$, which means they can only be used for qualitative purposes and not for accurate measurements. However, when these flexible sensors are used over a soft surface and calibrated on a flat surface using deadweights, they have reported pressures which were close to the ones reported by PicoPress sensors before applying correction factor. This is thought to be caused by the curved nature of the leg. These results suggest that it might be necessary to calibrate these sensors over a curved surface to reduce the error caused by bending.

Using pucks to target the forces towards the sensitive area of the sensor found to cause significant pressure overestimation. The results illustrate the impact of sensor aspect ratio on the measured pressure. This was echoed when correction factor was applied to the pressure measured by PicoPress sensors and found to result in pressures which are in good agreement with the computed pressure.

The outcomes of the research reported in this chapter can be summarized in the following points:

- The first study to compare the pressure computed from MCB elongation measurement to the pressure measured using pressure transducers.
- Elongation was found not to provide adequate and reliable feedback to control the pressure applied by MCBs. This was confirmed with the usage of FS01 sensors on both the PVC cylinder and mannequin leg.
- The first study to compare the pressures measured using a number of pressure measurement systems on a number of different surfaces.
- The design and development of multiple pressure measurement systems which can be used to study MCBs both in vivo and in vitro.
- PicoPress transducer was found to overestimate the pressure applied by MCBs. However, using a correction factor which is based on the aspect ratio of the sensor and the radius of the curvature was found to reduce the problem for curvatures with large radii.
- The usage of window averaging with FlexiForce sensors did resolve some of the accuracy and reliability problems associated with them. Testing these sensors over

rigid surfaces showed that they can provide more reliable and accurate pressure maps than PicoPress transducer for example.

- The usage of puck to direct the force towards the sensitive area of the Flexible sensor when these sensors are used over curved surfaces will result in overestimating the pressure.

Chapter 7

Pressure-Mapping Measurement System

This chapter presents the development of a pressure-mapping measurement system with custom arrays of flexible sensors that can be used to map pressures applied by compression bandages to the leg. It compares pressure maps obtained by this system to the pressures obtained by PicoPress sensors and pressures computed from extension when MCBs are applied to a real leg.

7.1 Introduction

The results and the data obtained from the pressure-mapping cylinders (Section 6.2), the pressure-mapping mannequin legs (Section 6.3) and the pressure-mapping soft leg model (Section 6.4) have been used to design a pressure measurement system that can be used over a human leg to map the pressure applied by MCBs. The chapter spells out the development of pressure-mapping systems based on custom arrays of flexible sensors that can be used in-vivo to map the pressure under MCBs, when applied to a limb. The chapter illustrates the use of such a system to map the pressure applied by MCBs to a human participant and compares the pressure maps to both computed pressures from extension and pressures measured using arrays of PicoPress sensors. The experiment also addresses the problem of calibration and how this can be partially fixed by calibrating sensors over rigid cylinders.

7.2 Design and Development

7.2.1 Hardware

The system developed is capable of providing pressure readings for up to 40 measurement points with modest accuracy. However, using window averaging can reduce the accuracy error to half of its value before applying averaging. The system consists of 40 FlexiForce

sensors with each 4 sensors bundled together using PVC tapes and cellular tape to ease attaching these sensors to the patient's or participant's leg. The sensors are connected to a processing unit that powers the sensors with a constant 5V. The processing unit amplifies the sensor output signals, filters it using a hardware low-pass filter and then passes it to Mass Term 6225 USB DAQ card through a screw terminal board (LPR-68) (Figure 7.1).

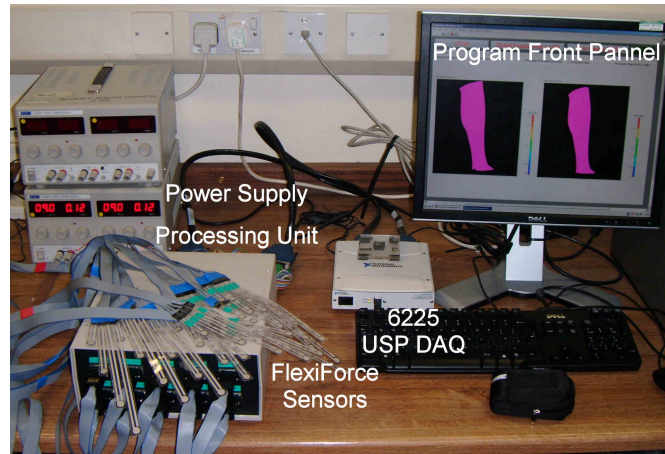


Figure 7.1: The pressure measurement system developed which can be used to map pressures under MCBs applied to human legs

The conditioning circuits in the processing unit are modified versions of the circuit described in Section 6.2.3 (Figure 7.2). Each conditioning circuit can power 8 FlexiForce sensors. As the previous design, the circuit has got two voltage followers to maintain the 5V supply to the sensors. Nevertheless, each voltage follower now powers only 4 sensors. Furthermore, the quad op-amps used in the previous version of the circuit was found to introduce DC offsets, have temperature and humidity dependencies, low noise rejection and current leakage resulting in cross talking between their channels; thus, these op-amps were replaced with OP07 op-amps. Moreover, the output signal from the previous version of the circuit could only be connected to the DAQ card using single ended inputs with common ground, which resulted in cross-talk between channels. In this new version of the circuit, the output of the circuit can be connected to the DAQ card using either differential or single ended inputs. The usage of differential inputs would result in reducing the noise and channels cross talk.

7.2.2 Sensors Calibration

As it was reported in Sections 6.2.5 and 6.4.4 calibrating FlexiForce sensors over a flat surface using deadweights will result in sensors reporting higher pressures than the ones expected from mathematical models. However, it is not possible to calibrate the sensors directly on the participants leg as the calibration process takes very long time. In addition, skin softness might affect the process. Fergenbaum et al. [154] showed that calibrating F-scan on a cylinder and then using it over a curved surface will result in improving

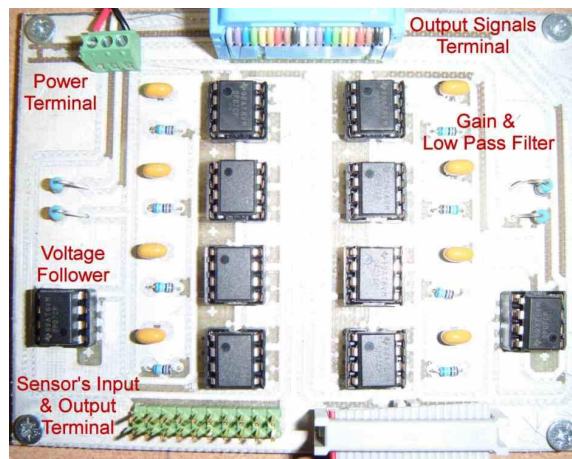


Figure 7.2: The conditioning circuit used to power up 8 sensors and process their output signals

the sensors accuracy. Therefore, the sensors utilized in this measurement system were calibrated using deadweights on a flat surface and an aneroid sphygmomanometer on a $0.114m$ diameter PVC cylinder. The experiments which were conducted to validate the system were used to conclude which of the calibration processes should be used in future trails.

Each sensor was calibrated first using deadweights from $0-125mmHg$. The calibration process involved stacking 15 loads on top of each other on the sensor sensitive area and then removing the loads. The process was repeated five times. The sensors were then calibrated again using an aneroid sphygmomanometer for the pressure range $0-120mmHg$. The aneroid sphygmomanometer cuff was inflated by $10mmHg$ increments from $0mmHg$ to $120mmHg$ and then deflated by $10mmHg$ decrements to $0mmHg$. The process was also repeated for five times for each sensor. The stacking and un-stacking process was used to address the hysteresis problem associated with these sensors and it follows other researchers' recommendations [169]. Repetition of the calibration process was conducted in order to reduce the effect of the repeatability error on the calibration process. A program written in LabView 8.6 environment was used to acquire the sensors signals in the calibration process and a program written in LabView 8.6 was used to obtain the best 5^{th} order polynomial fitting line for deadweights calibration, and the best linear fitting line for the aneroid calibration.

7.2.3 Interface and Pressure Measurement Program

The program was written in LabView 8.6 to acquire and display the signals, remove DC offset from the signals, convert voltages to pressure values using both deadweights and aneroid sphygmomanometer calibration fitting-lines, perform window averaging for the pressure values, display the measured and average pressure values numerically, map the measured pressures on a 3D representation for the leg and store the voltages, the voltages

after removing the DC offset, the measured pressures and the average pressure values in separate files for further processing. The signals were sampled at $1kHz$ and a software based 2^{nd} order low-pass filter with $10Hz$ cut-off frequency was used to filter out the acquired signals. Figures 7.3 and 7.4 show the front panel of the program and the flow chart of the program respectively.

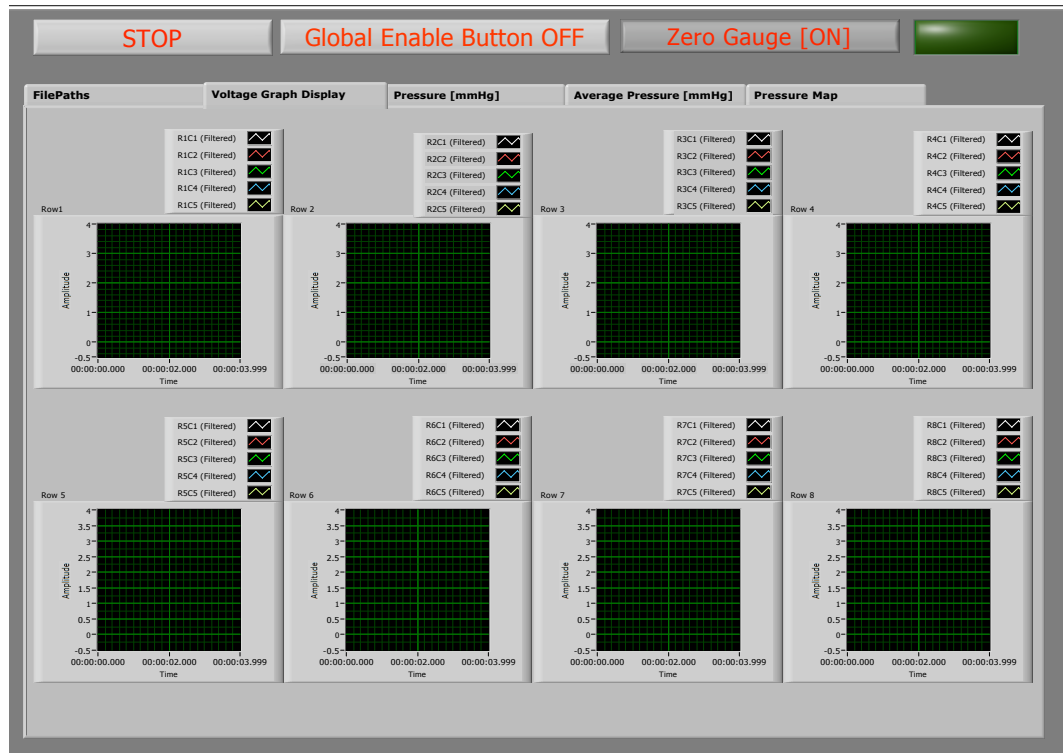


Figure 7.3: The front panel of the display program for the pressure-mapping system

7.3 3D scan and Curvature Measurements for Human Participant Leg

In order to calculate the pressures applied by MCBs to the human participant's leg, the change in the radius of curvature of the participant's leg needs to be measured. The left leg of a healthy participant was scanned using NextEngine 3D scanner (Figures 7.5 and 7.6) from ankle to knee with the same procedure explained in Section 6.3.1.

7.4 Validation Using Computational Pressure From Extension

As there is no gold standard which can be used to validate the new pressure-mapping system with, the system described above was tested by comparing the pressures reported

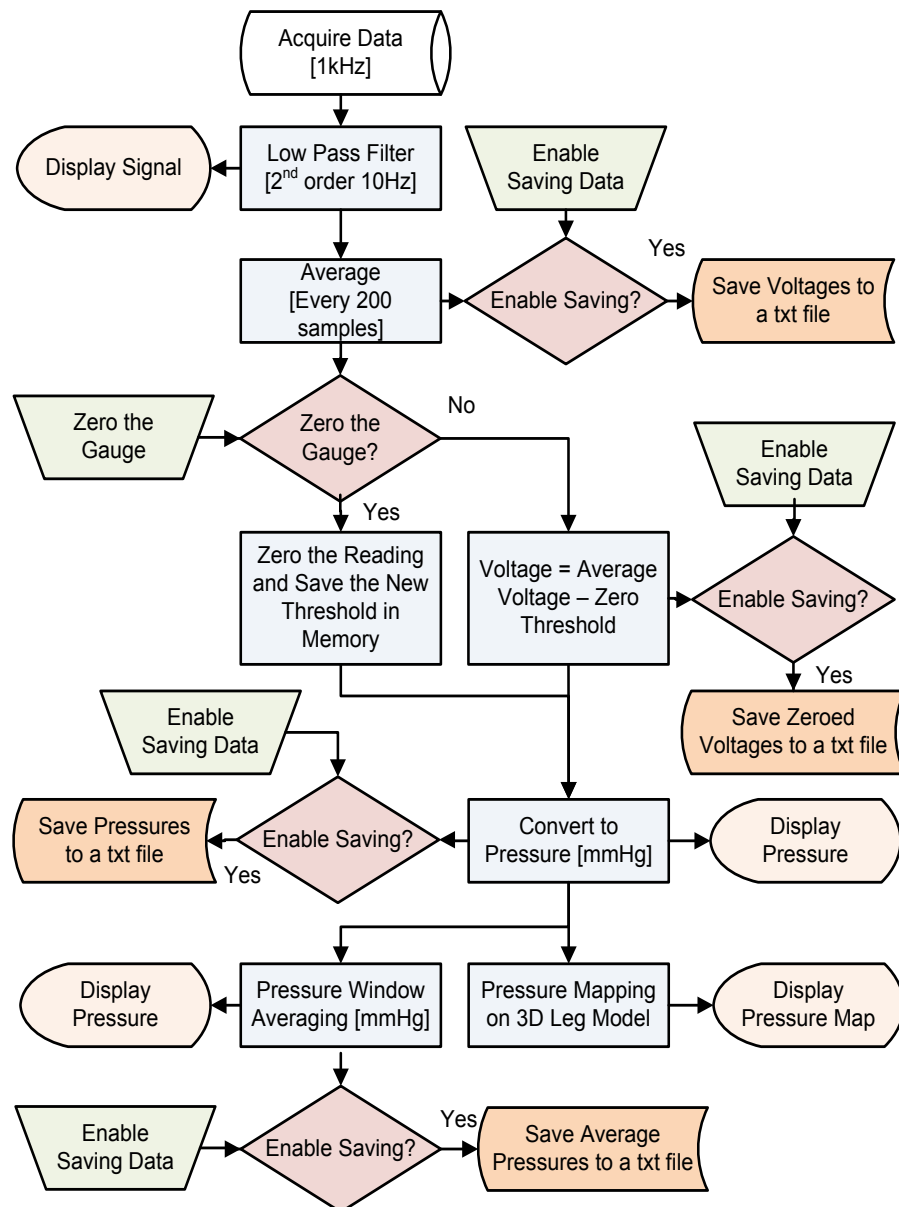


Figure 7.4: The flow chart of the display program for the pressure-mapping system

by the system with the pressures estimated from elongation when MCBs are applied to a healthy leg. This section will report experiments carried out with the measurement system to test which of the two sensor calibration methods agrees more with the computational pressure and to quantify the levels of agreement between the computed and measured pressures, when MCBs are applied to the leg of a healthy subject. The study was approved by the MEEC Faculty Research Ethics Committee at the University of Leeds (Appendix A).

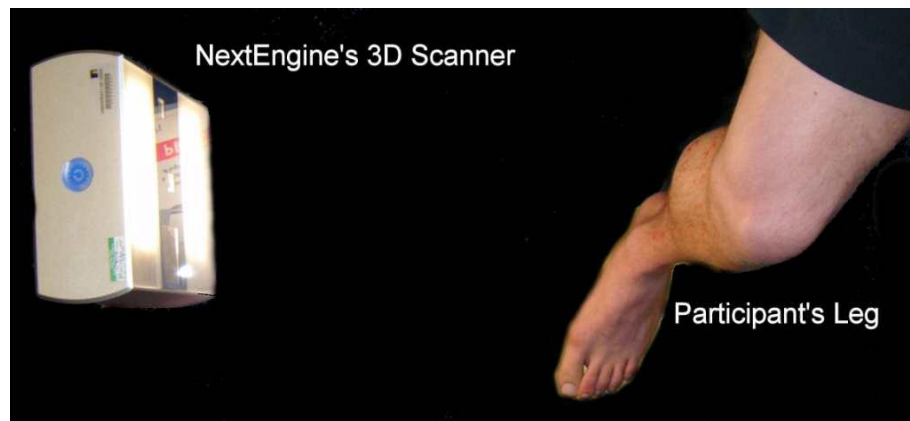


Figure 7.5: NextEngine's 3D scanner and the left leg of the participant in the study. The red marks on the participant skin were used for scanning purposes

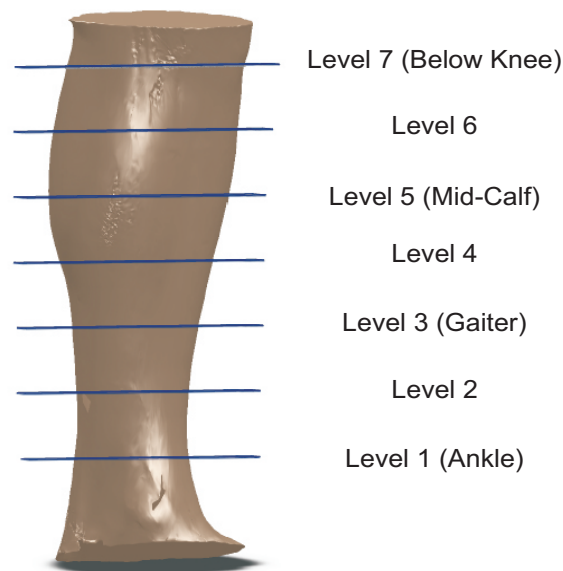


Figure 7.6: The 3D ankle-to-knee solid model of the left leg of the participant showing the planes where the cross sectional digital profiles were obtained

7.4.1 Methods and Materials

Bandages: SurePress bandages were used only in this experiment as it was clear from all the other experiments conducted and reported in Sections 4.4, 6.2, 6.3 and 6.4 that SurePress bandages are more consistent in their performance and show higher levels of agreement with measured pressures, particularly on hard surfaces.

Human subjects: Only one healthy person was involved in this experimental study. A signed consent was obtained from him to participate in the study.

3D scan: The participant's left leg was scanned from ankle to knee using a 3D scanner. The radius of curvature at the required cross sections was obtained using the scanned 3D model of the leg and SolidWorks 2009 as per Section 7.3.

Extension measurement and pressure computation: Prof. E.A. Nelson applied three pre-marked SurePress bandages to the participant's leg after the sensors were attached to the leg (Figure 7.7). She was asked to apply the bandages using spiral 50% overlap with target pressure of 40mmHg at the ankle and 20mmHg at the knee. After applying each bandage, the amount of extension was recorded using a measurement tape at 28 points (7×4 matrix), which corresponds to the spaces between sensor rows and the four sides of the leg. The extension was recorded at both the inner and outer layers of the bandage. MATLAB R2009b was used to compute the theoretical pressures from the measured extension values using the method detailed in Section 6.3.2.

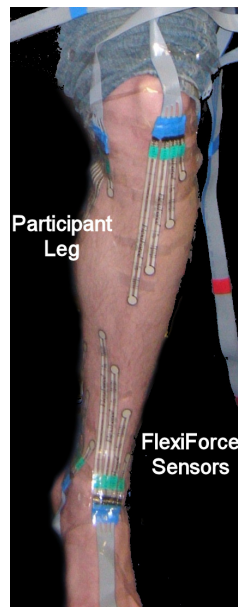


Figure 7.7: FlexiForce sensors attached to the participant's leg

Pressure measurement: The pressure measurement system described in Section 7.2 was used to measure the pressure. Despite the system being able to measure and report pressure readings for up to 40 measurement points, only 32 sensors were used in this experiment. The participant's leg was small in size and only 32 sensors could be fit to his leg without overlapping in the short time available before conducting the experiment (approximately 30 minutes to attach the sensors). The sensors were organized in 8×4 matrix format. The program reported in Section 7.2 was modified to acquire and map the signal from the 32 sensors, which were distributed in 8×4 matrix format. The modified program was applying window averaging to the acquired pressure matrix. The output of the window averaging was a pressure map with 7×4 matrix format. MATLAB R2009b

was used to post-process the acquired data and compare the computed and measured pressures.

Statistical analysis: Bland-Altman plots and percentage frequency counts were used to check the levels of agreement between the computed and measured pressures for the output of the window averaging for the two calibration methods. The computed and measured pressures were considered to be in agreement if the difference between the computed and measured pressures were within $\pm 5mmHg$. PASW 17, MATLAB R2009b and Excel 2007 were used to carry out the statistical analysis and the comparisons.

7.4.2 Results, Analysis and Discussion

From the calibration process, the median accuracy for the sensors used was found to be $\pm 14\%FS$ and $\pm 17\%FS$ for the deadweights calibration and aneroid sphygmomanometer calibration respectively. FS here is $125mmHg$ and $120mmHg$ for deadweights calibration and aneroid sphygmomanometer calibration respectively. The accuracy in both cases is the combined error of the calibration fitting line, the repeatability and the hysteresis of the sensors. However, with deadweights the impact of placing the load exactly on the sensitive area of the sensor without causing a shear stress might have had an impact on the accuracy of deadweights calibration while using different sides of the aneroid sphygmomanometer cuff might have had an impact on the accuracy reported for the aneroid sphygmomanometer calibration. Accuracy in terms of pressures means that the median accuracy for each sensor is $\pm 17.5mmHg$ and $\pm 20.4mmHg$ for deadweights calibration and aneroid sphygmomanometer calibration respectively. The decrease in accuracy reported for aneroid calibration might mainly be caused by the variation in the sphygmomanometer cuff performance. After window averaging the accuracy would be $\pm 8.75mmHg$ and $\pm 10.2mmHg$ for deadweights calibration and aneroid sphygmomanometer calibration respectively.

Figure 7.8 shows that the computed pressure map, measured pressure map and the averaged measured pressure map obtained for both calibration techniques (the maps are for the first of the three bandages used in the experiment). The computed map shows that the bandage was applied with a pressure gradient. Both the measured pressure and the averaged pressure maps show that the aneroid sphygmomanometer calibration reports lower pressures than deadweights calibration.

The computed pressure map shows that the bandage applied high pressure at the anterior just above level C, where the shin bone is palpable. The measured pressures report this peak in pressure at anterior level C. However, the lower position of this peak compared to the computed pressures might be explained by the fact that sensors positions might not correspond exactly to where the cross sectional profiles were obtained or where the extensions were measured.

It is also clear from the maps that using window averaging will result in reporting pressures which are not exactly at the same locations where pressures are computed. For

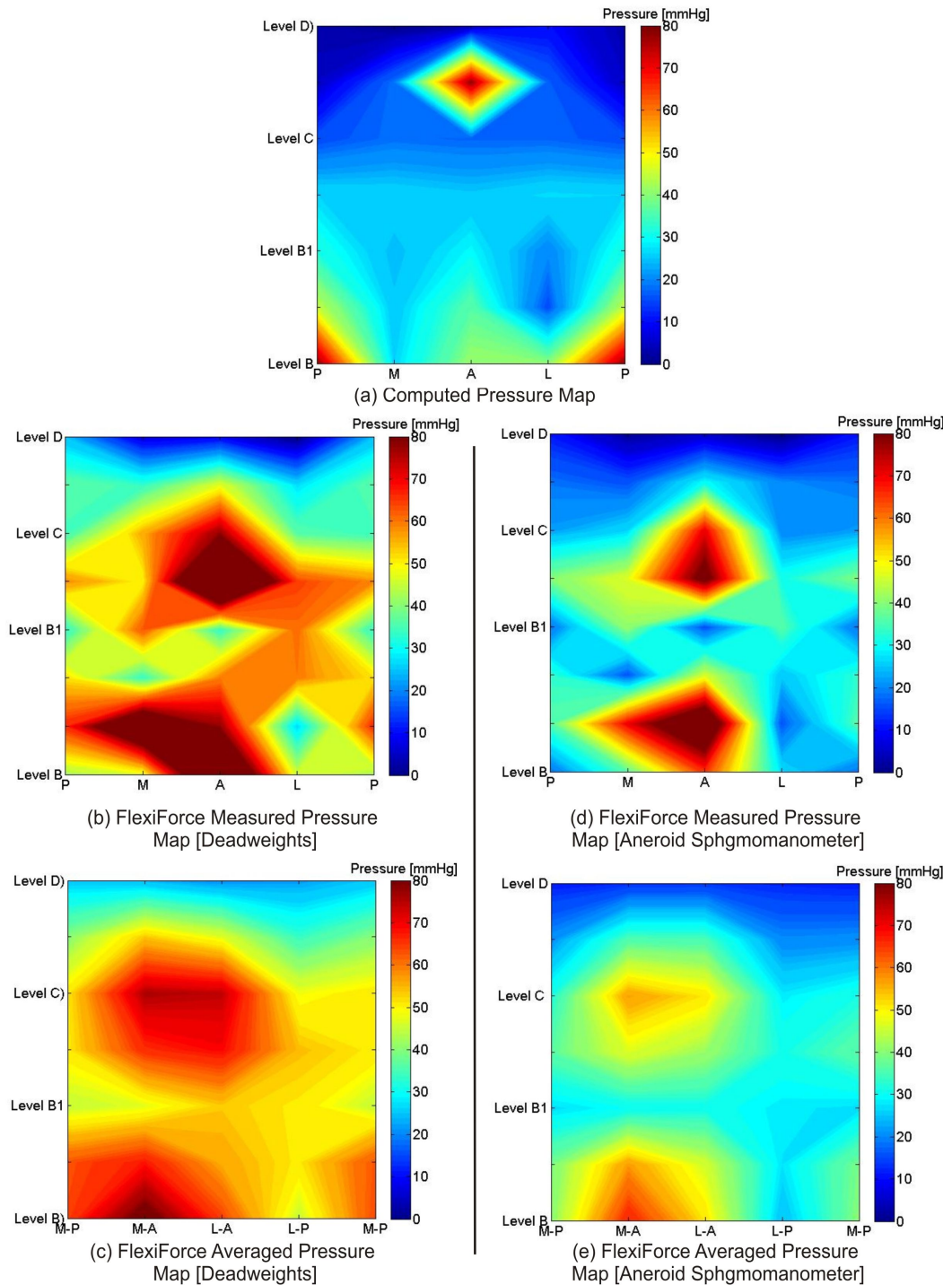


Figure 7.8: SurePress pressure maps: (a) SurePress computed pressure map, (b) SurePress measured pressure map using deadweights calibration method, (c) SurePress averaged pressure map using deadweights calibration method, (d) SurePress measured pressure map using aneroid sphygmomanometer calibration method and (e) SurePress averaged measured pressure map using aneroid sphygmomanometer calibration method. The maps are shown with the first column “Posterior” being repeated at the start and end for better clarity. ‘L’ = Lateral, ‘A’= Anterior, ‘M’ = Medial and ‘P’ = Posterior

example, the window averaging for sensors at medial and anterior level B will result in a pressure that corresponds to the side between the medial-anterior and neither of them, while the computed pressures are for either the medial or the anterior sides. This might have had an effect on the comparison between the computed and measured pressures.

Table 7.1 summarizes the measured extensions, averaged pressures, and the calculated tensions and pressures. Figure 7.9 illustrates the computed pressures and the averaged pressures for both deadweights and aneroid sphygmomanometer calibration methods.

Table 7.1: Summary of SurePress measured extensions, calculated tensions and pressures and averaged measured pressures for both calibration methods. The upper and lower 95% *spread* = $mean \pm (1.96 \times SD)$, and the upper and lower 95% *CI* = $mean \pm (t \times SE)$, where “*t*” is critical point at 95% for the data degrees of freedom obtained from the student’s t-distribution look-up table [189]

Statistical Analysis			Computed pressure [mmHg]	Averaged measured pressure (deadweights calibration) [mmHg]	Averaged measured pressure (aneroid sphygmomanometer calibration) [mmHg]	Averaged pressure (deadweights calibration) / computed pressure	Averaged pressure (aneroid sphygmomanometer calibration) / computed pressure
	Extension [%]	Tension [N]					
Median	32.00	4.97	16.87	40.76	23.64	2.49	1.47
Mean	31.62	5.21	20.34	43.37	27.23	3.10	1.85
SD	10.48	2.14	13.87	12.38	11.38	3.51	1.91
SE	1.14	0.23	1.51	1.21	1.24	0.38	0.21
Upper 95% spread	52.17	9.41	47.51	67.64	49.54	9.98	5.59
Lower 95% spread	11.07	1.01	-6.84	19.11	4.93	-3.77	-1.89
Upper 95% CI	33.86	5.67	23.30	45.74	29.67	3.85	2.26
Lower 95% CI	29.38	4.75	17.37	41.01	24.80	2.35	1.44

As it was reported previously, using deadweights for calibration will result in reporting higher pressures than using aneroid sphygmomanometer (Section 6.2.5). This is echoed in results reported in Table 7.1.

Using aneroid sphygmomanometer for calibration resulted in pressures which are closer to the computed pressures than using deadweights for calibration. This is further demonstrated in Figures 7.10 and 7.11. In the case of deadweights calibration, the computed and averaged measured pressures were found to be in agreement in 1% of the cases and in the case of aneroid sphygmomanometer they agreed in 27% of the cases. This indicates that using aneroid sphygmomanometer and a cylinder with 0.114m diameter might possibly result in reporting pressures which are more in agreement with the computed pressures than using deadweights for calibration.

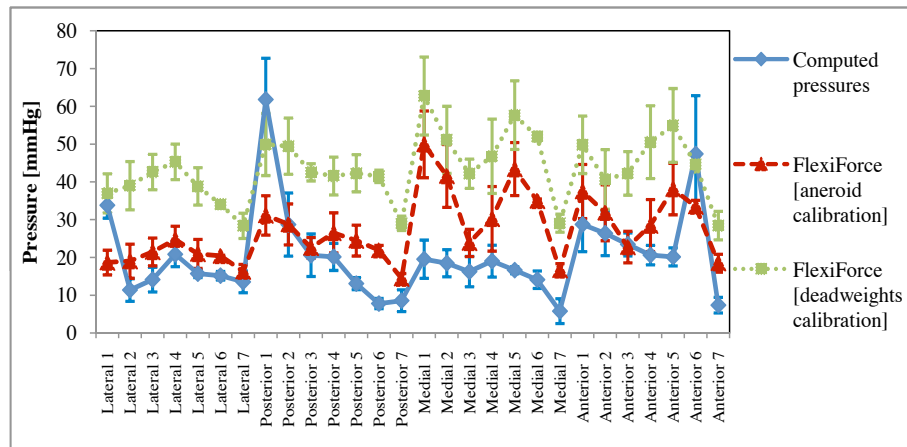


Figure 7.9: SurePress: computed and averaged measured pressures for both deadweights and aneroid sphygmomanometer calibration methods. Error bars are the standard error of the mean of the three bandage applications. Lines connecting the measurement points are for illustrative purposes

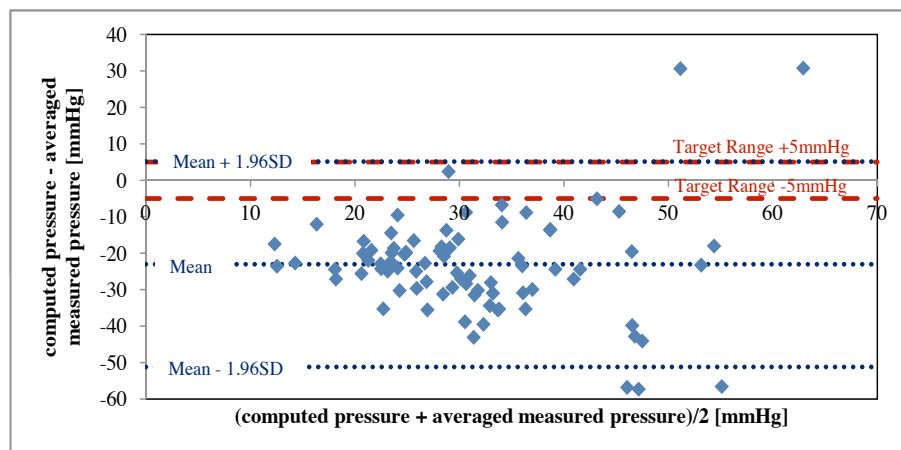


Figure 7.10: Bland-Altman plot for computed pressures and averaged measured pressures using deadweights calibration for SurePress

7.5 Validation Using PicoPress Measured Pressures

As it was shown in Section 7.4 using aneroid sphygmomanometer with a cylinder to calibrate FlexiForce sensors results in much higher levels of agreement with the computed pressures compared to the deadweights calibration. Computing pressures from elongation is not the only practice used in clinics to control the pressures applied by MCBs. Some researchers have used and recommended the usage of pressure measurement devices such as PicoPress and Kikuhime for quality control purposes [126]. This section will describe and report experiments carried out with the pressure measurement system to validate it by comparing the pressures measured using the system with the pressures measured using PicoPress sensors, pressures measured using PicoPress sensors plus correction and

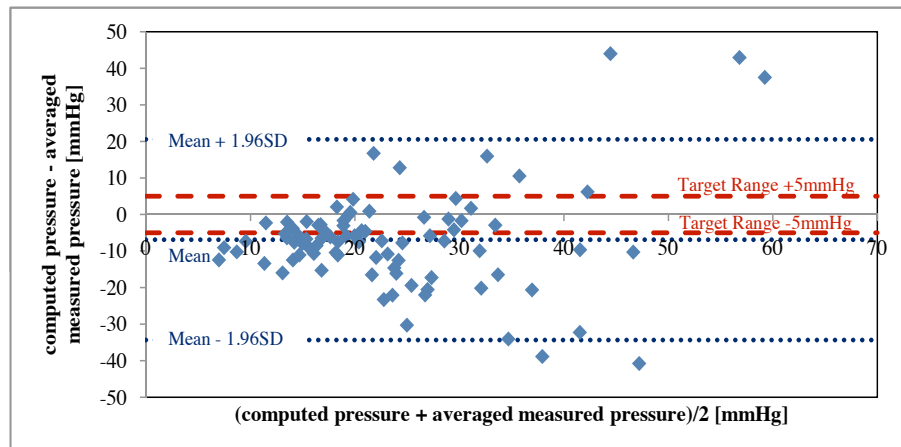


Figure 7.11: Bland-Altman plot for computed pressures and averaged measured pressures using aneroid sphygmomanometer calibration for SurePress

pressures computed for elongation when MCBs are applied to the leg of a healthy subject. Computed pressures were added in order to make sure that introducing PicoPress balloons next to FlexiForce sensors with the very small space available on the leg did not result in any degradation in the FlexiForce performance. The study was approved by the MEEC Faculty Research Ethics Committee at the University of Leeds (Appendix A).

7.5.1 Methods and Materials

Bandages: The same as Section 7.4.

Human subjects: The same as Section 7.4.

3D scan: The same as Section 7.4.

Extension measurement and pressure computation: Prof. E.A. Nelson applied three pre-marked SurePress bandages to the participant's leg after the FlexiForce sensors and PicoPress balloons were attached to the participant's leg (Figure 7.12). The rest of this section is the same as Section 7.4.

Pressure measurement: The pressure measurement system described in Section 7.2 was used to measure the pressure. Once the bandage is applied, PicoPress balloons were used to measure the pressure by first calibrating the transducer and inflating the probe and then recording the pressure reading into a spreadsheet. The pressures measured using PicoPress probes were then multiplied with correction factors (see Section 6.2.1 for more details about the correction factor).

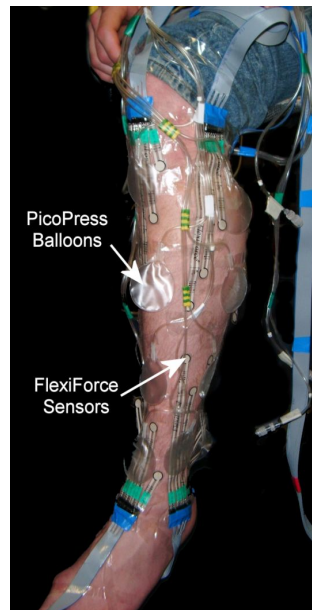


Figure 7.12: FlexiForce sensors and PicoPress transducer attached to the participant leg

Statistical analysis: Bland-Altman plots [197] and percentage frequency counts were used to check the levels of agreement between:

- the computed pressures and the PicoPress measured pressures
- the computed pressures and the PicoPress corrected measured pressures
- the computed pressures and the averaged measured pressures of the output of the window averaging of FlexiForce sensors (deadweights calibration).
- the computed pressures and the averaged measured pressures of the output of the window averaging of FlexiForce sensors (aneroid sphygmomanometer calibration).

In addition, Bland-Altman plots [197] and percentage frequency counts were also used to check the levels of agreement between:

- the PicoPress measured pressures and the averaged measured pressures of the output of the window averaging of FlexiForce sensors (deadweight calibration).
- the PicoPress measured pressures and the averaged measured pressures of the output of the window averaging of FlexiForce sensors (aneroid sphygmomanometer calibration).
- the PicoPress corrected measured pressures and the averaged measured pressures of the output of the window averaging of FlexiForce sensors (deadweight calibration).

- the PicoPress corrected measured pressures and the averaged measured pressures of the output of the window averaging of FlexiForce sensors (aneroid sphygmomanometer calibration).

Pressures were considered to be in agreement if the difference between the pressures were within $\pm 5\text{mmHg}$. PASW 17, MATLAB R2009b and Excel 2007 were used to carry out the statistical analysis and the comparisons.

7.5.2 Results, Analysis and Discussion

Table 7.2 summarizes the measured extensions, calculated tensions and pressures, averaged pressures for both calibration methods for the pressure measurement system, and the measured and corrected measured pressures for PicoPress.

Table 7.2: Summary of SurePress measured extensions, calculated tensions and pressures, averaged measured pressures for both FlexiForce calibration methods and measured and corrected pressures for PicoPress sensor. The upper and lower 95% spread = $mean \pm (1.96 \times SD)$, and the upper and lower 95% CI = $mean \pm (t \times SE)$, where “ t ” is critical point at 95% for the data degrees of freedom obtained from the student’s t-distribution look-up table [189]

Statistical Analysis	Statistical Analysis											
	Extension [%]	Tension [N]	Computed pressure [mmHg]	PicoPress measured pressure [mmHg]	PicoPress plus correction factor measured pressure [mmHg]	FlexiForc deadweights calibration averaged measured pressure [mmHg]	FlexiForc aneroid sphygmomanometer calibration averaged measured pressure [mmHg]	PicoPress measured pressure / computed pressure	PicoPress plus correction measured pressure / computed pressure	FlexiForc deadweights calibration averaged measured pressure / computed pressure	FlexiForc aneroid sphygmomanometer calibration averaged measured pressure / computed pressure	
Median	31.00	4.76	14.34	39.50	25.00	40.03	22.71	2.44	1.51	2.52	1.54	
Mean	30.13	4.69	17.46	41.95	27.66	40.31	23.91	2.80	1.80	2.70	1.57	
SD	6.48	1.24	10.52	16.72	13.92	14.11	10.06	1.45	1.01	1.23	0.71	
SE	0.93	0.18	1.52	2.41	2.01	2.04	1.45	0.21	0.15	0.18	0.10	
Upper 95% spread	42.82	7.12	38.07	74.73	54.95	67.97	43.63	5.64	3.77	5.11	2.96	
Lower 95% spread	17.43	2.26	-3.16	9.18	0.37	12.65	4.19	-0.04	-0.18	0.29	0.17	
Upper 95% CI	31.96	5.04	20.43	46.69	31.60	44.30	26.76	3.21	2.08	3.05	1.77	
Lower 95% CI	28.29	4.34	14.48	37.22	23.72	36.32	21.07	2.39	1.51	2.35	1.37	

Figure 7.13 illustrates the computed pressures, PicoPress measured and corrected measured pressures and FlexiForce averaged pressures for both calibration techniques.

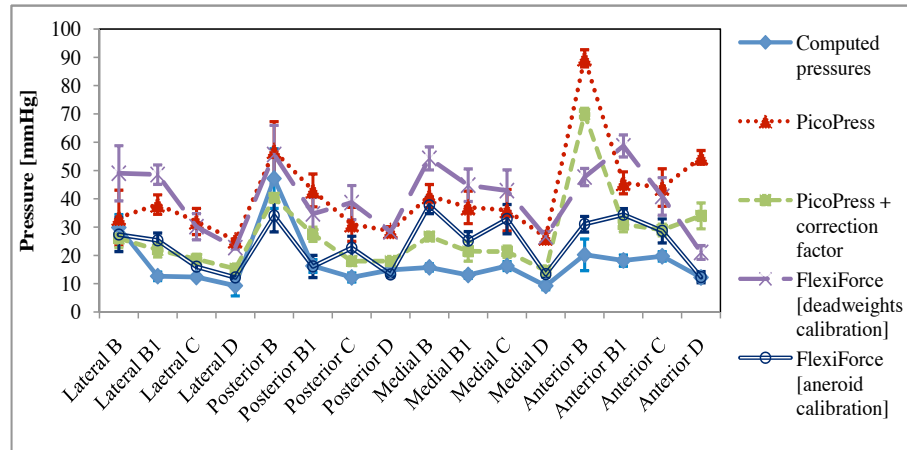


Figure 7.13: SurePress: computed pressures, PicoPress measured and corrected measured pressures and FlexiForce averaged measured pressures for both calibration methods. Error bars are the standard error of the mean of the three bandage application. Lines connecting the measurement points are for illustrative purposes

As it was reported previously, using deadweights for calibration will result in reporting higher pressures than using aneroid sphygmomanometer (Section 6.2.5). This is echoed in results reported in Table 7.1.

The pressures reported using PicoPress transducer after applying the correction factor and FlexiForce with aneroid sphygmomanometer calibration are much closer to the computed pressures. This is further demonstrated in Figures 7.14, 7.15, 7.16 and 7.17.

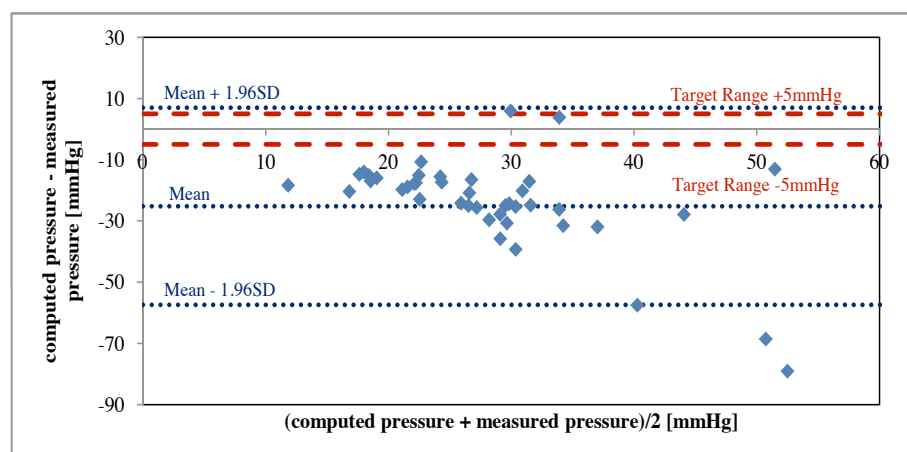


Figure 7.14: Bland-Altman plot for computed pressures and PicoPress measured pressures

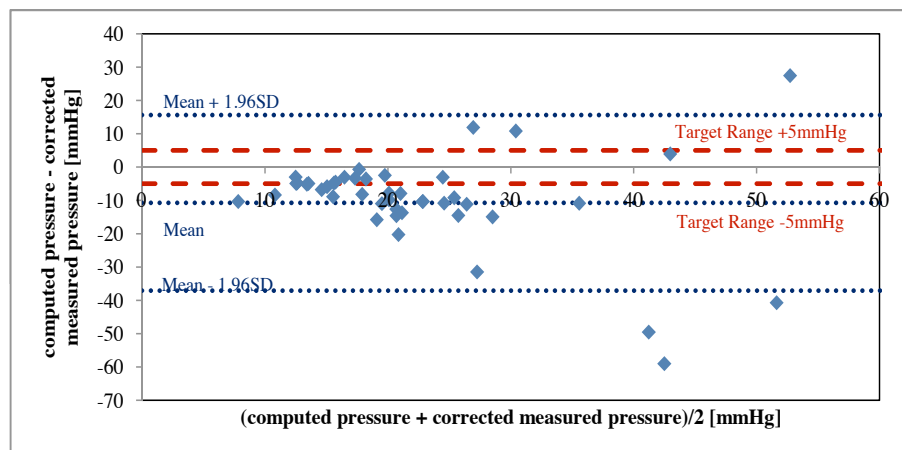


Figure 7.15: Bland-Altman plot for computed pressures and PicoPress corrected measured pressures

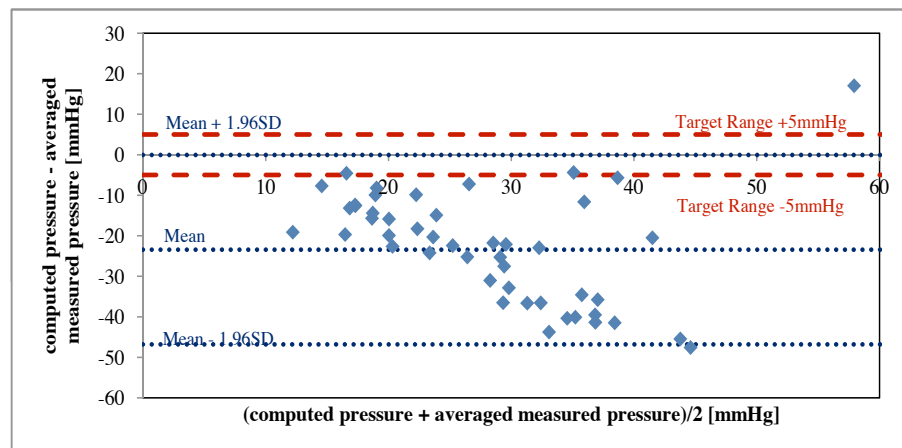


Figure 7.16: Bland-Altman plot for computed pressures and FlexiForce sensors averaged measured pressures using deadweights calibration

Summary of the percentage frequency count for the number of cases where compared pressures are within $\pm 5mmHg$ is provided in Table 7.3. Clearly, PicoPress plus correction factor and FlexiForce with aneroid sphygmomanometer calibration are showing much higher levels of agreement with the computational pressures than PicoPress and FlexiForce with deadweights calibration. In addition, results illustrate that introducing PicoPress sensors had a minimum effect, if any, on the FlexiForce sensors performance, which means that any deviation in the level of agreements between the FlexiForce and PicoPress measured pressures will not be caused by the introduction of PicoPress sensors next to FlexiForce sensors.

Additionally, Tables 7.2 and 7.3 and Figure 7.13 illustrate that the pressures measured using FlexiForce with deadweights calibration are close to the ones measured using PicoPress transducer and the pressures measured using FlexiForce with aneroid sphyg-

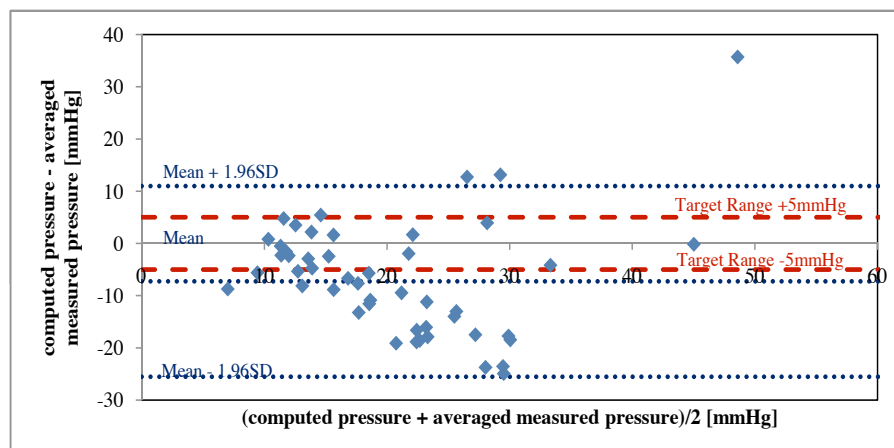


Figure 7.17: Bland-Altman plot for computed pressures and FlexiForce sensors averaged measured pressures using aneroid sphygmomanometer calibration

Table 7.3: The percentage of cases where the difference between the pressures being within $\pm 5\text{mmHg}$

Statistical Analysis	Percentage of cases where the difference is within $\pm 5\text{mmHg}$
Computed pressures and PicoPress measured pressures	2%
Computed pressures and PicoPress corrected measured pressures	30%
Computed pressures and FlexiForce deadweights calibration measured pressures	4%
Computed pressures and FlexiForce aneroid sphygmomanometer calibration measured pressures	35%
PicoPress measured pressures and FlexiForce deadweights calibration measured pressures	43%
PicoPress measured pressures and FlexiForce aneroid sphygmomanometer calibration measured pressures	11%
PicoPress corrected measured pressures and FlexiForce deadweights calibration measured pressures	5%
PicoPress corrected measured pressures and FlexiForce aneroid sphygmomanometer calibration measured pressures	52%

momanometer calibration are close to the ones reported by PicoPress transducer after applying correction. These are further demonstrated in Figures 7.18, 7.19, 7.20 and 7.21.

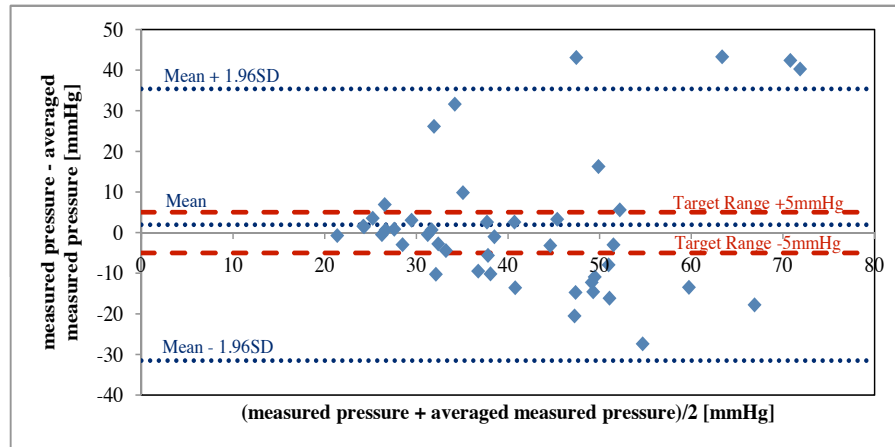


Figure 7.18: Bland-Altman plot for PicoPress measured pressures and FlexiForce load calibration measured pressures

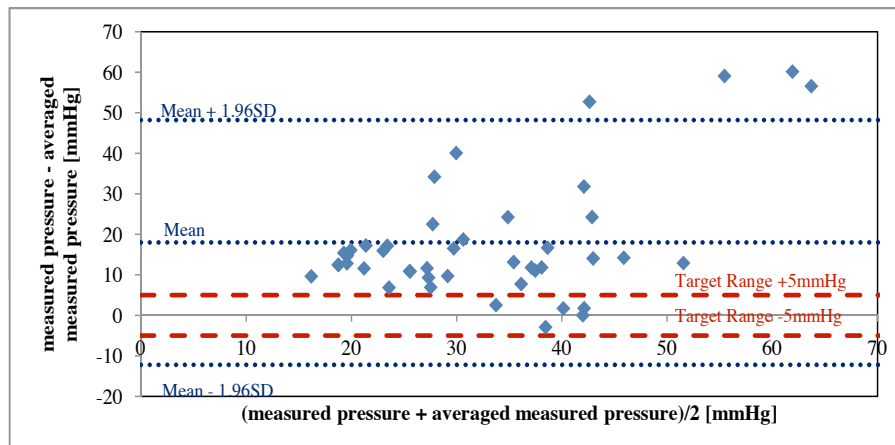


Figure 7.19: Bland-Altman plot for PicoPress measured pressures and FlexiForce aneroid sphygmomanometer calibration measured pressures

The high levels of agreement between the PicoPress corrected measured pressures and FlexiForce aneroid calibrations reported in Table 7.3 shows that the pressure measurement system can be used to map the pressure under compression bandages for qualitative purposes only, as accuracy and reliability are still an issue which needs to be improved in future work. However, in spite of the deficiencies with FlexiForce sensors accuracy, they provided much more reliable pressure maps compared to current commercial pressure measurement systems like PicoPress (without correction) when FlexiForce sensors were calibrated with aneroid sphygmomanometer over a curved surface like a rigid cylinder.

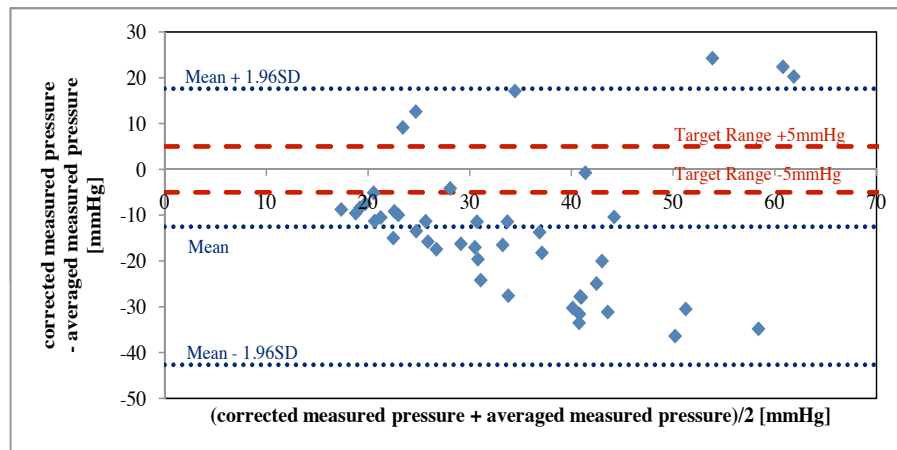


Figure 7.20: Bland-Altman plot for PicoPress corrected measured pressures and FlexiForce load calibration measured pressures

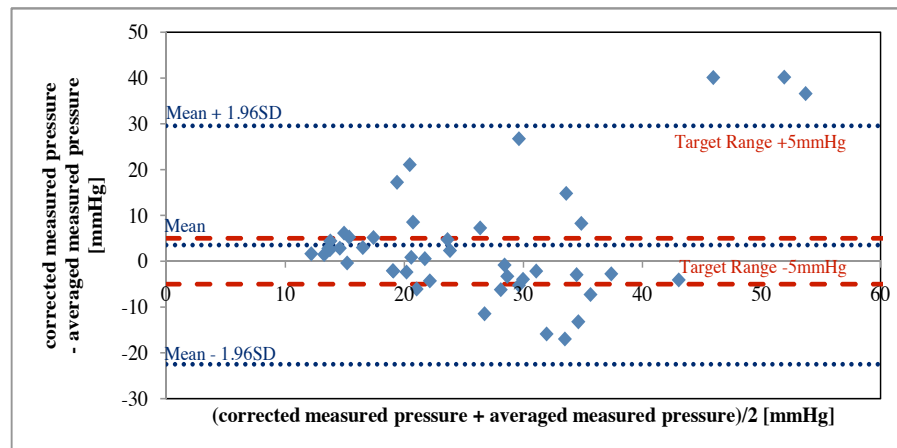


Figure 7.21: Bland-Altman plot for PicoPress corrected measured pressures and FlexiForce aneroid sphygmomanometer calibration measured pressures

7.6 Summary

The chapter demonstrated that FlexiForce arrays when calibrated on a curved surface using aneroid sphygmomanometer and window averaging have outperformed PicoPress transducer, which is a typical example of medical pressure transducers used to measure the pressure applied by MCBs to the patient's leg. Even after window averaging, FlexiForce arrays accuracy error is still higher than $\pm 5\text{mmHg}$, which means they can only be used for qualitative purposes and not for accurate measurements. This might be adequate, for example, to detect areas with dangerous levels of pressures or to check if MCBs are applied with graduated pressure.

The outcome of this chapter can be summarized in the following points:

- The usage of window averaging with FlexiForce sensors did resolve some of the

accuracy and reliability problems associated with FlexiForce sensors. Testing these sensors over a real leg showed that they can provide more reliable and accurate pressure maps than PicoPress transducer.

- 3D scans for the ankle to knee segment of the lower limb was used to compute the interface pressure and can be used as a great tool to study the interface pressure and identify sites where pressure might peak and cause tissue damage.
- The development of a pressure measurement system which uses arrays of FlexiForce sensors can be used to map the pressure at 40 measurement points. This study reported the use of the system to investigate the pressures applied by MCBs to a participant's leg at 32 points. This is twice as much measurement points as the largest number of measurement points reported by any other study.

Chapter 8

Pressure-Mapping Bandage

This chapter presents the development of two pressure-mapping bandage prototypes to map the pressure applied by compression products at multiple points, and reports on the preliminary experimental validation for these prototypes using a pressure-mapping mannequin leg embedded with FS01 sensors. The question that this chapter will address is whether flexible pressure sensors can be attached to or potentially integrated in bandages and be used to measure the pressure applied by MCBs.

8.1 Introduction

Chapter 7 showed that arrays of FlexiForce sensors can be used to map the pressure under MCBs for qualitative purposes when multiple sensors are used, sensors are calibrated with an aneroid sphygmomanometer over a curved surface (PVC cylinder) and the average of the sensors output is used to report the pressure reading. This chapter will illustrate the development of two pressure-mapping bandage prototypes which can be used to provide nurses with qualitative feedback about the pressures they apply to the leg with bandages. This could potentially replace the current feedback method, which is based on the amount of elongation in the applied bandage. This was shown not be an adequate and reliable feedback method in Sections 6.2, 6.3 and 6.4 and Chapter 7.

The chapter is divided into two parts. Section 8.2 will report on the development of a pressure-mapping bandage with attached FlexiForce sensors, which can provide pressure readings at 4 measurement sites. The section will also detail the experimental validation for the pressure-mapping bandage prototypes using a pressure-mapping mannequin leg with embedded FS01 force sensors and describe the pros and cons of the tested prototypes.

Section 8.3 will illustrate the development of a pressure-mapping tubular bandage with attached FlexiForce sensors, which can provide pressure measurements at 3 locations. It will also highlight the outcome of the experimental validation for this second pressure-mapping prototype using a pressure-mapping mannequin leg with embedded FS01 force sensors. This will be concluded with an evaluation of the advantages and disadvantages of the second pressure-mapping prototype.

8.2 Pressure-Mapping Bandage: First Prototype

This section will present the design and development of the first pressure-mapping prototype and will report on experimental validation for its performance.

8.2.1 Bandage Selection

SurePress bandage was selected to be the medium to which FlexiForce sensors were to be attached. Its consistency, low hysteresis, elasticity and ability to apply high pressure with low elongations are the main reasons for its selection (Section 4.4).

8.2.2 Sensors, Sensors Attachments, Processing Unit and Data Acquisition

16 FlexiForce sensors were attached to a SurePress bandage. This was achieved by sewing the bandage with inelastic cotton yarn to form a number of loops that the sensor can be passed under. For each sensor, three stitching sites were used to secure the sensor in its place. The sensor itself was not stitched to the bandage so it can be re-washed and to allow bandage extension. Every four FlexiForce sensors were attached to the bandage next to each other so the average of the output could be used to report the pressure at that particular point. Sensors were attached to the bandage at 4 different sites, corresponding approximately to the ankle, gaiter, mid-calf and below knee. The sensors were attached in right angles to the bandage long axis (Figure 8.1). The sensors were attached to the bandage so the sensitive area of the sensor was in the top half of the bandage. This was to ensure that sensors report the pressure applied by the two layers of the bandage when the bandage is applied with spiral 50% overlap. This design also solves the problem of wiring, as sensors could be connected to the processing unit after the bandage was applied to the leg. This limits pressure measurement to after applying the bandage.

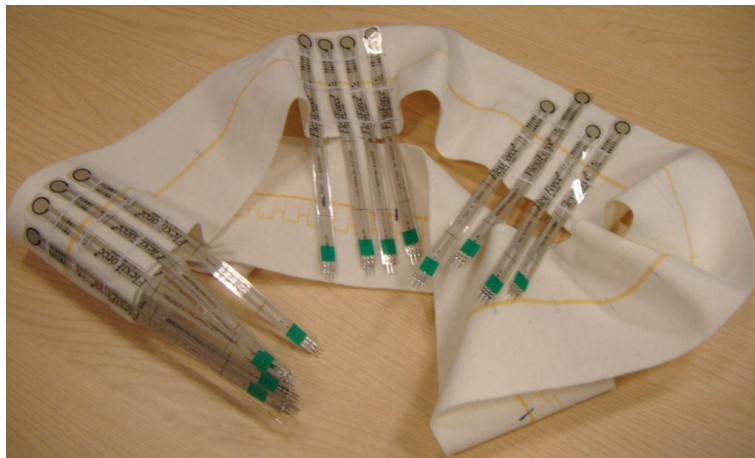


Figure 8.1: SurePress bandage with attached FlexiForce sensors

Once the bandage is applied to the leg, sensors were connected to a processing unit that powers the sensors with a constant $5V$. The processing unit amplifies the sensor output, filters it using hardware low-pass filter and then passes it to Mass Term 6225 USB DAQ card through a screw terminal board (LPR-68). The processing unit consists of two conditioning circuits, each to power and handle the signal of 8 FlexiForce sensors (see Section 7.2 for more details)

8.2.3 Sensors Calibration

As it has been shown in Chapter 7, FlexiForce sensors report pressures which are in agreement with the computed pressures from extension and measured pressures with PicoPress plus correction factor and FS01 force sensor when calibrated using an aneroid sphygmomanometer; thus, the sensors were calibrated using an aneroid sphygmomanometer for the pressure range $0 - 120mmHg$. The calibration was carried out on a cylinder with $0.114m$ diameter. The aneroid sphygmomanometer cuff was inflated by $10mmHg$ increments from $0mmHg$ to $120mmHg$ and then deflated by $10mmHg$ decrements to $0mmHg$. The process was repeated ten times for each sensor. The inflating and deflating process was used to address the hysteresis problem associated with these sensors as per recommendations [169]. Repetition of the calibration process was conducted in order to reduce the effect of the repeatability error on the calibration process. A program written in LabView 8.6 environment was used to acquire the sensor signals in the calibration process and a program written in LabView 8.6 was used to obtain the best 5^{th} order polynomial fitting line for the calibration that describes the pressure in $mmHg$ obtained by transformation from the measured voltage.

8.2.4 Pressure-Mapping Bandage Interface and Program

The program was written in LabView 8.6 to acquire the signals, display them, convert them to pressure values using calibration fitting lines, average the output of each 4 adjacent sensors, display the measured and average pressure values numerically, map the averaged measured pressures on a 3D representation for the bandage, and store the voltages, the measured pressures and the average pressure values in separate files for further processing. The signals were sampled at $1kHz$ and a software based 2^{nd} order low-pass filter with $10Hz$ cut-off frequency was used to filter out the signal. The program has the capability to zero the pressures on demand. In addition, a piece of code was written in the program to compare the average pressure with the target pressure profile $40mmHg$ at ankle decreasing to $20mmHg$ below knee. After comparing the average and target pressures, the program provides the user with textual feedback about the pressure applied; higher or lower than target pressure, and visual feedback in terms of mapping the difference between the target and applied pressures to a diagnostic map. The map displays white for pressures $20mmHg$ higher than target pressure values, red for for pressures $10mmHg$ higher than target pressure values, green for no difference, light blue for pressures $10mmHg$ lower than

target pressure values and pink for pressures 20mmHg lower than target pressure values. Figures 8.2 and 8.3 show the program front panel and flow chart of the pressure-mapping bandage program.

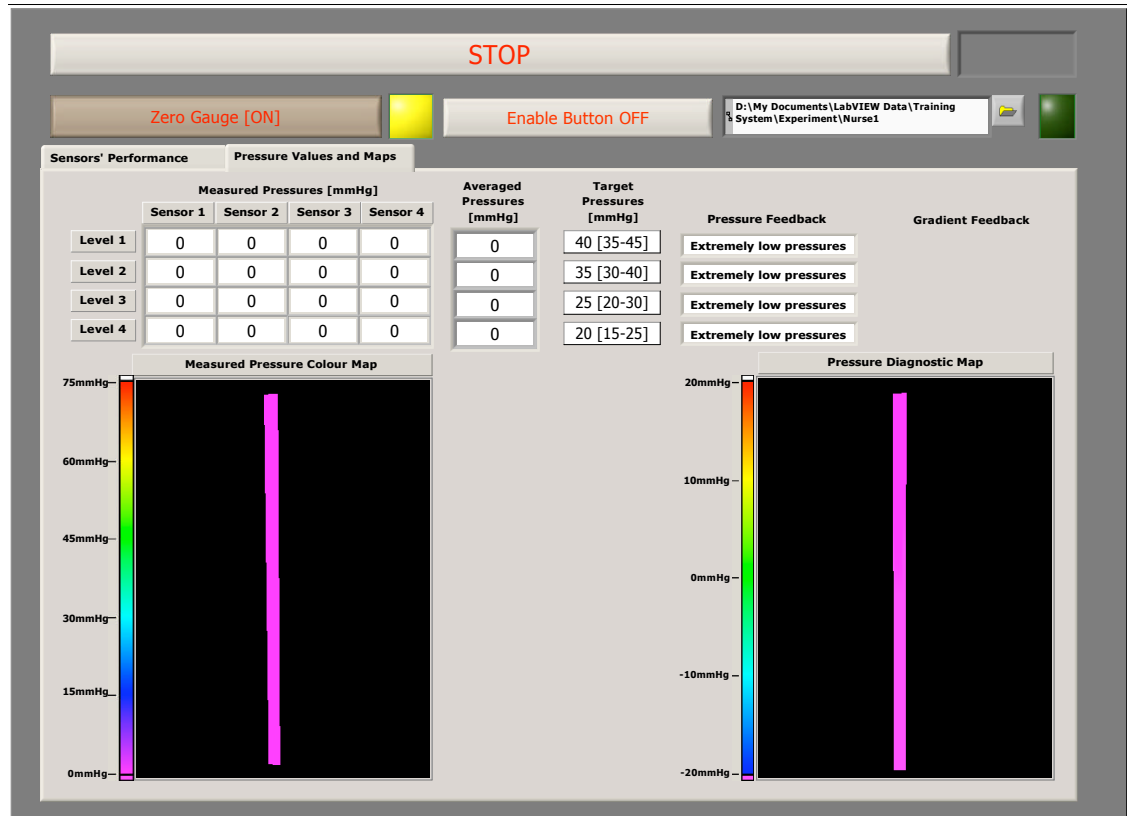


Figure 8.2: The front panel of the display program for the first prototype pressure-mapping bandage.

8.2.5 Experimental Validation for the Pressure-Mapping Bandage

The first pressure-mapping bandage prototype was tested using a pressure-mapping mannequin leg with embedded FS01 force sensors. The objectives of the experiment were:

- to quantify the levels of agreement between the pressures reported by the pressure-mapping bandage and the pressures reported by the pressure-mapping mannequin leg.
- to compare the pressure profile reported by the two pressure-mapping systems to quantify the ability of the pressure-mapping bandage to provide qualitative information about pressure gradient.

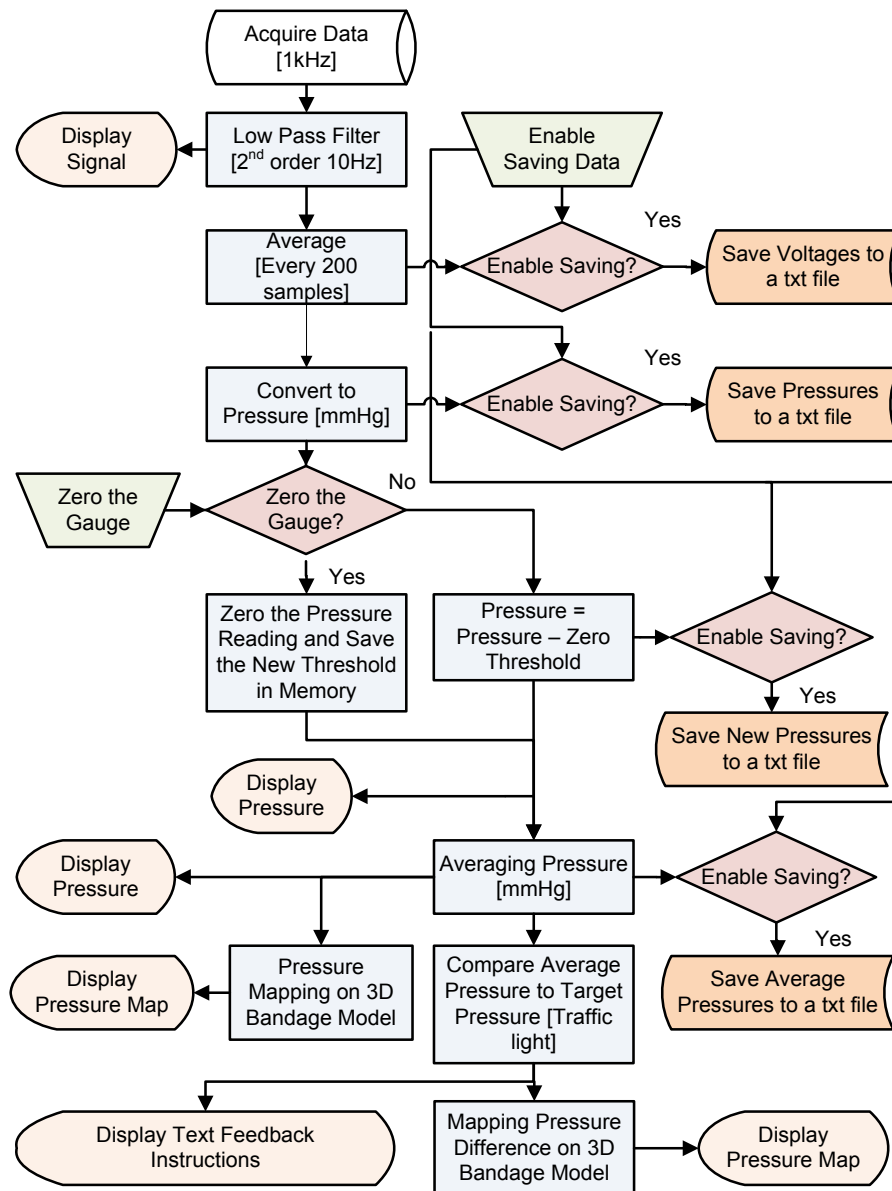


Figure 8.3: The flow chart of the display program for the first prototype pressure-mapping bandage.

Methods and Materials

As the bandage was to be tested with a pressure-mapping mannequin leg, a program was written in LabView 8.6 to acquire, display and save the pressure maps reported by the pressure-mapping bandage and the pressure-mapping mannequin leg (Figure 8.4).

The author applied the pressure-mapping bandage to the pressure-mapping mannequin leg 7 times (Figure 8.5). Each time, sensors were connected after applying the bandage, the pressures reported by both the pressure-mapping leg and the pressure-mapping bandage were saved for post processing. As the position of measurement points on the pressure-

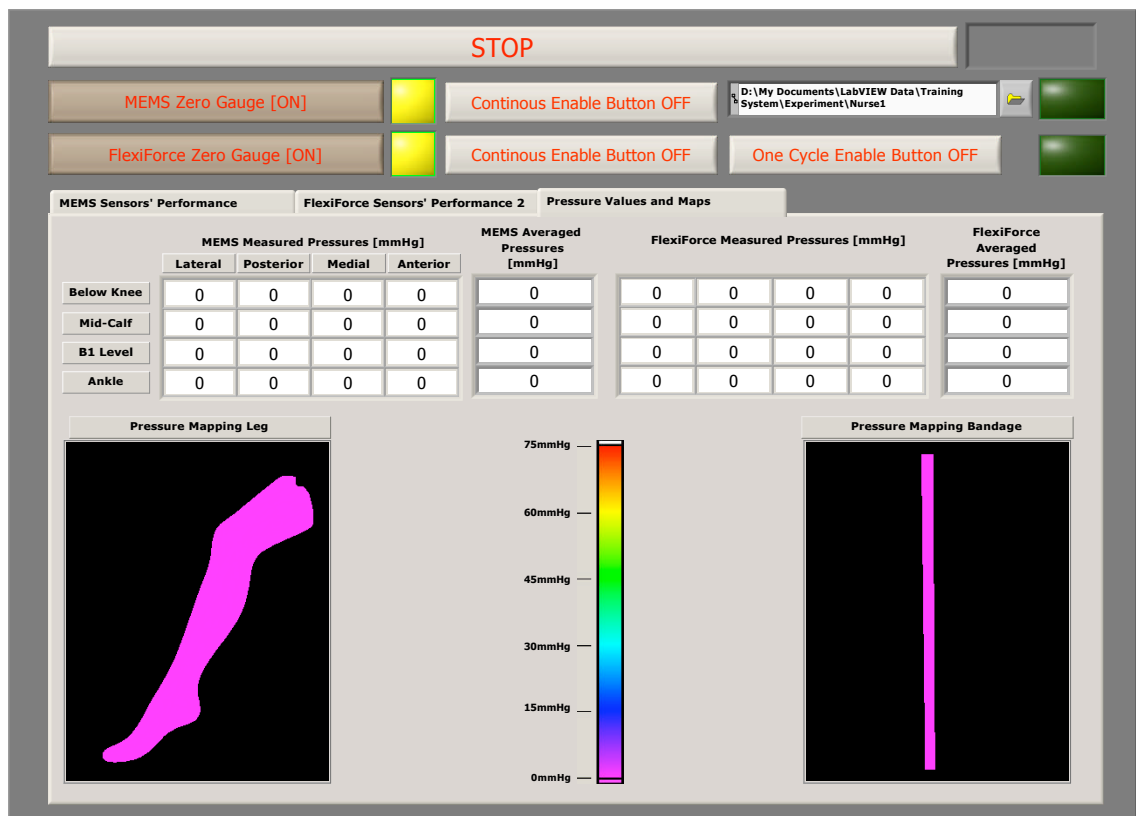


Figure 8.4: The front panel of the display program for the program used in the experiment.

mapping bandage differed each time the bandage was applied to the leg, the locations were noted manually. This information was used to select the appropriate readings from the leg for comparison with the pressure-mapping bandage. Furthermore, before the pressure-mapping bandage was applied to the mannequin leg, a stocking was applied to the leg in order to protect FlexiForce sensors from any damages. This resulted in pre-loading the FS01 sensors which was solved by zeroing the pressure gauge in the software.

Bland-Altman plots [197] and percentage frequency counts were used to check the levels of agreement between the averaged pressures reported by the pressure-mapping bandage and the corresponding measured pressures reported by the pressure-mapping mannequin leg. In addition, Bland-Altman plots [197] and percentage frequency counts were used to check the levels of agreement between the averaged pressures reported by the pressure-mapping bandage and the averaged pressures for the ankle, gaiter, mid-calf and below knee reported by the pressure-mapping mannequin leg. The pressures are considered to be in agreement if the difference between the measured pressures are within $\pm 5mmHg$.

Furthermore, the pressure ratio: gaiter/ankle, mid-calf/ankle, below-knee/ankle, mid-calf/gaiter, below-knee/gaiter and below-knee/mid-calf for the pressure-mapping bandage and the pressure-mapping mannequin leg measured and averaged pressures were calculated. Then, the number of cases where both pressure-mapping bandage and pressure-

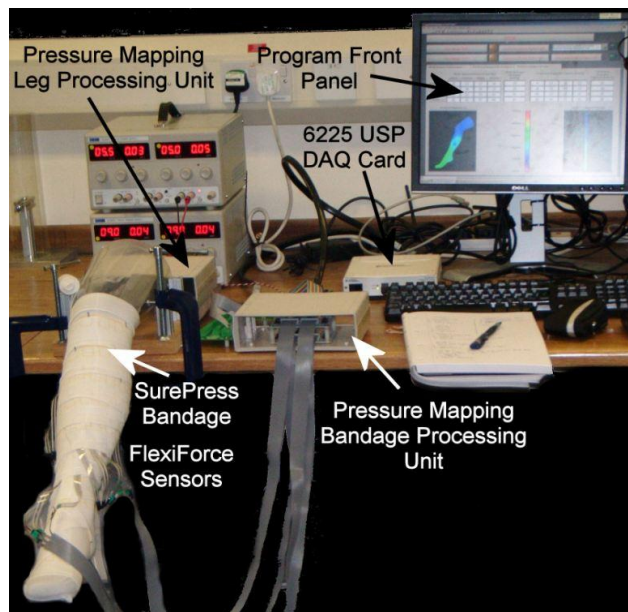


Figure 8.5: Pressure-mapping bandage applied to the pressure-mapping mannequin leg

mapping mannequin leg reported the same gradient description, lower than one and equal or higher than one, was calculated. This was done for both the corresponding measured pressures reported by the mannequin leg and the anatomical level averaged pressures reported by the mannequin leg i.e. the average pressures reported by four FS01 sensors at each of the anatomical levels: ankle, gaiter, mid-calf and knee. PASW 17, MATLAB R2009b and Excel 2007 were used to carry out the statistical analysis and the comparisons.

Results, Analysis and Discussion

From the calibration process, the median accuracy for the FlexiForce sensors used found to be $\pm 16\%FS$, where FS here is $120mmHg$. The accuracy here is the combined error of the calibration fitting line, the repeatability and the hysteresis of the sensors. Median accuracy in terms of pressures is $\pm 19.2mmHg$ for each sensor. After averaging the accuracy will be $\pm 9.6mmHg$ for each measurement site.

Figure 8.6 summarizes the mean of the averaged pressures reported by the pressure-mapping bandage and the mean of the averaged and measured pressures reported by the pressure-mapping mannequin leg. Clearly, the pressure-mapping bandage reports values similar to the pressure-mapping mannequin leg, which is supported by the outcome of the statistical analysis.

Figure 8.7 illustrates the Bland-Altman plots for the measured pressures reported by the pressure-mapping mannequin leg and the average pressures reported by the pressure-mapping bandage. Figure 8.8 shows the Bland-Altman plot for the average pressures reported by the pressure-mapping mannequin leg and the average pressures reported by the

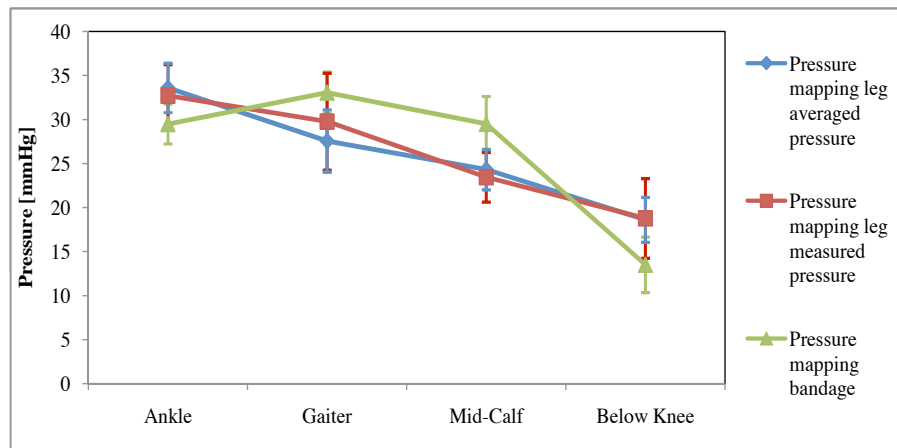


Figure 8.6: The average output for the pressure-mapping bandage and the pressure-mapping mannequin leg. The error bars are for the standard error of the mean. Lines connecting the pressure points are for illustrative purposes

pressure-mapping bandage. The pressure-mapping bandage was found to report pressures which agreed with the measured pressures and the averaged pressures reported by the pressure-mapping mannequin leg in 32% and 39% of the cases respectively. These results highlight the problem of accuracy of the pressure-mapping bandage.

Comparing the pressure ratios shows that the pressure-mapping bandage reported the same gradient description as the pressure-mapping mannequin leg measured and averaged pressures in 64% and 71% of the cases respectively. These results suggest that the pressure-mapping bandage can be used to help applying bandages with the appropriate pressure gradient.

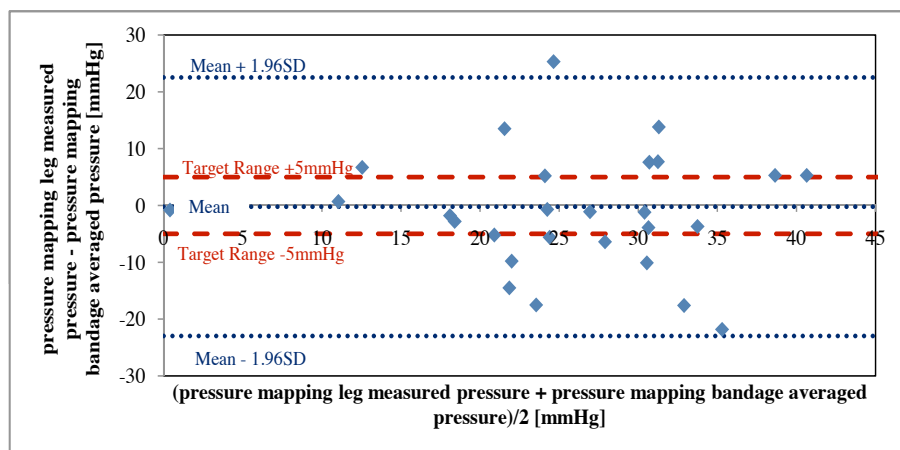


Figure 8.7: Bland-Altman plot for the measured pressures reported by the pressure mannequin leg and the averaged pressures reported by the pressure-mapping bandage

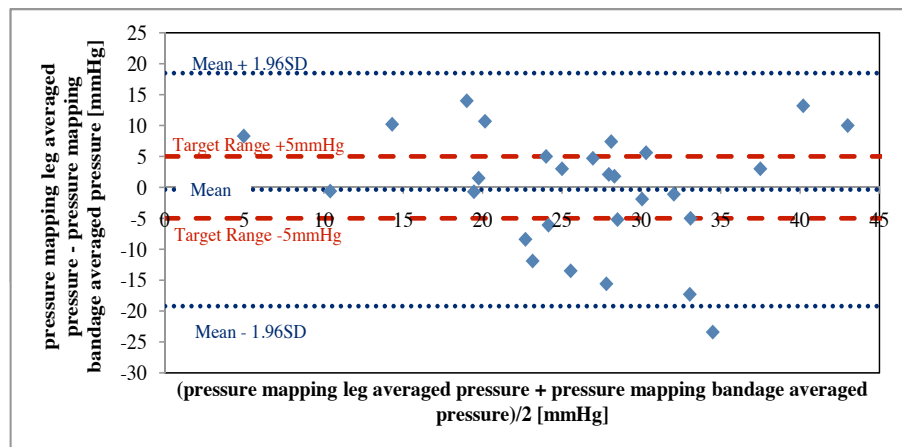


Figure 8.8: Bland-Altman plot for the anatomical level averaged pressures reported by the pressure mannequin leg and the averaged pressures reported by the pressure-mapping bandage

8.3 Pressure-Mapping Bandage: Second Prototype

The first pressure-mapping bandage prototype has one main drawback, that the pressure readings can only be obtained after applying the bandage and connecting the sensors. This means users will need to reapply the bandage fully in order to adjust the bandage application; thus, a second prototype of the pressure-mapping bandage with attached sensors was developed to overcome the mentioned limitation. This section will present the design and development of the second pressure-mapping bandage prototype and will report on the experimental validation of its performance.

8.3.1 Bandage Selection

SurePress Comfort first layer tubular bandage (ConvaTec Ltd, Deeside, UK) was used to host the FlexiForce sensors. This tubular bandage was used because it applies very low pressures to the leg ($< 10\text{mmHg}$).

8.3.2 Sensors, Sensor Attachments, Processing Unit and Data Acquisition

12 FlexiForce sensors were attached to a SurePress Comfort tubular bandage. This was achieved by sewing the tubular bandage with inelastic cotton yarn to form loops that the sensors can be passed under. For each sensor, three stitching sites were used to secure the sensor in its place. However, the sensor itself was not stitched to the tubular bandage, so that the bandage can be re-washed and to overcome the problem of bandage extension. Four FlexiForce sensors were attached to the tubular bandage next to each other so the average of the sensors output could be used to report the pressure at that particular point. Sensors were attached to the tubular bandage at 3 sites: the ankle, mid-calf and below

knee. The main reason to use only three sites and not four is the limited space available on the tubular bandage if the sensors are not to overlap each other (Figure 8.9).



Figure 8.9: Tubular bandage with attached FlexiForce sensors

Once the tubular bandage was applied to the leg, sensors could be attached to the bandage and be connected to the processing unit that powers the sensors with constant 5V. The processing unit amplifies the sensor output, filters it using hardware low-pass filter and then passes it to Mass Term 6225 USB DAQ card through a screw terminal board (LPR-68). The processing unit consists of two conditioning circuits, each of which can power and handle 8 FlexiForce sensors (see Section 7.2 for more details)

8.3.3 Sensors Calibration

The calibration procedure and the sensors used are the same as those detailed in Section 8.2.3.

8.3.4 Pressure-Mapping Bandage Interface and Program

The program used is reported in Section 8.2.4 except that the mannequin leg model was used to map the measured pressures and the diagnostic pressures. Figures 8.10 and 8.11 show the program front panel and flow chart of the second pressure-mapping bandage prototype program.

8.3.5 Experimental Validation for the Pressure-Mapping Bandage

The second pressure-mapping bandage prototype was tested using a pressure-mapping mannequin leg with embedded FS01 force sensors as before. The objectives of the experiment were:

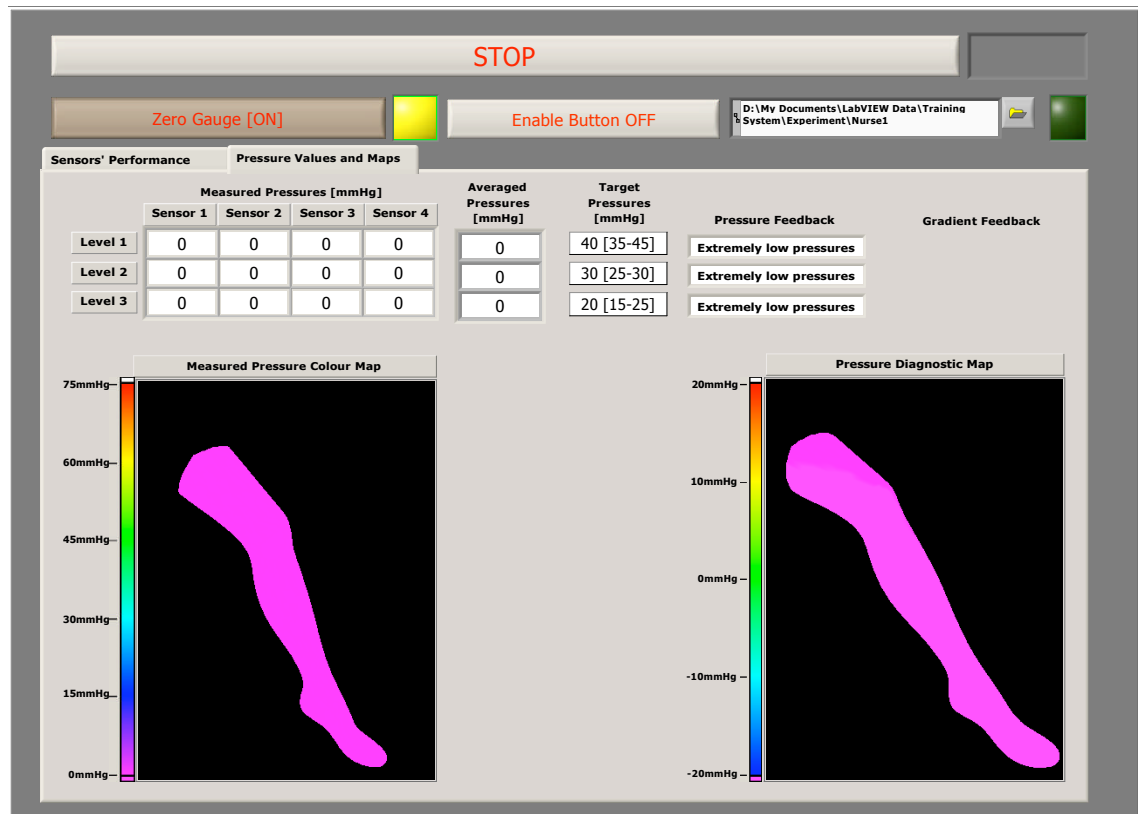


Figure 8.10: The front panel of the display program for the second prototype pressure-mapping bandage.

- to quantify the levels of agreement between the pressures reported by the pressure-mapping bandage and those reported by the pressure-mapping mannequin leg.
- to compare between the pressure profile reported by the two pressure-mapping systems to quantify the ability of the pressure-mapping bandage to provide qualitative information about pressure gradient.

Methods and Materials

A program was written in LabView 8.6 to acquire, display and save the pressure maps reported by the pressure-mapping bandage and the pressure-mapping mannequin leg (Figure 8.12). As the position of measurement points on the pressure-mapping tubular bandage are known, the program was written to display both the pressure-mapping mannequin leg averaged pressures and measured pressures that correspond to the same location where the pressure-mapping bandage is reporting.

The author applied the pressure-mapping bandage to the pressure-mapping mannequin leg, connected the sensors and then applied SurePress bandage to both measurement systems 10 times. Each time the pressures reported by both pressure-mapping leg and pressure-mapping bandage were saved for post processing. Due to the fact that the second

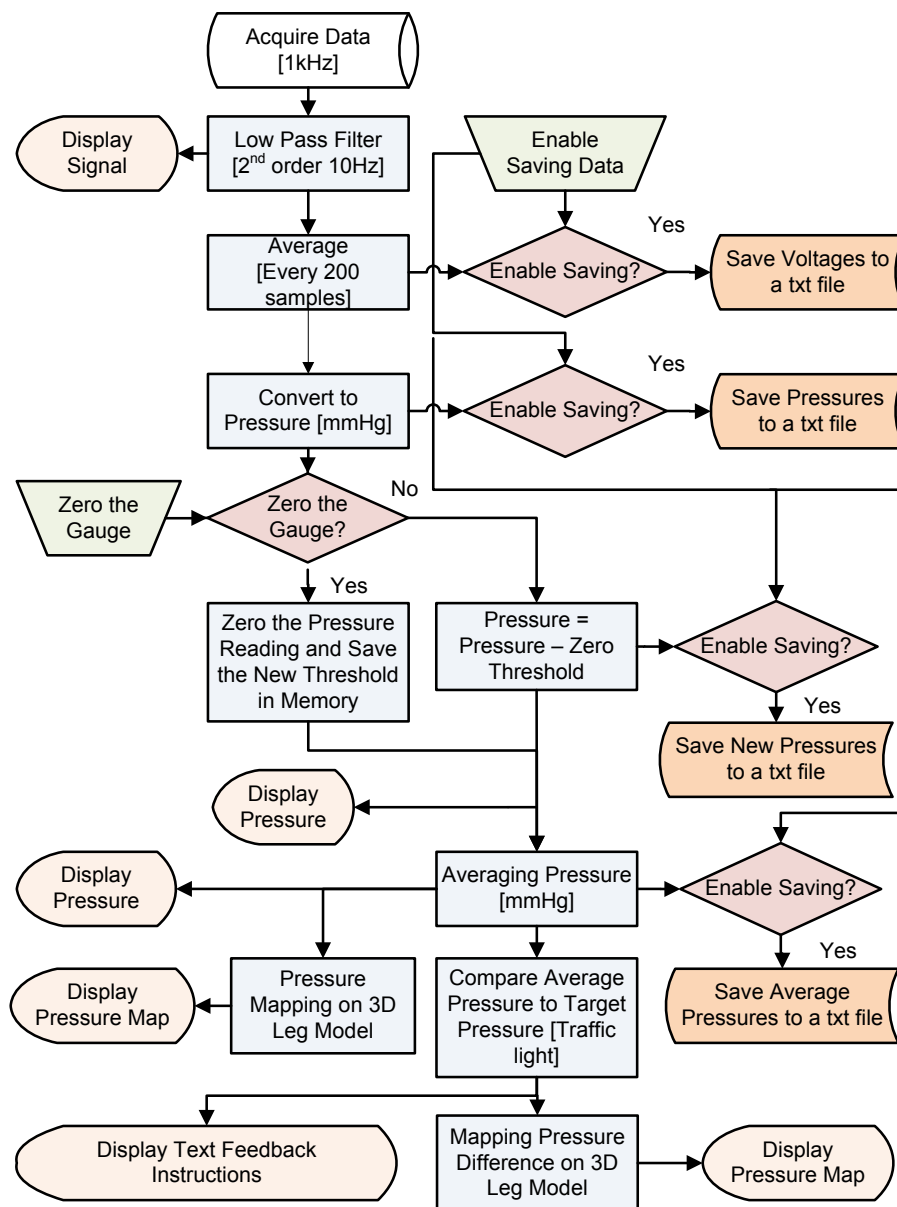


Figure 8.11: The flow chart of the display program for the second prototype pressure-mapping bandage.

pressure-mapping bandage prototype was applied to the mannequin leg before SurePress bandage being applied, the pressure reading for the FS01 sensors were zeroed before applying the SurePress bandage.

Bland-Altman plots [197] and frequency counts were used to check the levels of agreement between the averaged pressures reported by the pressure-mapping bandage and the corresponding measured pressures reported by the pressure-mapping mannequin leg. In addition, Bland-Altman plots [197] and frequency counts were also used to check the levels of agreement between the averaged pressures reported by the pressure-mapping bandage and the averaged pressures for the ankle, mid-calf and below-knee reported by



Figure 8.12: The front panel of the display program for the program used in the testing experiment.

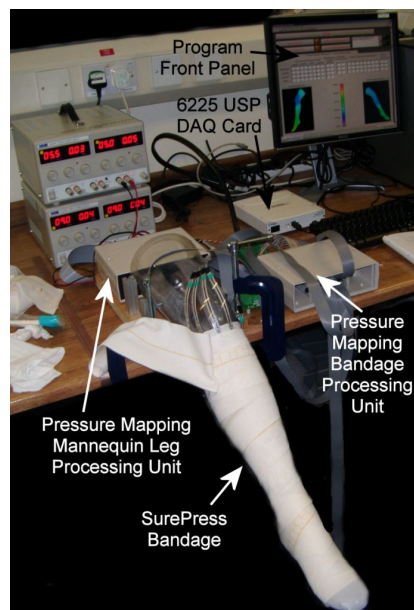


Figure 8.13: SurePress bandage applied to the second prototype pressure-mapping bandage and pressure-mapping mannequin leg

the pressure-mapping mannequin leg. The pressures were considered to be in agreement if the difference between the computed and measured pressures were within $\pm 5\text{mmHg}$.

Furthermore, the pressure ratio: mid-calf/ankle, below-knee/ankle and below-knee/mid-calf for the pressure-mapping bandage and the pressure-mapping mannequin both measured and averaged pressures were calculated. Then, the number of cases where both pressure-mapping bandage and pressure-mapping mannequin leg reported the same gradient description, lower than one or equal and higher than one, was calculated. This was done for both the corresponding measured pressures reported by the mannequin leg and the anatomical level averaged pressures reported by the mannequin leg i.e. the average pressures reported by four FS01 sensors at each of the anatomical levels: ankle, gaiter, mid-calf and knee. PASW 17, MATLAB R2009b and Excel 2007 were used to carry out the statistical analysis and the comparisons.

Results, Analysis and Discussion

Figure 8.14 summarizes the mean of the averaged pressures reported by the pressure-mapping bandage and the mean of the averaged and measured pressures reported by the pressure-mapping mannequin leg. Unlike the first prototype, the pressure profile is slightly different to the ones reported by the mannequin leg.

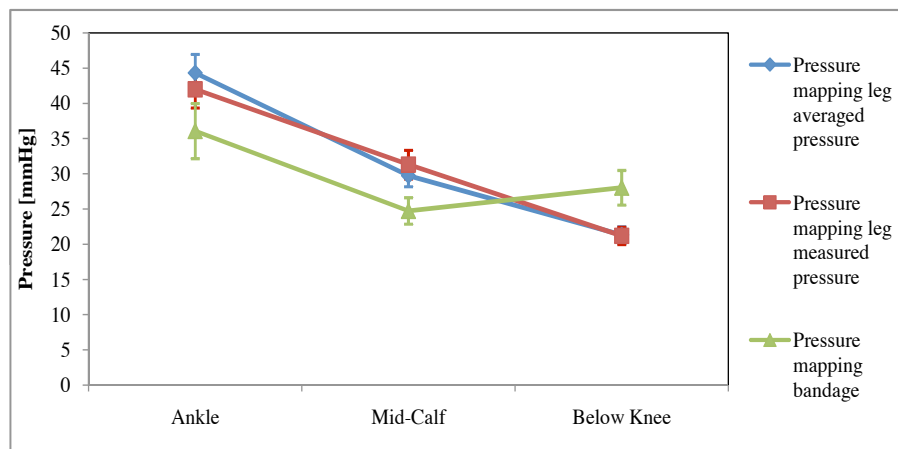


Figure 8.14: The average output for the second pressure-mapping bandage prototype and the pressure-mapping mannequin leg. The error bars are for the standard error of the mean. The lines connecting the measurement points are for illustrative purposes

Figure 8.15 illustrates the Bland-Altman plots for the measure pressures reported by the pressure-mapping mannequin leg and the average pressures reported by the pressure-mapping bandage. Figure 8.16 shows the Bland-Altman plot for the average pressures reported by the pressure-mapping mannequin leg and the average pressures reported by the pressure-mapping bandage. The pressure-mapping bandage reported pressures which agreed with the measured pressures and the averaged pressures reported by the pressure-mapping mannequin leg in 27% and 37% of the cases respectively. These results highlight

the problem of accuracy of the pressure-mapping bandage.

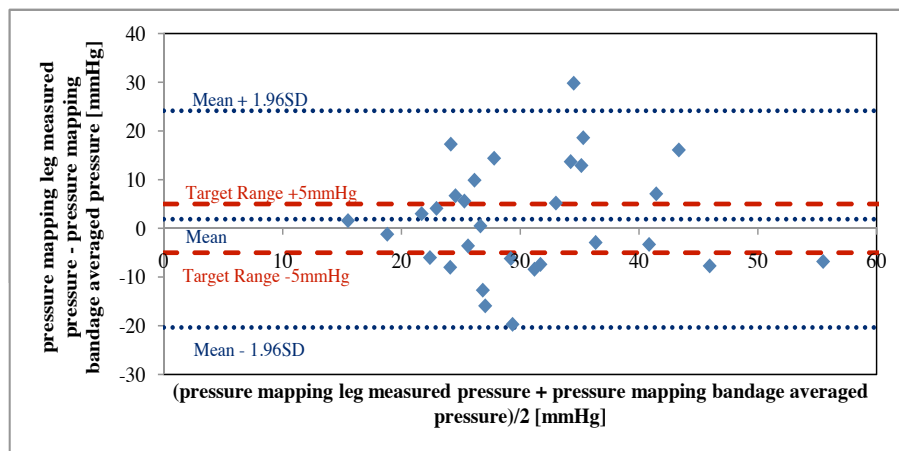


Figure 8.15: Bland-Altman plot for the measured pressures reported by the pressure mannequin leg and the averaged pressures reported by the second pressure-mapping bandage prototype

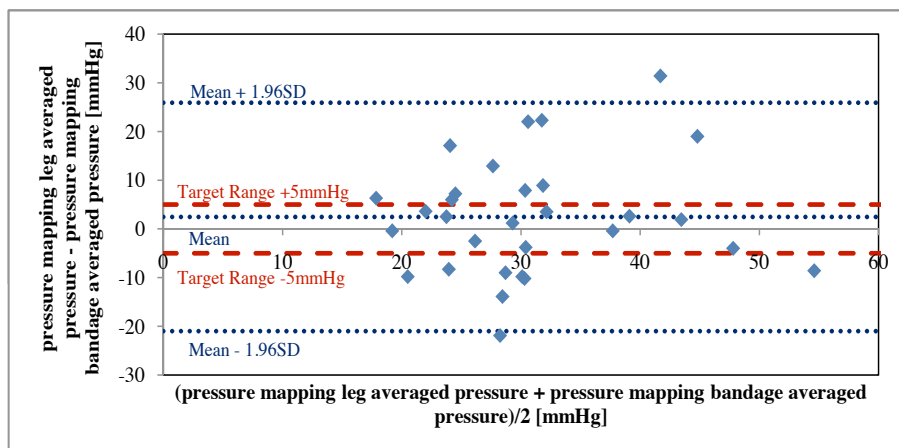


Figure 8.16: Bland-Altman plot for the anatomical level averaged pressures reported by the pressure mannequin leg and the averaged pressures reported by the second pressure-mapping bandage prototype

Comparing the pressure ratios shows that the pressure-mapping bandage reported the same gradient description as the pressure-mapping mannequin leg measured and averaged pressures in 57% and 60% of the cases respectively. These results suggest that the pressure-mapping bandage can be used for qualitative purposes.

8.4 Summary

This chapter presented the design and development of two pressure-mapping bandage prototypes and detailed the experimental work carried out to validate and test these

prototypes using pressure-mapping mannequin leg. These prototypes are believed to be the first of their kind and the results of the preliminary tests suggest that they could be used to provide qualitative feedback about the pressures applied by MCBs. In spite of their modest accuracy, they still showed agreement in pressure values with the pressure-mapping mannequin leg in 30 – 40% of the cases. They also provided similar information as the mannequin leg about the pressure gradient in 60 – 70% of the cases. These are promising initial results.

The first bandage prototype is an example for how a bandage could be transformed to a pressure-mapping system. However, its main drawback is that it can only provide pressure readings after applying the bandage and connecting the sensors. The second pressure-mapping bandage prototype is in the form of tubular bandage. Indeed, it did resolve the problem of providing information about pressure applied during bandage application, which could enable clinicians to tailor their bandaging application while they apply the bandage. However, the problem with this new design is that itself applies some pressure to the leg. This could be resolved by attaching the sensor to the inner side of the tubular bandage. In addition, wiring is still an issue, which could be fixed by using longer custom FlexiForce sensors.

Chapter 9

Compression Bandages Training System

This chapter reports an experimental study to assess the feasibility and acceptability of using model legs with embedded pressure sensors as a training tool for student nurses and identifies errors of application in bandaging techniques of student nurses.

9.1 Introduction

Research suggests that even experienced nurses are not able to apply compression bandages with the target pressure profile [67–69]. Researchers have recommended continuous learning for nurses [67–69; 126] and the usage of pressure measurement devices for quality control [69; 126]. To date, no work has been carried out to check the feasibility and acceptability of using model legs with embedded sensors as a training tool for nurses. In addition, according to the literature review, no research has been carried out to evaluate the early bandaging skills of student nurses to see if they make the same errors in application as experienced nurses. This chapter will report on an experimental study to assess the feasibility and acceptability of using model legs with embedded pressure sensors as a training tool for student nurses and identify errors of application in bandaging techniques of student nurses.

9.2 Methods and Materials

Training Pressure-Mapping System

The pressure-mapping leg mannequin reported in Section 6.3.3 was used in this experiment to train nurses and assess their performances. New circuitry was designed and placed within a plastic box to form a processing unit. The processing circuitry output was then connected to a Mass Term 6225 USB DAQ card through a screw terminal (LPR-68) Figure 9.1.

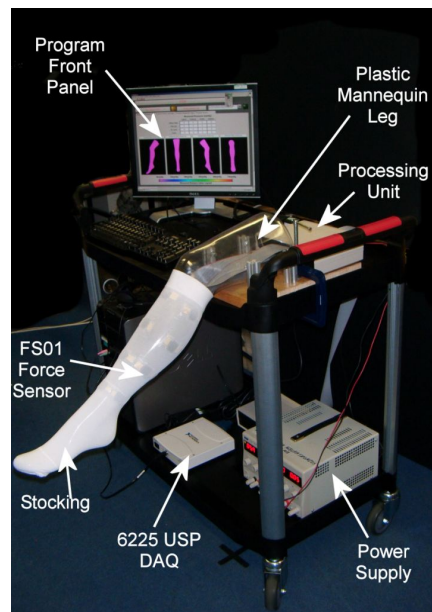


Figure 9.1: The training pressure-mapping system.

New calibration 5^{th} order polynomial fitting-lines were obtained for the FS01 sensors from the calibration data reported in Section 6.3.3 using a program written in LabView 8.6. The 5^{th} order polynomial fitting-line was used instead of a 3^{rd} order polynomial fitting line to improve the sensor accuracy at low pressure values.

A new program was written in LabView 8.6 to acquire the signals, display them, convert them to the equivalent pressure values using calibration fitting-lines and average the 4 FS01 sensor values at ankle, gaiter, mid-calf and below knee. It displayed the measured and average pressure values numerically, mapped the measured pressures on a 3D representation of the leg mannequin and stored the voltages, the measured pressures and the average pressure values in separate files for further processing. The signals were sampled at $1kHz$ and a software based 3^{rd} order low pass filter with $1Hz$ cut-off frequency was used to filter out the signal. The program was designed to zero the pressures on demand. In addition, a piece of code was written in the program to compare the average pressure with the target pressure profile $40mmHg$ at ankle decreasing to $20mmHg$ below knee. After comparing the average pressure and the target pressures the program provides the user with text feedback about the pressure applied; higher or lower than target pressure, and visual feedback by mapping the difference between the target and applied pressures on a diagnostic pressure map on the mannequin leg. This displays white for pressures $20mmHg$ higher than target pressure values, red for pressures $10mmHg$ higher than target pressure values, green for no difference, light blue for pressures $10mmHg$ lower than target pressure values and pink for pressures $20mmHg$ lower than target pressure values. Figures 9.2 and 9.3 show the program front panel and flow chart of the training pressure-mapping system program.

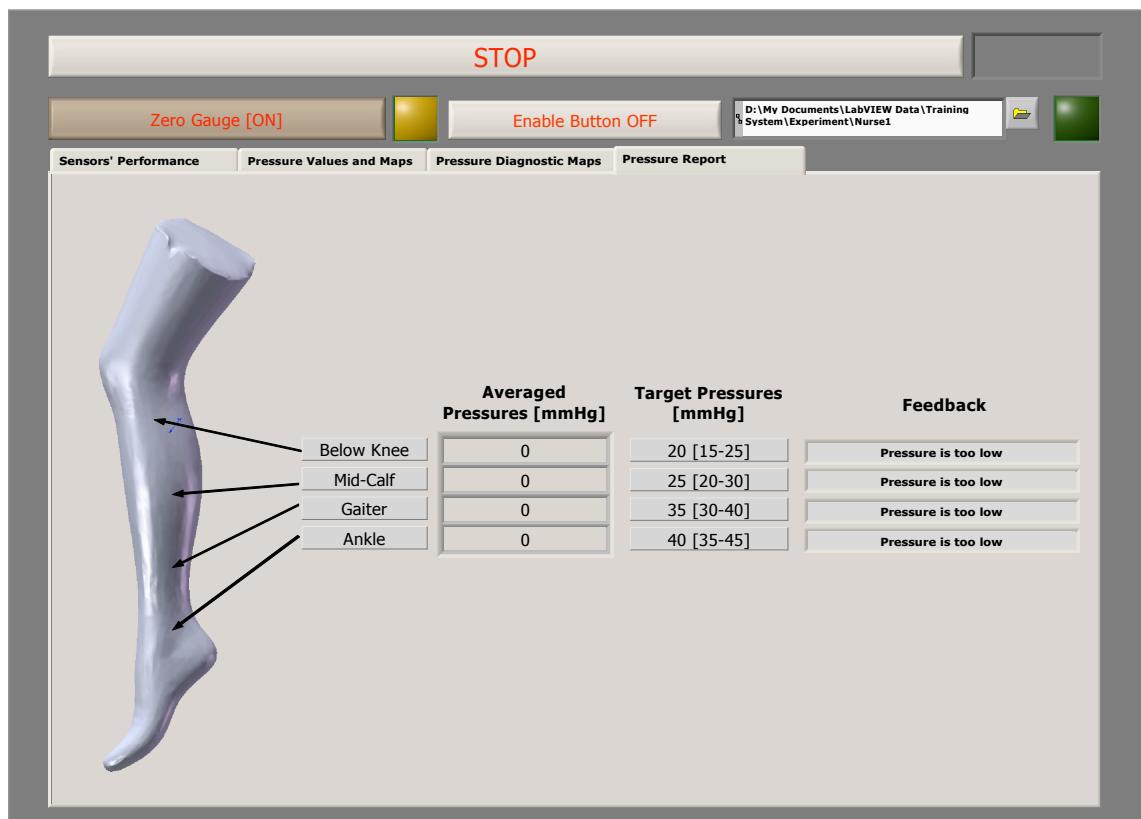


Figure 9.2: The front panel of the display program for the training system.

Subjects

21 student nurses participated in the study. They were offered the opportunity to check their bandaging skills with the pressure-mapping leg while attending bandaging workshops conducted by Prof. E.A. Nelson. These were held during the nursing skills week in the School of Healthcare at University of Leeds. Nurses attended one of six bandaging workshops, each of 90 minutes long. Nurses were offered the opportunity to test their bandaging skills in the last thirty minutes of each workshop session.

All nurses participated in the study did gave their consent to use the data gathered in the study and any photographic images for research publications. The study was approved by the School of Healthcare Research Ethics Committee at University of Leeds. A copy of the approval and the information sheet given to the students is provided in Appendix B. The information sheet was given to the nurses more a week in advance of the workshop.

Bandages and Bandaging Techniques

Participating students were asked to apply a padding layer followed by one SurePress bandage, using spiral 50% overlap technique to the pressure-mapping mannequin leg (Figure 9.4). The participants were asked to try to apply the compression bandage to achieve 40mmHg at the ankle, 35mmHg at the gaiter, 25mmHg at the widest girth of the calf

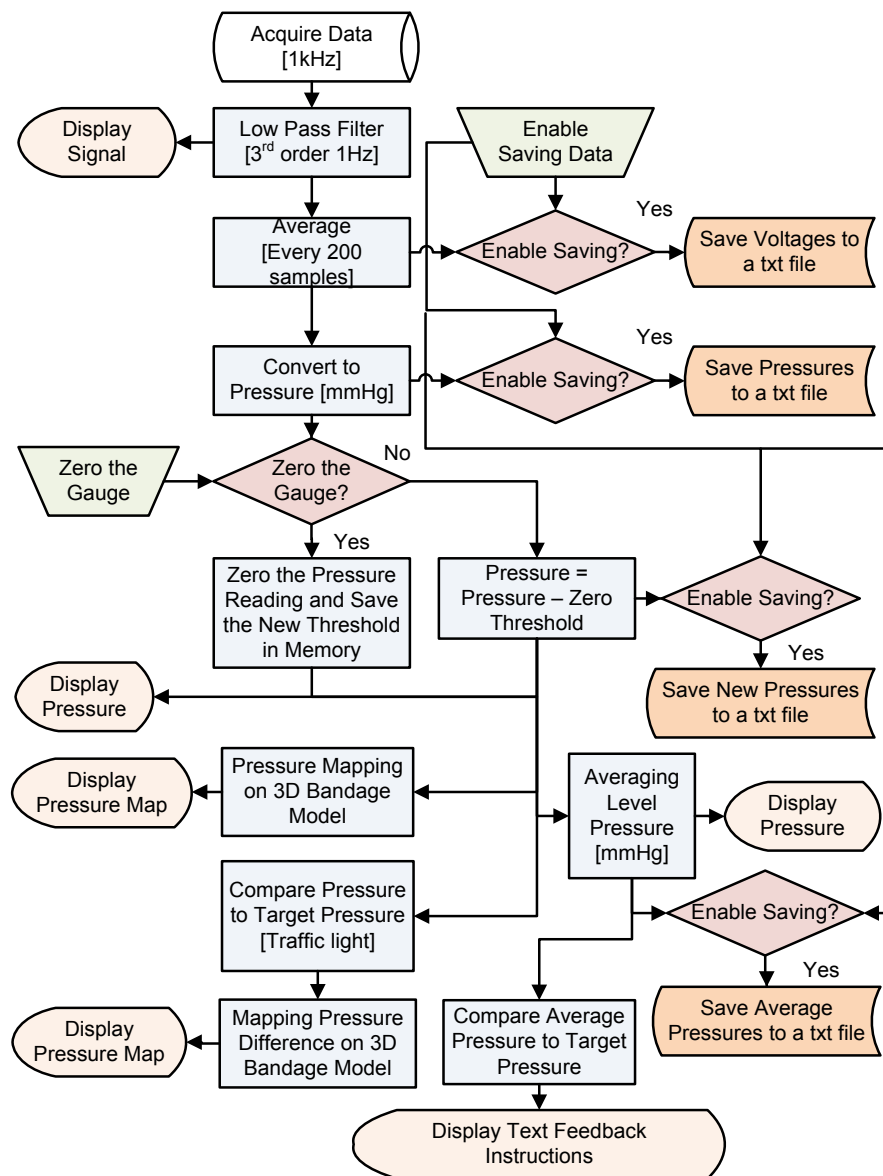


Figure 9.3: The flow chart of the display program for the training system.

and an average of 20mmHg at the knee. In order to achieve this the student had the help of the bandage skills session and the visual feedback from the SurePress bandage printed rectangles which transforms to squares when applied with the appropriate amount of extension.

Questionnaire

A questionnaire was used to evaluate the acceptability of the system by the student nurses. In addition, the questionnaire was used to check whether student nurses preferred having numbers or coloured maps as feedback on bandage application. The results of the ques-

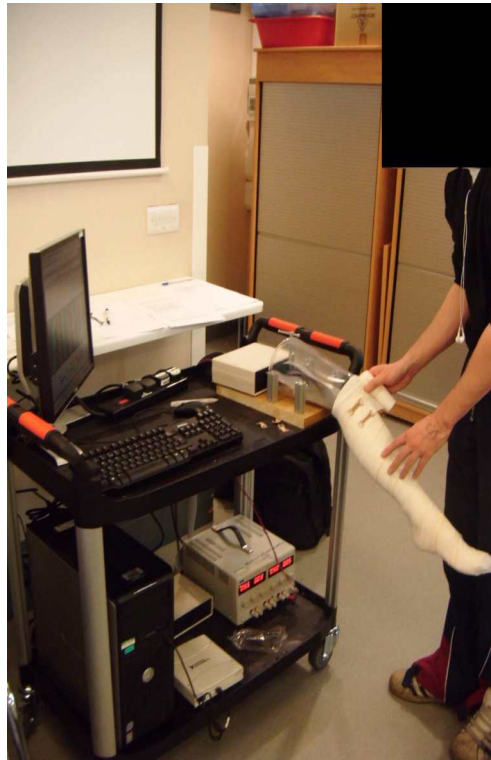


Figure 9.4: A nurse applying SurePress bandage to the training system.

tionnaire will be used as design recommendation for any further instrumentation to be developed for users of compression bandages. A copy of the questionnaire is available in Appendix B.

Statistical Analysis

Questionnaire: Frequency count is used to summarize nurses responses.

Amount of pressure applied: The overall bandaging performance is summarized using frequency count, where the average measured values for each level i.e. ankle, gaiter, calf and knee, is categorised into three groups: lower than target ($< (target - 5mmHg)$), around the target ($\pm 5mmHg$ of target), and ($> (target + 5mmHg)$) for each level. This is used to report the percentage of nurses who were able to achieve the target pressures regardless of the presence of the correct gradient or not.

In addition, the percentage of nurses who were able to apply average pressure within the target range for at least one level, at least two levels, at least three levels, all levels correct and none of the levels correct is also quantified.

Distribution of pressure applied: The overall performance with regards to achieving the desired mid-calf/ankle and below-knee/ankle pressure ratio is categorised into two groups: pressure ratio < 1 and pressure ratio $=$ or > 1 . Frequency count will again be

used to report the number of nurses who managed to achieve the correct ratio of less than 1 (indicating graduated pressure from ankle to knee).

9.3 Results, Analysis and Discussion

Feasibility of Using Training Pressure Measurement System to Train Student Nurses

The total amount of time available for the study was 540 minutes, which 180 minutes were allocated to introduce the system to the potential participants, answering their questions, asking them to sign the consent and photographic agreement forms, applying the cotton wool bandage and the SurePress bandage by nurses, providing the nurses with both vocal and printed feedback about their bandaging skills and then asking them to fill answer the questionnaire. Ten minutes was allowed for each nurse. Each nurse was expected to take 5 minutes to apply the two bandages. However, some nurses took less time applying the bandage, with average time being 4 minutes (Table 9.1). These results indicate that the usage of the system to train nurses is feasible. It is worth mentioning that no problems were noted during the study with respect to the system performance or its usage.

Acceptability of Using Training Pressure Measurement System to Train Student Nurses

The student nurses responses are summarized in Table 9.2. It shows that student nurses found the system extremely useful and with 84% saying that they would use the system to practice if it was available.

The Type of Feedback Preferred by Student Nurses

Table 9.2 shows that most nurses preferred the graphical display colour map. Mainly this was due to its ability to show them exactly where the problems with their bandaging technique were. This was made very easy using the pressure map, which analyzed the pressures applied, compared them to the target pressures and then illustrated the results on the 3D model of the mannequin leg. These results suggest that nurses would prefer a qualitative representation of the pressure they apply rather than exact numbers.

Amount of Pressure Applied

The nurses' pressure performance is summarized in Figure 9.5 and Tables 9.1 and 9.3. Average pressure results show that the vast majority of nurses were unable to apply the required pressures at the ankle and gaiter. This is echoed clearly in Figure 9.5, as results shows fewer nurses were able to apply the bandages with the right amount of pressure at the ankle and gaiter, with majority applying bandages with lower pressures than the target pressure. This reflects results reported by other researchers for experienced nurses

Table 9.1: Summary of average pressures applied by student nurses to the training pressure measurement system and the time they taken to apply the padding bandage and SurePress bandage.

Nurse No.	Ankle [mmHg]	Gaiter [mmHg]	Mid-Calf [mmHg]	Below Knee [mmHg]	Application Time [s]
1	37	35	20	16	179
2	18	18	16	9	167
3	17	15	21	15	130
4	49	27	24	15	169
5	28	22	30	14	464
6	20	19	23	11	339
7	75	43	27	25	289
8	24	25	20	9	275
9	24	33	24	22	266
10	20	24	23	10	314
11	33	33	33	26	154
12	27	24	21	21	474
13	30	30	25	16	117
14	21	24	25	7	213
15	25	27	35	19	260
16	39	29	17	24	182
17	32	24	30	19	163
18	47	39	46	24	242
19	47	29	18	12	170
20	34	17	18	16	231
21	27	24	20	16	256
Median	28	25	23	16	231
Mean	32	27	25	16	241
SE	3	2	2	1	21

[7; 67–69]. Results in Table 9.3 illustrate that only one of the nurses was able to apply the bandage with the correct amount of pressures at the four different levels.

Distribution of Pressure Applied

The student nurses ability to apply the bandages with graduated pressure is summarized in Figure 9.6 and Table 9.1. Average pressure results show that nurses were able to apply the SurePress bandage with a pressure gradient. This is also demonstrated in Figure 9.6, which shows that 62% of student nurses have achieved a mid-calf/ankle ratio of less than 1 and all of them achieving below-knee/ankle ratio of less than 1. Nelson [7] reported that even after training, 64% of experienced nurses applied bandages with higher pressure at the calf than ankle. Taylor et al. [68] reported that even after training, 50% of nurses applied bandages with higher calf/ankle pressure than 1. For knee/ankle ratio, Taylor et al. [68] found that 81% of experienced nurses applied the bandage with the desired pressure ratio of less than 1. This increased to 94% after training. Student nurses seem to be more able to apply bandages with correct pressure gradient more often than experienced nurses

Table 9.2: Summary of student nurses' response to the questionnaire.

Did you find the leg helped in providing you with feedback about your bandaging skills?				
Helped a lot	Helped a little	Neutral	Hindered a little	Hindered a lot
100%	0%	0%	0%	0%
If this system was available for you to use again would you use it?				
Definitely yes	Probably yes	Not sure	Probably not	Definitely not
86%	14%	0%	0%	0%
You have recieved both graphical colour map and average print-out numeric feedback.Which of these two more useful to interpret?				
Graphical colour map	Average numeric		Both methods	
79%	10%		10%	

Table 9.3: Percentage of nurses applied the correct amount of pressures for at least one level, two levels, three levels and four levels.

No level	One level at least	Two levels at least	Three levels at least	Four levels
10%	90%	52%	14%	5%

immediately after training but this needs to be further verified with a bigger study that involves both student and experienced nurses.

9.4 Summary

This chapter detailed a study conducted using the pressure-mapping mannequin leg to test the feasibility and acceptability of such a system for training purposes for student nurses. Results indicate that using such a system for training purposes is possible as the system was welcomed by the student nurses who took part in the study.

The study also evaluated the pressures and pressure gradient ratios applied by student nurses and compared them to pressure and pressure gradient ratios applied by experienced nurses published by other researchers. Results indicate, that student nurses apply bandages with lower than target pressures at the ankle and gaiter. However, more student nurses were able to apply bandages with graduated pressure compared to experienced

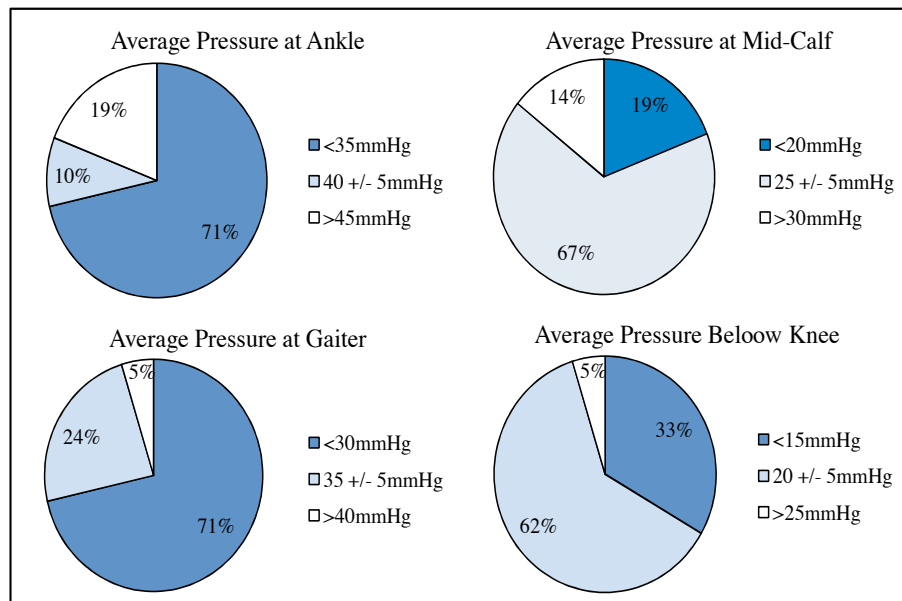


Figure 9.5: Percentage of nurses applying higher, within and lower than the target pressure at ankle, gaiter, mid-calf and below knee.

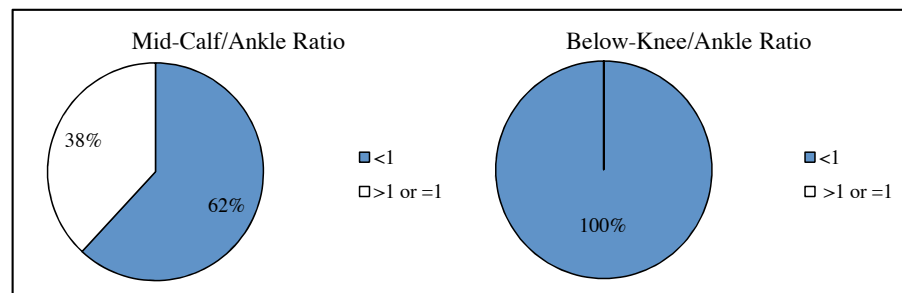


Figure 9.6: Percentage of nurses applying mid-calf/ankle and below-knee/ankle pressure ratio higher than or equal to one and lower than 1.

nurses. According to the literature review, this study is the first of its kind.

Furthermore, student nurses preferred a graphical coloured map as a feedback to a numerical report. This might indicate that nurses are more concerned about the quality of their bandaging in terms of pressure gradient and applying bandages with close pressure to the target pressures, than being concerned about the exact pressure values. This might provide a good support to further develop the pressure-mapping bandage reported in Chapter 8.

Chapter 10

Summary and Conclusions

This chapter summarizes the findings in this research, with reference to the new and novel investigations that have been conducted. It investigates whether the aims of the research have been successfully achieved, and it draws conclusions that can be derived from the previously discussed results. Finally, recommendations for future work in the field are made.

10.1 Summary of the Findings and Contribution to the Field

Venous ulcers are chronic open wounds which have a slow healing tendency and are caused, by definition, by chronic venous insufficiency. Compression therapy in the form of medical compression bandages and medical compression stockings is the corner stone in the treatment and prevention of re-occurrence of venous ulcers. It is known that pressure applied by compression bandages is proportional to the tension with which these bandages are applied and inversely proportional to the limb radius. Yet, very little work has been carried out to understand the factors influencing the pressure applied by compression therapy. Many devices have been developed in the last few years to measure the pressure under compression bandages. Nevertheless, very little has been done to evaluate the accuracy and reliability of these devices. In addition, none of these devices could be used to map the pressure under compression bandages as most of them support pressure measurement at one point only. This body of work has investigated the physics behind the ability of a bandage to apply pressure, some of the factors influencing compression therapy, and experimental validation for some of the mathematical concepts. In addition, it has demonstrated the development of a number of pressure-mapping systems and has reported on the experimental work carried out to test these devices. It has demonstrated the development of a pressure-mapping measurement system that can be used in vivo to map the pressure at 40 different measurement points with modest accuracy, which could be increased using averaging techniques. Furthermore, it has detailed the development of two pressure-mapping bandage prototypes and their experimental validation. The thesis also reports a study to test the feasibility and acceptability of a pressure-mapping system

for training student nurses in how to apply compression bandaging.

10.1.1 Mathematical Examination of the Interface Pressure

Analysis showed that the effect of bandage thickness on the pressure produced by one layer of bandage is clinically insignificant. However, the mathematical equations derived provided an explanation for the experimental results reported by other researchers and enabled a simulation of the pressures applied by a bandage to a 3D model for a real leg with known digital cross sectional profiles. The simulation, which is a novel contribution of this work, showed that pressure peaked on the Achilles tendon and upper parts of the shin bone, close to the tibial tuberosity. However, these peak pressures were not found over other crucial places like the lateral and medial malleolus. This might be due to the fact that the simulation was done for only the circumferential curvature of the leg. The models developed were compared to data obtained using an experimental setup which confirmed the validity of the model which takes in consideration the bandage thickness (Section 3.3).

Analysis also showed that Thomas's approach [75] of using simple multiplication of the number of MCB layers with the pressure applied with one layer to estimate the overall pressure will result in errors in pressure estimation, with significant errors even for a few small number of bandage layers over sharp edges. The results also helped to explain the so-called pressure damping effect when bandages are applied within multi-component MCBs compared to their performance when applied directly to the leg. Experimental results showed that the models, which take in consideration the increase in limb radius due to the former applied bandage layers, reported pressure values that are not statistically different from the measured pressure values, while the model, which does not take in consideration the increase in limb radius due to the former applied bandage layers, reported pressures which are statistically different from the measured pressure values (Section 3.4).

Moreover, the effect of biaxial tension-compression forces in bandage on the interface pressure was addressed for the first time and found to have a significant effect on the interface pressure at sites with sharp longitudinal curvatures like the malleolus for example. This, when combined with the impact of the MCB application angle, might explain why nurses apply a reverse gradient pressure profile even when they apply MCBs with constant tension over a leg with ankle circumference smaller than below knee circumference. This was attributed to nurses applying bandage with an angle at the ankle and at right angle below the knee to secure the bandage in position. In addition, modeling the application angle effect on the interface pressure illustrated that as the angle between the MCB and the limb vertical axis, parallel to the median plane, decreases the pressure applied by the bandage increases first and then decreases. The amount of increase will depend on the amount of tension forces developed in the transverse direction of the bandage, if all other variables were kept constant (Sections 3.5 and 3.6).

Additionally, the thesis explored the impact of the change in limb shape secondary to

calf muscle contraction on the interface pressure. A mathematical model based on thick wall cylinder theory was shown to simulate bandage performance in dynamic situations if the Chord modulus of that bandage is known (Section 3.7).

The Vinckx et al. [86] model was used to estimate the perturbation in pressure measurement due to sensor aspect ratio and it was experimentally tested and found to be not in agreement with the experimental results. However, the experimental work confirmed that increasing the sensor thickness will result in overestimating the pressure, which can be reduced by increasing its diameter or length of the sensor (Section 3.8).

10.1.2 Experimental Evaluation of Medical Compression Bandages

SurePress and Comprilan bandages' tension-elongation relationship was explored. The results indicated that SurePress bandage has more linearity, more consistent loading tension curves, smaller hysteresis, higher static forces at low extensions and more durable pressure than Comprilan. Tension forces developed in the transverse direction for both bandages were found to be $1 - 2N$ even when the bandage was compressed by as little as 2% in the transverse direction secondary to extension in the length direction (Sections 4.4 and 4.5).

A new method to classify compression bandages based on Chord modulus was presented in this thesis and the experimental setup to obtain these values was detailed. The outcomes suggest that Chord modulus can be used to classify compression bandages and hence can be used instead of other classification methods suggested by researchers in the field, which are based on expensive in vivo experiments (Section 4.6).

10.1.3 Pressure Sensors Characteristics

The PicoPress sensor was found to have low nonlinearity, repeatability and hysteresis errors. It overestimated the pressure applied by MCBs due to the sensor physical dimensions. This was as much as 48% when PicoPress sensors were used to measure the pressure applied by compression bandages to a cylinder with $0.114m$ diameter (Section 5.4).

FS01 force sensors had a good level of accuracy when tested over a flat surface. However, experimental results showed that the sensor's sensitivity to pressure when embedded in a cylinder (and pressure applied with aneroid sphygmomanometer) was twice as much as its sensitivity to pressures applied by deadweights on a flat surface. This suggests that these sensors, should be calibrated by applying pressure to them over a curved surface using material that is conformable like a sphygmomanometer cuff (Section 5.5).

Despite having more repeatability errors compared to $12mm$ diameter active sensing area FSR, FlexiForce sensor was selected to be used in the pressure measurement system and the pressure-mapping bandage. FlexiForce sensors showed better linearity, good sensitivity to low pressure values and the lowest drift errors. FSR sensors were not sensitive to low pressure values with high drift error. Tactilus sensor suffered from significant stability deficiencies (Section 5.6).

The dynamic response for a step input for a 1^{st} order system model for FlexiForce

sensors suggests that the sensor's time constant is much higher than $30ms$ reported by other researchers, and certainly higher than the $5\mu s$ response time claimed by the Tekscan. Results suggest that FlexiForce bandwidth is in the range of $0.126 - 0.594Hz$, which explains the degradation in its output when subjected to long-duration, low-frequency and high-amplitude force. Temperature variation had insignificant effects on the sensor's output for low pressure inputs, when the temperature and temperature variation were low. Calibration of sensors at room temperature is therefore sufficient for sensors in contact with human skin (Section 5.7).

Furthermore, using averaging for multiple FlexiForce sensors was confirmed experimentally to increase the accuracy of the measurement (Section 5.7).

10.1.4 Pressure-Mapping Reference Systems

A number of pressure-mapping reference systems were developed (Sections 6.2, 6.3 and 6.4). These systems could be used to study MCBs, report on bandaging skills and evaluate new pressure measurement products. Bandage extension was found to be an inadequate and unreliable feedback method to control the interface pressure applied by MCBs. This suggests that current practice of marking bandages with constant intervals and the usage of geometrical shapes that change during bandage application might need to be improved or replaced by another method (Sections 6.2, 6.3 and 6.4 and Chapter 7).

FlexiForce arrays, when calibrated on a curved surface using aneroid sphygmomanometer and window averaging, have outperformed PicoPress transducers. Even after window averaging, FlexiForce arrays accuracy error was more than $\pm 5mmHg$, which means they can only be used for qualitative purposes and not for accurate measurements. However, the results indicate that FlexiForce sensors have the potential to measure the interface pressure. It also raise concern about studies reported by other researchers, who used pressure transducers with thick probes, as all their measurement results might have been significantly overestimated (Sections 6.2, 6.3 and 6.4, and Chapter 7).

10.1.5 Pressure-Mapping Measurement System

A pressure-mapping measurement system which uses arrays of FlexiForce sensors was designed and developed. The system can be utilized to map the pressure at 40 measurement points. This study reported the use of the system to study the pressure applied by MCBs to a participant's leg at 32 points. This is twice as many pressure measurement points as any other study found in the literature. The maps obtained by the pressure-mapping measurement system were compared for validation purposes with the pressure maps computed from MCBs extension and the pressure maps obtained by using arrays of PicoPress probes. Results showed that FlexiForce arrays, when calibrated on a curved rigid surface using an aneroid sphygmomanometer and window averaging, might provide more reliable pressure maps than PicoPress sensor. However, the reported pressure-mapping system is only capable of providing pressure maps which could be used for qualitative purposes such

as: identifying the areas on the leg which are subjected to high pressures and assessing whether MCBs are applied with gradual pressure profile (Chapter 7).

10.1.6 Pressure-Mapping Bandage

Two pressure-mapping bandage prototypes were designed and developed. Preliminary experimental work was carried out to validate and test these prototypes using pressure-mapping mannequin leg. These prototypes are believed to be the first of their kind and the results of the preliminary tests suggest that they could be used to provide qualitative feedback about the pressures applied by MCBs. In spite of their modest accuracy, they still showed approximately 30 – 40% agreement in pressure values with the pressure-mapping mannequin leg. They also provided similar information to the data reported by the mannequin leg about the pressure gradient in 60 – 70% of the cases. These results are promising (Chapter 8).

10.1.7 Compression Bandages Training System

The use of a pressure-mapping mannequin leg for training purposes was feasible and welcomed by student nurses. The study also found that student nurses like experienced nurses apply bandages with lower pressures at the ankle and gaiter than the nominal target pressures. However, unlike experienced nurses, the majority of student nurses were able to apply bandages with a gradual pressure immediately after training in bandaging. According to the literature review, this study is the first of its kind (Chapter 9).

10.2 Assessment of the Research Objectives

In Chapter 1, the objectives of this research were set. This section evaluates the extent to which these objectives were achieved.

1. *To investigate theoretically the factors that influence the sub-bandage pressures and model them mathematically. The models then need to be verified experimentally.*

The impact of bandage thickness, multilayering, biaxial forces, angle of application and limb curvature were all investigated theoretically in Chapter 3. The models developed for single-layers and multi-layers of bandage were shown experimentally to report pressures which are not statistically different from the measured pressures. However, further experimental work is needed. In addition, the impact of sensor aspect ratio on the interface pressure was investigated. The experimental work failed to validate the model proposed by Vinckx et al. [86], The impact of friction was not studied.

2. *To explore flexible pressure sensors which can be utilized to design pressure-mapping bandages and evaluate their static performance in terms of accuracy, repeatability, hysteresis and drift.*

Comparative tests of the static performance of resistive based flexible sensors were conducted and reported in Chapter 5. FlexiForce sensors were found to have an overall better performance and hence were selected to be used in a custom pressure measurement system and to be attached to a bandage to form the pressure-mapping bandage.

3. *To design pressure-mapping leg systems with distributed embedded or mounted pressure sensors to study MCBs and validate pressure-mapping bandages.*

Eight pressure-mapping systems were developed using arrays of PicoPress sensors, arrays of FlexiForce sensors and embedded arrays of FS01 sensors (see Chapter 6). Three of these systems were constructed using a rigid cylinder, three were constructed using a plastic mannequin leg and two were mounted over a soft leg model. All these systems were used to study MCBs and to compare the sensing technologies. The FS01 pressure-mapping mannequin leg was used to test pressure-mapping bandage prototypes and also used for training purposes.

4. *To design a pressure measurement system using custom arrays of sensors in order to map the pressure applied by MCB to a real leg.*

This was fully achieved by constructing a pressure measurement system using custom arrays of FlexiForce sensors that could be used to map the pressure at 40 measurement points (see Chapter 7). The usage of window averaging limits the measurement points to 35, however, this increases the system accuracy. Nevertheless, the system could only be used for qualitative measurements and not for quantitative measurements due to its low accuracy.

5. *To design a user interface that can acquire the signals from distributed sensors, convert the acquired signals to the equivalent pressure values, display the calculated pressure values using a graphical map and store the measured values for post-processing.*

This was fully achieved and reported in Chapters 6, 7, 8 and 9. The current program could even provide the user with some assessment of the pressures applied comparing to a pre-defined pressure profile.

6. *To design a prototype pressure-mapping bandage by attaching flexible sensors to MCB and test their performance with the pressure-mapping leg systems.*

Chapter 8 demonstrated the development of two pressure-mapping bandage prototypes and reported on their testing using the pressure-mapping mannequin leg. These preliminary experiments show promising results. However, further experiments on softer tissues and real legs are required.

7. *To test the feasibility and acceptability of using pressure-mapping systems for training purposes.*

Chapter 9 reported on the feasibility and acceptability of using a pressure-mapping mannequin leg for training purposes. Results show that the system could be used in a teaching environment for training purposes. Student nurses who took part in the study provided very positive feedback with a majority showing their willingness to practice their bandaging skills on the device.

10.3 Conclusions

A summary of the conclusions drawn from this research are listed below:

- Bandage thickness should be considered in the process of estimating pressures from tension applied in the case of applying multi-layering MCBs.
- From theoretical simulations, areas with sharp bony curvatures in the lower limb would see much higher pressures than adjacent sites with a large radius of curvature. This supports the idea of covering these bony structures with wool cotton paddings to protect them from high pressures.
- Biaxial forces generated in the bandage transverse direction secondary to bandage extension and the angle of application would have a severe impact on the interface pressure theoretically. From analytical point of view, these factors will play a greater role in sites with small radius of curvature like the malleolus.
- Nonlinearity, hysteresis shape and inter-variation in the bandage tension-elongation curves and creep are among the most important factors that affect the accuracy of the pressure estimated from the elongation in the bandage, when it is applied to a curvature with known radius.
- Chord modulus which could be estimated from in vitro experimental setup can be used to classify MCBs.
- Sensors physical dimensions were found to impact on the interface pressure estimated by the sensor both analytically and experimentally. However, experimental results do not fit with the analytical calculation for the perturbation in pressure obtained using the model proposed by Vinckx et al. [86] for thin plate sensors.
- PicoPress sensor was found to have good accuracy in terms of low nonlinearity, repeatability and hysteresis errors. However, it overestimates the pressure applied to it due to its physical dimensions. In addition, its capability to be calibrated under compression bandages will result in local stress in the bandage, which will further increase the amount of pressure perturbation and hence error.
- FS01 sensor has very good accuracy (typical $\pm 2mmHg$), however, its rigid material creates sharp edges over any curvature resulting in an impact on the measured pressures where these sensors are embedded in a structure with curved shape.

- FlexiForce sensors outperformed other flexible sensors at low pressures. However, their accuracy is modest (typical $\pm 14\text{mmHg}$) and not sufficient for accurate measurements. However, they could be used for qualitative purposes when multiples of them are used in arrays and the average of the sensors readings is used to report the pressure.
- Extension was found not to provide adequate and reliable feedback for nurses on the pressure they apply to curvatures with known radii.
- Comparative analysis of the measured pressures using different systems with the computed pressures from elongation in the bandage showed low levels of agreement.
- Comparative analysis of pressures measured by FlexiForce sensors and PicoPress sensors suggested that the FlexiForce, when calibrated using aneroid sphygmomanometer and their values reported using averaging techniques, provide more reliable pressure measurements than PicoPress sensors when they are used without correction factors. The usage of correction factor for the pressures measured by PicoPress sensors could improve the reliability of their pressure readings, however, correction factors are calculated from the radius of curvature of the leg which is very difficult to determine within a clinical environment.
- The pressure measurement system constructed using arrays of FlexiForce sensors could be used to map pressures under MCBs when applied to real legs. The qualitative data maps could be used to study the pressures and detect regions with dangerous levels of pressures or low levels of pressures. The information could help clinicians to tailor their bandaging techniques accordingly.
- Pressure-mapping bandage prototypes were tested. Preliminary results demonstrated their ability to provide descriptive information about the pressure gradient. However, they are not suitable, as yet, to be used for accurate measurements. Compared with bandage elongation, these qualitative pressure maps are potentially a huge step forward to more reliable compression bandages for venous ulcers patients.
- The usage of the pressure-mapping mannequin leg for training purposes was welcomed by student nurses, who found it very useful in showing them their bandaging skills strengths and weaknesses.
- Analysis of the pressures applied by student nurses indicated that they apply bandages with low pressures at the ankle and gaiter regions like experienced nurses. Unlike experienced nurses, student nurses applied bandages with the right pressure gradient in the majority of the cases, immediately after a training workshop.

10.4 Future Work

Further work is recommended to address issues covered in this body of work:

- Experimental investigation of the effect of biaxial forces, angle of application and friction forces on the interface pressures.
- Experimental validation of the model proposed to study the impact of limb change on the interface pressures. This should be combined with computational simulation of the impact of change in limb shape on the interface pressures using FEA.
- Remodeling the impact of the sensors physical aspect ratio on the interface pressures and validating it using experimental data, as current models do not fit with the experimental results.
- Further investigation into the biaxial forces generated in the bandage in the transverse direction secondary to extension in the length direction of the bandage.
- Exploring the potential of using capacitive flexible sensors to measure the interface pressure applied by MCBs.
- Explore the usage of both the capacitive and resistive properties of the FlexiForce sensors to further improve their accuracy.
- Further investigation into the impact of temperature variation on the performance of the FlexiForce sensors.
- Explore the nonlinear modulation for the FlexiForce sensors in dynamic situation to enable using them to monitor the interface pressures during locomotion.
- Larger study which involves scanning a large number of legs and mapping the pressures applied to these legs when MCBs are applied to them using the pressure measurement system developed and reported in this body of work.
- The usage of the pressure measurement system and the 3D scanner to map the pressures applied by the MCBs to legs of patients with venous ulcers. This could be combined with MRI studies due to the fact that FlexiForce sensors would not interfere or be affected by the magnetic fields of the MRI system.
- Clinical trials of the pressure-mapping bandage prototypes to evaluate nurses' acceptance for such a system and their feedback about how it could be improved.
- The development of a portable drive and display for the pressure-mapping bandage.
- Further development of the pressure-mapping bandage which includes
 - Better sensor attachment.
 - Better wiring and miniaturizing of the processing circuits.
 - Integrating the sensor into the fabric.

-
- Further development of the training interface to include pattern recognition and intelligence to analyze the pressure maps applied by the user over a period of time and providing the users with instructions to improve their techniques.
 - Further improve the program to enable better usage of the computational power by using state machine programming technique.
 - Redesign the training devices to include a larger number of sensors.
 - Larger clinical trials for the training device with larger number of students and experienced nurses with multiple visits and follow up sessions to investigate the ability of the system to improve the bandaging skills of nurses, and use nurses feedback for further improvements.

References

- [1] J.L. Beebe-Dimmer, J.R. Pfeifer, J. S. Engle, and D. Schottenfeld. The epidemiology of chronic venous insufficiency and varicose veins. *Annals of Epidemiology*, 15(3): 175–184, March 2005.
- [2] J.S. Crane and N.W. Cheshire. Chronic ulceration of the leg. *Surgery*, 22(12): 327–330, 2004.
- [3] M.H. Criqui, M. Jamosmos, A. Fronck, J.O. Denenberg, R.D. Langer, J. Bergan, and B.A. Golomb. Chronic venous disease in an ethnically diverse population: The san diego population study. *Am. J. Epidemiol.*, 158(5):448–456, September 2003.
- [4] C. Ruckley. Socioeconomic impact of venous insufficiency and leg ulcers. *Angiology*, 46(1):67–69, 1997.
- [5] C.V. Ruckley, C.J. Evans, P.L. Allan, A.J. Lee, and F.G. Fowkes. Chronic venous insufficiency: Clinical and duplex correlations. the edinburgh vein study of venous disorders in the general population. *Journal of Vascular Surgery*, 36(3):520–525, 2002.
- [6] S. O’Meara, J. Tierney, N. Cullum, M.J. Bland, P.J. Franks, T. Mole, and M. Scriven. Four layer bandage compared with short stretch bandage for venous leg ulcers: systematic review and meta-analysis of randomised controlled trials with data from individual patients. *BMJ*, 338:b1344, April 2009.
- [7] E.A. Nelson. *A study of patient and nurse factors influencing sub-bandage pressure*. PhD thesis, 2001.
- [8] H. Partsch. The static stiffness index: A simple method to assess the elastic property of compression material in vivo. *Dermatologic Surgery*, 31(6):625–630, 2005.
- [9] H. Partsch, M Clark, S. Bassez, J. Benigni, F. Becker, V. Blazek, J. Caprini, A. Cornu-Thenard, J. Hafner, M. Flour, M. Junger, C. Moffatt, and M. Neumann. Measurement of lower leg compression in vivo: Recommendations for the performance of measurements of interface pressure and stiffness. *Dermatologic Surgery*, 32(2):224–233, February 2006.
- [10] C.M.A. Ashruf. Thin flexible pressure sensors. *Sensor Review*, 22(4):322–327, 2002.

- [11] D. Armstrong, J.A. Caprini, A.J. Comerota, P. Franks, K. Harding, C. Moffat, H. Partsch, T.J. Phillips, W. Vanscheidt, and F. Vin. *Chronic Venous Insufficiency and Venous Ulceration: Aetiology and Treatment*. ConvaTec, 1st edition, 2006.
- [12] B. Eklof. Classifying venous disorder. In J.J. Bergan, editor, *The Vein Book*, pages 111–117. Elsevier Academic Press, San Diego, CA, 1st edition, 2007.
- [13] P. Bachoo. Interventions for uncomplicated varicose veins. *Phlebology*, 24(suppl.1): 3–12, April 2009.
- [14] J.J. Bergan, G.W. Schmid-Schonbein, P.D. Smith, A.N. Nicolaides, M.R. Boisseau, and B. Eklof. Chronic venous disease. *N Engl J Med*, 355(5):488–498, August 2006.
- [15] G.M. Andreozzi, R. Cordova, M.A. Scomparin, R. Martini, A. D’Eri, and F. Andreozzi. Quality of life in chronic venous insufficiency. *International Angiology*, 24(3):272–277, 2005.
- [16] D. Bergqvist, C. Lindholm, and O. Nelzén. Chronic leg ulcers: the impact of venous disease. *Journal of Vascular Surgery*, 29(4):752–755, April 1999.
- [17] K. Finlayson, H. Edwards, and M. Courtney. Factors associated with recurrence of venous leg ulcers: A survey and retrospective chart review. *International Journal of Nursing Studies*, 46(8):1071–1078, August 2009.
- [18] J. Bergan. Risk factors, manifestations, and clinical examination of the patient with primary venous insufficiency. In J.J. Bergan, editor, *The Vein Book*, pages 119–124. Elsevier Academic Press, San Diego, CA, 1st edition, 2007.
- [19] M.H. Criqui, J.O. Denenberg, R.D. Langer, R.M. Kaplan, and A. Fronck. Epidemiology of chronic peripheral venous disease. In J.J. Bergan, editor, *The Vein Book*, pages 27–37. Elsevier Academic Press, San Diego, CA, 1st edition, 2007.
- [20] E.A. Nelson, D.R. Harper, R.J. Prescott, B. Gibson, D. Brown, and C.V. Ruckley. Prevention of recurrence of venous ulceration: randomized controlled trial of class 2 and class 3 elastic compression. *Journal of Vascular Surgery*, 44(4):803–808, October 2006.
- [21] K.L. Moore and A.F. Dalley. *Clinically Oriented Anatomy*. Lippincott Williams & Wilkins, 5th edition, 2006.
- [22] E.N. Marieb and K. Hoehn. *Human Anatomy and Physiology*. Pearson Benjamin Cummings, 7th edition, 2007.
- [23] S. Standring, editor. *Gray’s Anatomy*. Elsevier Churchill Livingstone, 39th edition, 2005.
- [24] G. Mozes and P. Głowiczki. Venous embryology and anatomy. In J.J. Bergan, editor, *The Vein Book*, pages 15–25. Elsevier Academic Press, San Diego, CA, 2007.

- [25] M.H. Meissner, G. Moneta, K. Burnand, P. Gloviczki, J.M. Lohr, F. Lurie, M.A. Mattos, R.B. McLafferty, G. Mozes, R.B. Rutherford, F. Padberg, and D.S. Sumner. The hemodynamics and diagnosis of venous disease. *Journal of Vascular Surgery*, 46(6):S4–S24, December 2007.
- [26] Oxford University. *The New Oxford American Dictionary*. Oxford University Press, 2nd edition, 2005.
- [27] A.M.N. Gardner and R.H. Fox. *The return of blood to the heart: venous pumps in health and disease*. John Libbey & company Ltd, 2nd edition, 1993.
- [28] H. Partsch. Understanding the pathophysiological effects of compression. *EWMA Position Document. Understanding compression therapy*. London: MEP Ltd, pages 2–4, 2003.
- [29] C.N. Etufugh and T.J. Phillips. Venous ulcers. *Clinics in Dermatology*, 25(1):121–130, February 2007.
- [30] C. Moffatt. *Compression Therapy in Practice*. Wound UK Publishing, 1st edition, 2007.
- [31] A. Bradbury and C.V. Ruckley. Clinical assessment of patients with venous disease. In P. Gloviczki and J.S.T. Yao, editors, *Handbook of Venous Disorder*. Oxford University Press, Oxford, 2nd edition, 2001.
- [32] J. Reichenberg and M. Davis. Venous ulcers. *Seminars in Cutaneous Medicine and Surgery*, 24(4):216–226, 2005.
- [33] J.K. Raines and J.I. Almeida. Role of physiology testing in venous disorders. In J.J. Bergan, editor, *The Vein Book*, pages 47–55. Elsevier Academic Press, San Diego, CA, 1st edition, 2007.
- [34] P.D. Coleridge-Smith. Leg ulcer treatment. *Journal of Vascular Surgery*, 49(3):804–808, March 2009.
- [35] S. O’Meara, N.A. Cullum, and E.A. Nelson. Compression for venous leg ulcers. *Cochrane Database of Systematic Reviews*, (1), 2009.
- [36] E.A. Nelson, S.E. Bell-Syer, and N.A. Cullum. Compression for preventing recurrence of venous ulcers. *Cochrane Database of Systematic Reviews (Online)*, (4), 2000.
- [37] H. Partsch. Mechanism and effects of compression therapy. In J.J. Bergan, editor, *The Vein Book*, pages 103–109. Elsevier Academic Press, San Diego, CA, 1st edition, 2007.

- [38] C. Moffatt. Four-layer bandaging: From concept to practice. part 1: The development of the four-layer system. *World Wide Wounds*, December 2004. URL <http://www.worldwidewounds.com/2004/december/Moffatt/Developing-Four-Layer-Bandaging.html>.
- [39] H. Partsch. Do we still need compression bandages? haemodynamic effects of compression stockings and bandages. *Phlebology*, 21(3):132–138, 2006.
- [40] R.S.A. Lord and D. Hamilton. Graduated compression stockings (20-30mmHg) do not compress leg veins in the standing position. *ANZ Journal of Surgery*, 74(7):581–585, 2004.
- [41] B. Partsch and H. Partsch. Calf compression pressure required to achieve venous closure from supine to standing positions. *Journal of Vascular Surgery*, 42(4):734–738, October 2005.
- [42] A. Mostbeck, H. Partsch, and L. Peschl. Änderungen der blutvolumenverteilung im ganzkörper unter physikalischen und pharmakologischen maßnahmen. *Vasa*, 6:137–142, 1977.
- [43] S.P. Downie, D.N. Firmin, N.B. Wood, S.A. Thom, A.D. Hughes, J.N.H. Wolfe, and X.Y. Xu. Role of MRI in investigating the effects of elastic compression stockings on the deformation of the superficial and deep veins in the lower leg. *Journal of Magnetic Resonance Imaging*, 26(1):80–85, 2007.
- [44] S.P. Downie, S.M. Raynor, D.N. Firmin, N.B. Wood, S.A. Thom, A.D. Hughes, K.H. Parker, J.H.N. Wolfe, and X.Y. Xu. Effects of elastic compression stockings on wall shear stress in deep and superficial veins of the calf. *Am J Physiol Heart Circ Physiol*, 294(5):H2112–2120, May 2008.
- [45] R.J. Damstra, E.R. Brouwer, and H. Partsch. Controlled, comparative study of relation between volume changes and interface pressure under short-stretch bandages in leg lymphedema patients. *Dermatologic Surgery*, 34(6):773–779, June 2008.
- [46] M.A. Murphy, W.P. Joyce, C. Condrón, and D. Bouchier-Hayes. A reduction in serum cytokine levels parallels healing of venous ulcers in patients undergoing compression therapy. *European Journal of Vascular and Endovascular Surgery*, 23(4):349–352, April 2002.
- [47] G. Dai, J.P. Gertler, and R.D. Kamm. The effects of external compression on venous blood flow and tissue deformation in the lower leg. *Journal of Biomechanical Engineering*, 121(6):557–564, 1999.
- [48] G.W. John, A.J. Narracott, R.J. Morris, J.P. Woodcock, P.V. Lawford, and D.R. Hose. Influence of intermittent compression cuff design on interface pressure and

- calf deformation: experimental results. *EMBS 2007. 29th Annual International Conference of the IEEE*, pages 2122–2125, 2007.
- [49] A.J. Narracott, G.W. John, D.R. Hose, R.J. Morris, J.P. Woodcock, and P.V. Lawford. Influence of intermittent compression cuff design on calf deformation: computational results. *EMBS 2007. 29th Annual International Conference of the IEEE*, pages 6334–6337, 2007.
- [50] A. Coull, D. Tolson, and J. McIntosh. Class-3c compression bandaging for venous ulcers: comparison of spiral and figure-of-eight techniques. *Journal of Advanced Nursing*, 54(3):274–283, May 2006.
- [51] R. Stemmer, J. Marescaux, and C. Furderer. The compression therapy of the lower-extremities especially with compression stockings. *The Dermatologist*, 31:355–365, 1980.
- [52] K.G. Burnand and G.T. Layer. Graduated elastic stockings. *Br Med J*, 293:224–225, 1986.
- [53] R. Stemmer. Ambulatory elasto-compressive treatment of the lower extremities particularly with elastic stockings. *Der Kassenarzt*, 9:1–8, 1969.
- [54] D.J. Milic, S.S. Zivic, D.C. Bogdanovic, M.M. Jovanovic, R.J. Jankovic, Z.D. Milosevic, D.M. Stamenkovic, and M.S. Trenkic. The influence of different sub-bandage pressure values on venous leg ulcers healing when treated with compression therapy. *Journal of Vascular Surgery*, 51(3), March 2010.
- [55] K. Sigg. Compression with pressure bandages and elastic stockings for prophylaxis and therapy of venous disorder of the leg. *Fortschr Med*, 15:601–606, 1963.
- [56] A.J. Lee, J.J. Dale, C.V. Ruckley, B. Gibson, R.J. Prescott, and D. Brown. Compression therapy: Effects of posture and application techniques on initial pressures delivered by bandages of different physical properties. *European Journal of Vascular and Endovascular Surgery*, 31(5):542–552, May 2006.
- [57] P. Vowden and K. Vowden. Doppler assessment and abpi: Interpretation in the management of leg ulceration. *World Wide Wounds*, March 2001. URL <http://www.worldwidewounds.com/2001/march/Vowden/Doppler-assessment-and-ABPI.html>.
- [58] M.J. Callam, C.V. Ruckley, J.J. Dale, and D.R. Harper. Hazards of compression treatment of the leg: an estimate from scottish surgeons. *British Medical Journal*, 295, November 1987.
- [59] M Kosiak. Etiology and pathology of ischaemic ulcers. *Arch Phys Med Rehab*, 40: 62–69, 1959.

- [60] M. Clark. Compression bandages: principles and definitions. *EWMA Position document. Understanding compression therapy. MEP*, pages 5–7, 2003.
- [61] H. Partsch, M. Clark, G. Mosti, E. Steinlechner, J. Schuren, M. Abel, J. Benigni, P. Coleridge-Smith, A. Cornu-Thenard, M. Flour, J. Hutchinson, J. Gamble, K. Issberner, M. Juenger, C. Moffatt, H.A.M. Neumann, E. Rabe, J. F. Uhl, and S. Zimmet. Classification of compression bandages: Practical aspects. *Dermatologic Surgery*, 34(5):600–609, May 2008.
- [62] CEN. adopted european prestandard medical compression hosiery. Technical report, Brussels: Comite Europeen de Normalisation, 2001.
- [63] G.B. Mosti and V. Mattaliano. Simultaneous changes of leg circumference and interface pressure under different compression bandages. *European Journal of Vascular and Endovascular Surgery*, 33(4):476–482, April 2007.
- [64] C.P.M. Wegen-Franken, P. Mulder, B. Tank, and H.A.M. Neumann. Variation in the dynamic stiffness index of different types of medical elastic compression stockings. *Phlebology*, 23(2):77–84, April 2008.
- [65] R. Stolk, C.P.M. Wegen van der Franken, and H.A.M. Neumann. A method for measuring the dynamic behavior of medical compression hosiery during walking. *Dermatologic Surgery*, 30(5):729–736, 2004.
- [66] C. Moffatt. Variability of pressure provided by sustained compression. *International Wound Journal*, 5(2):259–265, May 2008.
- [67] A. Keller, M.L. Müller, T. Calow, I.K. Kern, and H. Schumann. Bandage pressure measurement and training: simple interventions to improve efficacy in compression bandaging. *International Wound Journal*, 6(5):324–330, 2009.
- [68] A.D. Taylor, R.J. Taylor, and S.S.S. Said. Using a bandage pressure monitor as an aid in improving bandaging skills. *Journal of Wound Care*, 7(3):131–133, March 1998.
- [69] J. Hafner, W. Lüthi, H. Hänsle, G. Kammerlander, and G. Burg. Instruction of compression therapy by means of interface pressure measurement. *Dermatologic Surgery*, 26(5):481–488, 2000.
- [70] S. Thomas. Bandages and bandaging: the science behind the art. *Care Sci Pract*, 8(2):50–60, 1990.
- [71] S. Thomas and P. Fram. Laboratory-based evaluation of a compression-bandaging system. *Nursing Times*, 99(40):24–28, 2003.

- [72] G. Mosti, V. Mattaliano, and H. Partsch. Inelastic compression increases venous ejection fraction more than elastic bandages in patients with superficial venous reflux. *Phlebology*, 23(6):287–294, December 2008.
- [73] S. Ghosh, A. Mukhopadhyay, M. Sikka, and K.S. Nagla. Pressure mapping and performance of the compression bandage/garment for venous leg ulcer treatment. *Journal of Tissue Viability*, 17(3):82–94, August 2008.
- [74] R. Liu, Y.L. Kwok, Y. Li, T.T. Lao, and X. Zhang. Quantitative assessment of relationship between pressure performances and material mechanical properties of medical graduated compression stockings. *Journal of Applied Polymer Science*, 104(1):601–610, 2007.
- [75] S. Thomas. The use of the laplace equation in the calculation of sub-bandage pressure. *EWMA journal*, 3(1):21–23, 2003. URL <http://www.worldwidewounds.com/2003/june/Thomas/Laplace-Bandages.html>.
- [76] P. De Bruyne and T. Dvořák. The pressure exerted by an elastic stocking and its measurement. *Medical and Biological Engineering and Computing*, 14(1):94–96, January 1976.
- [77] J.R. Basford. The law of laplace and its relevance to contemporary medicine and rehabilitation. *Archives of Physical Medicine and Rehabilitation*, 83(8):1165–1170, August 2002.
- [78] L. Macintyre, M. Baird, and P. Weedall. The study of pressure delivery for hypertrophic scar treatment. In S.C. Anand, J.F. Kennedy, M. Mirafteb, and S. Rajendran, editors, *Medical Textiles and Biomaterials for Healthcare*, pages 224–232. Woodhead Publishing Limited, Cambridge, 2006.
- [79] J. Cheng, J. Evans, K. Leung, J. Clark, T. Choy, and P. Leung. Pressure therapy in the treatment of post-burn hypertrophic scar critical look into its usefulness and fallacies by pressure monitoring. *Burns*, 10(3):154–163, February 1984.
- [80] D. Wertheim, J. Melhuish, R. Williams, and K. Harding. Measurement of forces associated with compression therapy. *Medical and Biological Engineering and Computing*, 37(1):31–34, January 1999.
- [81] I. Gaiied, S. Drapier, and B. Lun. Experimental assessment and analytical 2d predictions of the stocking pressures induced on a model leg by medical compressive stockings. *Journal of Biomechanics*, 39(16):3017–3025, 2006.
- [82] A. Reicher. Design of a compression bandage or stocking. *Care Sci Pract*, 8(2):61–62, 1990.
- [83] S. Thomas. *Bandages and Bandaging*, chapter 13. Pharmaceutical Press, 1990.

- [84] J.M. Melhuish, M. Clark, R. Williams, and K.G. Harding. The physics of sub-bandage pressure measurement. *Journal of Wound Care*, 9(7):308–310, July 2000.
- [85] E.J. Hearn. *Mechanics of Materials Volume 1: An Introduction to the Mechanics of Elastic and Plastic Deformation of Solids and Structural Materials*. Butterworth-Heinemann, 3 edition, August 1997.
- [86] L. Vinckx, W. Boeckx, and J. Berghmans. Analysis of the pressure perturbation due to the introduction of a measuring probe under an elastic garment. *Medical and Biological Engineering and Computing*, 28(2):133–138, March 1990.
- [87] M.W. Ferguson-Pell. Design criteria for the measurement of pressure at body/support interfaces. *Eng Med*, 9(4):209–214, 1980.
- [88] V. Allen, D.W. Ryan, N. Lomax, and A. Murray. Accuracy of interface pressure measurement systems. *Journal of Biomedical Engineering*, 15(4):344–348, July 1993.
- [89] M.D. Stinson, A.P. Porter-Armstrong, and P.A. Eakin. Pressure mapping systems: reliability of pressure map interpretation. *Clin Rehabil*, 17(5):504–511, May 2003.
- [90] J. Woodburn and P.S. Helliwell. Observations on the f-scan in-shoe pressure measuring system. *Clinical Biomechanics*, 11(5):301–304, July 1996.
- [91] A.W.P. Buis and P. Convery. Calibration problems encountered while monitoring stump/socket interface pressures with force sensing resistors: Techniques adopted to minimise inaccuracies. *Prosthetics and Orthotics International*, 21(3):179–182, 1997.
- [92] A.A. Polliack, R.C. Sieh, D.D. Craig, S. Landsberger, D.R. Mcneil, and E. Ayyappa. Scientific validation of two commercial pressure sensor systems for prosthetic socket fit. *Prosthetics and Orthotics International*, 24(1):63–73, 2000.
- [93] D.A. Rikli, P. Honigmann, R. Babst, A. Cristalli, M.M. Morlock, and T. Mittlmeier. Intra-articular pressure measurement in the radioulnocarpal joint using a novel sensor: In vitro and in vivo results. *The Journal of Hand Surgery*, 32(1):67–75, January 2007.
- [94] D. Wilson, M.V. Aperleva, M.J. Eichler, and F.R. Harrold. Accuracy and repeatability of a pressure measurement system in the patellofemoral joint. *Journal of Biomechanics*, 36(12):1909–1915, December 2003.
- [95] D. Wilson, C. Niosi, Q. Zhu, T. Oxland, and D. Wilson. Accuracy and repeatability of a new method for measuring facet loads in the lumbar spine. *Journal of Biomechanics*, 39(2):348–353, 2006.

- [96] H.P. Giele, K. Liddiard, K. Currie, and F.M. Wood. Direct measurement of cutaneous pressures generated by pressure garments. *Burns*, 23(2):137–141, March 1997.
- [97] C.H.Y. Lai and C.W.P. Li-Tsang. Validation of the pliance x system in measuring interface pressure generated by pressure garment. *Burns*, 35(6):845–851, September 2009.
- [98] E. Van den kerckhove, S. Fieuws, P. Massage, R. Hierner, W. Boeckx, J. Deleuze, J. Laperre, and M. Anthonissen. Reproducibility of repeated measurements with the kikuhome pressure sensor under pressure garments in burn scar treatment. *Burns*, 33(5):572–578, August 2007.
- [99] F. Lurie, V. Scott, H. Yoon, and R.L. Kistner. On the mechanism of action of pneumatic compression devices: Combined magnetic resonance imaging and duplex ultrasound investigation. *Journal of Vascular Surgery*, 48(4):1000–1006, October 2008.
- [100] H. Partsch and G. Mosti. Thigh compression. *Phlebology*, 23(6):252–258, December 2008.
- [101] S.D. Blair, D.D.I. Wright, C.M. Backhouse, E. Riddle, and C.N. McCollum. Sustained compression and healing of chronic venous ulcers. *BMJ (Clinical research ed.)*, 297(6657):1159–1161, November 1988.
- [102] J. Horner, L.C. Lowth, and A.N. Nicolaides. A pressure profile for elastic stockings. *British Medical Journal*, 280(6217):818–820, March 1980.
- [103] R. Liu, Y.L. Kwok, Y. Li, T.T.H. Lao, X. Zhang, and X.Q. Dai. Objective evaluation of skin pressure distribution of graduated elastic compression stockings. *Dermatologic Surgery*, 31(6):615–624, 2005.
- [104] R. Liu, Y. L. Kwok, Y. Li, T.T. Lao, and X. Zhang. The effects of graduated compression stockings on cutaneous surface pressure along the path of main superficial veins of lower limbs -wounds. *Wounds*, 18(6):150–157, June 2006.
- [105] H. Partsch, G. Menzinger, B. Borst-Krafek, and E. Groiss. Does thigh compression improve venous hemodynamics in chronic venous insufficiency? *Journal of Vascular Surgery*, 36(5):948–952, November 2002.
- [106] A. Satpathy, S. Hayes, and S.R. Dodds. Measuring sub-bandage pressure: comparing the use of pressure monitors and pulse oximeters. *J Wound Care*, 15(3):125–128, March 2006.
- [107] J.J. Dale, C.V. Ruckley, B. Gibson, D. Brown, A.J. Lee, and R.J. Prescott. Multi-layer compression: Comparison of four different four-layer bandage systems applied

- to the leg. *European Journal of Vascular and Endovascular Surgery*, 27(1):94–99, January 2004.
- [108] S. Rajendran and S.C. Anand. Evaluation of pressure profile of bandages using mannequin leg. In S.C. Anand, J.F. Kennedy, M. Mirafteb, and S. Rajendran, editors, *Medical Textiles and Biomaterials for Healthcare*, pages 233–242. Woodhead Publishing Limited, Cambridge, 2006.
- [109] C.P.M. van der Wegen-Franken, B. Tank, T. Nijsten, and H.A.M. Neumann. Changes in the pressure and the dynamic stiffness index of medical elastic compression stockings after having been worn for eight hours: a pilot study. *Phlebology*, 24(1):31–37, February 2009.
- [110] J.C. Barbenel, S. Sockalingham, and D. Queen. In vivo laboratory evaluation of elastic bandages. *Care Sci Pract*, 8(2):72–74, 1990.
- [111] M. Hirai, H. Iwata, H. Ishibashi, T. Ota, and H. Nakamura. Interface pressure and stiffness of various elastic stockings during posture changes and exercise. *Vascular*, 16(2):95–100, 2008.
- [112] M. Hirai, K. Niimi, H. Iwata, I. Sugimoto, H. Ishibashi, T. Ota, and H. Nakamura. A comparison of interface pressure and stiffness between elastic stockings and bandages. *Phlebology*, 24(3):120–124, June 2009.
- [113] G. Lee, S. Rajendran, and S. Anand. New single-layer compression bandage system for chronic venous leg ulcers. *British Journal of Nursing*, 18(15):S4–S18, 2009.
- [114] G. Mosti, V. Mattaliano, and H. Partsch. Influence of different materials in multi-component bandages on pressure and stiffness of the final bandage. *Dermatologic Surgery*, 34(5):631–639, May 2008.
- [115] H. Partsch. The use of pressure change on standing as a surrogate measure of the stiffness of a compression bandage. *European Journal of Vascular and Endovascular Surgery*, 30(4):415–421, October 2005.
- [116] S. Rajendran and S. Anand. Design and development of novel bandages for compression therapy. *British Journal of Nursing*, 12(6 Suppl):S20–S29, March 2003.
- [117] R Liu, L.Y. Kwok, Y. Li, T.T. Lao, and X. Zhang. Skin pressure profiles and variations with body postural changes beneath medical elastic compression stockings. *International Journal of Dermatology*, 46(5):514–523, May 2007.
- [118] D. Wertheim, J. Melhuish, R. Williams, I. Lane, and K. Harding. Movement-related variation in forces under compression stockings. *European Journal of Vascular and Endovascular Surgery*, 17(4):334–337, April 1999.

- [119] T.B. Raj, M. Goddard, and G.S. Makin. How long do compression bandages maintain their pressure during ambulatory treatment of varicose veins? *British Journal of Surgery*, 67(2):122–124, February 1980.
- [120] S. Sockalingham, J.C. Barbenel, and D. Queen. Ambulatory monitoring of the pressures beneath compression bandages. *Care Sci Pract*, 8(2):75–78, 1990.
- [121] H. Partsch, B. Partsch, and W. Braun. Interface pressure and stiffness of ready made compression stockings: Comparison of in vivo and in vitro measurements. *Journal of Vascular Surgery*, 44(4):809–814, October 2006.
- [122] G. Mosti and S. Rossari. The importance of measuring sub bandage pressure and presentation of new measuring device. *Acta Vulnol*, 6:31–36, 2008.
- [123] J. Fraden. *Handbook of modern sensors - physics, designs and applications*. Springer, New York, 3rd edition, 2004.
- [124] Microlab Electronica. PicoPress, last accessed on 18/04/2010. URL www.microlabitalia.it.
- [125] AMI Techno. Air-pack type contact surface pressure continuously measuring system, last accessed on 10/04/2010. URL <http://www.ami-tec.co.jp/eindex.htm>.
- [126] A. Satpathy, S. Hayes, and S. Dodds. Is compression bandaging accurate? the routine use of interface pressure measurements in compression bandaging of venous leg ulcers. *Phlebology*, 21(1):36–40, March 2006.
- [127] Salzmänn AG (SAG). MST MK IV, last accessed on 12/04/2010. URL <http://www.salzmänn-group.ch>.
- [128] A. Finnie. Interface pressure measurements in leg ulcer management. *British Journal of Nursing*, 9(6):S5–S18, March 2000.
- [129] C.J. Wildin, A.C. W. Hui, C.N.A. Esler, and P.J. Gregg. In vivo pressure profiles of thigh-length graduated compression stockings. *British Journal of Surgery*, 85(9):1228–1231, 1998.
- [130] E. Brizzio, F. Amsler, B. Lun, and W. Blättler. Comparison of low-strength compression stockings with bandages for the treatment of recalcitrant venous ulcers. *Journal of Vascular Surgery*, 51(2):410–416, February 2010.
- [131] R.J. Taylor and A.D. Taylor. Construction and calibration of a low-cost bandage pressure monitor. *Journal of Wound Care*, 7(3):125–128, March 1998.
- [132] Gaelttec. Fontameter, last accessed on 13/04/2010. URL <http://www.gaeltec.com/pdf/Font.pdf>.

- [133] Gaelttec. Intracranial catheter tip pressure transducer (ICT/B), last accessed on 13/04/2010. URL <http://www.gaeltec.com/pdf/ICT-B.pdf>.
- [134] D. Wertheim, J. Melhuish, M. Llewellyn, A. Hoppe, R. Williams, and K. Harding. An integrated instrumentation approach to the study of wound healing. In *Proc. of the 20th Annual International Conference of the IEEE Engineering in Medicine and Biology Society*, volume 20, pages 1760–1761, 1998.
- [135] D. Wertheim, J. Melhuish, K. Trenary, S. Shutler, R. Williams, and K. Harding. Assessment of forces associated with compression therapy under static and dynamic conditions. In *Proc. of the 18th Annual International Conference of the IEEE Bridging Disciplines for Biomedicine.*, volume 1, pages 173–174, 1996.
- [136] D. Wertheim, G. Harinath, J.M. Melhuish, R.J. Williams, K.G. Harding, and R. J. Whiston. In vivo pressure profiles of thigh-length graduated compression stockings. *British Journal of Surgery*, 86(4):572, 1999.
- [137] D. Wertheim, J. Melhuish, R. Williams, and K. Harding. Measurement of sub-bandage forces. *IEE Colloquium on Innovative Pressure, Force and Flow Measurements*, pages 4/1–4/3, 1999.
- [138] R. J. Williams, D. Wertheim, J. Melhuish, and K.G. Harding. How compression therapy works. *Journal of Wound Care*, 8(6):297–298, June 1999.
- [139] J.C. Barbenel and S. Sockalingham. Device for measuring soft tissue interface pressures. *Journal of Biomedical Engineering*, 12(6):519–522, 1990.
- [140] M. Taylor. Bandage pressure sensor. *United States Patent Application 20080306407 A1*, 2008.
- [141] A. Ouchene and J. Counord. Device for measuring pressure points to be applied by a compressive orthotic device. *WO 2004/000183 A1*, 2003.
- [142] A. Cornu-Thenard, P. Boivin, P.H. Carpentier, F. Courtet, and P. Ngo. Superimposed elastic stockings: Pressure measurements. *Dermatologic Surgery*, 33(3): 269–275, March 2007.
- [143] J. Testud, M. Sennoune, J. Prudhomme, and A. Ouchene. Device for measuring pressure points to be applied by a compressive orthotic device. *United States Patent Application 6334363 B1*, 2002.
- [144] D Kuenzli, W. Braun, and M. Ruettiger. Apparatus for the testing elastic textile garments. *United States Patent Application 2007/0012120 A1*, 2007.
- [145] Salzmann AG (SAG). MST Professional, last accessed on 12/04/2010. URL <http://www.salzmann-group.ch>.

- [146] W. Hansjoerg, O. Ulrich, and J. Harald. Device for the determination of parameters particularly for therapeutic compression measures on limbs. *DE102004038421 A1*, 2006.
- [147] Pressure Profile Systems. PPS, last accessed on 18/04/2010. URL <http://www.pressureprofile.com/>.
- [148] Pressure Profile Systems. ConTacts Discrete Tactile Sensors, last accessed on 18/04/2010. URL <http://www.pressureprofile.com/products-contacts>.
- [149] Pressure Profile Systems. ConTacts C500, last accessed on 18/04/2010. URL <http://www.pressureprofile.com/products-tactarray-sensors>.
- [150] Novel. Novel single sensors, last accessed on 18/04/2010. URL <http://www.novel.de/productinfo/sensors-single.htm>.
- [151] R. Cork. Xsensor technology: a pressure imaging overview. *Sensor Review*, 27(1): 24–28, 2007.
- [152] XSENSOR. X3 PX100 pressure imaging sensor, last accessed on 19/04/2010. URL <http://www.xsensor.com/pressure-imaging/x3-px100>.
- [153] M.A. Fergenbaum, L. Hadcock, J.M. Stevenson, E. Morin, and S.A. Reid. Dynamic assessment of pressure measurement system for the dynamic biomechanical model of human load carriage: Phase 4: Part C1: Assessment of pressure measurement systems on flat surfaces for use in human load carriage. Technical report, Queen’s University, 2005.
- [154] M.A. Fergenbaum, L. Hadcock, J.M. Stevenson, J.T. Bryant, E. Morin, and S.A. Reid. Development of a dynamic biomechanical model for load carriage: Phase 4, part C2: Assessment of pressure measurement systems on curved surfaces for the dynamic biomechanical model of human load carriage. Technical report, Queen’s University, 2005.
- [155] XSENSOR. X3 LX100 pressure imaging sensor, last accessed on 19/04/2010. URL <http://www.xsensor.com/pressure-imaging/x3-Lx100>.
- [156] E. Ochoteco, J.A. Pomposo, T. Sikora, F. Vidal, F. Martinez, G. Obieta, and H. Grande. All-plastic distributed pressure sensors: taylor-made performance by electroactive materials design. *Microsystem Technologies*, 14(8):1089–1097, 2008.
- [157] E. Ochoteco, J.A. Pomposo, H. Macicior, M.A. Arregui, F. Martinez, G. Obieta, and H. Grande. Design of all-plastic distributed pressure sensors based on electroactive materials. In T. Becker, C. Cané, and S.N. Barker, editors, *Smart Sensors, Actuators, and MEMS III*, volume 6589. SPIE, 2007.

- [158] Interlink-Electronics. FSR force sensing resistor integration, last accesses on 20/04/2010. URL http://www.interlinkelectronics.com/force_sensors/products/forcesensingresistors/standardsensors.html.
- [159] F. Vecchi, C. Freschi, S. Micera, A.M. Sabatini, P. Dario, R. Sacchetti, S.S. di Sant'Anna, and C.I. Rtr. Experimental evaluation of two commercial force sensors for applications in biomechanics and motor control. In *Proc. 5th Ann IEFES Conf in Alaborg (DK)*, 2000.
- [160] M.C.F. Castro and A. Cliquet, Jr. A low-cost instrumented glove for monitoring forces during object manipulation. *IEEE Transactions on Rehabilitation Engineering*, 5(2):140–147, 1997.
- [161] R.S. Hall, G.T. Desmoulin, and T.E. Milner. A technique for conditioning and calibrating force-sensing resistors for repeatable and reliable measurement of compressive force. *Journal of Biomechanics*, 41(16):3492–3495, December 2008.
- [162] C. Lebosse, B. Bayle, M. de Mathelin, and P. Renaud. Nonlinear modeling of low cost force sensors. *ICRA 2008. IEEE International Conference on Robotics and Automation, 2008.*, pages 3437–3442, 2008.
- [163] L. Marechal, C. Barthod, G. Gautier, J. Lottin, and J.C. Jeulin. Instrumentation and labview based continuous processing for chest physiotherapy. In *Proc. BIODEVICES 2008, International Conference on Biomedical Electronics and Devices (2)*, pages 41–46, 2008.
- [164] L. Maréchal, C. Barthod, J. Lottin, G. Gautier, and J.C. Jeulin. Measurement system for gesture characterization during chest physiotherapy act on newborn babies suffering from bronchiolitis. In *Proc. 29th Annual International Conference of the IEEE Engineering in Medicine and Biology Society*, pages 5770–5773, 2007.
- [165] L. Maréchal, C. Barthod, G. Gautier, J. Lottin, and J.C. Jeulin. Mechatronical approach for the definition of future functionalities for a torso simulator. *Mechatronics 2008 Conference*, 2008. URL http://damien.marechal.neuf.fr/Site_Luc/files/Mecatronics2008_Marechal.pdf.
- [166] K.N. Bachus, A.L. DeMarco, K.T. Judd, D.S. Horwitz, and D.S. Brodke. Measuring contact area, force, and pressure for bioengineering applications: using fuji film and tekscan systems. *Medical Engineering & Physics*, 28(5):483–488, June 2006.
- [167] A. Kalamdani, C. Messom, and M. Siegel. Tactile sensing by the sole of the foot: part I: apparatus and initial experiments toward obtaining dynamic pressure maps useful for stabilizing standing, walking and running of humanoid robots. In *Proc. HAVE'2006 IEEE International Workshop on Haptic Audio Visual Environment and their Applications*, Ottawa, Canada, 2006.

- [168] A.A. Kalamdani. Development and characterization of a high-spatial-temporal-resolution foot-sole-pressure measurement system. Master's thesis, Citeseer, 2006.
- [169] E.R. Komi, J.R. Roberts, and S.J. Rothberg. Evaluation of thin, flexible sensors for time-resolved grip force measurement. *Journal of Mechanical Engineering Science*, 221:1687–1699, November 2007.
- [170] E.R. Komi, J.R. Roberts, and S.J. Rothberg. Measurement and analysis of grip force during a golf shot. *Journal of Sports Engineering and Technology*, 222(1): 23–35, 2008.
- [171] M. Lowe, A. King, E. Lovett, and T. Papakostas. Flexible tactile sensor technology: bringing haptics to life. *Sensor Review*, 24(1):33–36, 2004.
- [172] Tekscan Inc. The garment system, last accessed on 24/04/2010. URL <http://www.tekscan.com/medical/system-garment.html>.
- [173] Tekscan. FlexiForce®: Single button force sensing resistor, last accessed on 24/04/2010. URL <http://www.tekscan.com/flexiforce/flexiforce.html>.
- [174] Tekscan. *FlexiForce® Sensors User Manual*, May 2009. URL <http://www.tekscan.com/pdfs/FlexiforceUserManual.pdf>.
- [175] A. Balakrishnan, D.F. Kacher, A. Solcum, C. Kemper, and S.K. Warfield. Smart retractor for use in image guided neurosurgery. *2003 Summer Bionengineering Conference*, 2003.
- [176] M. Ferguson-Pell, S. Hagiwara, and D. Bain. Evaluation of a sensor for low interface pressure applications. *Medical Engineering & Physics*, 22(9):657–663, November 2000.
- [177] Y.K. Kong and B.D. Lowe. Optimal cylindrical handle diameter for grip force tasks. *International Journal of Industrial Ergonomics*, 35(6):495–507, June 2005.
- [178] R.A. Lee, A.A.J. van Zundert, R.L.J.G. Maassen, R.J. Willems, L. P. Beeke, J.N. Schaaper, J. van Dobbelsteen, and P. A. Wieringa. Forces applied to the maxillary incisors during video-assisted intubation. *Anesthesia & Analgesia*, 108(1):187–191, January 2009.
- [179] M.L. Lu, T. James, B. Lowe, M. Barrero, and Y.K. Kong. An investigation of hand forces and postures for using selected mechanical pipettes. *International Journal of Industrial Ergonomics*, 38(1):18–29, January 2008.
- [180] M. Monroy, M. Ferre, J. Barrio, V. Eslava, and I. Galiana. Sensorized thimble for haptics applications. *ICM 2009. IEEE International Conference on Mechatronics, 2009.*, pages 1–6, 2009.

- [181] A. Nikonovas, A.J.L. Harrison, S. Hoult, and D. Sammut. The application of force-sensing resistor sensors for measuring forces developed by the human hand. *Journal of Engineering in Medicine*, 218(2):121–126, 2004.
- [182] L. Paredes-Madrid, P. Torruella, P. Solaeche, I. Galiana, and P. Gonzalez de Santos. Accurate modelling of low-cost piezoresistive force sensors for haptic interface. *ICRA 2010. IEEE International Conference on Robotics and Automation, 2010.*, pages 1828–1833, 2010.
- [183] D. Wasserman, J. Wasserman, and J. I. Ahn. Instrumentation for measuring coupling forces of hand-held tools. *J. Sound and Vibration*, 35(7):22–25, July 2001.
- [184] Vista Medical Ltd. FSA, last accessed on 23/04/2010. URL <http://www.pressuremapping.com>.
- [185] Peratech. The science of quantum tunnelling composites, last accessed on 21/04/2010. URL <http://www.peratech.com/qtscience.php>.
- [186] Eleksen. Eleksen a Peratech Company, last accessed on 21/04/2010. URL <http://www.eleksen.com>.
- [187] Sensor Product Inc (SPI). Tactilus, last accessed on 23/04/2010. URL <http://www.sensorprod.com/tactilus.php>.
- [188] Sensor Product Inc (SPI). Tactilus free form sensor system, last accessed on 23/04/2010. URL <http://www.sensorprod.com/freeform.php>.
- [189] W Bolton. *Measurement and instrumentation systems*. Newnes, Oxford, 1st edition, 1996.
- [190] K. van der Wegen-Franken, W. Roest, B. Tank, and M. Neumann. Calculating the pressure and the stiffness in three different categories of class II medical elastic compression stockings. *Dermatologic Surgery*, 32(2):216–223, February 2006.
- [191] S. Drapier and I. Gaied. Identification strategy for orthotropic knitted elastomeric fabrics under large biaxial deformations. *Inverse Problems in Science and Engineering*, 15(8):871–894, December 2007.
- [192] B.P. Saville. *Physical testing of textiles*. Woodhouse Publishing Limited, 1st edition, 1999.
- [193] S. Smith, B. Norris, and L. Peebles. OLDER ADULT DATA: The handbook of measurements and capabilities of the older adult - data for design safety. Technical report, University of Nottingham, Product Safety and Testing Group, Nottingham, 2000.
- [194] J.P. Bentley. *Principles of measurement systems*. Pearson Education Limited, Harlow, 4th edition, 2005.

-
- [195] P.F. Dunn. *Measurement and data analysis for engineering and science*. McGraw-Hill Professional, 1st edition, 2004.
- [196] Honeywell. FS01, last accessed on 16/05/2010. URL http://sensing.honeywell.com/index.cfm/ci_id/140301/la_id/1/pr_id/144041.htm.
- [197] S.K. Hanneman. Design, analysis, and interpretation of method-comparison studies. *AACN Advanced Critical Care*, 19(2):223–234, 2008.

Appendix A

Documentation for the Clinical Study: Lower Limb Shape, Temperature and Pressure Measurement Under Compression Bandages

Information Sheet

Research Project Title: Lower Limb Shape, Temperature and Pressure Measurement Under Compression Bandages

Dear Reader,

You are being invited to take part in a research project. Before you decide, it is important for you to understand why the research is being done and what it will involve. Please take time to read the following information carefully and discuss it with others if you wish. Ask us if there is anything that is not clear or if you would like to have more information. Take your time to decide whether or not you wish to take part. Thank you for reading this.

What is the project's purpose?

Chronic venous ulceration is a medical condition that affects 1% of the population in developed countries. The main treatment for this medical problem is compression therapy, for example, compression bandages and stockings are some examples of compression therapy. Compression bandages are used more frequently to treat active venous ulcers. However, the level of the pressure produced by these bandages is subject to many factors. Researchers around the world use many different pressure measurement systems to measure the pressure produced by compression bandages. We have developed a new pressure measurement system which we want to study. We intend to check its performance and compare it against a pressure measurement system that is already widely used. The project's main aims are as follows:

- Measuring the change in lower limb skin temperature when compression bandages are applied. This will enable us to fine tune the pressure measurement system that we have developed in the University of Leeds.
- Scanning the leg from ankle to the knee. The scans will enable us to measure the different physical dimensions of the leg. This will enable us to compute indirect pressure maps from the extension in the bandage material when it is applied to the leg.
- Measuring the sub-bandage pressure map when compression bandage is applied to the leg using a commercial pressure measurement system.
- Measuring the sub-bandage pressure map when compression bandage is applied to the leg using a pressure measurement system developed in University of Leeds.

The study will recruit people between January 2010 and April 2010

Why have I been chosen?

This investigation needs five healthy participants and we are inviting you to take part as you are a research student in Mechanical Engineering in the University of Leeds. This enables flexible timing arrangement for both you and the investigator in charge.

Do I have to take part?

It is up to you to decide whether or not to take part. If you do decide to take part, you will be given this information sheet to keep (and be asked to sign a consent form) and you can still withdraw at any time without it affecting any benefits that you are entitled to in any way. You do not have to give a reason.

What will happen to me if I take part?

You are going to be asked to attend two sessions on two different days in the school of Mechanical Engineering in the University of Leeds. One of these sessions will last for two hours and the other one will last for four hours. You are going to get paid £10 for each session you attend. However, you are expected to attend both sessions.

Visit 1

In the first session, a 3D scanner will be used to scan your leg [ankle to knee] while you are sitting. You are going to be asked to wait until the researcher finishes recording the data that will allow them to construct a 3D computer model of your leg.

Visit 2

In the second session, a trained nurse will first evaluate the blood pressure supply at your left foot and will decide whether applying compression bandages to your leg is safe or not. If it is safe to apply compression bandages to your leg, she will then evaluate if your skin is sensitive to adhesive tapes. If your skin is not sensitive, then the investigator will attach the pressure measurement system developed in University of Leeds to your leg. Once the system is attached and fully checked that it is operating, the trained nurse will apply compression bandages to your left leg for three times and each time the pressure induced will be measured and stored for further analysis. In addition, the extension in the bandage material will be recorded using measurement tape. The application of the bandage will be recorded using a digital camera (video and still), and this record will not include your face or allow you to be identified in any way. The sole purpose of this record to note how the bandage has been applied. Bandage application, pressure and extension measurement will be taken while you are sitting.

Next, 16 ultra thin balloons are going to be attached to your left leg next to the pressure measurement system developed in University of Leeds. These balloons are used commercially to measure the pressure under compression bandages when they are connected to pressure transducer. In addition, to these two pressure measurement system, 4 temperature sensors will be attached to your leg. Another four temperature sensors will be attached to your right leg. Once the two pressure measurement systems and the temperature sensors are attached to your leg, the investigator first, will measure your skin temperature using these temperature sensors. Then, the trained nurse will apply compression bandages for three times to your left leg. For each bandage application, pressure and temperature under the bandage and the extension in the bandage material will be measured.

What do I have to do?

You are going to be asked to attend the sessions and then remove any clothing that covers your legs [3cm above knee and below] (e.g. socks).

What are the possible disadvantages and risks of taking part?

In the second session of the experiment, the pressure measurement system is an electronic system and like any other electrical system, there is a very small chance of electrocution. However, this risk is very low as we have tested the system many and many times. In addition, we are going to use very low voltages to power up the sensors.

The sensors are going to be applied directly to your skin using adhesive tapes. Some people are sensitive to adhesive tapes. A trained nurse will evaluate if your skin is sensitive to adhesive tapes before any sensor is attached to your leg.

Compression bandages might cause pressure ulcers if they are applied wrongly or with very high pressure for a long period of time. However, the risk is very small as a trained nurse is going to apply these compression bandages to your leg. Also, the nurse will evaluate the blood circulation in your leg to make sure that it is safe for you to wear compression bandages. Moreover, you are going to wear these bandages for a very short time [maximum 10 min for each bandage].

What are the possible benefits of taking part?

Whilst there are no immediate benefits for those people participating in the project, it is hoped that this work will enable us to design pressure measurement system that can be used to design better compression products and provide researchers with more comprehensive dynamic picture about the changes in sub-bandage pressure and the factors that influence these changes.

What happens if the research study stops earlier than expected?

We do not expect the research study to stop for any reason as the period of study is short. However, we might ask you to withdraw from the study if the blood circulation in your leg was not within the safe levels prescribed for compression bandages.

Will my taking part in this project be kept confidential?

All the information that we collect about you during the course of the research will be kept strictly confidential. You will not be able to be identified in any reports or publications.

What type of information will be sought from me and why is the collection of this information relevant for achieving the research project's objectives?

The only information will gathered about you is your height, weight , age, the shape of your left leg, the temperature variation when a compression bandage is applied to your leg and the change in pressure under compression bandages when a compression bandage is applied to your leg.

What will happen to the results of the research project?

The research outcomes will be used to fine-tune the pressure measurement system developed in University of Leeds. Also, it might be used for further improvement and development for other monitoring devices. In addition, the data gathered might be used for additional research work.

All results will published in two to three years time in medical, bioengineering and engineering conferences and journal papers. However, in all our future publications, you are not going to be identified.

Will I be recorded, and how will the recorded media be used?

The audio and/or video recordings of your activities made during this research will be used only for analysis and for illustration in conference presentations and lectures. No other use will be made of them without your written permission, and no one outside the project will be allowed to have access to the original recordings.

Who is organising and funding the research?

This research is funded by ConvaTec Limited, a supplier of compression products .

Contacts for further information

For further information please contact:

Mr Jawad Al Khaburi

University of Leeds, School of Mechanical Engineering, Room G54b, LS2 9JT

Mobile No. 07912289090

Dr. Abbas A. Dehghani-Sanij

University of Leeds, School of Mechanical Engineering, Room 4.48, LS2 9JT

Tel No. 0113 343 32906

Prof. E. Andrea Nelson

University of Leeds, School of Healthcare, Baines Wing, Room 1.28, LS2 9JT

Telephone: 0113 343 1373

Please, keep this information sheet and if you are willing to take place in this project, please, sign the consent form.

Many thanks for your time to read this information sheet. If you are going to take part in this project, many thanks for your participation

Participant Consent Form

Title of Research Project: Lower Limb Shape, Temperature and Pressure Measurement Under Compression Bandages

Name of Researcher: Jawad Al Khaburi

Please initial box

1. I confirm that I have read and understand the information sheet
[Please Specify the Date: _____] explaining the
above research project and I have had the opportunity to ask
questions about the project.
2. I understand that my participation is voluntary and that I am free to
withdraw at any time without giving any reason and without there being
any negative consequences. In addition, should I not wish to answer
any particular question or questions, I am free to decline.
3. I understand that my responses will be kept strictly confidential. I give
permission for members of the research team to have access to my
anonymised responses. I understand that my name will not be linked
with the research materials, and I will not be identified or identifiable in
the report or reports that result from the research.
4. I agree for the data collected from me to be used in future subsequent
research.
5. I agree to take part in the above research project.

Name of Participant

Date

Signature

Lead Researcher

Date

Signature

To be signed and dated in presence of the participant

Copies:

Once this has been signed by all parties the participant should receive a copy of the signed and dated participant consent form, the letter/pre-written script/information sheet and any other written information provided to the participants. A copy of the signed and dated consent form should be kept with the project's main documents which must be kept in a secure location.

Agreement to Photographic and Video Records

I agree that the photographic images and video records (where your identity will not be shown through face blackout) taken during this experiment (lower limb shape, temperature and pressure measurement under compression bandages) may be used for the following purposes (please circle):

- a) Can be used in publications (i.e. journals, conference paper, thesis which are the part of this PhD)
- b) Can be used in a presentation (i.e. conferences and societies)
- c) Can be used for educational purposes (i.e. lectures)
- d) All of the above

This type of permission you give will not affect your treatment in any way. If in the future you wish to change your mind, you have the right to do so at any time by contacting the main investigator [Mr. Jawad Al Khaburi].

Name of Participant

Date

Signature

Main Investigator

Date

Signature

To be signed and dated in presence of the participant

Research Support

3 Cavendish Road
University of Leeds
Leeds LS2 9JT

Tel: 0113 343 1561
e-mail: l.m.sawiuk@adm.leeds.ac.uk



**MEEC Faculty Research Ethics Committee
University of Leeds**

c/o Laura Sawiuk
Senior Research Ethics Administrator
Research Support
3 Cavendish Road
University of Leeds
LS2 9JT

Tel: 0113 343 1561
Email: l.m.sawiuk@adm.leeds.ac.uk

5th January 2010

Mr Jawad Al Khaburi
Room G54b
Mechanical Engineering
University of Leeds

Dear Mr Al Khaburi,

Title of study: Lower Limb Shape, Temperature and Pressure Measurement Under
Compression Bandages
Ethics reference number: MEEC 09-006

The above project was reviewed by the MEEC Faculty Research Ethics Committee at its meeting of 4th January 2010.

The following documentation was considered:

Document	Version	Date
University Ethical Review Form	1	16/11/2009
Information Sheet	1	Undated
Consent form	1	Undated
Agreement to Audio / Video Recordings	1	Undated
Protocol	1	Undated
Advertisement	1	Undated

On the basis of the information provided, the Committee requested further information / clarification on the following matters:

1. *In your exclusion criteria (C9) you should add the information that you will be excluding individuals who have an ABPI less than 0.8 or higher than 1.3, as well as individuals who are sensitive to the tapes used.*

2. *You might want to consider describing the use of digital cameras in the design of the research as you do in the information sheet.*
3. *You should describe in the information sheet that the expectation is that participants will be able to attend both sessions, after explaining that they will get £10 for each session they attend.*
4. *Whilst members of the Committee found the advert "Can I borrow your leg for £20?" humorous, they felt that today's sensitivities are such that perhaps more information about the project should go on the poster and perhaps you might use a photograph of the experiment as opposed to a bare leg?*
5. *Members were concerned that you will only be recruiting volunteers from the research group, this could go against the principal of not exerting pressure on participants. What if there are not enough group volunteers for example?*
6. *Members also questioned whether the study group was appropriate. Are volunteers the same age as those suffering from this condition? Do they have the same anthropometric profile?*

A response should be sent to the Committee which addresses each of these points. Further consideration will be given to your response and we will write to you with a further and final opinion.

Yours sincerely

Laura Sawiuk
Senior Research Ethics Administrator
Research Support
On Behalf of
Professor Richard Hall
Chair, MEEC FREC.

Email: l.m.sawiuk@adm.leeds.ac.uk

Copy to: Dr Abbas Dehghani-Singh
Educational Supervisor
Mechanical Engineering
Room 4.48
University of Leeds

Professor E Andrea Nelson
Educational Supervisor
School of Healthcare
Room 1.28
Baines Wing
University of Leeds

Title of study: Lower Limb Shape, Temperature and Pressure Measurement Under Compression Bandages
Ethics reference number: MEEC 09-006

Dear MEEC Faculty Research Ethics Committee members,

I have received your request for more clarification about the following points. I have addressed each of the mentioned points both in here and in the original document.

1. *In your exclusion criteria (C9) you should add the information that you will be excluding individuals who have an ABPI less than 0.8 or higher than 1.3, as well as individuals who are sensitive to the tapes used.*

I have added the requested information to the original document. So the exclusion criteria now clearly states the above two groups also.

2. *You might want to consider describing the use of digital cameras in the design of the research as you do in the information sheet.*

The usage of digital cameras is now described in the design of the research section.

3. *You should describe in the information sheet that the expectation is that participants will be able to attend both sessions, after explaining that they will get £10 for each session they attend.*

The information sheet is now corrected and participants are informed that they are expected to attend both sessions just after explaining they will get £10 for each session they attend.

4. *Whilst members of the Committee found the advert "Can I borrow your leg for £20?" humorous, they felt that today's sensitivities are such that perhaps more information about the project should go on the poster and perhaps you might use a photograph of the experiment as opposed to a bare leg?*

We have limited the information on the poster as we wanted to provide the potential participants with all the required information using the information sheet. However, I have taken the members comment on board and changed the poster so it includes now some of the details about what is going to happen. In addition, I have changed the picture with a picture of sensors attached to the soft leg model that we have in the lab.

5. *Members were concerned that you will only be recruiting volunteers from the research group, this could go against the principal of not exerting pressure on participants. What if there are not enough group volunteers for example?*

I agree with the committee concern and I have changed the form so it will be open for everyone. However, we are still going to limit the advertisement to the three mentioned places.

6. *Members also questioned whether the study group was appropriate. Are volunteers the same age as those suffering from this condition? Do they have the same anthropometric profile?*

Elderly people are usually more vulnerable to this medical condition, therefore, volunteers are not at the same age. The effect of a bandage on the temperature change at the bandage/skin interface should not depend on the age of the participant. The **range** of values for the shape of the leg should also not vary between younger and older participants, and the range is what is required from our study in order to be able to model with upper and lower limits derived from real measurements. We acknowledge that the muscle tone is expected to be different, and this is a potential limitation to the external validity (generalisability) of the study, but we will make this clear in the discussion of our results.

However, after analysing the results and improving our measurement system we might consider a medical trial, which involves people with the same medical condition.

Research Support

3 Cavendish Road
University of Leeds
Leeds LS2 9JT

Tel: 0113 343 4873
e-mail: j.m.blaikie@adm.leeds.ac.uk



**MEEC Faculty Research Ethics Committee
University of Leeds**

10/06/10

Mr J Al Khaburi
G54b and G52
Mechanical Engineering
University of Leeds

Dear Mr Al Khaburi

Title of study: Lower Limb Shape, Temperature and Pressure Measurement Under
Compression Bandages
Ethics Reference Number: MEEC 09-006

Amendment Number: 1
Amendment Date: 03/02/10

The above amendment was reviewed by the Chair of the MEEC Faculty Research Ethics
Committee on 17th February 2010

The following documentation was considered:

<i>Document</i>	<i>Version</i>	<i>Date</i>
MEEC 09-006 Ethical Review Form version 2.doc	1	03/02/10

On the basis of the information provided, the Chair was happy to approve this project on behalf
of the Committee.

Yours sincerely

Jennifer Blaikie
Research Ethics Administrator
Research Support
On Behalf of
Professor Richard Hall
Chair, MEEC FREC.

Appendix B

Documentation for the Clinical Study: Using a Model Leg With Embedded Pressure Sensors for Training Student Nurses to Apply Compression Bandages: Feasibility, Acceptability and Initial Results

Information Sheet

Research Project Title: Using a model leg with embedded pressure sensors for training student nurses to apply compression bandages: feasibility, acceptability and initial results.

Dear Reader,

You are being invited to take part in a research project. Before you decide, it is important for you to understand why the research is being done and what it will involve. Please take time to read the following information carefully and discuss it with others if you wish. Ask us if there is anything that is not clear or if you would like to have more information. Take your time to decide whether or not you wish to take part. Thank you for reading this.

What is the project's purpose?

Chronic venous ulceration is a medical condition that affects 1% of the population in developed countries. The main treatment for this medical problem is compression therapy, for example, compression bandages and stockings are some examples of compression therapy. Compression bandages are used more frequently to treat active venous ulcers. The optimum pressure profile is most commonly described as a pressure of 40-45mmHg at the ankle, reducing to approximately 15-20mmHg at the knee. These values do not appear to have been determined through systematic empirical enquiry and some recent studies recommend much higher levels of pressure. In addition, some researchers found that experienced nurses are not able to achieve the target pressure levels and profile. We are developing a training tool – a model leg that tells you how much pressure there is beneath a bandage – to help nurses adjust their bandage technique during training. The training tool has been tested extensively to establish the accuracy and reliability of the pressure readings it provides for the user. This means that we know that it reads pressure levels accurately and reliably, but we still do not know if this information will be useful for nurses in training. This project's main aims are to address the following two aims:

- To assess the feasibility and acceptability of using model legs with embedded pressure sensors as a training tool for student nurses.
- To identify errors of application in bandaging techniques of student nurses.

The study will recruit people and be conducted in the compression bandages workshop during the week [Monday 12th of April 2010 until Friday 16th of April 2010]

Why have I been chosen?

The project aims to study the acceptability and feasibility of using leg models with embedded sensors in training student nurses and identify their main bandaging techniques pitfalls. You have been approached as you are a student nurse in the School of Healthcare at the University of Leeds.

Do I have to take part?

It is up to you to decide whether or not to take part. If you do decide to take part, you will be asked to sign a consent form and you can still withdraw at any time without it affecting any of your education in any way. You do not have to give a reason for not taking part or for stopping being in the study or if you decide to withdraw. Whether you decide to take part in the study or not, there will be no impact on your academic progress or any assessments in the School of Healthcare. In addition, there will be no impact on your academic progress if your bandaging skill is recorded as being imperfect by the model leg. The investigators (Prof Nelson and MR Al Khaburi) will not share the data on your bandaging skill with anyone in

the School of Healthcare or in clinical practice. This information will be treated as confidential. In addition, Prof Nelson will not be involved in assessing any of your work in this course.

What will happen to me if I take part?

You are going to be asked to apply a compression bandage to the training leg using a spiral overlap technique. Your target pressures are 40-45mmHg at the ankle, 35mmHg at the gaiter, 25mmHg at the widest girth of the calf and 20mmHg just below the knee. Once you have applied the bandage, a 3D representation with pressure colour map will be used to provide you with a graphical feedback (it looks a bit like a weather map of the UK, only on a leg shape). A print out for your average measured values of pressure will also be given to you. You are then going to be handed a very short questionnaire about your experience with the training tool and asked to complete it. Overall, the procedure of applying the bandage should take approximately 10 minutes, and as we have only one model leg, you may need to wait for 10-20 minutes to be able to take part.

What are the possible disadvantages and risks of taking part?

We do not anticipate any harm or discomfort from taking part. It is important to tell you that we are using a leg model with some electronics embedded in it, and there is a power supply attached to the leg. We are using very low power in the electronics and you are not going to be in direct contact with any electronic components. In addition, all the electronics to be used and all the wires and electronic components are going to be covered with insulated plastic tubes and placed within insulated enclosures. For additional safety, the high tech leg model will be covered with a thin cotton layer net. All of these electronic have been checked by staff at the University of Leeds in the School of Mechanical Engineering to check that they are safe for us to use.

Also, you might get disappointed if you did not manage to achieve the target pressures. However, as research shows even the very experienced nurses are not able to achieve these target pressures and we believe that the feedback you will receive in this session will enable you to improve your bandaging skills.

What are the possible benefits of taking part?

The immediate benefit for you will be the verbal and the printed out feedback for your bandaging skills. The leg training model was tested extensively in the lab to check the accuracy of the pressure measurements it provides. In addition, your response about your experience will enable us to evaluate whether we should carry more investigation for introducing training leg models within the curriculum of teaching bandaging skills. Moreover, the data we gather will be used to identify the main problems with early bandaging techniques. This will enable us to recommend what bandaging skills trainers might focus on in their future workshops.

What happens if the research study stops earlier than expected?

We do not expect the research study to stop for any reason as the period of study is short.

Will my taking part in this project be kept confidential?

All the information that we collect about you during the course of the research will be kept strictly confidential. You will not be able to be identified in any reports or publications.

What type of information will be sought from me and why is the collection of this information relevant for achieving the research project's objectives?

The only information will gathered about you is the pressure map that you generate when you apply the compression bandage to the leg model, the time you have taken to apply the bandage and your response to the questionnaire.

What will happen to the results of the research project?

The outcome of the research will enable us to check the acceptability feasibility of using leg models with embedded sensors to train student nurses and identify the main problems with their early bandaging techniques, which will be compared to the available information about the mistakes made by experienced nurses. The data gathered might be used for additional research work.

All results will published in two to three years time in medical conferences and journal papers. However, in all our future publications, you are not going to be identified.

Will I be recorded, and how will the recorded media be used?

The images that will be captured for your bandaging once you have applied it to the leg model will be used only for analysis purposes and for illustration in conference presentations, lectures and written publications. No other use will be made of them without your written permission, and no one outside the project will be allowed to have access to the original images.

Who is organising and funding the research?

The research is organised by Mr Jawad Al Khaburi a PhD student in the School of Mechanical Engineering at the University of Leeds. His supervisors are Prof Andrea Nelson (School of Healthcare) and DR Abbas Dehghani (School of Mechanical Engineering).

This research is funded by ConvaTec Limited, a supplier of compression products.

Contacts for further information

For further information please contact:

Mr Jawad Al Khaburi
University of Leeds, School of Mechanical Engineering, Room G54b, LS2 9JT
Mobile No. 07912289090

Prof. E. Andrea Nelson
University of Leeds, School of Healthcare, Baines Wing, Room 1.28, LS2 9JT
Telephone: 0113 343 1373

Dr. Abbas A. Dehghani-Sanij
University of Leeds, School of Mechanical Engineering, Room 4.48, LS2 9JT
Tel No. 0113 343 32906

Please, keep this information sheet and if you are willing to take place in this project, please, sign the consent form.

Many thanks for your time to read this information sheet. If you are going to take part in this project, many thanks for your participation

Using a model leg with embedded pressure sensors for training student nurses to apply compression bandages: feasibility, acceptability and initial results

Questionnaire

Dear student,

We would be very grateful if you could please spare some time to provide us with feedback about your experience with the training device you have used in this workshop.

1. **Did you find the leg helped in providing you with feedback about your bandaging skills?** Please circle the most appropriate answer for your response.

Helped a lot	Helped a little	Neither helped nor hindered	Hindered a little	Hindered a lot
-----------------	--------------------	-----------------------------------	----------------------	-------------------

Is there any reason for your answer to Question 1 that you can share?

2. **If this system was available for you to use again would you use it?**
Please circle the most appropriate answer for your response.

Definitely yes Probably yes Not sure Probably not Definitely not

Is there any reason for your answer to Question 2 that you can share?

Agreement to Photographic and Video Records

I agree that the photographic images (where your identity will not be shown through face blackout) taken during this experiment (Using a model leg with embedded pressure sensors for training student nurses to apply compression bandages: feasibility, acceptability and initial results) may be used for the following purposes (please **circle** all that apply):

- a) Can be used in publications
(i.e. journals, conference paper, thesis which are the part of this PhD)
- b) Can be used in a presentation
(i.e. conferences and societies)
- c) Can be used for educational purposes (i.e. lectures)
- d) All of the above

If in the future you wish to change your mind, you have the right to do so at any time by contacting the main investigator [Mr. Jawad Al Khaburi].

_____	_____	_____
Name of Participant	Date	Signature
_____	_____	_____
Main Investigator	Date	Signature

To be signed and dated in presence of the participant

School of Healthcare

Dr Janet Holt
0113 343 1296
hcsjh@leeds.ac.uk

Baines Wing
University of Leeds
Leeds LS2 9JT

1st March 2010

Mr Jawad Al Khaburi
School of Mechanical Engineering
University of Leeds
Woodhouse Lane
LEEDS LS2 9JT

Dear Jawad

Research Projects for Ethical Approval (SHREC/RP/180)

Thank you for submitting your research proposal "Using a model leg with embedded pressure sensors for training student nurses to apply compression bandages: feasibility, acceptability and initial results". The committee discussed your proposal and agreed that ethical approval would be granted subject to receiving amendments with the following changes:

Participant Information Sheet

- (i) Please provide more detail about the leg testing in particular how it will be of benefit to nurses.
- (ii) Please be explicit that there will be no impact on the students' progress or assessment whether they chose to participate or not
- (iii) With regards to the use of photographs, on the document 'Agreement to Photographic Record' the word 'treatment' should be changed
- (iv) The time commitment required from participants should be clear

Clarification

- (v) It was suggested that the information sheet could be given to the students in advance of the workshop so they could have more time to consider participation.

Please submit a copy of the amendments to your proposal and supporting documentation to Rachel de Souza r.e.desouza@leeds.ac.uk A final approval letter will be issued following Chair's action on receipt of the revised documentation.

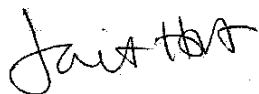
Ethical approval does not infer you have the right of access to any member of staff or student or documents and the premises of the University of Leeds. Nor does it imply any right of access to the premises of any other organisation, including clinical areas. The SHREC takes no responsibility for you gaining access to staff, students and/or premises prior to, during or following your research activities.

Professor Dawn Freshwater
Head of School of Healthcare



It is our policy to remind everyone that it is your responsibility to comply with Health and Safety, Data Protection and any other legal and/or professional guidelines there may be.

Yours sincerely



Dr Janet Holt
Chair
School of Healthcare Research Ethics Committee

Thursday, 04 March 2010

Title of study: Using a model leg with embedded pressure sensors for training student nurses to apply compression bandages: feasibility, acceptability and initial results.

Ethics reference number: SHREC/PR/180

Dear Dr. Janet Holt,

I have received your request for amendments to the information sheet and the agreement to the photographic record documents. I have carried out these changes and have attached the relevant documents. Track changes has been used on the original document to enable you to identify these changes. I also have attached a final, amended version of the document, without the changes being visible, for your records.

In addition, a more detailed response is provided below.

1. *"Please provide more detail about the leg testing in particular how it will be of benefit to nurses".*

I have added few lines to the information sheet to indicate that the pressure sensor system has been tested by me during the course of my PhD studies at the University of Leeds, and found to be accurate and reliable. However, I did not include the level of accuracy of the pressure readings as I believe it is unnecessarily detailed information. It may be useful for you to know that the system accuracy is +/-1mmHg for the range of 0-120mmHg. Nevertheless, if the Committee believe that I should include it in the information sheet, then I will do that.

2. *"Please be explicit that there will be no impact on the students progress or assessment whether they chose to participate or not."*

This has now been made very clear on the first page of the information sheet.

3. *"With regards to the use of photographs on the document 'Agreement to Photographic Record' the word treatment should be changed."*

The requested change has been made to the mentioned document.

4. *The time commitment from participants should be clear*

This is now clearly indicated on the second page of the information sheet.

You have also suggested that we provide the students with the information sheet in advance of the workshop. This has now been arranged and the information sheet will be handed out to the students when they attend a session taught by Prof nelson on the 18th March, on wound care, at the end of the session. In addition, it will be uploaded to the VLE documents for the module to allow any non-attendees at the wound care session on the 18th March, to consider taking part in the study. This will be at least 24 hours before the workshop.

Thank you for considering the application. Any other comments or suggestions are more than welcome.

Yours sincerely,

Jawad Al Khaburi

School of Healthcare

Dr Janet Holt
0113 343 1296
hcsjh@leeds.ac.uk

Baines Wing
University of Leeds
Leeds LS2 9JT



UNIVERSITY OF LEEDS

10 March 2010

Jawad Al Khaburi
BEng in Mechatronics Engineering
PhD Student
School of Mechanical Engineering
University of Leeds
Woodhouse Lane
LEEDS LS2 9NL

Dear Jawad

Re: Research Project for Ethical Approval (SHREC/RP/180)
Title: 'Using a model leg with embedded pressure sensors for training student nurses to apply compression bandages: feasibility, acceptability and initial results'

Thank you for making the necessary changes and submitting the amended documents for approval.

This has been reviewed and I can confirm that the issues raised by the School of Healthcare Research Ethics Committee (SHREC) have been fully addressed and consequently ethical approval is granted.

The committee wishes you every success with your project.

Yours sincerely

A handwritten signature in black ink, appearing to read 'Janet Holt', written in a cursive style.

Dr Janet Holt
Chair
School of Healthcare Research Ethics Committee

Appendix C

List of Publications

- J. Al Khaburi, A.A. Dehghani-Sanij, E.A. Nelson and J. Hutchinson, "Relationship between extension and pressure in compression bandages used in leg ulcers for the control of interface pressure". *In Proc. of the 12th Mechatronics Forum Biannual International Conference, ETH, Zurich, Switzerland*, v1:62-69, 2010.
- J. Al Khaburi, A.A. Dehghani-Sanij, E.A. Nelson and J. Hutchinson, "Comparison between sub-bandage interface computed and measured pressures when bandages are applied to a mannequin leg". *In Proc. of the 12th Mechatronics Forum Biannual International Conference, ETH, Zurich, Switzerland*, v1:70-77, 2010.
- J. Al Khaburi, A.A. Dehghani-Sanij, E.A. Nelson and J. Hutchinson, "The effect of sensor thickness on the interface pressure measurement induced by medical compression bandages". *In Proc. of the 12th Mechatronics Forum Biannual International Conference, ETH, Zurich, Switzerland*, v1:91-98, 2010.
- J. Al Khaburi, E.A. Nelson, J. Hutchinson and A.A. Dehghani-Sanij, "Impact of variation in limb shape on sub-bandage interface pressure". *Accepted for publication in Phlebology*.
- J. Al Khaburi, E.A. Nelson, J. Hutchinson and A.A. Dehghani-Sanij, "Impact of multi-layered compression bandages on sub-bandage interface pressure: a model". *Accepted for publication in Phlebology*.